Elucidating Novel Roles for Post-Transcriptional Regulation of Gene Expression in Neural Stem Cell Biology



Tamsin Joy Samuels

Christ Church

University of Oxford

A thesis submitted for the degree of

Doctor of Philosophy

Trinity 2018

To Jayne Samuels.

ABSTRACT

The brain develops from a relatively small number of neural stem cells whose highly regulated divisions lead to a large and diverse population of neurons. The major focus of the field has been on transcriptional regulation of protein expression, to direct this important process. The precise expression of different transcription factors and regulators determines the behaviour of the stem cell throughout development. In parallel to transcriptional regulation, RNA-binding proteins regulate the processing and fate of their target mRNAs, controlling when and where the encoded proteins are expressed, known as post-transcriptional regulation. In *Drosophila*, two conserved RNA-binding proteins IGF II mRNA-binding protein (Imp) and Syncrip (Syp) are known to act in neural stem cells to specify progeny fate, stem cell shrinkage and termination of division (Liu et al., 2015; Yang et al., 2017a). This thesis examines the importance of post-transcriptional regulation in controlling neural stem cell behaviour, illustrated by two key examples, *myc* and *prospero*.

In order to understand the action of Imp and Syp, I identified their RNA binding targets in the brain by RNA immunoprecipitation and sequencing, with analysis in collaboration with Dr Aino Järvelin. I found a large number of targets, and an enrichment of binding to transcripts encoding transcription factors and RNA-binding proteins. This illustrates the broad roles of Imp and Syp, and their influence on key regulatory proteins. I then designed a gene-by-gene approach to quantitatively and functionally characterise the post-transcriptional regulation of different targets. I particularly focused on the regulation of neural stem cell size, proliferation rate and termination.

I showed that the proto-oncogene *myc* is a target of both Imp and Syp. Myc is known to regulate cell size and cell cycle progression and the human homolog, *c-myc*, is frequently dysregulated in brain cancers. I was interested in the function of Myc in regulating neural stem cell size and proliferation. I used single molecule fluorescent *in situ* hybridisation and immunofluorescence in the intact *Drosophila* larval brain to examine the regulation of *myc* by Imp and Syp. This method allowed precise measurement of the levels of *myc* transcription, cytoplasmic mRNA and protein in individual cells within the brain. I found that Imp stabilises *myc* mRNA, increasing its half life and Myc protein levels. I examined the phenotype of Myc overexpression and found an increase in neural stem cell size and division rate. Myc may be the key Imp target regulating these important aspects of neural stem cell behaviour.

I then examined the regulation of *prospero* (*pros*) by Syp, building on work by Dr Lu Yang in the Davis lab. The key regulatory transcription factor, *pros,* is a target of both Imp and Syp, and is stabilised through Syp binding to a long mRNA isoform with a huge 15 kb extended 3' UTR. The extended isoform of *pros* is highly stable in the *wild type*, and is destabilised by loss of Syncrip. I used clonal analysis and endogenous deletions to begin to dissect the functional roles of the different *pros* isoforms. I uncovered a novel unannotated *pros* transcript, and a complex network of expression and regulation.

The large numbers of Imp and Syp targets identified in this thesis, many with known functions in neurogenesis, show the breadth of post-transcriptional regulation in the brain. The examples of *myc* and *pros* illustrate the importance of precise post-transcriptional regulation of two key transcription factors in neural stem cells. We expect that many further cases of post-transcriptional regulation will be uncovered, with far-reaching consequences for our understanding of neurodevelopment.

DECLARATION

I hereby declare that this Thesis is my own work and the experiments described in the following pages were performed by myself, unless otherwise stated. The experiments were carried out in the Department of Biochemistry, University of Oxford. This Thesis has not been submitted for any other degree or professional qualification.

Tamsin Joy Samuels

ACKNOWLEDGEMENTS

I wish first and foremost to thank my supervisor **Professor Ilan Davis** for his support and guidance throughout the project. I appreciate the freedom I was given to take the project in my own direction, and the thoughtful discussions which helped steer me.

I am extremely grateful to all of the members of the Davis and Castello labs for their practical support and for making the last four years so enjoyable. In particular, I thank **Dr Darragh Ennis** for his constant willingness to help and remarkable ability to fix any problem. **Dr Aino Järvelin** kindly lent her time and skills to analyse the bioinformatics data presented in this thesis. I benefitted greatly from **Dr Francesca Robertson**'s expertise on fly genetics and CRISPR, as well as many brainstorming sessions while tipping flies. This project was developed from initial work by **Dr Lu Yang** and I benefitted hugely from her introduction to the field of *Drosophila* neurobiology. Discussions with **Professor David Ish-Horovicz**, **Dr Mary Thompson, Jeff Lee** and **Martin Hailstone** were essential in the development of this work. I also appreciate **Dr Richard Parton** and all of the staff at Micron for their assistance in microscopy.

I am in debt to the following people for fly stocks, reagents and discussion: **Professor Paul MacDonald, Professor Robert Eisenman, Dr Tzumin Lee** and **Dr Ching-Po Yang.** I thank the **University of Cambridge Department of Genetics Fly Facility** for their injection work. I gratefully acknowledge the **Wellcome Trust** for funding this project, as well as the effort made by **Professor Matthew Whitby** for the smooth running of the Chromosome and Developmental Biology programme.

ABBREVIATIONS

AKT	protein kinase B
Alk	Anaplastik lymphoma kinase
APF	after pupal formation
aPKC	atypical protein kinase C
Baz	Bazooka
bHLH	basic Helix Loop Helix
Brat	Brain tumour protein
BSA	bovine serum albumin
Cas	Castor
CB	central brain
cDNA	complementary deoxyribonucleic acid
Chinmo	chronologically inappropriate morphogenesis
ChIP	chromatin immunoprecipitation
CHX	cycloheximide
CLIP	crosslinking and immunoprecipitation
CNS	central nervous system
DAPI	4’,6-diamidino-2-phenylindole
Dpn	Deadpan
DEPC	diethylpyrocarbonate
Dm	Diminutive
DMP	dimethyl pimelimidate
DMSO	dimethyl sulfoxide
DNA	deoxyribonucleic acid

dNTP	deoxynucleotide
DRB	5,6-dichloro-1-beta-D-ribofuranosylbenzimidazole
EcR	ecdysone receptor
EdU	5-ethynyl-2′-deoxyuridine
EJC	exon junction complex
EM	electron microscopy
EtOH	ethanol
FMR1	fragile X mental retardation
GMC	ganglion mother cell
Grh	Grainyhead
gRNA	guide RNA
Hb	Hunchback
HR	homologous recombination
iCLIP	individual nucleotide resolution crosslinking and immunoprecipitation
IF	immunofluorescence
Imp	IGFII mRNA-binding protein
INP	intermediate neural progenitor
InR	insulin receptor
Insc	Inscuteable
KH	hnRNP K homology domain
Klu	Klumpfuss
Kr	Krüppel
LB	lysogeny broth
MB	mushroom body
Mbm	Mushroom body miniature
Mbt	Mushroom bodies tiny

Mira	Miranda
NB	neuroblast
NHEJ	non-homologous end joining
NMD	nonsense mediated mRNA decay
NMJ	neuromuscular junction
NSC	neural stem cell
ON	overnight
PAK	p21-activated kinase
PBS	phosphate buffered saline
PBST	phosphate buffered saline with Tween
PBSTX	phosphate buffered saline with Triton-X
PCR	polymerase chain reaction
PFA	paraformaldehyde
PI3K	phosphatidylinositol 3-kinase
Pon	Partner of Numb
Pros	Prospero
qPCR	quantitative polymerase chain reaction
RBP	RNA-binding protein
RBD	RNA-binding domain
RIPseq	RNA immunoprecipitation and sequencing
RNA	ribonucleic acid
RNP	ribonucleoprotein
RRM	RNA recognition motif
RT	room temperature
RT-PCR	reverse transcription polymerase chain reaction
SELEX	systematic evolution of ligands by exponential enrichments
SMA	spinal muscular atrophy

smFISH	single molecule RNA fluorescent *in situ* hybridisation
SOC	Super optimal broth with catabolite repression
SSC	saline sodium citrate
Stau	Staufen
Svp	Sevenup
Syp	Syncrip
TF	transcription factor
TOR	target of rapomycin
TSS	transcriptional start site
UTR	untranslated region
VNC	ventral nerve cord
Wor	Worniu
Yki	Yorkie

TABLE OF CONTENTS

ABSTRACT i

DECLARATION iii

ACKNOWLEDGEMENTS iv

ABBREVIATIONS v

TABLE OF CONTENTS ix

List of Tables and Figures xiii

INTRODUCTION 1

1.1 NEUROGENESIS IN DROSOPHILA 2

1.1.1 Drosophila as a model organism 2

1.1.2 Drosophila neural stem cells 3

1.1.3 Asymmetric neuroblast division 5

1.2 NEUROBLAST DIVISION THROUGH DEVELOPMENT 9

1.2.1 Two waves of neurogenesis 9

1.2.2 Neuroblast termination 11

1.2.3 Neuroblast growth control 12

1.2.4 Neuroblast division rate 16

1.3 TRANSCRIPTIONAL REGULATION OF NEUROGENESIS 17

1.4 POST-TRANSCRIPTIONAL REGULATION OF NEUROGENESIS 19

1.4.1 RNA-binding proteins 21

1.4.2 RBP binding motifs 23

1.4.3 mRNA localisation in neurons 24

1.4.4 Brat: an asymmetrically localised cell fate determinant 25

1.4.5 RBP levels define neuron fates 25

1.5 IMP AND SYP REGULATION OF NEUROGENESIS 26

1.5.1 Imp 27

1.5.2 Syncrip 29

1.5.3 The regulatory relationship of Imp and Syp 30

1.6 RELEVANCE TO MAMMALIAN NEUROGENESIS 32

1.7 AIMS OF THESIS 33

MATERIALS AND METHODS 36

2.1 REAGENTS AND FLY STOCKS 36

2.1.1 Solutions and Reagents 36
2.1.2 Fly stocks 37
2.1.3 Clonal analysis 38
2.2 BIOCHEMICAL TECHNIQUES 39
2.2.1 Genomic DNA extraction from Drosophila 39
2.2.2 BAC purification 39
2.2.3 Standard PCR 39
2.2.4 DNA gel electrophoresis 40
2.2.5 Gel purification 40
2.2.6 Sanger sequencing 41
2.2.7 RNA extraction 41
2.2.8 Reverse transcription PCR (RT-PCR) 41
2.2.9 qPCR 42
2.2.10 Antibody crosslinking to magnetic beads 42
2.2.11 RNA immunoprecipitation 43
2.2.12 Western blot 44
2.2.13 polyA selection 44
2.2.14 RNA sequencing 45
2.3 Staining and Imaging 45
2.3.1 Antibody staining for immunofluorescence (IF) in larval brains 45
2.3.2 single molecule RNA fluorescent in situ hybridisation (smFISH) for larval brains 46
2.3.3 smFISH with IF for larval brains 47
2.3.4 Staining with dyes 48
2.3.5 5-ethynyl-2'deoxyuridine (EdU) labelling 48
2.3.6 Image acquisition 48
2.3.7 Image analysis 49
2.4 CRISPR Drosophila methods 50
2.4.1 CRISPR guide design 50
2.4.2 Guide cloning 51
2.4.3 Homology template cloning 52
2.4.4 Embryo injection and selection 53
2.5 Bioinformatics methods 53
2.5.1 Statistical analysis 53
2.5.2 Analysis of RNAseq and RIPseq (with Dr Aino Järvelin) 54
2.5.3 Bioinformatic analysis of Imp iCLIP-seq dataset in S2 cells 56
2.5.4 Analysis of 3' UTR length 56
2.5.5 Functional annotation 57

THE ROLE OF IMP AND SYP IN NEUROGENESIS 58
3.1 INTRODUCTION 58
3.1.1 Specific aims 60
3.1.2 Experimental rationale 60
3.2 WHAT mRNA TARGETS DO IMP AND SYP BIND? 62
3.2.1 RIPseq identified Imp and Syp mRNA targets 62
3.2.2 Which mRNA targets are bound by both Imp and Syp? 71
3.2.3 Enrichment of RBPs and TFs among Imp and Syp targets 72
3.2.4 Imp and Syp bind genes with long 3' UTRs 74
3.3 ARE mRNA LEVELS OF SYP TARGETS ALTERED IN A syp MUTANT? 76
3.3.1 RNAseq identified changes in mRNA levels in syp mutant 76
3.3.2 Changes in target transcript levels in the syp mutant 80
3.4 SELECTING TARGETS TO FOLLOW UP 84
3.4.1 Experimental rationale 85
3.4.2 How do Imp and Syp behave in type I NBs? 89
3.4.3 Phenotypes of imp and syp in type I NBs 91
3.4.4 Choosing targets to follow up 97
3.5 CONCLUSION AND DISCUSSION 98
MYC IS POST-TRANSCRIPTIONALLY REGULATED TO CONTROL NB SIZE 101
4.1 INTRODUCTION 101
4.1.1 Specific aims 104
4.2 IS MYC OR MNT LEVEL REGULATED BY IMP/SYP? 105
4.2.1 Where are Myc and Mnt expressed? 105
4.2.2 Are Myc or Mnt levels regulated by Imp/Syp? 107
4.2.3 Which isoform of myc is expressed in NBs? 109
4.2.4 Is there an isoform switch in the syp mutant? 112
4.3 IS MYC POST-TRANSCRIPTIONALLY REGULATED IN THE NB? 112
4.3.1. Measuring post-transcriptional regulation 112
4.3.2 Quantitating post-transcriptional regulation of myc 114
4.3.3 Cycloheximide treatment stabilises myc mRNA in wild type 117
4.4 IS MYC ELEVATION RESPONSIBLE FOR THE PHENOTYPES OF IMP/SYP DYSREGULATION? 119
4.5 WHERE DOES IMP BIND TO myc? 121
4.5.1 iCLIP analysis in S2 cells shows most binding in the extended 3' UTR 121
4.5.2 Endogenous myc 3' UTR deletions 123
4.6 IMP AND NB SHRINKAGE IN THE PUPA 125
4.7 CONCLUSION AND DISCUSSION 128

mRNA STABILITY REGULATES CELL-TYPE SPECIFIC EXPRESSION OF PROS 133

5.1 INTRODUCTION 133

5.1.1 Specific aims 135

5.2 PROS IS POST-TRANSCRIPTIONALLY REGULATED BY SYP 136

5.2.1 Syp binds pros and is expressed in the same cells of the brain 136

5.2.2 pros isoform choice determines protein level 137

5.2.3 Syp regulates pros mRNA stability 140

5.2.4 proslong is stabilised by Syp 142

5.3 WHAT IS THE FUNCTION OF PROS REGULATION BY SYP? 144

5.3.1 Clonal analysis shows normal exit from proliferation 144

5.3.2 Syp is required for nuclear Pros in terminating NBs (Dr Lu Yang and Dr Ching-Po Yang) 146

5.4 CRISPR MUTANTS PROVIDE INSIGHT INTO PROS ISOFORM FUNCTIONS 148

5.4.1 Removing proslong through NMD 148

5.4.2 Using CRISPR to delete the pros 3' UTR extension 150

5.4.3 Deleting the proslong promoters 151

5.4.4 Ongoing strategies to delete the pros UTR extension 156

5.5 CONCLUSION AND DISCUSSION 157

DISCUSSION AND FUTURE PERSPECTIVES 162

Bibliography 169

Appendix 184

A. qPCR primers 184

B. smFISH probe sequences 184

C. CRISPR/Cas9 Deletions 193

D. RIPseq target tables 198

E. syp mutant RNAseq comparison 240

List of Tables and Figures

Figure 1.1 Neurogenesis in the Drosophila larva (adapted from Homem et al. 2015) 4

Figure 1.2 Asymmetric segregation in the NB (adapted from Homem et al. 2012) 7

Figure 1.3 NB size is regulated through development 10

Figure 1.4 Nutritional regulation of NB size 13

Figure 1.5 Transcription factors and transcriptional cascades 17

Figure 1.6 Post-transcriptional regulation: RBPs and RBP binding motifs 20

Figure 1.7 Imp and Syp are conserved RBPs 27

Table 2.1 Solutions and Reagents 36

Table 2.2 Fly Stocks 37

Table 2.3 Antibodies for Western Blot 44

Table 2.4 Antibodies for immunofluorescence 46

Figure 3.1 RIPseq strategy to identify Syp targets 63

Figure 3.2 Syp IP sample correlation plots show reproducibility 64

Figure 3.3 Syp targets identified by RIPseq 66

Figure 3.4 RIPseq strategy to identify Imp targets 68

Figure 3.5 Imp IP sample correlation plots show reproducibility 69

Figure 3.6 Imp targets identified by RIPseq 70

Figure 3.7 Targets binding both Imp and Syp 71

Table 3.1 Expression of targets in NBs or neurons 72

Table 3.2 Enrichment of TFs and RBPs among Imp and Syp targets 73

Figure 3.8 Imp and Syp bind genes with long 3’ UTRs 75

Figure 3.9 Changes in the transcriptome of syp mutant brains 77

Table 3.3 TFs which change in the syp mutant 79

Table 3.4 RBPs which change in the syp mutant 80

Figure 3.10 syp mutant data and overlap with targets 81

Table 3.5 Syp targets changed in the syp mutant 82

Table 3.6 Imp targets changed in the syp mutant 83

Figure 3.11 Diagram illustrating the microscopy experimental rationale 87

Figure 3.12 Imp and Syp expression 88

Figure 3.13 Syp represses Imp in type I NBs 90

Figure 3.14 Manipulating Imp and Syp levels 91

Figure 3.15 Imp regulates type I NB size in the larva 93

Figure 3.16 Imp overexpression increases NB mitotic index 95

Figure 3.17 Imp overexpression increases rate of progeny production 97

Figure 4.1 Myc protein, but not myc mRNA, is restricted to the NB 106

Figure 4.2 Mnt protein and mRNA is expressed in NBs and progeny 107
Figure 4.3 Myc, but not Mnt, level is regulated by Imp 109
Figure 4.4 myclong is expressed in NBs 111
Figure 4.5 Workflow of transcript counting in NBs 114
Figure 4.6 smFISH quantitation shows Imp regulates myclong half life 116
Figure 4.7 myc mRNA is unstable in wild type brains 118
Figure 4.8 myc overexpression phenocopies Imp elevation 120
Figure 4.9 Imp binds myc in the 3' UTR extension 122
Figure 4.10 CRISPR homologous repair and deletion lines 125
Figure 4.11 Imp binds to mRNAs encoding Mediator components. 127
Figure 5.1 pros mRNA and protein are correlated in Syp expressing cells 136
Figure 5.2 pros is transcribed in all cells in the Type I NB lineage 137
Figure 5.3 pros has a hugely extended 3' UTR 138
Figure 5.4 Syp regulates pros stability 140
Figure 5.5 Imp does not contribute to Pros regulation 141
Figure 5.6 Syp specifically increases proslong stability 143
Figure 5.7 Model depicting Syp regulation of pros 144
Figure 5.8 Clonal analysis shows normal GMC differentiation in syp mutant 145
Figure 5.9 Syp stabilises proslong in pupal NBs 147
Figure 5.10 Introducing an NMD mutation does not remove proslong 149
Figure 5.11 Deletion of the 3' UTR extension 150
Figure 5.12 Deletion of the upstream TSSs does not remove all pros-long signal 152
Figure 5.13 Deletion of the upstream TSSs reveals a new pros isoform 154
Figure 5.14 Pupal termination is unaffected by loss of upstream TSSs 155
Figure 5.15 Ongoing strategies to study the pros extended 3' UTR 157
Table C.3 gRNAs 195
Table D.1 Syp RIPseq targets 198
Table D.2 Imp RIPseq targets 213
Table E.1 Upregulated in syp mutant 240
Table E.2 Downregulated in syp mutant 246

1.

INTRODUCTION

The brain is the most complex organ in the vertebrate body, and is responsible for diverse and essential functions from controlling behaviour, to memory, to secretion of hormones. It must combine flexibility and learning with established responses and structures. The human brain contains approximately 86 billion neurons and a roughly equivalent number of non-neuronal cells such as glia (Azevedo et al., 2009). This vast number and diversity of neurons is derived from a relatively small population of neural stem cells (NSCs), which undergo multiple asymmetric division cycles to generate all the cells of the brain.

Tight regulation of NSC behaviour is critical to ensure correct development of a functional brain, and to avoid uncontrolled proliferation. The risk of dysregulated division must be minimised through redundant controls, and yet NSCs require flexibility to allow spatio-temporally specific behaviour. There is a large body of literature describing the regulation of NSC processes at a transcriptional level. However, key questions remain in the field. To what extent does post-transcriptional regulation coordinate NSC biology? How is NSC division and growth regulated through developmental progression in changing conditions? This thesis aims to examine the regulatory roles of two differentially expressed RNA-binding proteins

(RBPs), and to identify key genes which are post-transcriptionally regulated to control NSC growth and division.

In this Chapter, I will introduce the characteristics of neurogenesis and NSC behaviour in *Drosophila*. I will then discuss the regulation of neurogenesis: the well studied transcriptional regulation, and the newly emerging role of post-transcriptional regulation. I will finally introduce Imp and Syncrip, two RBPs which play a key role in regulation of neurogenesis, and which will be the main focus of this thesis.

1.1 NEUROGENESIS IN *DROSOPHILA*

1.1.1 *Drosophila* as a model organism

The model organism *Drosophila melanogaster* is widely used to study the nervous system. Its relative simplicity and small size allow the use of microscopy to study processes in the intact brain at a sub-cellular level. The adult *Drosophila* central nervous system (CNS) contains approximately 100,000 neurons, while the 3rd instar larval CNS (wL3, the final larval stage before pupation) contains 10,000 neurons. This relatively simple model has allowed researchers using electron microscopy (EM) to map the entire neural connectome of the mushroom body (MB, the centre for memory) in both larvae and pupae (Eichler et al., 2017; Takemura et al., 2017).

More generally, the *Drosophila* model system is well established, with a highly annotated genome and sophisticated genetic tools to perturb the system. Along with the rapid generation time of *Drosophila,* this opens up wide possibilities for experimentation. Discoveries in *Drosophila* pave the way for mammalian research, as up to 75% of human disease-causing genes have a functional homolog in *Drosophila* (Pandey and Nichols, 2011). Therefore, using *Drosophila* to study NSC regulation

allows rapid experimentation and discovery, and provides valuable insight to human processes.

1.1.2 *Drosophila* neural stem cells

The *Drosophila* larval nervous system simultaneously functions to control larval behaviour, and undergoes extensive neurogenesis to produce the adult brain. The larval brain is made up of two brain lobes and the ventral nerve cord (VNC) (Figure 1.1 A). NSCs, called neuroblasts (NBs), produce all the neurons required for a functional nervous system. The NBs are very large cells, which divide asymmetrically to produce another large NB, as well as a much smaller daughter cell, which proceeds down the path of differentiation. *Drosophila* neurogenesis occurs in two waves, first in the embryo and then the larva, separated by a period of quiescence (Homem and Knoblich, 2012; Homem et al., 2015).

This thesis will focus on the larval central brain (CB), which contains mainly type I and type II NBs, classified by their division pattern (Figure 1.1 B). Type I NBs divide asymmetrically to produce another NB, and a smaller progeny cell called the ganglion mother cell (GMC). The GMC divides only once more, symmetrically, to produce a pair of terminally differentiated neurons or glia. Type II NBs have a more complex division hierarchy, where the NB produces an intermediate neural progenitor cell (INP), which itself can asymmetrically divide a further 3 - 5 times, with each division producing an INP and a GMC (Bello et al., 2008). There are about 90 type I NBs per brain lobe, and just 8 type II NBs. However, the transit amplifying population of INPs makes the type II NBs the majority contributor to the adult neural cell population.

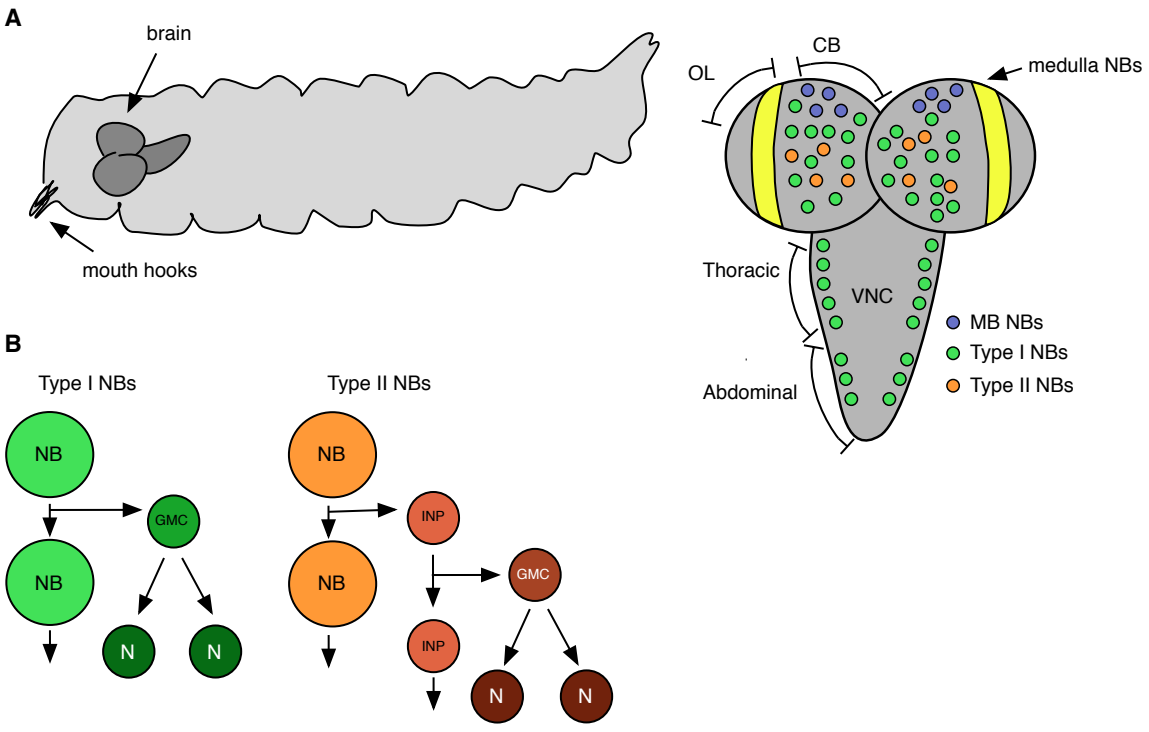


Figure 1.1 Neurogenesis in the *Drosophila* larva (adapted from Homem *et al*. 2015)

A The wandering 3rd instar larval brain is found in the head region behind the mouth hooks. A dorsal view of the larval brain shows the location of different neuroblast (NB) lineages. The optic lobe (OL) is produced by medulla NBs. The ventral nerve cord (VNC) contains thoracic and abdominal type I NBs. The central brain (CB) contains both type I and type II NBs, as well as the mushroom body NBs. **B** Type I NBs divide asymmetrically to produce a progeny ganglion mother cell (GMC) and another NB. The GMC divides only once more to produce neurons or glia (N). Type II NBs have an additional intermediate progenitor cell (INP), which itself undergoes asymmetric divisions and acts as an amplifying population.

There are also 4 MB NBs per hemisphere in the central brain, which specifically contribute the neurons for the MB (and follow the same division sequence as a type I NB). Medulla NBs build the optic lobes, which will make up half of the volume of the adult brain. Finally the VNC contains the abdominal and thoracic NBs.

1.1.3 Asymmetric neuroblast division

Each type I NB division produces two distinct cell types: the NB is renewed, and a GMC buds off. The cells are different in size, with the small GMC budding off from a much larger NB, and have very different proliferative potential. Type I NBs divide approximately every 90 minutes in the larva, while the GMC divides just once, after more than 4 hours (Homem et al., 2013). The progeny cells from the GMC division exit mitosis entirely and undergo terminal differentiation. It is crucial that the GMCs do not inherit the NB's drive for rapid proliferation, as reversion of the GMC to a proliferative fate leads to uncontrolled tumour growth. At the same time, the NB must maintain its own proliferative fate through each division, in order to produce further neurons required for the brain.

The production of two cells with different fates from a single stem cell division can be achieved either through extrinsic cell signalling (between the two cells after division, or with the environment), or through segregation of an intrinsic determinant (Horvitz and Herskowitz, 1992). Larval NB asymmetric divisions do not require external factors, as they can continue normally in isolated culture (Ceron et al., 2006). The intrinsic factors required for *Drosophila* NB asymmetric division have been highly studied and the process is well understood. Briefly, cell polarity must be established, the spindle is oriented, cell fate determinants are differentially localised in the cell,

and finally these determinants are segregated to different cells at division (Homem and Knoblich, 2012) (Figure 1.2).

Establishing the axis of NB division

Embryonic NBs originate from the ventral neuroectoderm and inherit the polarity of this epithelium to orient their first division (Knoblich, 2008). However, subsequent NB divisions are aligned relative to the previous division axis, which may be inferred from the centrosome (Rebollo et al., 2009). The cell polarity is established by localisation of the Par complex to the apical cortex of the NBs during interphase (Homem and Knoblich, 2012) (Figure 1.2). The Par complex consists of Bazooka (Baz)/Par-3, Par-6 and atypical protein kinase C (aPKC), and it is conserved through almost all circumstances of cell polarity (Suzuki and Ohno, 2006). Mutants for any of these proteins leads to loss of division asymmetry as various other fate determinants are mislocalised.

The spindle is responsible for dividing the two cells at mitosis and therefore must be aligned appropriately with respect to the segregating factors. Baz recruits Inscuteable (Insc) to the apical cortex and, in a cascade of protein binding, Insc brings Pins, Gαi and Mud into the complex (Knoblich, 2008). Mud is a microtubule and dynein binding protein (the *Drosophila* homolog of NuMA) and acts as a docking site for astral microtubules to bring one of the spindle poles and anchor it to the apical cortex.

Cell cleavage occurs at the mid-plane of the spindle which usually results in two equally sized daughter cells. However, in NBs the spindle is asymmetrically shaped with a larger apical half, and is displaced such that the cleavage site is shifted basally (Kaltschmidt and Brand, 2002).

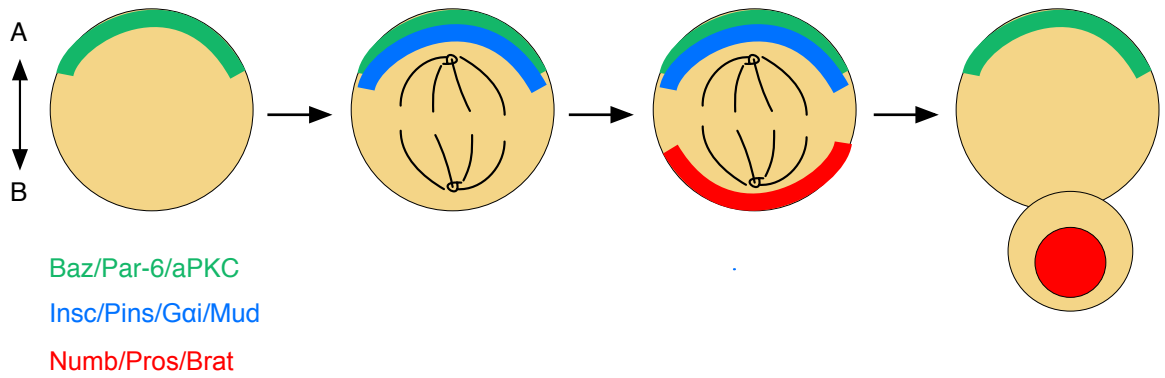


Figure 1.2 Asymmetric segregation in the NB (adapted from Homem *et al*. 2012) During interphase the Par complex (Baz/Par6/aPKC) is recruited to the NB apical cortex. Baz then recruits Insc, which then brings in Pins, Gαi and Mud. Astral microtubules bind to Mud and anchor on spindle pole at the apical cortex. Numb, Pros and Brat are segregated to the basal side of the cortex such that they are inherited only by the GMC at the asymmetric division. Pros is then allowed to enter the nucleus where it promotes neural differentiation. A = apical, B = basal.

Asymmetry of cell fate determinants

The apical Par complex itself does not confer any cell fate, but it induces accumulation of cell fate determinants at the opposite, basal side of the cell so that they are inherited by the GMC. There are three key cell fate determinants segregated to the GMC: Numb, Prospero (Pros) and Brain tumour protein (Brat) (Knoblich, 2008) (Figure 1.2).

Numb is asymmetrically localised to the basal side of the cortex through binding to Partner-of-numb (Pon), which is itself activated through phosphorylation by Polo kinase (Wang et al., 2007). Numb is inherited by the GMC, where it promotes endocytosis of the Notch receptor and therefore inhibits Notch signalling in a cell-type-specific way (Berdnik et al., 2002). Chromatin Immunoprecipitation (ChIP) experiments to identify Notch targets reveal many genes for NB proliferation and temporal specification including *worniu (wor), deadpan (dpn), klumpfuss (klu), grainy head (grh), myc* and *castor (cas),* among others (Zacharioudaki et al., 2016). High

levels of Notch are a determinant of NB fate and therefore Numb inhibition of Notch promotes differentiation in the GMC.

Pros (the *Drosophila* homolog of Prox1) is a homeodomain-containing transcription factor (TF), which represses genes for self-renewal and activates genes for neural differentiation. Pros is asymmetrically segregated in the NB through binding to Miranda (Mira) (Chia et al., 2008). Mira itself is recruited to the basal side of the NB through activation by Lethal giant larvae (Lgl), which is repressed at the apical side through phosphorylation by aPKC. Therefore, Mira is only recruited at the basal side of the NB, where it tethers Pros until after division (Hirata, 1995; Ikeshima-Kataoka, 1997; Spana and Doe, 1995). In the GMC, Mira is degraded and allows Pros to enter the nucleus. The targets of Pros have been identified genome-wide and include downregulation of NB determinants *mira* and *dpn,* and upregulation of neuronal specifiers *zfh1* and *lim1* (Choksi et al., 2006). *pros* mRNA is also asymmetrically localised by Insc in the embryo, requiring Staufen (Stau) for this process (Li et al., 1997). In embryos, *pros* mutants lead to excess cell divisions in GMCs (Choksi et al., 2006). However, in larval brains *pros* mutants cause tumours (Bello et al., 2006).

Brat is co-segregated into the GMC with Pros via Mira (Betschinger et al., 2006). It acts together with Pros to promote a GMC fate. Brat is an RNA-binding protein which may regulate several important targets at a post-transcriptional level. *brat* mutants cause tumour growth due to reversion of the INP population to an NB fate.

Together, Numb, Pros and Brat promote differentiation in the progeny GMC. The mechanism of asymmetric protein localisation is advantageous due to the immediate action in the daughter cell upon cell division, compared to the slower effect of switching on a gene transcriptionally.

1.2 NEUROBLAST DIVISION THROUGH DEVELOPMENT

NBs are formed in the embryo through delamination from the neuroectoderm, followed by a process of lateral inhibition (Skeath and Thor, 2003). There are then two waves of neurogenesis, in the embryo and then the larva, separated by a period of stem cell quiescence (Homem and Knoblich, 2012) (Figure 1.3 A). In the early pupal stages most NBs exit division through various mechanisms depending on their lineage. The CNS is remodelled during metamorphosis in the pupa through pruning and cell death, but limited further cell division.

1.2.1 Two waves of neurogenesis

The neuroectoderm emerges after gastrulation and NBs delaminate in five successive waves in embryonic stages 9 - 11 (Hartenstein and Wodarz, 2013). Small clusters of cells express pro-neural genes and, within each cluster, Notch signalling between cells results in the selection of a single NB. The NB then enters mitosis and begins a wave of asymmetric divisions. Throughout the embryonic and larval stages each NB produces a highly reproducible sequence of specific neuron types. In the embryo, this is regulated through a sequential cascade of TFs, which is key to producing all the correct neurons for the brain and is discussed further below (section 1.3). Embryonic NBs do not grow sufficiently to maintain their volume with each division and therefore gradually shrink, limiting their proliferative potential (Fuse et al., 2003; Hartenstein et al., 1987). After completing these divisions, producing all of the neurons for the larval brain, most NBs in the abdominal regions undergo apoptosis. The remaining NBs in the cephalic and thoracic regions enter a period of quiescence until 8-10 hours after larval hatching (with the exception of the mushroom body neuroblasts which do not undergo quiescence (Syed et al., 2017a)).

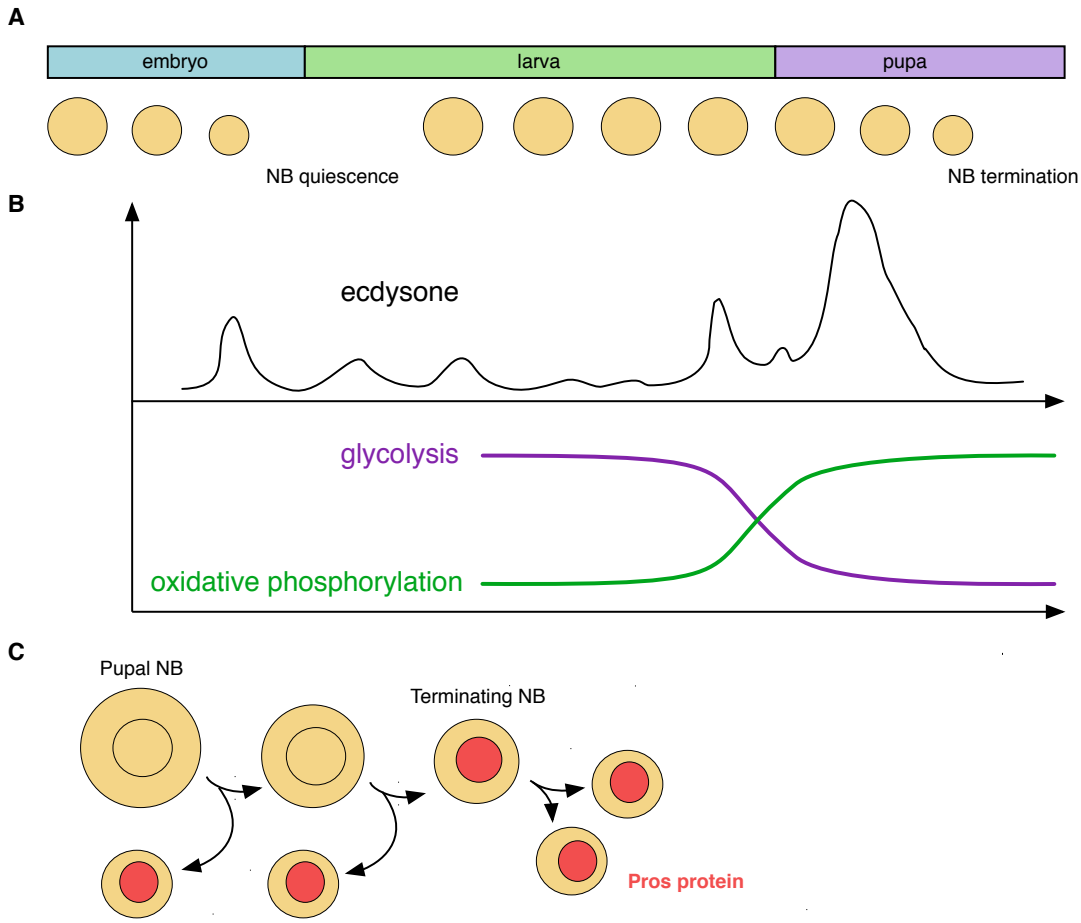


Figure 1.3 NB size is regulated through development
A NBs undergo two waves of division. In the embryo the neuroblast does not regrow between divisions and therefore gradually shrinks until it reaches a stage of quiescence. In the larva, feeding triggers NB growth and re-entry into the division cycle. NB size is maintained through the larval stages but in the pupae, NBs begin to shrink again, eventually leading to termination of division. **B** A pulse of ecdysone at the larval-pupal transition triggers a shift in metabolism from glycolysis to oxidative phosphorylation, reducing cell growth. **C** In the pupae each NB division leads to gradual shrinkage of the NB. At the terminal division, Pros enters the nucleus of the type I NB, and this drives a symmetrical division to produce two GMCs.

In the early larval stages, feeding activates insulin pathways to induce an increase in NB size and re-entry into the cell cycle (Chell and Brand, 2010). The second wave of neurogenesis provides about 90% of the neurons required for the adult brain. Type I NBs divide about every 90 minutes and the NBs regrow between each division to maintain their volume. The NB is maintained within a stem cell niche including glial cells, which provide signalling information. Each central brain NB produces around 100 progeny cells and these are pushed further from the NB and deeper into the lobe

with each subsequent division. During terminal differentiation, each neuron sends out axon projections, which join the central neuropil of the brain. As in the embryo, each NB produces progeny with a reproducible sequence of neuronal types. The NB divides into the early pupal stages before terminating (Truman and Bate, 1987).

1.2.2 Neuroblast termination

NBs exit from the division cycle at different times in the pupae, suggesting there is not a single systemic termination signal. Different sub-populations of NBs terminate through different mechanisms. In the VNC NBs undergo apoptosis via a burst of Abdominal-A Hox protein which activates the Reaper, Hid and/or Grim pro-apoptotic proteins (Bello et al., 2003). The long-lived MB NBs are lost through apoptosis and autophagy (Siegrist et al., 2010).

The CB type I NBs decrease in size over several divisions in the pupa and the stem cell is lost through a final, symmetrical division, in which both progeny lose their stem cell character and differentiate (Maurange et al., 2008). Shrinkage is triggered through signalling by the steroid hormone ecdysone at the larval to pupal transition (Homem et al., 2014) (Figure 1.3 B). The Mediator complex is required to make NBs responsive to ecdysone, allowing a metabolic shift from glycolysis to oxidative phosphorylation. This depletes essential building blocks for cell growth, so that with continued division the NBs shrink.

The final symmetric division, resulting in loss of the type I NB, is driven by nuclear accumulation of Pros in the terminating NB (Maurange et al., 2008) (Figure 1.3 C). In larval and early pupal NBs, Pros is undetectable in the nucleus. However, a burst of nuclear Pros is detected immediately prior to the terminal division. At the same time Mira delocalises from the cortex, presumably allowing Pros entry to the nucleus.

Furthermore, overexpressing Pros in young NBs induces premature termination. It is not clear how this pulse of Pros expression is achieved.

1.2.3 Neuroblast growth control

At different stages of *Drosophila* neurogenesis, a reduction in NB size limits proliferative potential. To maintain a constant cell size, growth must exactly replenish the volume lost through each cell division. Any imbalance in this equation results in net growth or shrinkage of the cell with each division cycle. In *Drosophila* NBs, reduced growth with continued cell division results in the cell shrinkage required for embryonic NB quiescence and pupal NB termination. In the early larva, NBs regrow before re-entering the proliferative cell cycle.

The rate of cell growth can be modified through a number of pathways. In the early larva, NB growth depends on feeding, indicating a favourable environment. The embryo contains its own nutritional reserves so is isolated from the effects of nutritional restriction. In the early larval stages, feeding is detected systemically by the insulin pathway (Homem and Knoblich, 2012) (Figure 1.4 A). The fat body detects increased circulating amino acid levels and activates the target of rapamycin (TOR) pathway (Chell and Brand, 2010; Sousa-Nunes et al., 2011). This leads to release of an unknown signal, which is received by glial cells in the NB niche and prompts them to release insulin-like peptides (ILPs). The insulin receptor (InR) on the NBs recognises these ILPs and activates phosphatidylinositol 3-kinase (PI3K) and Protein Kinase B (AKT) (Hietakangas and Cohen, 2009). The TOR pathway is also activated in the NB, both through PI3K/AKT and as a direct response to the increased cellular levels of amino acids and energy. Therefore, NBs are alerted to the nutritional status of the animal via several convergent pathways.

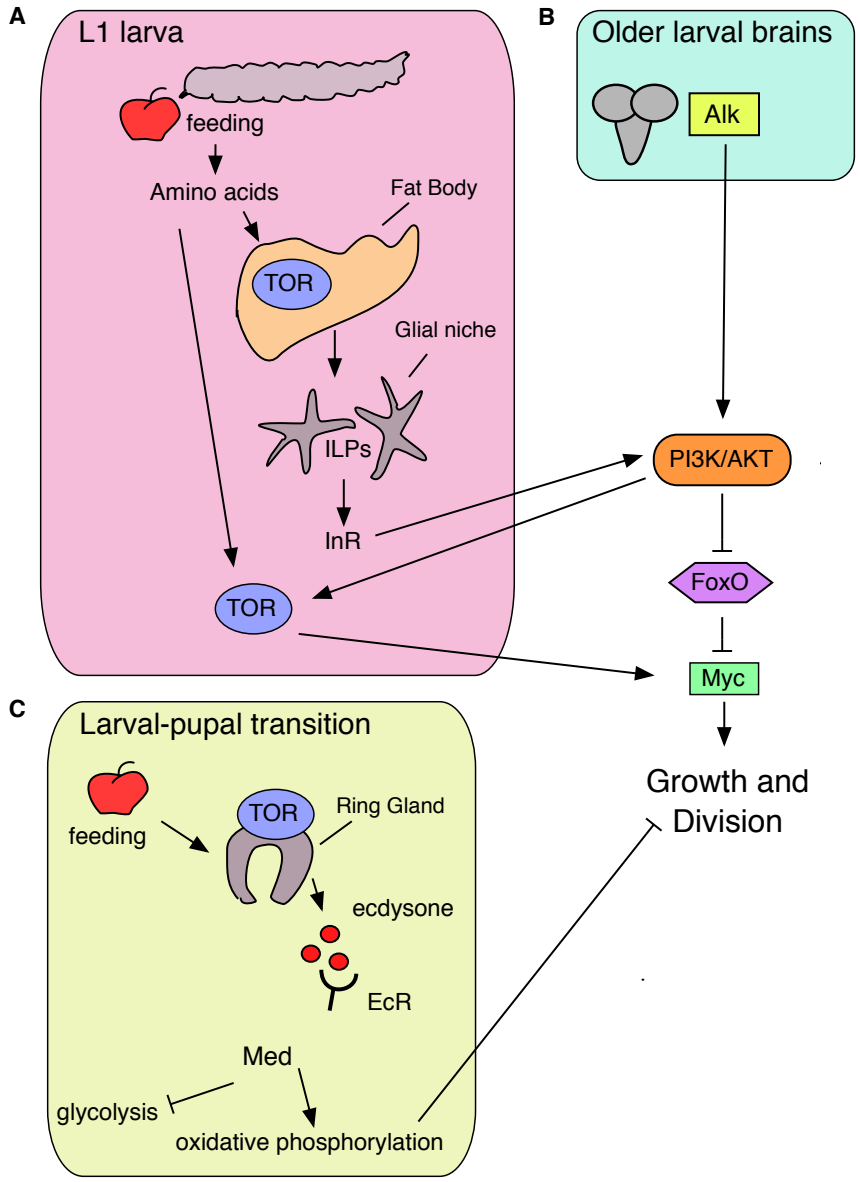


Figure 1.4 Nutritional regulation of NB size
A Feeding in L1 larvae activates the TOR pathway in the NB as well as in the fat body, which initiates insulin signalling. Insulin signalling activates the PI3K/AKT signalling pathway in the NB. These signalling pathways converge on transcriptional activation of Myc, which leads to cell growth and division. **B** In older larval brains constitutive expression of Alk activates the PI3K/AKT pathway independently of nutritional status. **C** At the pupal transition, feeding triggers ecdysone release from the ring gland. This leads to a metabolic shift to oxidative phosphorylation, inhibiting growth.

Downstream of the TOR and PI3K/AKT signalling pathways, there are targets promoting growth and division. One of the targets of AKT signalling is the Forkhead box class O (FoxO) TFs. AKT phosphorylates FoxO, which leads to its nuclear export, followed by ubiquitin-mediated proteasomal degradation (Matsuzaki et al.,

2003). FoxO inhibits expression of cell cycle genes, promoting cell cycle arrest in G1. Therefore, AKT signalling drives re-entry into the cell cycle. In other systems, FoxO and TOR also convergently regulate protein biosynthetic capacity through Myc (the *Drosophila* homolog of the human c-myc) (Teleman et al., 2008). Myc is likely to be the link between PI3K/AKT signalling and cell growth in the NBs, though the pathway is understudied in this context.

The TF Myc promotes ribosome biogenesis via increasing rRNA transcription, as well as expression of ribosomal proteins and proteins required to construct ribosomes (van Riggelen et al., 2010). Ribosome biogenesis is essential for increased cell growth. This is supported by an RNAi screen examining NB size, which identified a cluster of genes involved in ribosome biogenesis (Neumuller et al., 2011). The human c-myc is proto-oncogene upregulated in medulloblastomas and gliomas (Swartling, 2012). The *Drosophila* homolog of c-myc was originally named Diminutive (Dm) due to the small size of the mutant fly, but has since been renamed Myc to reflect its human homolog. In the *Drosophila* larval brain, Myc expression is restricted to the NB and this may be due to post-transcriptional regulation by Brat (Betschinger et al., 2006).

After successful exit from quiescence in the larva, NB growth and division becomes independent of nutritional status. This brain-sparing phenomenon is conserved in human brain growth. In older *Drosophila* brains, Anaplastic lymphoma kinase (Alk) is constitutively expressed, and substitutes for InR so that downstream targets are switched on and normal growth occurs even during nutrient scarcity (Cheng et al., 2011) (Figure 1.4 B).

Nutritional status becomes important once again at the pupal transition (Figure 1.4 C). Ecdysone signalling drives NB shrinkage at the larval to pupal transition by driving a metabolic shift from glycolysis to oxidative phosphorylation, which reduces NB growth (Homem et al., 2014). Ecdysone is released by the prothoracic gland which is part of the ring gland (Homem et al., 2015). The TOR pathway controls ecdysone production from the prothoracic gland and therefore links nutritional status of the larva to the timing of pupation (Layalle et al., 2008).

The growth regulator Myc is also downstream of other well-studied signalling pathways. The Hippo pathway is a key controller of cell growth and tissue homeostasis and has been recently been implicated in NB size regulation (Gailite et al., 2015; Poon et al., 2016). The Hippo pathway leads to phosphorylation of the transcriptional coactivator Yorkie (Yki), excluding it from the nucleus (Stocker, 2011). Myc is a target of Yki and is expressed during low Hippo signalling conditions (Neto-Silva et al., 2010). Myc also regulates levels of Yki, and therefore a feedback mechanism stabilises growth. In a pathway independent of Hippo signalling, Liver kinase B1 (LKB1) also inhibits Yki activity via AMPK (AMP-activated protein kinase) (Gailite et al., 2015). AMPK is a nutrient sensor and is more easily activated by LKB1 in low energy conditions, inactivating Yki (Shaw et al., 2004). Therefore, in low energy conditions Yki is inactive and Myc transcription is not switched on. Interestingly, the LKB1 pathway appears to be active in the CB/VNC NBs, while the parallel Hippo dependent pathway is active in the optic lobe NBs (Gailite et al., 2015).

Myc is also a transcriptional target of Notch (Zacharioudaki et al., 2016). Notch signalling enhances type II NB regrowth after division through upregulation of translation elongation factor 4E (eIF4E) and Myc (Song and Lu, 2011). The

asymmetric inheritance of Numb by the GMC, limits Myc activity and cell growth in these progeny cells.

1.2.4 Neuroblast division rate

The growth of NBs is differentially regulated through development, but less is understood about the regulation of division timing. In most normal cell proliferation systems, the length of the cell cycle is dependent on the length of the first gap phase, G1, during which growth is monitored until it is sufficient to transition to the DNA synthesis, S, phase (Lloyd, 2013; Turner et al., 2012). This monitoring system leads to maximal proliferation while ensuring cell size is sufficient for daughter survival. Such a mechanism could exist in larval NBs: a certain cell size must be achieved before a GMC can be produced. However, a size threshold for division must be switched off or altered in the embryonic and pupal NBs, which repeatedly divide at ever smaller cell sizes.

It has not been shown whether NB division rate changes through development (with the exception of quiescence). Several mutants have been found which alter both NB size and division rate. For example, loss of the p21-activated kinase (PAK) Mushroom bodies tiny (Mbt) causes smaller NBs with lower mitotic activity (Melzer et al., 2013), while impairment of the Hippo pathway leads to larger NBs which divide faster (Poon et al., 2016). Interestingly, these examples suggest that NB division is not simply triggered when the cell reaches a certain size and may be independently regulated.

Myc promotes cell proliferation as well as cell growth (Johnston et al., 1999). Upregulation of Myc shortens the G1 phase by elevating Cyclin E levels. On its own, this does not lead to shortening of the cell cycle as the G2/M transition is limited by

cdc25/string. Upregulation of both of these factors can drive a faster cell cycle. Perhaps changing levels of Myc alter NB division rate as well as NB growth through the progression of larval development.

1.3 TRANSCRIPTIONAL REGULATION OF NEUROGENESIS

The behaviour and fate of a cell depends on its protein complement, which varies despite all cells containing the same genetic information. This is due to differences in gene expression levels, which can be measured in specific cell types. Investigating how gene expression is controlled in different cells is important in order to understand processes in development and disease. The bulk of these studies have focused on transcriptional regulation.

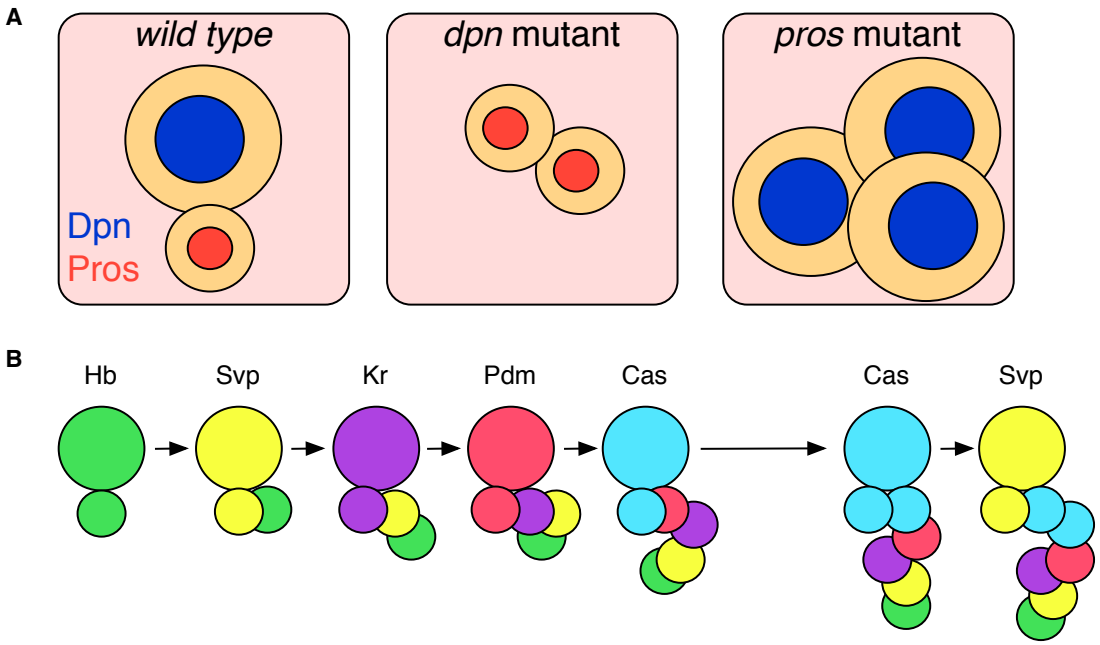


Figure 1.5 Transcription factors and transcriptional cascades
A Key TFs define proliferative or differentiating character of a cell. Dpn promotes a proliferative fate, so *dpn* mutants display premature differentiation and have a reduction in NB number. Pros drives differentiation, so *pros* mutants have the opposite phenotype - differentiation is blocked, so cells take a proliferative fate and form tumours. **B** NB progeny fate in the embryo is determined by a sequential TF cascade in the NB (adapted from Homem and Knoblich, 2012). Hunchback (Hb) > Sevenup (Svp) > Krüppel (Kr) > Pdm > Castor (Cas). The progeny cells inherit the TFs expressed in the NB at the time of their birth, determining their fate. In the larva, Cas and the Svp are re-expressed.

Each TF has a cohort of targets which are upregulated or downregulated at the level of mRNA synthesis. TFs with key roles in differentiation have been identified in *Drosophila* neurogenesis (Figure 1.5 A). Finding these key TFs is of particular interest to cancer biologists, as failure to differentiate leads to tumours (Wodarz and Nathke, 2007). Dpn is a basic Helix-Loop-Helix (bHLH) transcriptional repressor, which defines NB character (San-Juan and Baonza, 2011; Zhu et al., 2012). Loss of Dpn results in a significant reduction in NB number, while Dpn overexpression leads to reversion of progeny cells to a NB-like fate. Acting in concert, Pros is homeobox TF and a determinant of neuron fate. As discussed above, Pros is segregated to the NB cell cortex and only allowed to enter the nucleus in the progeny cells. Its target genes promote exit from the cell cycle and differentiation (Choksi et al., 2006).

TFs are also important in determining the different fates of the diverse progeny generated by a single NB. NBs produce invariant sequences of distinct neuronal types, which results in the functional population of neurons required to build the brain. Producing these cells in the right place at the right time is essential, but requires tight regulation. Various experiments using cell ablation and transplantation have shown that the main determinant of GMC fate is birth order (Doe and Goodman, 1985; Weigmann and Lehner, 1995). In the embryo, this is achieved through the expression of a sequential TF cascade in the NB, with the GMC inheriting the TF expressed at the time it is born. In embryonic NBs, TFs are expressed in a defined but overlapping sequential cascade of Hunchback (Hb) > Sevenup (Svp) > Krüppel (Kr) > Pdm > Castor (Cas) (Isshiki, 2001) (Figure 1.5 B). In post-embryonic NBs, Cas is first re-expressed and then Svp is switched on (Maurange et al., 2008). Each GMC maintains the expression pattern of the parent NB at the time it is born and this defines the fate of its progeny neurons. It is so far unclear how the switches

through the cascade occur. The transitions are not simultaneous in different NBs, so there is no global timer. There may be some regulation by cell cycle number but this is poorly understood (Homem and Knoblich, 2012).

In some cases, key TFs determine cell fate or behaviour, but transcriptional networks can also be powerful to fine-tune regulation and produce more precise outcomes. Transcriptomics experiments on isolated NBs have been used to compare the expression patterns in particular subgroups of NBs, to understand how different NBs produce different neuron lineages (Yang et al., 2016). This study identified complex combinations of TFs characterising different NB lineages which may drive the production of specific neuron fates.

The prevalent approach in understanding the regulation of neurogenesis has been using genome-wide studies to identify key cell-type defining TFs, followed by specific follow up of each TF to find its targets and understand its action. This approach has been very powerful and helpful to our understanding of *Drosophila* neurogenesis. Clearly TF activity defines the gene expression landscape of a cell, but this does not exclude further pathways of modification and regulation. Furthermore the regulation of these key TFs themselves is poorly understood, suggesting more complex levels of control.

1.4 POST-TRANSCRIPTIONAL REGULATION OF NEUROGENESIS

Most work on *Drosophila* and mammalian neurogenesis has focused on key TFs and transcriptional networks. Transcription fundamentally determines which genes are switched on in a cell. However, transcriptional regulation has limitations: different sub-cellular compartments cannot be differentially regulated, and responses to

rapidly changing requirements are slow. Post-transcriptional regulation includes all processes between transcription of a gene and the production of the protein, including splicing, nuclear export, mRNA localisation, degradation, and translation (Figure 1.6 A). Combinations of regulation at these various stages can provide additional complexity, precision, speed or redundancy, depending on the situational requirements. These characteristics are very desirable in the regulation of neurogenesis.

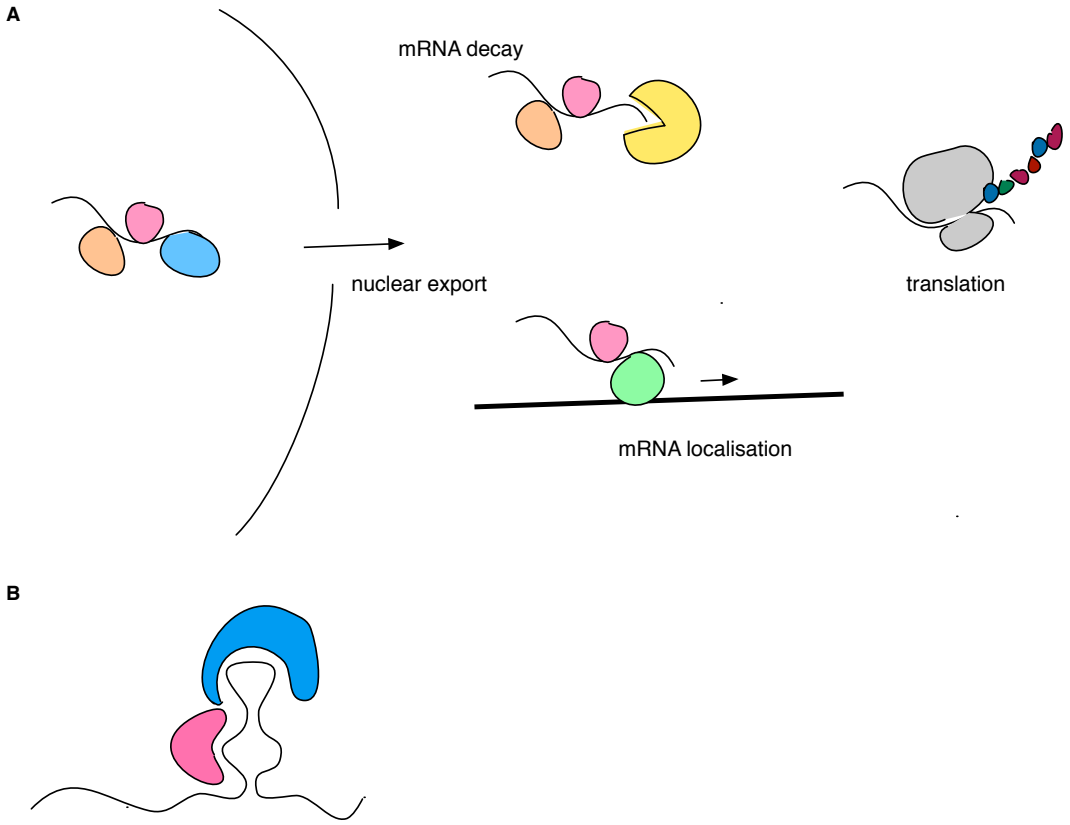


Figure 1.6 Post-transcriptional regulation: RBPs and RBP binding motifs
A Post-transcriptional regulation controls mRNA nuclear export, decay, localisation and translation rates. The mRNA is bound by RBPs to form an RNP. The composition of these binding proteins directs the mRNA fate. **B** Distortions of the mRNA secondary structure such as loops and bulges expose the bases for RBP binding.

A few important examples of post-transcriptional regulation have been uncovered in the nervous system, but these are likely to be just the tip of the iceberg. Taking into account the findings from other fields, it seems likely that a layer of post-transcriptional regulation adds precision and accuracy to many aspects of neurogenesis.

1.4.1 RNA-binding proteins

RBPs act on an RNA to determine how it is processed in the cell. The RBP is a key regulator of its downstream mRNA targets. RBPs are the effectors of post-transcriptional regulation, analogous to TFs as the effectors of transcriptional regulation. Some RBPs have broad roles, such as the neuronal ELAV which influences processes from polyadenylation, to mRNA localisation and translation (Pascale et al., 2008). It is not unusual for these RBPs to act on different levels regulating different target cohorts. Others perform highly specific actions such as splicing or RNA nuclear export. RBPs also bind and regulate non-coding RNAs, which can have functional consequences for cell behaviour.

A conventional RBP has at least one RNA-binding domain (RBD) such as an RNA recognition motif (RRM) or an hnRNP K homology (KH) domain. They bind to sequence or structural motifs in RNA with varying affinity and specificity. RBPs very often act in combination, forming a ribonucleoprotein (RNP) complex. The protein complement of an RNP shifts through the lifetime of the mRNA, directing its fate within the cell.

As the importance and breadth of post-transcriptional regulation has gained recognition, great efforts have been made to systematically identify all RBPs in the genome (Hentze et al., 2018). This process has identified huge numbers of novel

RBPs lacking a conventional RBD (Baltz et al., 2012; Castello et al., 2012). Many of these proteins instead bind RNAs through intrinsically disordered regions (Castello et al., 2016). The identification of such a large cohort of novel RBPs poses many more questions on their roles and the potential breadth of post-transcriptional regulation. There have not been very many studies on RBPs in the central brain, compared to the emphasis on TFs, so further investigation in this context is highly likely to uncover many more developmentally significant RBPs.

RBPs exert their function through the regulation of their target RNAs. The targets of an RBP can be identified using RNA immunoprecipitation (RIP) experiments (reviewed in (Wheeler et al., 2018)). Simply, antibody against the RBP (or an endogenously fused tag such as FLAG or GFP) is used to pull down the RBP and its bound RNAs from a cell lysate. The RNA is extracted and can be analysed using qPCR to identify specific targets of interest, or next generation sequencing (RIPseq) to identify all bound RNAs. UV crosslinking can be used to ensure only directly bound RNAs are recovered (CLIP). Identifying the targets of an RBP is useful to understand its regulatory role. In some cases it is thought that mRNAs encoding functionally related proteins are bound and co-regulated by common RBPs - the regulon hypothesis (Keene, 2007).

RBPs form networks where they regulate each other both post-transcriptionally and post-translationally, with parallels to the well studied transcriptional networks (Mittal et al., 2011). One category of RBPs tends to interact stably with a limited number of protein partners, with which they share many targets. These RBPs often control single steps of the post-transcriptional process such as splicing. Another group of RBPs have a much wider and more transient binding pool, and these are likely to link steps of the post-transcriptional processing together. Many of the highly connected

RBPs autoregulate, lowering the noise in their expression and allowing quick responses to changes. These types of coregulatory network provide efficiency and redundancy, but also mean that large perturbations (e.g. mutants) have far reaching indirect effects.

1.4.2 RBP binding motifs

Each RBP binds to a specific cohort of mRNAs, and this is mediated through interactions with RBP binding motifs. mRNAs are produced as single stranded molecules but form complex secondary and tertiary structures through intra-molecular interactions. These can include stems, hairpin loops, internal loops or bulges, and pseudoknots (Hermann and Patel, 1999). RBPs recognise motifs consisting of a combination of sequence and structure. Double stranded RNA using Watson-Crick base pairing forms an A form helix, which has a deep and narrow major groove that excludes RBPs. Therefore, features of the RNA which distort this structure allow access to the base pairs for sequence recognition (Hermann and Patel, 2000) (Figure 1.6 B). RBP binding sites are frequently but not exclusively found within the 5' or 3' untranslated regions (UTRs) of an mRNA, as this sequence can evolve regulatory functions without affecting the protein sequence.

Uncovering the recognition motif for an RBP is a useful tool to understand the mechanism of regulation (for example through deletion of the motif at the endogenous locus), as well as to predict mRNA targets. There are various experimental and computational techniques to identify the specific recognition motif for an RBP (Li et al., 2014). SELEX (systematic evolution of ligands by exponential enrichments) is an *in vitro* technique, which uses randomised RNA oligonucleotides to identify preferred binding sequence in an iterative fashion. *in vivo,* CLIP-based experiments use UV light to cross link RNAs to RBPs. The RNA can be partially

digested to leave only the bound region, which is sequenced to find the binding sites. A modification on this technique called iCLIP provides individual nucleotide resolution of the RBP binding sites (Huppertz et al., 2014). Binding sites from iCLIP data can be computationally processed to predict binding motifs. RNA folding predictors are important to understand the structural context of these motifs, which will often affect RBP binding. However, understanding the interactions between mRNAs and RBPs must be supplemented by investigating the function of these interactions.

1.4.3 mRNA localisation in neurons

mRNA localisation has been one of the best examined mechanisms of post-transcriptional regulation in the nervous system. Intuitively it is easy to see its value, as a neuron is a highly polarised cell with many synapses at great distance from the cell body. These synapses must respond rapidly to stimuli and must be differentially regulated as compartments of the same cell. mRNA localisation could allow storage of various mRNAs at the axon ends, which would only be translated in response to a specific stimulus (Jung et al., 2012). One of the first examples of this was *camkII* (Calcium/calmodulin-dependent protein kinase II), which is localised to dendrites and locally translated (Burgin et al., 1990). Since then many studies have aimed to identify more transcripts in dendrites and axons (Cajigas et al., 2012; Gumy et al., 2011; Holt and Schuman, 2013; Misra et al., 2016; Zivraj et al., 2010).

mRNA localisation is also observed at the asymmetric division of the neuroblast. During neuroblast division the primary challenge is to ensure GMC inheritance of pro-differentiation mRNAs and proteins, while preventing inheritance of those promoting proliferation and stem cell character. This fate decision must occur rapidly, as the GMC immediately exits from the short NB cell cycle. As discussed extensively above (section 1.1.3), cell fate determinants are localised to the basal cortex of the NB and

segregated into the GMC daughter cell. While these determinants are primarily proteins, some RNAs are also segregated, including *pros* and the lncRNA *cherub* (Landskron et al., 2018; Li et al., 1997). This mechanism allows a faster determination of cell fate in the progeny cell, than a transcriptional switch after division.

1.4.4 Brat: an asymmetrically localised cell fate determinant

Brat is an RNA-binding protein, and is one of the key cell fate determinants that is segregated to the GMC upon NB asymmetric division (as described in section 1.1.3). Brat is an evolutionarily-conserved tumour suppressor (Arama et al., 2000). The fact that one of the key cell fate determinants is an RBP underlines the importance of post-transcriptional regulation in NB biology. In *brat* mutant larvae, INPs (the progeny of the type II NBs) fail to downregulate NB-specific genes such as *mira* and w*or* (Betschinger et al., 2006). This allows continued growth and division, leading to tumours. Blocking asymmetric segregation of Brat mimics the phenotype of *brat* mutation.

The levels of Brat regulate the character of immature and mature INPs. Brat represses the translation of *dpn* and *zelda* (*zld*) by binding to a specific motif in their 3' UTRs (Reichardt et al., 2018). Brat levels are high in immature INPs, but reduce in mature INPs, allowing Dpn re-expression. However, Zld requires less Brat for translational repression and therefore is not re-expressed in the mature INP.

1.4.5 RBP levels define neuron fates

RBP levels have also been shown to define NB age, determining the sequences of neuronal progeny (Liu et al., 2015). In the embryo, the neuron sequence is regulated by a cascade of TFs, which combinatorially define NB age (section 1.3). However,

the TF cascade does not continue with sufficient complexity to regulate the longer and more diverse neuron sequences in the larval central brain. Several studies have aimed to identify the regulators of larval NB age.

Mutant screening in MB NBs was used to identify genes that disrupt the normal progression of cell fates (Zhu et al., 2006). This screen identified the BTB-zinc finger protein, Chinmo, which is expressed in a decreasing gradient through the MB lifespan. Chinmo was so named due to the chronologically inappropriate morphogenesis of mutant progeny cells: manipulating levels of Chinmo alters the numbers of different classes of neuron. Building on this, a later study reasoned that the levels of a putative progeny fate regulator would vary over developmental time (Liu et al., 2015). MB and antennal lobe (AL) NBs were isolated at various larval and pupal stages for transcriptomic analysis, aiming to identify highly dynamic genes. This study identified two evolutionarily conserved RNA-binding proteins, IGF-II mRNA-binding protein (Imp) and Syncrip/hnRNPQ (Syp), which are expressed in opposing temporal gradients (Figure 1.7 A). Manipulating the levels of Imp and Syp resulted in temporal fate transformations of the neurons. Understanding the action of these RBPs is the focus of this thesis.

1.5 IMP AND SYP REGULATION OF NEUROGENESIS

Imp and Syp are expressed in opposing gradients in larval NBs, and the levels of these two RBPs regulates the progeny fate of the MB NBs. RBPs act through post-transcriptional regulation of their target genes and *chinmo* is one example of a target of Imp and Syp, which influences NB progeny fate. However, RBPs generally regulate many different targets, with different functions. This thesis will explore other targets of Imp and Syp, their roles and their mechanisms of regulation.

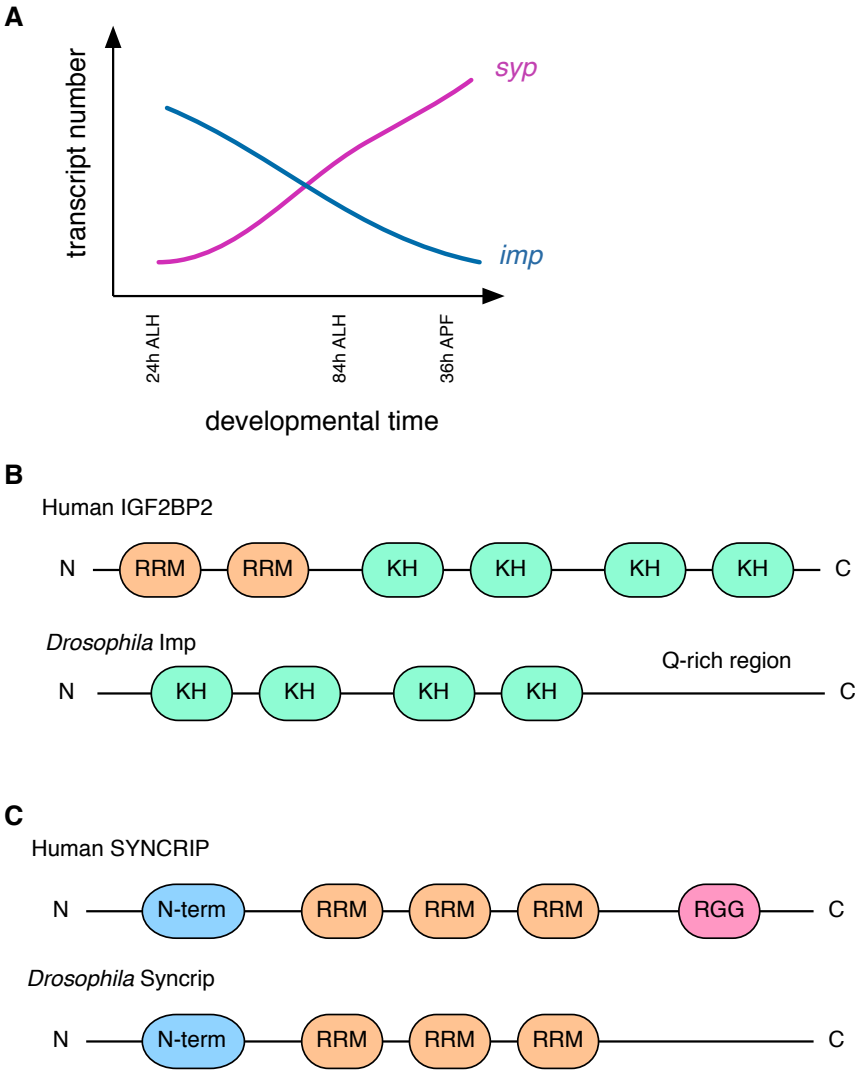


Figure 1.7 Imp and Syp are conserved RBPs
A Representation of transcriptomics analysis from Liu *et al.,* 2015. In sorted MB NBs, *imp* and *syp* mRNA are expressed in opposing gradients. *imp* is highest in early larval NBs and decreases through development, while *syp* level increases in the late larva and pupa. ALH: after larval hatching, APF: after pupal formation **B** Diagram illustrating the RNA-binding domains of the human IGF2BP2, compared to the *Drosophila* Imp (adapted from Hansen *et al.,* 2015). **C** Diagram illustrating the RNA-binding domains of the Human SYNCRIP, compared to the *Drosophila* Syp (adapted from Hobor *et al.,* 2018).

1.5.1 Imp

The *Drosophila* Imp was first identified in a visual screen for motile proteins in the egg chamber (Boylan et al., 2008). Imp is the *Drosophila* homolog of the human Insulin-like growth factor 2 mRNA-binding protein (IGF2BP) family, the chicken zipcode-binding protein 1 (ZBP-1), and the *Xenopus* Vg1 RBP. These proteins play roles which are among the most well-known examples of post-transcriptional

regulation in developmental biology. ZBP-1 binds *β-actin* mRNA and drives its localisation to the leading edge of the fibroblast for cell migration (Farina et al., 2003). Vg1 RBP binds *Vg1* mRNA and tethers it to the vegetal pole to establish embryonic axes (Havin et al., 1998).

The mouse homolog of Imp is named Coding Region Determinant-Binding Protein (CRD-BP), due to its binding to the Coding Region mRNA stability Determinant (CRD) region of *c-myc* (the mouse homolog of Myc). In mouse, the CRD is a 180 nt region of the coding sequence of *c-myc* which encodes for 60 amino acids at the C terminus of the protein (Bernstein et al., 1992). This sequence determines mRNA stability through binding of a protein, shown by competition experiments with a synthetic CRD RNA which led to 8-fold destabilisation of the *c-myc* transcript. The binding protein, CRD-BP/IGF2BP, was studied and purified in both mouse and human (Bernstein et al., 1992; Prokipcak et al., 1994). IGF2BP family members have been implicated in a wide variety of cancers including colon, kidney and pancreas (Bell et al., 2013). Overexpression of IGF2BP2 promotes proliferation in diverse human cancer cells (Dai et al., 2017).

The *Drosophila* Imp has roles in the oocyte and synaptic growth (Boylan et al., 2008). Loss-of-function *imp* mutants are zygotic lethal. *Drosophila* Imp contains four KH domains, which are conserved in the human IGF2BP2 (Figure 1.7 B). However, the human homolog contains two additional RRM motifs, while the *Drosophila* Imp includes a unique C-terminal Q-rich domain. Imp is observed to be transported in the *Drosophila* nurse cells, suggesting a role in localisation of maternal RNA determinants (Boylan et al., 2008). Mutant and overexpression studies show that Imp is involved in *gurken* localisation, and *oskar* localisation and translation, but this role is largely redundant (Geng and Macdonald, 2006; Munro et al., 2006).

Imp is required for regrowth of axon branches after pruning, and is actively transported to axons being remodelled (Medioni et al., 2014). Imp binds to the 3' UTR of the *Drosophila profilin* homolog, *chickadee* (*chic*). This binding promotes *chic* transport to the axon, where Chic promotes actin polymerisation for axon extension. Some individual mRNA targets of Imp have been identified and functionally validated. However, there has been significant interest to understand the breadth of Imp regulation. One study identified Imp targets in *Drosophila* S2 cells using three complementary genome-wide techniques: RIPseq, iCLIP and PAR-iCLIP (Hansen et al., 2015). A subset of 86 genes were among the top 200 targets of all three techniques, and showed an enrichment in GO categories for biological processes including reproduction, neural development and cell polarity. Motif analysis showed an enrichment of UA-rich regions flanked by CA-rich regions, with most binding in the 3' UTRs. This study provides useful insight into the binding preferences of Imp, but is limited to transcripts that are expressed in S2 cells.

1.5.2 Syncrip

The *Drosophila* Syncrip (previously CG17838) was first identified in the oocyte, where it contributes to *gurken* localisation and translation (McDermott et al., 2012). *Drosophila* Syp contains three RRMs and an N-terminal non-canonical RNA-binding domain (Hobor et al., 2018) (Figure 1.7 C). The human SYNCRIP/hnRNPQ has an additional RNA-binding RGG domain in the C-terminus. SYNCRIP is found in neuronal RNA transport granules (Bannai et al., 2004) and has been shown to compete with PolyA binding proteins to inhibit translation (Svitkin et al., 2013). The human SYNCRIP has been identified to have mutations associated with human intellectual disability (Lelieveld et al., 2016).

In *Drosophila,* Syncrip is known to have roles in regulation of RNA localisation and translation (McDermott et al., 2012). At the *Drosophila* neuromuscular junction (NMJ), Syp is involved in synaptic growth (McDermott et al., 2014). Syp is expressed in the muscle nuclei and in the post-synaptic density. *syp* mutants have an overgrowth of the NMJ, and RIPseq experiments in the whole larva showed Syp binding to various transcripts with key roles at the synapse, including *msp-300, discs large 1* and *neurexin-1.* Furthermore, Syp regulates retrograde bone morphogenic protein signalling, which is required for correct pre-synapse neurotransmitter release (Halstead et al., 2014).

1.5.3 The regulatory relationship of Imp and Syp

While Imp and Syp have been individually studied across different systems and model organisms, their roles in NB regulation are tightly linked. Relative levels of Imp and Syp appear to define NB age: Imp is expressed at its highest in early NBs and declines throughout the larval stages, while Syp increases to become highly abundant in the late larval NB (Liu et al., 2015; Ren et al., 2017). In the MB, Imp specifies the early γ neurons, while Syp promotes the late α/β neurons. Therefore, the changing levels of Imp and Syp direct the proportions of the neuron fates produced. Manipulating Imp and Syp levels through overexpression and knockdown experiments led to predictable shifts of progeny fate to early or late neuron types in the MB (Liu et al., 2015).

Syp and Imp mutually repress each other at the transcript level (i.e. through transcription or mRNA stability) (Liu et al., 2015). Knockdown of Syp results in elevated Imp levels, and vice versa. Therefore, the high levels of Imp in the early larval NBs would be expected to prevent any accumulation of Syp. There must be an additional input to drive the gradient change in expression, leading to the switch from

Imp/Chinmo +ve NBs, to Syp +ve NB. The short larval TF cascade of Cas, followed by Svp, is required to make this switch and places Syp as the dominant partner in the mutually repressive balance (Narbonne-Reveau et al., 2016; Ren et al., 2017). Svp activates expression of the ecdysone receptor (EcR), allowing NBs to respond to ecdysone signalling (Syed et al., 2017b). This triggers the switch from Chinmo/Imp expression to Syp expression. The varied timing of the Cas and Svp expression sequence across different NBs may explain their differing switch timings.

As well as being co-regulated themselves, Imp and Syp perform coordinated regulatory roles in neurogenesis. Imp activates translation of *chinmo*, while Syp has the opposite effect, to specify MB neuron fates (Liu et al., 2015). Imp and Syp also cooperate to regulate NB termination. We found that Syp-depleted NBs (with elevated Imp) are prolonged into the pupa and do not shrink correctly (Yang et al., 2017a). Imp/Syp double knockdown experiments were then used to assign the individual roles the two RBPs. Imp regulates NB shrinkage, so NBs with high Imp do not correctly shrink in the pupa. Syp then controls cell cycle exit through the symmetric division. Work in our lab, on which I am a co-author, showed that the *syp* mutant has an enlarged larval brain, suggesting a defect in regulation of cell size or proliferation (Hailstone et al., 2018).

Imp and Syp have been shown to regulate both NB behaviour and progeny fate. Coordination of these processes by the same regulators may ensure production of the correct number and type of neurons to build the brain. However, it is unclear exactly how Imp and Syp regulate these processes. As RBPs, Imp and Syp act through controlling the levels of their different target genes through mRNA stability, localisation or translation. Therefore, identifying their target genes is a key step to understanding their actions, and this is one goal of this thesis.

1.6 RELEVANCE TO MAMMALIAN NEUROGENESIS

The *Drosophila* larval brain has many experimental advantages to study neural stem cells and neurogenesis. But how do developments in our understanding of *Drosophila* neurogenesis contribute to the field of mammalian neurogenesis?

Mammalian neurogenesis has many strong similarities to *Drosophila* neurogenesis. All neurons of the mouse cortex are produced by the asymmetric cell divisions of a small number of progenitor cells (Homem and Knoblich, 2012). Radial glia in the mammalian cortex divide to produce one self-renewing daughter and a second daughter that is either an intermediate progenitor cell (IPC) or differentiates to become a post mitotic neuron (Homem et al., 2015). Like a *Drosophila* GMC, the IPC typically divides only once to produce a pair of cortical neurons. In primates, but not rodents, there is an additional amplification progenitor called the outer radial glial cell, which acts like a *Drosophila* INP, dividing asymmetrically to produce many more neurons. Simply put, rodent neurogenesis is similar to the *Drosophila* type I neuroblast division lineage, while primate neurogenesis follows a lineage more like the *Drosophila* type II neuroblast.

Many key players in *Drosophila* neurogenesis are conserved in humans. The asymmetric division machinery to direct cell polarity and spindle orientation are conserved in the mammalian brain (Suzuki and Ohno, 2006). The mammalian homolog of Pros, Prox1, plays a similar role directing neuronal differentiation and suppressing proliferation (Stergiopoulos et al., 2014). The RBPs Imp and Syp, the focus of this thesis, both have human homologs, which have been associated with brain cancers and intellectual disability, respectively. While IGF2B and SYNCRIP have not yet been shown to regulate human neural stem cells, the improved

understanding of their roles in *Drosophila* may lead to the uncovering of similar functions in humans.

While not all regulators of *Drosophila* neurogenesis have a direct mammalian homolog playing the same role, the conceptual regulatory processes may be conserved. For example, in the mouse cerebral cortex, specific types of neuron are born in a predictable sequence (Shen et al., 2006). Although the neuron sequences are far more complex than in *Drosophila,* there is evidence that TFs such as COUP-TFI and II promote a switch from early to late fate neurons, in a similar manner to the TF cascades of embryonic *Drosophila* neurogenesis (Kohwi and Doe, 2013).

Further examination may identify more complex TF sequences. Similarly, a growing understanding of the extensive roles of post-transcriptional regulation in *Drosophila* neuroblasts is very likely to inspire similar research in mammalian systems. This is likely to uncover important insights into human neurogenesis.

1.7 AIMS OF THESIS

The cellular processes of neurogenesis have been well studied in the *Drosophila* larva and our understanding of the regulation of these processes is increasing rapidly. The asymmetric NB division is particularly well understood, involving protein and mRNA segregation to the GMC to ensure its exit from proliferation. mRNA localisation is also classically appreciated at the synapse to allow strengthening or weakening of connections depending on signals received. These examples of post-transcriptional regulation illustrate the need for multiple layers of regulation of processes where tight spatio-temporal control is required. However, the prevailing view of the fundamental processes of neurogenesis, generating a large number and diversity of neurons, is still primarily at the level of transcriptional regulation.

In embryonic NBs, a sequentially expressed cascade of TFs defines the fate of progeny neurons. In larvae, the cascades are insufficiently complex to explain all of the neuron fates. TFs define the available gene expression landscape in each cell, but it is becoming clear that this is overlaid with a complex cross-regulatory network including post-transcriptional regulatory processes. Regulated mRNA stability or translation can significantly change the protein complement of the cell. Furthermore, how are the TFs themselves regulated? The tightly limited spatio-temporal expression of TFs is likely to require multiple layers of regulation. In the progression of larval NB development, opposing gradients of two RBPs, Imp and Syp, define NB age and progeny fate. This finding opens up the possibility of a far more significant role of post-transcriptional regulation than previously appreciated.

This thesis aims investigate the post-transcriptional regulation of neural stem cell biology. I focus on the RBPs Imp and Syp, as they have been shown to regulate key aspects of NB behaviour and age. In Chapter 3, I perform genome-wide studies to find the mRNA binding targets of Imp and Syp in the larval brain. I find an enrichment for binding to transcripts encoding TFs and RBPs, and transcripts with extremely long 3' UTRs. I define an approach to examine the regulation and function of specific targets, focusing on the growth, division and termination of type I NBs. Among other targets, I show that Imp and Syp both bind the mRNAs encoding two key TFs in neurogenesis: *myc* and *pros.* I investigate these further in the subsequent chapters.

In Chapter 4, I examine the regulation of the conserved TF and proto-oncogene Myc. Myc is a key regulator of cell size and division and is the convergent regulatory point of many signalling pathways. I find that Imp regulates *myc* post-transcriptionally, and use microscopy techniques to quantitate this. I show that Imp stabilises *myc* mRNA,

thereby upregulating Myc protein levels. I then explore the functional importance of this regulation through phenotypic analysis, including producing endogenous deletion lines at the *myc* locus.

In Chapter 5, I investigate the post-transcriptional regulation of the TF Pros, extending the work of Dr Lu Yang in the Davis lab. *pros* mRNA stability is regulated by Syp. I examine the levels of different mRNA isoforms, using imaging techniques to visualise transcription, mRNA and protein. I then explore the functions of these different isoforms, producing deletion lines at the endogenous locus.

Collectively, this work provides insight into the breadth of post-transcriptional regulation in the nervous system. Pros and Myc are two highly-studied TFs, but their post-transciptional regulation in neural stem cell lineages was unknown. The lists of Imp and Syp targets are sure to include many more important examples of post-transcriptional regulation. Uncovering the cooperation of transcriptional and post-transcriptional regulation will further our understanding of neurogenesis.

In summary the key aims of the thesis are:

1. Elucidate the mRNA binding targets of Imp and Syp
2. Identify and quantitate key examples of post-transcriptional regulation by Imp and Syp
3. Uncover the functional significance of the post-transcriptional regulatory processes

2.

MATERIALS AND METHODS

2.1 REAGENTS AND FLY STOCKS

2.1.1 Solutions and Reagents

The Department of Biochemistry media kitchen prepared LB-agar plates with antibiotics, and Apple juice plates. They also prepared and autoclaved the Phosphate buffered saline (PBS), Saline-sodium citrate (SSC) and Lysogeny Broth (LB) media.

Table 2.1 Solutions and Reagents

Media	Composition
TE Buffer	10 mM TrisHCl, 1 mM EDTA in diethylpyrocarbonate (DEPC) treated water
10X TAE Buffer	0.4 M Tris, 10 mM EDTA (pH 8.0), 1.2% (v/v) glacial acetic acid
10X PBS, pH 7.4	1.37 M NaCl, 27 mM KCl, 100 mM Na_2HPO_4, 20 mM KH_2PO_4
20X SSC	For 1 L: 175.3 g NaCl, 100.5 g Tri-Sodium Citrate ($2H_2O$) in 800 ml of distilled H_2O, pH balanced to 7.0 with HCl
LB	For 1 L: 10g Bacto tryptone (Difco), 5g Bacto yeast extract, 5g NaCl

2.1.2 Fly stocks

Drosophila melanogaster fly stocks were kept at 18 °C, but transferred to 25 °C for crosses and experimental use. OrR was the *wild type* strain. Flies were raised on standard cornmeal-agar medium.

Table 2.2 Fly Stocks

	Genotype	Description	Origin
wild type	OregonR	*wild type*	
***syp* mutant**	*w[11180]; PBac(PB)Syp[e00286]/ TM6B*	Syncrip P element insertion mutation	Harvard Exelixis Collection
nanos-Cas9	*y[1] sc[1] v[1];; {y[+t7.7] v[+t1.8]=nanos-Cas9} attp2*	TH_attP2. nanos-Cas9 on the 3rd chromosome	The University of Cambridge Department of Genetics Fly Facility
vas-Cas9	*y_1 M{vas-Cas9.RFP-} ZH-2A w^{1118}*	vas-Cas9 on the X chromosome	Bloomington (stock 55821)
Cre recombinase	*y[1] w[67c23]; MKRS, P{ry[+t7.2]=hsFLP}86E/ TM6B, P{w[+mC]=Crew} DH2, Tb[1]*	Cre recombinase on the 3rd chromosome	Bloomington (stock 1501)
***syp* RNAi**	*;P(GD9477)v33011*	UAS-syp RNAi	VDRC stock 33011
***imp* RNAi line**	*y[1] sc[*] v[1]; P{y[+t7.7] v[+t1.8]=TRiP.HMS01168}attP2*	UAS-imp RNAi	Bloomington (stock 34977)
Myc OE line	*M{UAS-Myc.ORF. 3xHA.GW}*	UAS-Myc construct	FLY-ORF stock F001801
Imp OE line	*UAS-ImpRM-FLAG*	UAS-Imp construct	Liu *et al.,* 2015
hsFLP	*hsFLP;Pin/ CyO;Tm3,Sb,TM6B*	Heat shock flippase	Awasaki *et al.*, 2014

	Genotype	Description	Origin
act>FOT>Gal4	*act-FRT>-dSTOP-FRT>-Gal4,UAS-mCD8::GFP/ CyO; TM3,Sb/TM6B*		Harris *et al.* 2015
Imp::GFP	*Imp[CB04573]*	Endogenously GFP-tagged Imp	Toledano *et al.*, 2012
insc-GAL4		GAL4 driver in NB and GMCs	Betschinger *et al.* 2006
UAS-mCD8::GFP	*UAS-mCD8::GFP*	Membrane bound GFP	Bloomington (stock 5137)
pros-longSTOP		26 bp deletion in the unique coding exon of $pros^{long}$	Dr Lu Yang
prosΔpromUP		Deletion of the upstream three *pros* transcription start sites	This study

2.1.3 Clonal analysis

For *wild type*, female *hsFLP;Pin/CyO;Tm2,Sb/Tm6B* (Awasaki et al., 2014) were crossed to male *act-FRT>-dSTOP-FRT>-Gal4, UAS-mCD8::GFP/CyO;Tm3,Sb/Tm6b* (Harris et al., 2015). These lines were crossed to the *syp* mutant to produce parental lines to make the clones: female *hsFLP;Pin/CyO;Syp[e00286]/Tm6b* were crossed to male *act-FRT>-dSTOP-FRT>-Gal4,UAS-mCD8::GFP/CyO;Syp[e00286]/Tm6b*. Eggs were collected in a four hour egg lay on apple juice plates with yeast paste at 25 ˚C. 24 hours after the egg lay, newly hatched larvae were transferred to fly food vials and incubated in a 37 ˚C water bath for 25 minutes. Wandering larvae were dissected 96 hours after larval hatching. For *syp* mutant, only non-tubby larvae were dissected. Immunofluorescence was completed as described below and clones were imaged on the ventral side.

2.2 BIOCHEMICAL TECHNIQUES

2.2.1 Genomic DNA extraction from *Drosophila*

A single adult fly was homogenised in 50 µl of Squishing Buffer (10 mM TrisHCl pH 8.0, 1 mM EDTA, 25 mM NaCl, 200 µg/ml proteinase K (freshly added) in DEPC water) and incubated at 37 °C for 30 mins. The sample was then heated to 95 °C for 2 mins to inactivate the proteinase.

2.2.2 BAC purification

Bacterial artificial chromosomes (BACs) were ordered from BacPac Resources and received as an agar stab. The bacteria were streaked onto chloramphenicol plates (15 µg/ml, low salt agar) and grown overnight (ON) at 37 °C. Colonies were picked and grown up in 2 ml high salt LB with 17 µg/ml chloramphenicol as a day culture, and then in 50 ml at 37 °C ON. 500 µl of bacteria was added to 500 µl of 50% glycerol, mixed gently, and stored at -80 °C. BAC DNA was purified using an adaptation of the QIAGEN Large Construct Kit (Qiagen). Briefly, bacteria were pelleted by centrifugation at 3,000 rpm for 10 min and supernatant was discarded. Bacteria were resuspended in 2 ml P1 and then 2 ml of P2 was added and incubated at room temperature (RT) for 5 min. 2 ml of P3 was added and incubated on ice for 5 min. The sample was centrifuged at 10,000 rpm for 15 min. Supernatant was removed and the DNA pellet was washed with 3.3 ml of 70% ethanol (EtOH) and spun at 10,000 rpm for 5 min. The EtOH wash was repeated and all supernatant was aspirated. DNA was resuspended in 50 µl of DEPC water.

2.2.3 Standard PCR

For Sanger sequencing or building constructs, Phusion High-Fidelity DNA polymerase (NEB) was used. A 50 µl reaction consisted of 4 µl DNA template, 10 µl

5x Phusion High-Fidelity Buffer (NEB), 1 µl of 10 mM stock dNTPs, 2.5 µl of stock 10 µM forward and reverse primers, 1.5 µl of dimethyl sulfoxide (DMSO), 0.5 µl Phusion High-Fidelity DNA polymerase and DEPC water. The reaction followed this program: initial denaturation at 98 °C for 30 s, then 35 cycles of 98 °C for 10 s, 56-62 °C (depending on the melting temperature of the specific primer set) for 10 s and then elongation at 72 °C for 30 s per 1 kb of product length. There was a final elongation step of 72 °C for 10 min.

For colony PCR screening, Quick-load Taq 2X polymerase (NEB) was used. Single bacteria colonies were resuspended in 10 µl LB media with ampicillin (100 µg/ml). The reaction mixture includes 1 µl of bacterial suspension, 12.5 µl of 2X Taq master mix, 0.5 µl of stock 10 µM forward and reverse primers, and DEPC water up to 25 µl. The PCR cycle was 95 °C for 30 s, then 30 cycles of: 95 °C for 15 s, 60 °C for 15 s and 68 °C. The cycle finished with extension at 68 °C for 5 min. The master mix includes loading dye so the sample can be directly loaded to a gel.

2.2.4 DNA gel electrophoresis

Agarose was dissolved in 1x TAE buffer to the correct percentage (0.5% - 1%). 3 µl of Ethidium bromide was added per 50 ml of gel before setting. 10 µl of PCR product was added to 10 µl water and 5 µl of 5x gel loading dye (NEB). This was loaded onto the gel. 7 µl of Hyperladder 1 kb (Bioline) was used to mark the running sizes. The gel was run at 100 V in 1x TAE buffer. DNA was visualised under a UV transilluminator.

2.2.5 Gel purification

For gel purification purposes, DNA was run on gels with midori green dye and all sample was loaded with appropriate volumes of 5x gel loading dye, allowing an

empty lane between each sample. DNA was visualised under blue light and the correct bands were carefully excised into eppendorf tubes. PCR products were purified from the gel using the QIAQuick Gel Extraction Kit (Qiagen) according to manufacturer's instructions. DNA was eluted with 30 µl of DEPC water and concentration was measured with a NanoDrop spectrophotometer.

2.2.6 Sanger sequencing

Sanger sequencing was performed by Source Bioscience. Gel purified PCR products or plasmids were sent, along with sequencing primers at the required concentrations. Sequencing results were analysed using SnapGene.

2.2.7 RNA extraction

Third instar larval brains were dissected in Schneider's insect medium and then flash frozen in liquid nitrogen. Brains were homogenised using a pestle in IP buffer (50 mM Tris-HCl pH 8.0, 150 mM NaCl, 0.5% NP-40, 10% glycerol, 1 mini tablet of Complete EDTA-free protease inhibitor and 2 µl RNAse inhibitor (RNAsin Plus RNase Inhibitor, Promega). RNA was extracted using the RNASpin Mini kit (GE Healthcare) according to manufacturer's instructions. RNA concentration was measured using Qubit RNA HS assay (Life Technologies).

2.2.8 Reverse transcription PCR (RT-PCR)

Reverse transcription produces complementary DNA (cDNA) from RNA samples. RT-PCR was performed using random hexamers. 25 µl of extracted RNA was with 2 µl random hexamer (100 µM stock, Thermo Fisher Scientific), 2 µl of dNTPs (10 mM stock, Thermo Fisher Scientific) and 1 µl RNAse inhibitor (RNAsin Plus RNase Inhibitor, Promega). Samples were incubated at 65 °C for 5 min, then held on ice for 1 min to remove secondary structures before the reverse transcription reaction. 8 µl

of 5x RT buffer (Thermo Fisher Scientific) and 2 µl of reverse transcriptase (RevertAid Premium Reverse Transcriptase, Thermo Fisher Scientific) were added to the sample and the reaction was incubated at 25 °C for 10 min, 50 °C for 30 min, and 85 °C for 5 min.

2.2.9 qPCR

Real time quantitative PCR was performed using primers specific to a transcript of interest, and where possible spanning an exon junction. A 25 µl reaction consisted of 12.5 µl SYBR Green Master Mix, 0.75 µl forward and reverse primers, 8 µl of DEPC water, and 3 µl of cDNA. qPCR was performed with the CFX96 Touch Real-Time PCR Detection System (BioRad). Cycle threshold (C(T)) values were calculated from the BioRad CFX software using a second differential maximum method. Input samples were used for a dilution series and the percentage input of each gene was calculated in the IP samples as a measure of pulldown. For primer sequences see Appendix A.

2.2.10 Antibody crosslinking to magnetic beads

α-Syncrip antibody was crosslinked to magnetic Dynabeads Protein A (Life Technologies) using Dimethyl pimelimidate (DMP) according to the Abcam crosslinking protocol (https://www.abcam.com/protocols/cross-linking-antibodies-to-beads-protocol). Briefly, beads were washed in 1x PBS for at least 1 hr at 4 °C, then replaced with dilution buffer (1x PBS with 1 mg/ml BSA). Antibody was diluted in dilution buffer up to 50 µl (500 µg/ml anti-syp antibody (McDermott et al., 2014), 400 µg/ml anti-IgG), then incubated with the washed beads. Beads were incubated at 4 °C for 1 hr with gentle mixing and rotation. Beads were then washed in dilution buffer and then 1x PBS. A fresh stock of 13 mg/ml DMP was made in water, and then added 1:1 to wash buffer (0.2 M triethanolamine in 1x PBS). The solution should be pH 8-9.

50 µl DMP wash solution was added to the beads and rotated for 30 min at RT. Beads were washed 5 min at RT in wash buffer, then the DMP treatment and wash was repeated twice more (using fresh DMP from the stock each time). The reaction was quenched with 50 mM ethanolamine in 1x PBS by incubation for 5 min at RT. Quenching was repeated, then beads were washed in 100 µl 1x PBS. 50 µl of 1 M glycine was added to beads and incubated 10 min at RT. This glycine step was repeated and then beads were washed twice in 1x PBS. Beads were stored at 4 °C for use within a week. Crosslinking was confirmed by running on an SDS-PAGE gel and staining for 30 min with InstantBlue (Sigma) gel (see 2.2.12 for SDS-PAGE method).

2.2.11 RNA immunoprecipitation

Wandering larval brains brains were dissected and homogenised in IP buffer (50 mM Tris HCl (pH 8), 150 mM NaCl, 0.5% NP40, 10% glycerol, protease inhibitor, RNase inhibitor). Input samples were taken. Each experiment was done in triplicate.

For Syp IP, 100 OrR *wild type* brains were used per IP. anti-Syp antibody was cross linked to magnetic beads as described above. The lysate was incubated with beads at 4 °C overnight, then the unbound supernatant was collected. Beads were washed in cold IP buffer 5x 5 min.

For Imp IP, 200 *Imp::GFP* brains were used per IP. The lysate was incubated with GFP-Trap agarose beads (Chromotek) at 4 °C for two hours and the unbound supernatant was collected. Beads were washed in cold IP buffer for 4x quick washes.

For both IPs, the bound material was eluted by incubation for 30 min at 65˚C in Elution buffer (50 mM Tris HCl (pH 8), 10 mM EDTA, 1.3% SDS, protease inhibitor, RNase inhibitor). The elution step was repeated and the supernatants were pooled.

RNA was extracted for IP samples and inputs (2.2.7) and used for RT-qPCR (2.2.9) or sequencing libraries (2.2.14).

2.2.12 Western blot

Proteins were separated by SDS-PAGE on a 4-12% Novex gradient gel then transferred to nitrocellulose membrane with the Trans-Blot Turbo Transfer System (BioRad). Membranes were blocked in 50% Odyssey Blocking Buffer in 0.3% PBST (1x PBS with 0.3% Tween) for 1 hr at RT. The membrane was incubated with primary antibody overnight at 4 °C. After rinsing, the membrane was incubated with fluorescently labelled secondary antibodies for LICOR (1:2000) for 2 hr at RT. Membranes were washed in 0.3% PBST and imaged with the LI-COR Odyssey.

Table 2.3 Antibodies for Western Blot

Antibody	WB concentration	Source
α-Syncrip (guinea pig)	1:2000	McDermott *et al.* 2014
α-GFP (rat)	1:1000	Chromotek
α-αTubulin (mouse)	1:500	Sigma

2.2.13 polyA selection

For RNA sequencing, mRNA was enriched through polyA selection. After RNA extraction above (2.2.7), rRNA was depleted with by Poly(A) selection with the NEBNext Poly(A) mRNA Magnetic Isolation Module (NEB) according to manufacturer's instructions. Briefly RNA sample was added to washed beads with Binding buffer. Samples were incubated at 65 °C for 5 min and then cooled to 4 °C for RNA binding. Beads were washed in Wash Buffer and RNA was eluted at 80 °C for 2 min. Binding, washing and elution steps were repeated to improve purification with final elution in 17 µl of Tris Buffer.

2.2.14 RNA sequencing

Three biological replicates (n = 3) were produced for each sample (whole transcriptome/input or immunoprecipitation). RNA extraction and polyA selection were performed as above. Poly(A) enriched RNA was then used for library production using the Ion Total RNA-Seq Kit v2 for Whole Transcriptome Libraries (Life Technologies). Libraries were produced according to the Ion Total RNA-Seq Kit v2 protocol. Following quality control steps, adaptors were hybridised to the RNA fragments and RT reaction was performed followed by cDNA amplification with Ion Xpress RNA Barcode primers. Prior to sequencing, quality of cDNA libraries were assessed using Agilent High Sensitivity DNA Kit with the Agilent 2100 Bioanalyser. Libraries were pooled to a total concentration of 100 pM, with three samples multiplexed per chip. Sequencing was performed on an in house Ion Proton Sequencer, using the Ion PI IC 200 Kit (Life Technologies). Ion PI chips were prepared following manufacturer's instructions and loaded using the Ion Chef System.

2.3 Staining and Imaging

2.3.1 Antibody staining for immunofluorescence (IF) in larval brains

Larvae were washed briefly in 70% ethanol followed by water. Brains were carefully dissected in Schneider's medium and collected into 0.2 ml PCR tubes. Samples were rinsed once with 0.3% PBSTX (0.3% Triton-X in 1x PBS) and then fixed in 4% paraformaldehyde (PFA) (4% PFA in 0.3% PSTX) for 25 min at room temperature (RT). Samples were rinsed briefly 3x in 0.3% PBSTX, and then washed 3x 15 min in 0.3% PBSTX at RT. Blocking was for 1 hr at RT in Blocking Buffer (1% bovine serum albumin (BSA) in 0.3% PBSTX). Primary antibody was added at the correct dilution to Blocking Buffer and samples were incubated overnight at 4 °C on a rocker. Samples were rinsed briefly 3x in Blocking Buffer, and then washed 3x 15 min in Blocking

Buffer at RT. Alexa Fluor secondary antibody (Thermofisher) was added at 1:200 in Blocking Buffer and samples were incubated for 1 hr at RT in the dark. Samples were rinsed briefly 3x in 0.3% PBSTX, and then washed 3x 15 min in 0.3% PBSTX at RT. For nuclear staining DAPI (4',6-diamidino-2-phenylindole) was included at 1:500 in the second 15 min wash. Brains were transferred to the dissecting dish to allow final cleaning and then mounted in VECTASHIELD anti-fade mounting medium (Vector Labs). Slides were either imaged immediately or stored at -20 °C.

Table 2.4 Antibodies for immunofluorescence

Antibody	Concentration for IF	Origin
α-Syncrip (guinea pig)	1:500	McDermott *et al.* 2014
α-Imp (rabbit)	1:600	Gift from P. M. Macdonald
α-Pros (mouse)	1:10	Developmental Studies Hybridoma Bank (DSHB)
α-Deadpan (rat)	1:200	abcam
α-pH3 (rabbit)	1:200	abcam
α-Elav (rat)	1:10	DSHB
α-Myc (mouse)	1	Gift from R. N. Eisenman
α-Mnt (mouse)	1	Gift from R. N. Eisenman

2.3.2 single molecule RNA fluorescent *in situ* hybridisation (smFISH) for larval brains

smFISH probes were designed using the Stellaris® Probe Designer version 4.2. The sequences against which the probes were designed are shown in Appendix B. Stellaris® DNA probes were gently resuspended in 95 µl fresh TE buffer and 5 ul RNAse inhibitor (RNAsin Plus RNase Inhibitor, Promega), and frozen at -80 °C in 10 µl aliquots. Dissected brains were rinsed once with 0.3% PBSTX (0.3% Triton-X in 1x PBS) and then fixed in 4% PFA (4% PFA in 0.3% PSTX) for 25 min at RT. Samples were rinsed briefly 3x in 0.3% PBSTX, and then washed 3x 15 min in 0.3% PBSTX at

RT. Samples were washed for 5 min in Wash Buffer (10% deionised formamide (stored at -80 °C) and 2x SSC in DEPC water) and then incubated with 250 nM Stellaris® DNA probes in Hybridisation Buffer (10% deionised formamide, 2x SSC and 5% dextran sulphate in DEPC water) overnight at 37 °C on a rocker. Samples were rinsed briefly 3x in Wash Buffer, and then washed 3x 15 min in Wash Buffer at 37 °C. For nuclear staining DAPI (4',6-diamidino-2-phenylindole) was included at 1:500 in the second wash. Brains were mounted in VECTASHIELD anti-fade mounting medium (Vector Labs). Slides were either imaged immediately or stored at -20 °C.

2.3.3 smFISH with IF for larval brains

For anti-Dpn antibody with smFISH, the smFISH protocol was followed exactly as above. After washes on day 2, samples were blocked in Blocking Buffer for 1 hr at RT. Samples were incubated with anti-Dpn primary antibody in Blocking Buffer for 3 hr at RT, then washed in Blocking Buffer and incubated with secondary antibody for 1 hr at RT. Samples were then washed in 0.3% PBTX, once including DAPI.

For all other antibodies, the primary antibody was included in the probe hybridisation step. Before hybridisation, samples were blocked for 1 hr at RT in Blocking Buffer. The appropriate dilution of primary antibody was included with the Stellaris® DNA probes in Hybridisation Buffer for overnight incubation at 37 °C. Samples were washed in Wash Buffer and then incubated with secondary antibody in Wash Buffer for 1 hr at RT. After final washing in Wash Buffer, samples were mounted in VECTASHIELD anti-fade mounting medium and immediately imaged or stored at -20 °C.

2.3.4 Staining with dyes

DAPI was used to stain nuclei, and was added at 1:500 in one of the final wash steps before mounting. Phalloidin was used to label F-actin and was added in one of the final wash steps and incubated for 1 hr at 37 °C. Fluorescein 488 phalloidin was used at 5 µl per 100 µl, 647 Phalloidin was used at 2.5 µl per 100 µl.

2.3.5 5-ethynyl-2'deoxyuridine (EdU) labelling

Brains were dissected in Schneider's medium and then transferred to Brain Culture Medium (BCM) (80% Schneider's medium, 20% fetal bovine serum (Gibco ThermoFisher), 0.1 mg/ml insulin (Sigma), 1:50 larval lysate) with 50 µM EdU for 4 hr. Brains were then washed with Schneider's medium and fixed for 25 min in 4% PFA in 0.3% PBSTX at RT. The samples were rinsed and then washed 3x 15 min in 0.3% PBSTX at RT before blocking for 1 hr at RT in Blocking Buffer. The Click-iT reaction was carried out with the Click-iT EdU Alexa Fluor 488 Imaging Kit (Invitrogen) following manufacturer's instructions for 30 min at RT. Samples were washed in 0.3% PBST, once including DAPI, and then mounted in VECTASHIELD anti-fade mounting medium (Vector Labs).

2.3.6 Image acquisition

An inverted Olympus FV1000 Laser Scanning Microscope or Olympus FV3000 Laser Scanning Microscope were used for fixed imaging of larval brains. Images were acquired using x20 0.75 NA UPlanSApo, x40 1.3 NA Oil UPlan FLN and x60 1.4 NA Oil UPlanSApo objective lenses. Note, for smFISH images, pixel size was 74 nm in x and y, and 200 nm in z.

2.3.7 Image analysis

smFISH

Using FIJI, single NBs were cropped and substacks were made to span the depth of each NB. I used the phalloidin staining to create a mask with the FIJI plugin MorphoLibJ, using the morphological segmentation feature (Legland et al., 2016). I then removed all transcripts outside the boundary of the NB. FishQuant (Mueller et al., 2013) was used to count spots and calculate nascent transcripts. For a single cell example, spots were detected and then thresholds adjusted by to ensure all spots were counted. mRNA spots were averaged and used to calculate nascent transcript number by the integrated intensity. Settings for detection and nascent transcript calculation were then applied to all images in the batch setting. This resulted in a count of the cytoplasmic transcripts and the nascent transcripts for each cell.

To convert transcript counts to rates of transcription and decay, the rate of elongation (v) was estimated at 1.5 kb per minute. This is an estimate based on a variety of methods in different *Drosophila* tissues, which gave measurements from 1.1 to 1.5 kb/min (Ardehali and Lis, 2009). A probe library weighting factor was calculated using the TransQuant software to account for the position of the probe set along the gene (Bahar Halpern and Itzkovitz, 2016). For *myc long* smFISH probes, this factor was 0.15264. Transcription and decay rates were calculated using the equations below. Decay rates were then converted to half lives.

1. Transcription rate (mRNA/hr) = ((nascent transcript number/weighting factor) x elongation rate) / gene length

2. Decay rate (per hour) = (chromosome fraction x transcription rate x number of chromosome copies) / transcripts in the cell

3. Half life (mins) = (ln2/decay rate) x 60

Measuring NB size

With the same method used to mask the smFISH data, I segmented the NB with the FIJI plugin MorphoLibJ, and then measured the masked volume. I used the DAPI staining of the chromatin to select only NBs in interphase (without condensed chromatin), as cells are larger during mitosis which may confound the result.

Measuring proliferation rates

Proliferation rate was measured both through mitotic index and EdU labelling of progeny cells. For mitotic index, the number of Dpn +ve NBs was counted in the ventral central brain. Dpn +ve NBs were then scored for PH3 staining, identifying condensed chromatin in mitosis. Mitotic index = Dpn +ve, PH3 +ve / Dpn +ve.
The number of EdU +ve progeny per NB were counted manually.

2.4 CRISPR *Drosophila* methods

2.4.1 CRISPR guide design

For the CRISPR experiments at the *pros* locus, guide RNAs (gRNAs) were designed and tested by Dr Andrew Bassett. The best guides in S2 cells were selected to use to make the transgenic *Drosophila* lines.

In order to make the *myc* deletions, I designed three gRNAs for each site, which were designed to cut within a few nucleotides of each other to maximise the chance of successful homologous recombination repair. PCR primers were designed around these sites to sequence the region in the Cas9 expressing fly line which would be injected, in order to check for SNPs which would affect guide efficiency. Each SNP PCR was done in duplicate to distinguish between PCR errors and SNPs.

Guides were designed using the FlyCRISPR tool: http://flycrispr.molbio.wisc.edu/tools and were double checked for off-targets with https://apps.molbiol.ox.ac.uk/CRISPR/cgi-bin/CRISPR.cg . Off-targets on different chromosomes were accepted but noted to be crossed out at later stages. Guides were designed to have cut sites within a few nucleotides of each other but far enough away to prevent complementarity of primers. Guide lists Appendix Table C.3.

2.4.2 Guide cloning

The guide sequences were cloned into the pCFD5 plasmid designed by the crisprflydesign group (Appendix C.1). This plasmid expresses multiple tRNA-flanked Cas9 gRNAs, using the ubiquitous RNA pol III promoter U6:3 (Port et al., 2014). Cloning primers and procedures were followed according to the protocol instructions with the noted alterations. For cloning of three gRNAs, two fragments must be inserted into the plasmid using Infusion cloning. Briefly, primers were designed to prime directly from the plasmid and add the guide sequences to each end. Priming directly from the plasmid was difficult with the long primers, therefore internal primers was used to produce a PCR product without the homologous sequence. This was then used as template for the further fragments. Phusion High-Fidelity DNA polymerase was used for these reactions, and the products were sequenced as described above.

In-Fusion cloning

Homology between the guide sequences at the ends of each fragment were used for In-Fusion cloning (Clontech). The pCFD5 plasmid was linearised using Bbs1 (NEB). 1.6 µg of the plasmid was added to a 10 µl reaction with 1 µl of Bbs1 and 3 µl of the buffer 2.1. This was incubated at 37 °C for 4 hr and then raised to 65 °C for 20 min to inactivate the enzyme. A 10 µl In-Fusion reaction was set up using 2 µl 5X In-Fusion

HD enzyme premix (Clontech), 50 ng of the linearised vector, and 50 ng of each insert. The mix was incubated at 50 °C for 15 min, and then immediately placed on ice.

Bacterial Transformation

The In-Fusion product was transformed into Stellar competent cells. An aliquot of cells was thawed on ice and 25 µl of cells was added to 2.5 µl of In-Fusion reaction mix for each reaction. The cells were incubated on ice for 30 min, then given a 45 sec heat shock at 42 °C and returned to ice for 1-2 min. 250 µl of warm SOC media was added, and the cells were incubated at 37 °C for 1 hr with 200 rpm shaking. 10 µl of cells were plated onto LB agar plates with ampicillin (100 µg/ml). These were incubated overnight at 37 °C. Individual colonies were screened for the guide insertion by colony PCR as described above (2.2.3).

Positive colonies were grown up in 3 ml of high salt LB with ampillicin overnight at 37 °C. Plasmid DNA was purified using the QIAprep Spin Miniprep Kit (Qiagen) according to manufacturer's instructions. DNA was eluted in 30 µl of DEPC water and the concentration was measured with a NanoDrop spectrophotometer. Sanger sequencing was performed as above to confirm the insertions.

2.4.3 Homology template cloning

For each deletion line, two CRISPR cuts were made and the deletion was repaired using homologous recombination. The donor construct included a ds-RED marker for selection, flanked by lox sites to remove the dsRED, and an attP site to allow future insertions at the site. This inserted cassette was flanked by 1 kb homology arms to facilitate repair. The pDsRED-attP vector 51019 was used (Appendix C.2).

For the *pros* promoter deletions, PCRs were done using gDNA prepared from the injected fly genotype. For all other homology arms, PCRs were done using purified BAC DNA. For *pros,* the BAC was CH322-133M22, and for *myc* it was CH322-74L1. The homology arms were designed for In-Fusion cloning as above, and colonies were screened and checked by Sanger sequencing.

2.4.4 Embryo injection and selection

For injection, plasmids were prepared by pooling 6 preparations from the QIAprep Spin Miniprep Kit (Qiagen) and then further purified using the QIAquick PCR Purification Kit (Qiagen). DNA was eluted in 10 µl of nuclease free, non-DEPC water. DNA concentration was measured and diluted appropriately (100 ng/µl each guide plasmid, 500 ng/µl donor plasmid, in 20 µl), before sending for injection at the University of Cambridge Department of Genetics Fly Facility. 200 embryos were injected and the larvae were returned for selection and crosses. For *pros* deletions, the injected line was BL 55821 with vas-Cas9 on the X chromosome. For *myc* deletions, the injected line was TH_attP2, with nanos-Cas9 on the 3rd chromosome. Injected flies were crossed to balancers as appropriate and positives were selected using the ds-RED marker. After validation of the insertion by PCR, the marker was removed with Cre recombinase and the final deletion was again validated by PCR. Sanger sequencing was used to identify the exact deletion.

2.5 Bioinformatics methods

2.5.1 Statistical analysis

Statistical analysis was performed using Prism (GraphPad Software). For image analysis (smFISH and phenotypic analysis), one-way ANOVA was used to identify difference between the results of different phenotypes and the *wild type* value.

Dunnett's multiple comparison test was then used to calculate significance values of each comparison.

The qPCR data was analysed with a comparison for each gene between the test and control pulldowns. The significance was calculated using t-tests with correction for multiple comparisons with the False Discovery Rate method, using an allowance of 5%.

2.5.2 Analysis of RNAseq and RIPseq (with Dr Aino Järvelin)

The following datasets were analysed:

- 3 biological replicates of RNAseq in *wild type* wL3 larval brains ("input" samples to Syp RIPseq)
- 3 biological replicates of RNAseq in *Imp::GFP* wL3 larval brains ("input" samples to Imp RIPseq)
- 3 biological replicates of RNAseq in *syp* mutant wL3 larval brains
- 3 biological replicates of Syp RIPseq in *wild type* wL3 larval brains
- 3 biological replicates of Imp RIPseq in *Imp::GFP* wL3 larval brains
- 2 biological replicates of RNAseq in S2 cells from (Hansen et al., 2015) (Short Read Archive (SRA) references SRR1640741 and SRR1640742)

The Hansen et al. S2 cell RNA-seq datasets were downloaded from the Short Read Archive (SRA) in native sra format using SRA toolkit (2.9.0) (SRA Toolkit Development Team, http://ncbi.github.io/sra-tools/) and converted to fastq files. The reads from all datasets and replicates were separately mapped to *Drosophila melanogaster* genome (genome assembly BDGP6, ENSEMBL release 92) downloaded from ENSEMBL on 19 May 2018 using the STAR aligner (2.5.3a) (Dobin et al., 2013).

Read counts per gene were calculated using HTSeq-count (0.8.0) (Anders et al., 2015). Given the bam output alignment files from STAR, HTSeq-count reports the number of uniquely mapped reads overlapping gene exons on the alignment strand in the annotation. Correlation between different replicates was visualised with a custom R script.

To identify differentially expressed genes, we used the Bioconductor package DESeq2 (1.20.0) with normal shrinkage estimation (Love et al., 2014) in a custom R script on the above count tables. RIPseq datasets were compared to their corresponding RNAseq samples ("inputs"). The results were visualised in custom MA plots in R.

To compare Syp RIPseq targets to transcriptomic changes seen in *syp* mutant, a custom R script was used to calculate the average read count between replicates normalised to library size for Syp RIPseq samples and *wild type* and *syp* mutant RNAseq samples. The ratios of RIPseq over *wild type* RNAseq and *syp* mutant RNAseq over *wild type* RNAseq was then plotted and data points for significant Syp targets and significantly differentially expressed genes (determined above with DESeq2) were highlighted in yellow and green, respectively, or in red if significant in both comparisons (Figure 3.10).

To make the coverage plots for *myc* (Figure 4.9), uniquely aligned reads were extracted from the alignment bam files using samtools (1.1) (Li et al., 2009) and further separated strand using samtools. The files were then converted into bedgraph format using bedtools (v2.26.0) (Quinlan and Hall, 2010), and the resulting coverage (count per base) was visualised with a custom R script using the Bioconductor package Sushi (1.18.0) (Phanstiel et al., 2014). Chromosome sizes needed for this

analysis were calculated with custom R scripts using Bioconductor packages Biostrings (2.48.0) (Pagès et al. 2018). The Bioconductor package intervals (0.15.1) (Bourgon 2015) was used in a custom script to determine coding exons for *myc* in *D. melanogaster* (BDGP6) annotation that provides coordinates for all exons and UTR exons of genes, but not coding exons explicitly.

2.5.3 Bioinformatic analysis of Imp iCLIP-seq dataset in S2 cells

The Hansen *et al*. (2015) two replicate Imp iCLIP datasets were downloaded from SRA (references SRR1640733. and SRR1640734) and converted to fastq format as described above. Illumina sequencing adapters were trimmed off reads using cutadapt (1.10) (Martin, 2011) and the first five bases (corresponding to molecular barcodes) were removed from sequence and appended to read name using a custom python script. The reads were then mapped to the *D. melanogaster* genome (genome assembly BDGP5, ENSEMBL release 78; downloaded on 8 January 2015) sequence using iCount *mapstar* (Curk et al., 2016; Dobin et al. 2013). iCount *xlsites* was used to determine the number of unique crosslinked sites (unique cDNA molecules) for any given position. This gives a measure Imp interaction strength with target RNA. The resulting Imp binding site bed files were then separated by strand using awk from the command line, converted to bedgraph format and visualised with the Bioconductor package Sushi (Phanstiel et al., 2014).

2.5.4 Analysis of 3' UTR length

A custom R script was used to determine the 5' and 3'UTR lengths for *D. melanogaster* protein coding genes based on the BDGP6 annotation. Briefly, the 'three_prime_utr' and 'five_prime_utr' features per transcript were extracted from the annotation gtf file, and UTR lengths calculated from these coordinates (summed up if they spanned multiple exons). To provide UTR lengths per gene, we calculated the

minimum, maximum, median, and mean of transcript UTR lengths. These lengths were plotted in a boxplot with help of R package ggplot2 (2.2.1) (Wickham, 2009) (Figure 3.8).

2.5.5 Functional annotation

The curated gene lists in GLAD (Gene List Annotation for *Drosophila*) tools (Hu et al., 2015) were used to analyse the genes identified in the genome-wide sequencing experiments. I retrieved the lists of different gene targets, and cross-referenced the lists with the targets.

3.

THE ROLE OF IMP AND SYP IN NEUROGENESIS

3.1 INTRODUCTION

In order to make a fully functional nervous system, it is essential to produce the correct number and sequence of neurons throughout neurogenesis. All neurons are produced by neuroblast (NB) divisions and it is thought that their fates are determined by their birth order (Doe and Goodman, 1985; Weigmann and Lehner, 1995). Embryonic neuroblasts can be placed in a timeline of development based on their expression of a sequential cascade of transcription factors (TFs) (discussed further in section 1.3). These TFs are inherited and maintained by the GMC to determine the fate of their neuron progeny. Several studies have aimed to identify the equivalent regulators of larval NB age through development. Opposing gradients of the RNA-binding proteins (RBPs) Imp and Syp in the NB were shown to regulate the temporal fate of the mushroom body NB progeny neurons (Figure 1.7) (Liu et al., 2015). Furthermore these RBPs negatively regulate each other, maintaining the directionality of the gradients. However, the mechanism of action of Imp and Syp is poorly understood.

RBPs, such as Imp and Syp, act by controlling the fate of their target mRNAs (as well as non-coding RNAs), thereby altering the isoform choice, level or localisation of the encoded proteins. Therefore, I aimed to identify the Imp and Syp mRNA targets: an important step towards understanding the function of an RBP. Imp and Syp are known to have roles in regulation of RNA localisation, translation and stability (discussed in section 1.5) (Geng and Macdonald, 2006; McDermott et al., 2012; Svitkin et al., 2013). One functional target of Imp and Syp has been identified in the brain: translational regulation of *chinmo* mRNA determines the fate of MB neurons (Liu et al., 2015). Chinmo was identified because it had previously been found to regulate the normal progression of cell fates (Zhu, 2006). A genome-wide approach to identify Imp and Syp targets would provide an unbiased list of potentially regulated transcripts. This is very likely to lead to unexpected insights into the mechanisms of Imp and Syp regulation.

The regulation of *chinmo* translation by Imp and Syp determines progeny fate, but Imp and Syp have also been shown to regulate various other aspects of NB behaviour. The mechanisms of this regulation are incomplete or unknown. The *syp* mutant has a significantly enlarged central brain region, published in a preprint from the Davis Lab on which I am a co-author (Hailstone et al., 2018). This gross brain phenotype might be due to neuroblast overproliferation, generating excess cells. We found that Imp and Syp also regulate the termination of NB division in the pupa (Yang et al., 2017a). Specifically, loss of Imp allows NB shrinkage in the pupa, then elevated Syp is required for termination by a final symmetrical division. I aimed to identify key examples of post-transcriptional regulation of mRNA targets to explain the phenotypes of *imp* and *syp*. The broad functions of Imp and Syp show that these RBPs are highly important for coordination of neurogenesis and therefore understanding their mechanisms of action is essential.

In this Chapter, I aimed to identify the mRNA binding targets of both Imp and Syp in the larval brain, using RIPseq. I examined the targets as a group, identifying an enrichment of binding to transcripts encoding TFs and RBPs, and transcripts with highly extended 3' UTRs. I compared these targets to changes in the transcriptome in the *syp* mutant, to identify transcripts which might be regulated through mRNA stability. I then narrowed my focus to the phenotypes and regulation by Imp and Syp in the type I NBs. I examined the expression of Imp and Syp in the type I NB lineages using single molecule fluorescent *in situ* hybridisation (smFISH) and immunofluorescence (IF), and then defined an approach to follow up targets with the most potential.

3.1.1 Specific aims

1. To identify the mRNA targets of Imp and Syp
2. To analyse changes in target levels in the *syp* mutant
3. To examine expression and phenotypes of Imp and Syp in type I NB lineages
4. To select potential candidates for follow up experiments

3.1.2 Experimental rationale

I wanted to understand how Imp and Syp regulate NB behaviour in the larval brain. Many genes or transcript isoforms are specifically expressed in the nervous system (Mohr and Hartmann, 2014). Furthermore, the binding of Imp and Syp may depend on the transcript isoform, as well as the other RBPs present in the cells, mediating interactions. For these reasons, I aimed to identify the Imp and Syp targets specifically in the brain, using brain lysates. This is the most effective way to maximise the number and relevance of targets identified.

There are several methods to identify the mRNA binding targets of an RBP, which have different advantages and disadvantages (discussed in section 1.4, and reviewed in (Wheeler et al., 2018)). RIPseq is the simplest technique, where the RBP is directly immunoprecipitated from a cell lysate without crosslinking. This means that gentle washes must be used, which may lead to recovery of some indirect interactions. CLIP protocols use exposure to UV radiation, resulting in covalent crosslinks between closely bound proteins and RNA molecules (within just a few ångströms). Crucially, it does not induce protein-protein crosslinks and therefore, using much more stringent washes, only directly bound mRNAs are purified. The RNA is then digested into small fragments of ~50 nt to allow identification of the binding sites of the RBP in each transcript. iCLIP takes this one step further to allow individual nucleotide resolution of RBP binding sites. However, iCLIP is a very difficult protocol, requiring many months of optimisation for each protein studied. Furthermore, due to the low efficiency of crosslinking and limited penetration into tissue, a very large amount of starting material is needed.

The priority for this project was to identify mRNA targets of Imp and Syp, without an immediate requirement to find the specific binding sites. In order to identify mRNA targets specifically in the central nervous system, wL3 brains have to be individually dissected before pooling to make a lysate. This is hugely time consuming in large numbers, so collection of sufficient material is a key limiting factor in the methodology choice. For these reasons, RIPseq was chosen as the most appropriate technique.

3.2 WHAT mRNA TARGETS DO IMP AND SYP BIND?

mRNA-binding proteins such as Imp and Syp exert their function through regulation of various target mRNAs. This could include modulating mRNA localisation, stability or translation, to eventually alter the amount or localisation of the protein at different times. Therefore, identifying the mRNA targets of Imp and Syp is important to understand their regulatory mechanisms.

3.2.1 RIPseq identified Imp and Syp mRNA targets

To identify the mRNA targets of Imp and Syp, I performed RIPseq on wL3 brains. Full details of the protocol can be found in the Materials and Methods (section 2.2.10-15). Briefly, brains were dissected and then lysed in IP buffer (50 mM Tris-HCl pH 8.0, 150 mM NaCl, 0.5% NP-40, 10% glycerol). A fraction of the brain lysate was taken as an input sample. I used beads with specific conjugated antibodies to pull down either Imp or Syp and the associated RNAs from the brain lysate. The beads were washed in the IP buffer to remove non-specifically bound proteins or RNA. The bound protein was then eluted from the beads (at 65 ˚C in elution buffer (50 mM Tris HCl (pH 8), 10 mM EDTA, 1.3% SDS)), and the associated mRNA was purified. I produced and sequenced libraries from the IP samples and input samples on an in-house Ion Proton machine (Rothberg et al., 2011). All experiments were done in triplicate. Dr Aino Järvelin, a bioinformatician in the Davis lab, performed alignment and differential expression analysis to identify targets that were enriched in the pulldown samples compared to the inputs.

Syp RIPseq

The simplest way to perform an IP is to use a line with endogenous tagging of the protein, for example with FLAG tag or GFP, which can be used for the pulldown. However, there was no appropriate endogenously tagged Syp line. Therefore, I used anti-Syp antibody (McDermott et al., 2014) in the *wild type* background, to pull down endogenous Syp (Figure 3.1 A). I crosslinked anti-Syp antibody to magnetic beads and used these to pull down Syp and its bound mRNAs. I used a Western blot to show that the immunoprecipitation selectively enriches Syp, and α-Tubulin is left in the unbound fraction (Figure 3.1 B).

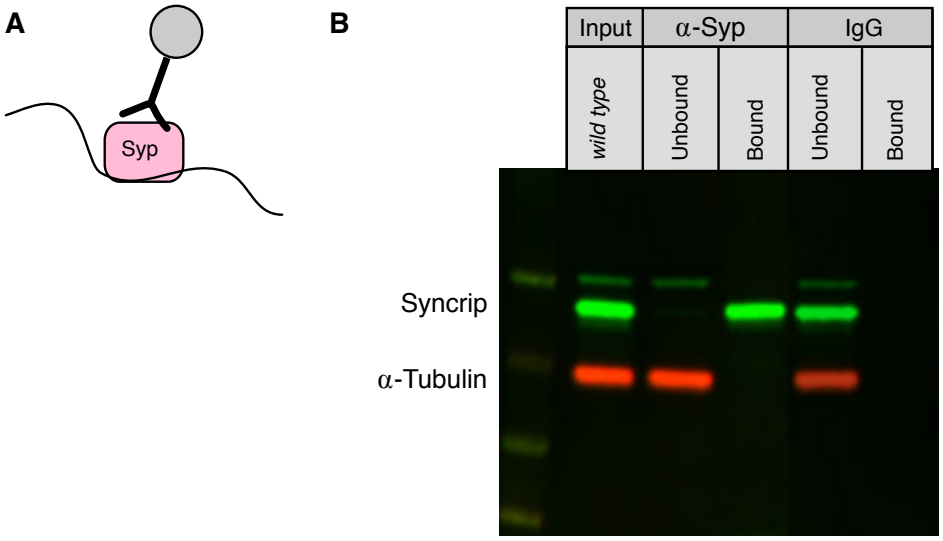


Figure 3.1 RIPseq strategy to identify Syp targets
A anti-Syp antibody was conjugated to magnetic beads. These beads were incubated with a brain lysate (100 brains per IP, in IP buffer (50 mM Tris HCl (pH 8), 150 mM NaCl, 0.5% NP40, 10% glycerol)), allowing binding of Syp to the antibody. The beads were washed in IP buffer to remove non-specific binders, then Syp protein was eluted at 65 ˚C in elution buffer (50 mM Tris HCl (pH 8), 10 mM EDTA, 1.3% SDS) and the bound mRNA was sequenced on an Ion Proton platform to identify the bound targets. **B** A Western blot to show efficiency of the Syp IP. The control IP used IgG conjugated beads, which do not pull down Syp. α-Tubulin and Syp are identified by specific antibodies in the input (*wild type*) sample. In the Syp pulldown, α-Tubulin is detected in the unbound fraction, but not in the bound fraction, while Syp is specifically depleted from the unbound fraction and detected in the bound fraction (note the larger background band detected by the α-Syp is not IPed). In the control IgG pulldown, Syp and α-Tubulin are both found in the unbound fraction and not in the bound fractions.

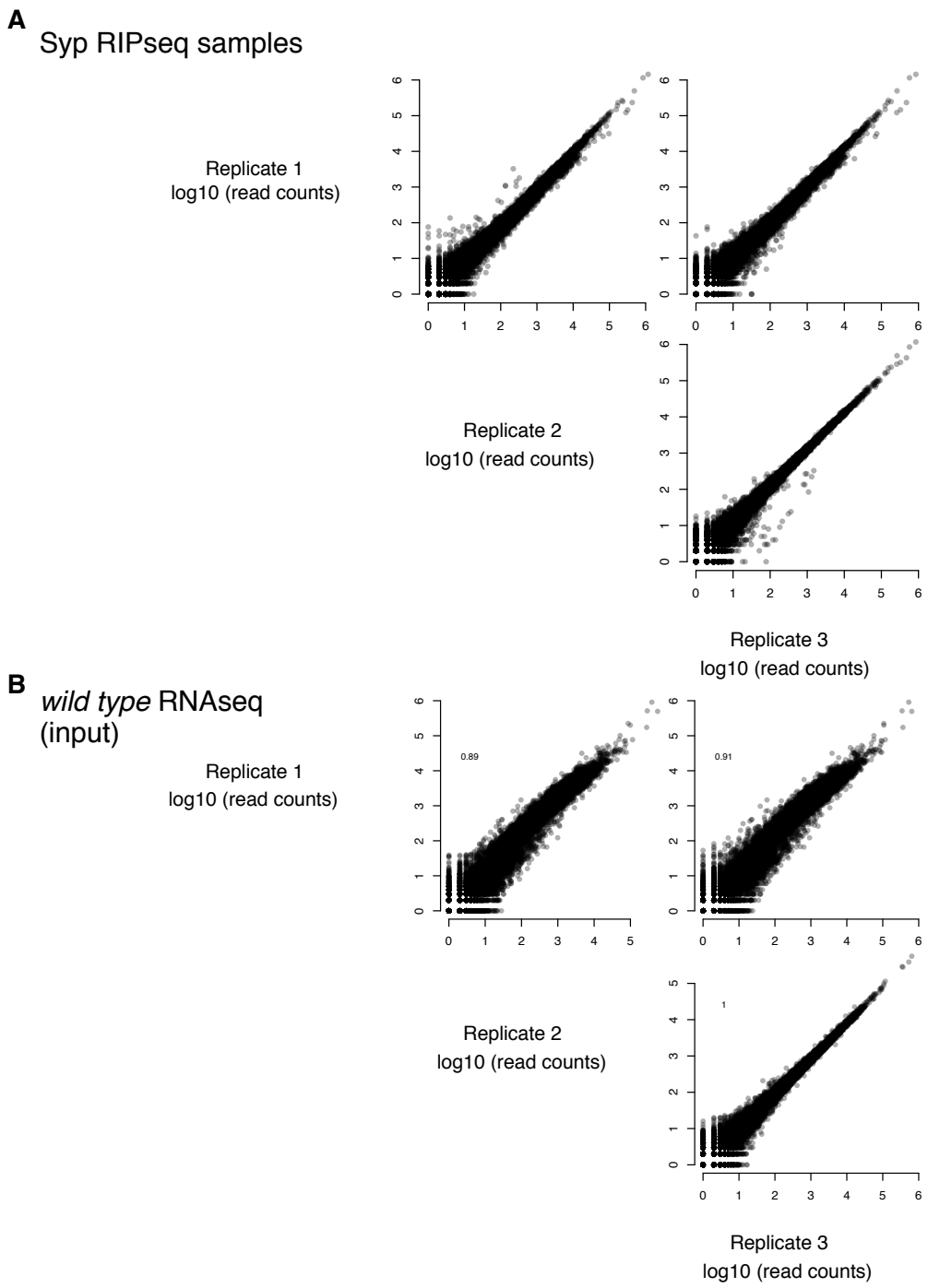


Figure 3.2 Syp IP sample correlation plots show reproducibility
Dr Aino Järvelin produced plots to show the correlations between the triplicate repeats in the RIPseq (**A**) and input (**B**) samples. The RIPseq samples are extremely well correlated. Replicate 1 of the input samples is slightly more different to the other two samples. This is most likely because the library was made separately to the other samples. The correlations were measured using the Pearson correlation, noted on each graph. The Pearson correlation has a value between +1 for total positive correlation, and -1 for total negative correlation.

For sequencing, Syp protein was immunoprecipitated from a lysate of 100 *wild type* (Oregon R) brains in triplicate. I purified the mRNA from the RIP samples and input samples and produced libraries, which I then sequenced using an in-house Ion Proton sequencer. Dr Aino Järvelin analysed the data and produced correlation plots, which show that the RIP replicates are very well correlated (Figure 3.2 A). The input samples show that the first replicate is most different, most likely because this library was made separately from the others (Figure 3.2 B).

Dr Aino Järvelin performed differential expression analysis to identify genes that were enriched in the Syp IP (Figure 3.3 A). 642 targets were found to be significantly enriched in the Syp IP compared to the input RNAseq (log2FC > 1, adjp < 0.01) (full list Appendix Table D.1). This is a large but not unexpected number of targets compared to other RIPseq experiments (Mittal et al., 2011), as Syp has broad functions, and RIPseq may identify some indirect mRNA interactions in addition to the direct targets. The targets included both *syp* and *imp*, as expected due to the cross-regulatory relationship between the RBPs. *chinmo* was also bound by Syp, supporting the previously published regulatory relationship (Liu et al., 2015).

I used RIP-qPCR to validate a small number of Syp targets and negative controls from the RIPseq data. For RIP-qPCR, the pulldown was performed as for the RIPseq, and IPed mRNA was calculated as a percentage of the input mRNA from a dilution curve. The % input from the Syp RIP, was compared to a control RIP with IgG antibody, which does not pull down Syp (Figure 3.3 B). Eight non-binding transcripts were tested, with five showing no significant Syp IP compared to the IgG control. Those which did show significant binding had very low % input pulled down. Five binding targets from the RIPseq were also tested and four of these showed significant binding in the IP.

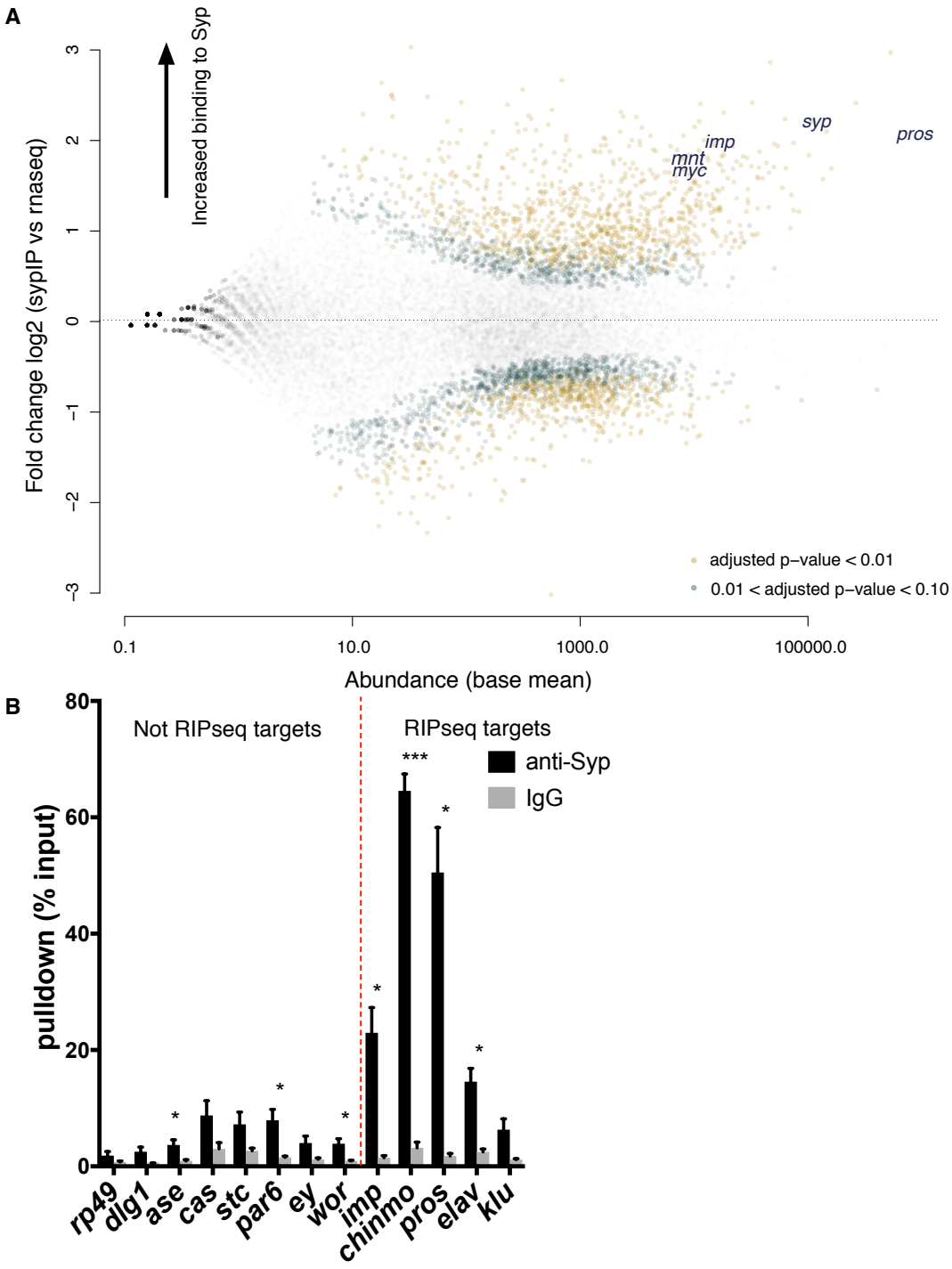


Figure 3.3 Syp targets identified by RIPseq

A Differential expression analysis shows targets that are enriched compared to the input samples (graph made by Dr Aino Järvelin). *imp* and *syp* are both targets of Syp. Targets which will be discussed in Chapters 4 and 5 are also marked (*myc, mnt* and *pros*). **B** qPCR was used to validate Syp targets, comparing pulldown with anti-Syp compared to anti-IgG. 4 of 5 targets from the RIPseq were also statistically significant in the qPCR, while 5 of 8 non-binding transcripts were significantly IPed in the qPCR. Statistical significance was calculated for each transcript between the Syp IP and the IgG control, using t-tests, with correction for multiple comparisons using a False Discovery Rate allowance of 5%. * q < 0.05, ** q < 0.01, *** q < 0.001

Syp targets identified by RIPseq have previously been published in whole wL3 larvae, finding many targets with key synaptic functions (McDermott et al., 2014). The previous Syp RIPseq in whole larvae identified 275 mRNA targets (log2FC > 1) (McDermott et al., 2014). 30 of these overlapped with the targets identified in the brain. Therefore, 612 additional brain-specific targets were identified in this study. Syp is expressed in the cytoplasm in cells of the brain, but in the nucleus in many other cell types such as muscle, which is likely to lead to a different complement of targets. Furthermore, many brain-specific transcripts would be present at an extremely low level in the whole larval samples and therefore may not be identified as significant. This novel cohort of Syp targets in brain tissue is a valuable resource to explore the function of Syp in the brain.

Imp RIPseq

The mRNA targets of Imp were identified using a very similar RIPseq method. A line with an endogenously tagged Imp::GFP (Toledano et al., 2012) was used for the Imp IP, allowing use of agarose GFP-Trap beads (Chromotek) to pull down Imp (Figure 3.4 A). I used a Western blot to show that the immunoprecipitation with the GFP-Trap beads enriches Imp from Imp::GFP brains, but not *wild type* (Figure 3.4 B). α-Tubulin is not bound, so remains in the unbound fraction.

For the Imp RIPseq experiment, I dissected 300 wandering L3 brains per replicate and took one third for input and two thirds for IP. The experiment was performed in triplicate, and Dr Aino Järvelin produced correlation plots, showing a good correlation between replicates (Figure 3.5). Dr Aino Järvelin analysed the data using differential expression analysis and found 1109 targets which were significantly enriched in the Imp IP (log2FC > 1, adjp < 0.01) (Figure 3.6 A, full list Appendix Table D.2). The targets include *imp* and *syp*, supporting the cross-regulatory relationship between

these RBPs. Imp pulls down *chic* in this system, as previously shown (Medioni et al., 2014). Imp also binds *chinmo,* which it is known to regulate in the MB NBs (Liu et al., 2015). There are almost twice as many mRNA targets of Imp than Syp. This may be due to technical differences in the pulldown strategy, or may be a real biological difference.

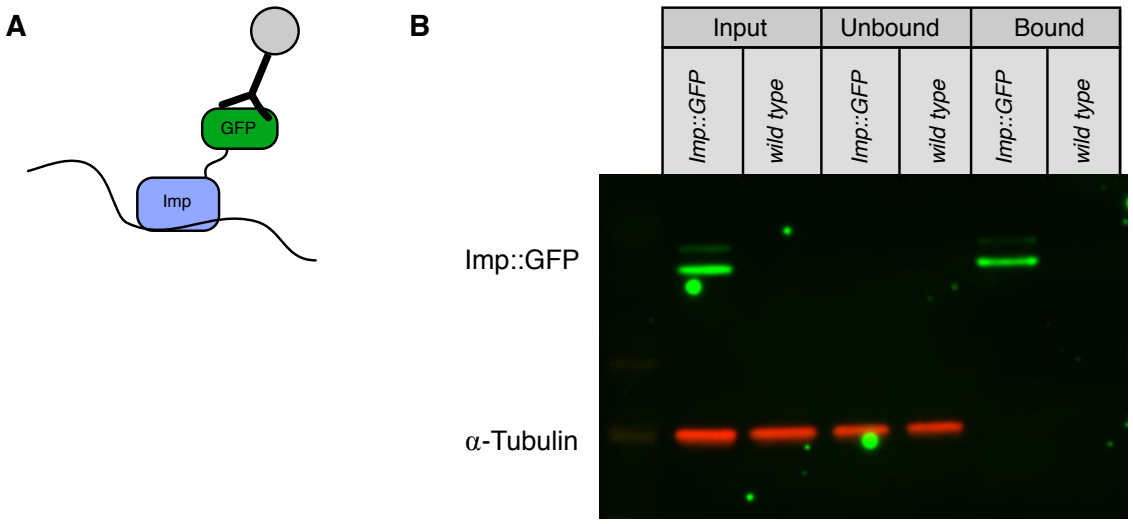


Figure 3.4 RIPseq strategy to identify Imp targets
A The *Imp::GFP* line was used for RIPseq. GFP trap agarose beads (Chromotek) bind to the endogenously tagged Imp::GFP in a brain lysate (200 brains per IP, in IP buffer (50 mM Tris HCl (pH 8), 150 mM NaCl, 0.5% NP40, 10% glycerol)). After washes in IP buffer, Imp protein was eluted at 65 ˚C in elution buffer (50 mM Tris HCl (pH 8), 10 mM EDTA, 1.3% SDS) and the bound mRNA was sequenced using an Ion Proton platform, to identify the targets. **B** I performed a Western Blot to validate the specificity of the IP. I used *wild type* brain lysate with GFP trap beads as a control as the Imp has no GFP tag, so will not be pulled down. Imp::GFP can be detected in the *Imp::GFP* but not the *wild type.* Imp::GFP is detected in the bound fraction of the IP. α-Tubulin is detected in the unbound but not the bound fractions in both the experimental and control IPs.

I used RIP-qPCR to validate a small number of the Imp targets. GFP trap beads were used to pulldown Imp from *Imp::GFP* or *wild type* brain lysate. Pulldown of each transcript was measured as a % input (Figure 3.6 B). Of six targets from the RIPseq, all showed significant binding to Imp. The negative control *rp49* also showed a significant pulldown in the *Imp::GFP* compared to the control. However, the %

pulldown was extremely low (0.7%), so is not considered a likely biologically significant target.

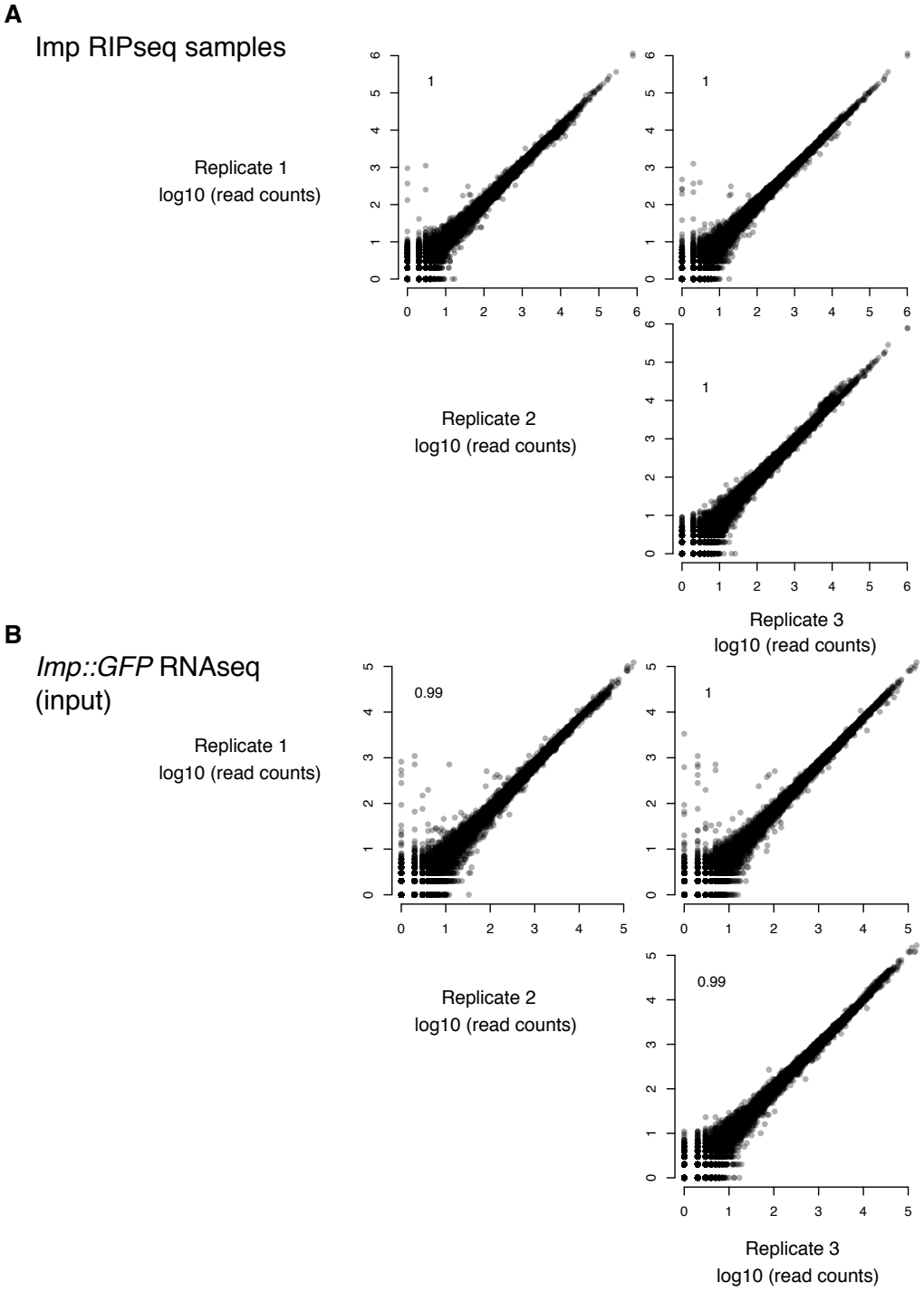


Figure 3.5 Imp IP sample correlation plots show reproducibility
Dr Aino Järvelin produced plots to show the correlations between the triplicate repeats in the RIPseq (**A**) and input (**B**) samples. The samples are very well correlated. The correlations were measured using the Pearson correlation, noted on each graph.

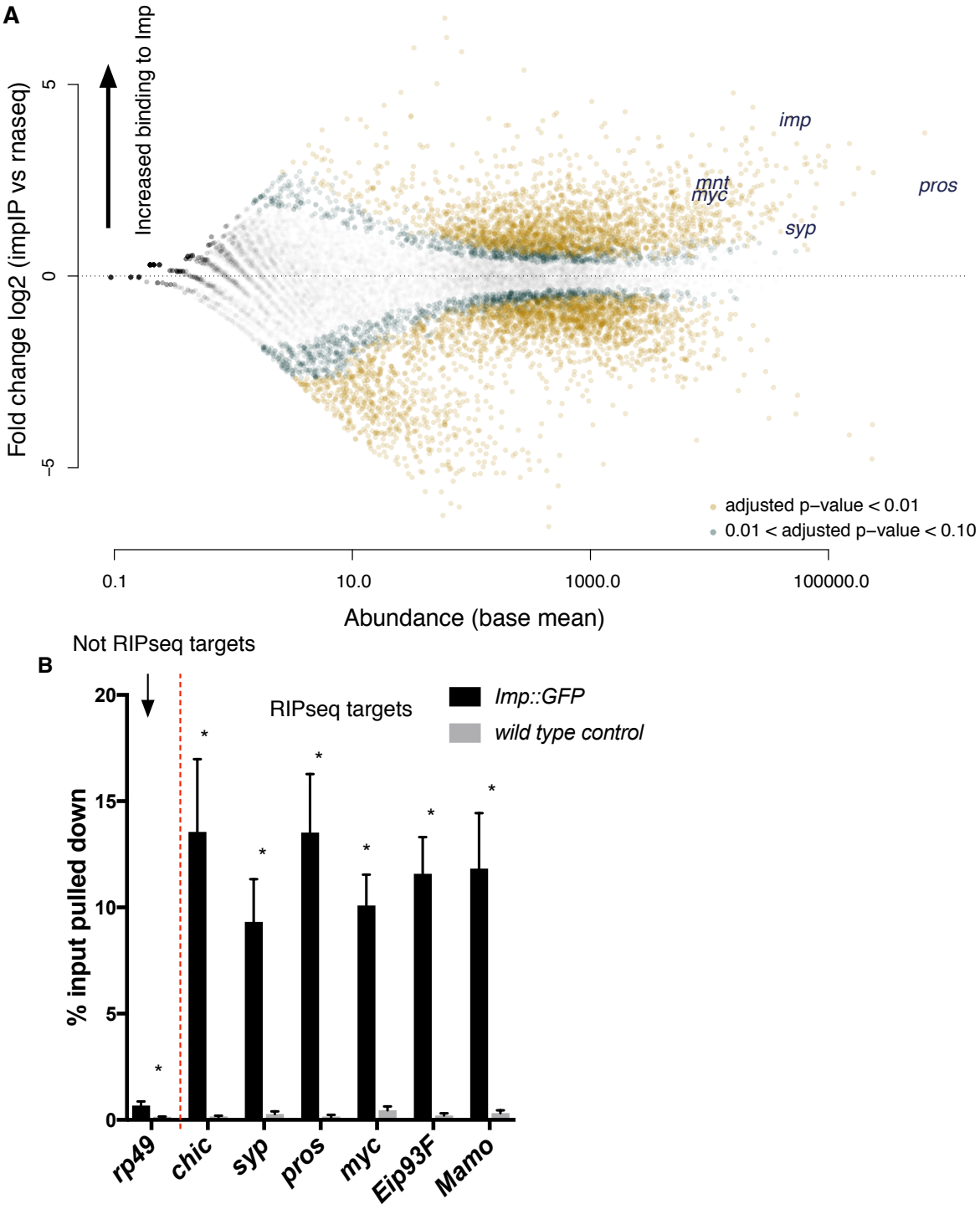


Figure 3.6 Imp targets identified by RIPseq

A Differential expression analysis shows Imp targets which are enriched compared to the input samples (graph by Dr Aino Järvelin). Targets which will be discussed in Chapters 4 and 5 are marked (*myc, mnt* and *pros*). **B** qPCR was used to validate Imp targets, comparing pulldown with anti-GFP in the *Imp::GFP* line, compared to *wild type* brains. Statistical significance was calculated for each transcript between the *Imp::GFP* and the *wild type* control, using t-tests with correction for multiple comparisons using a False Discovery Rate allowance of 5%. * q < 0.05, ** q < 0.01

3.2.2 Which mRNA targets are bound by both Imp and Syp?

We have proposed that co-regulation of progeny fate and NB termination by the same regulators, Imp and Syp, is important to coordinate production of the correct neurons for the brain (Yang et al., 2017a). I was interested to examine the regulatory relationship between Imp and Syp, so I asked whether Imp and Syp bind similar cohorts of mRNAs. RIPseq in the wL3 brain identified 642 Syp targets and 1109 Imp targets: 366 targets are shared by both RBPs (Figure 3.7). This includes transcripts regulated in the same way by Imp and Syp, in opposing ways (like *chinmo*), as well as some possible indirect interactions.

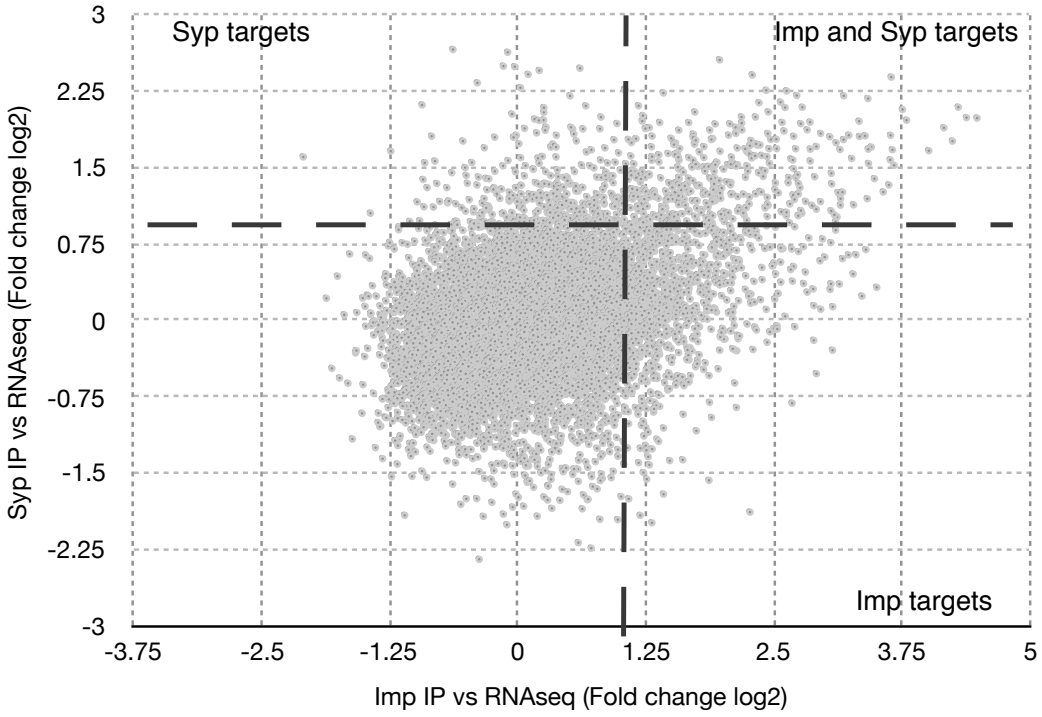


Figure 3.7 Targets binding both Imp and Syp
Plotting the fold change enrichment of all genes in both the Imp and Syp RIPseq experiments identifies shared targets, as well as targets bound singly by either Imp or Syp. Dotted lines indicate a 2-fold enrichment in the RIPseq experiment. The top right hand corner contains the shared targets.

Imp and Syp are not expressed highly in the same cells at the wL3 stage, when Syp is very high in the NBs, but Imp is almost entirely absent, and instead is expressed in

mature progeny cells (Figure 3.12). Therefore, I was interested where the targets of Imp and Syp are expressed. A previous study used FACS to identify genes enriched in either NBs or neurons (Berger et al., 2012), so I cross-referenced these lists with the RIPseq targets (Table 3.1). I found that more Imp targets are enriched in the neurons, compared to NBs. This is consistent with higher Imp expression in neurons compared to NBs at this stage. Similarly, more shared targets are enriched in the neurons, where Imp and Syp expression overlap more. However, targets which are enriched in either NBs or neurons may still be significantly expressed in other cell types and pulled down by Imp or Syp there.

Table 3.1 Expression of targets in NBs or neurons

	Total number	Enriched in NBs	Enriched in neurons
Whole genome	13924	12.1% (1678)	12.7% (1775)
Syp targets	642	12.9% (83)	19.9% (128)
Imp targets	1109	7.3% (81)	34.7% (385)
Imp + Syp targets	366	10.4% (38)	29.0% (106)

During the immunoprecipitation, Imp and Syp may be exposed to transcripts from other cells broken down in the brain lysate (Mili and Steitz, 2004). Therefore, perhaps some binding interactions may not be present *in vivo*. In the follow up of individual targets, microscopy can be used to validate expression in the same cells.

3.2.3 Enrichment of RBPs and TFs among Imp and Syp targets

I was also interested to explore the types of targets bound by Imp and Syp. I used GLAD (Gene List Annotation for *Drosophila*), a curated set of gene annotations, to identify characteristics of the bound mRNAs (Hu et al., 2015). Compared to the frequency in the whole genome, Imp and Syp targets are enriched for TFs/DNA binding and RBPs (Table 3.2, full RIPseq lists annotated as TF or RBP Appendix

Table D.1,2). This suggests that Imp and Syp bind more than expected to transcripts encoding regulatory proteins.

Classically, the expression of different TFs is thought to determine cell fate. Transcripts encoding TFs that are bound by both Imp and Syp include *pros*, *myc*, *homothorax,* and *mamo*. Some of these, such as *pros* are highly studied in neurogenesis, and their target genes have been identified. Many more are much less well understood. The dysregulation of target TFs may explain the phenotypes of *imp* and *syp.*

Table 3.2 Enrichment of TFs and RBPs among Imp and Syp targets

	Total number	TF/DNA binding	RBPs
Whole genome	13924	8.2% (1146)	4.1% (576)
Syp targets	642	17.6% (113)	9.0% (58)
Imp targets	1109	16.2% (180)	5.0% (55)
Imp + Syp targets	366	23.3% (85)	11.5% (42)

Imp and Syp also show an enrichment of binding to transcripts encoding RBPs, which could suggest that Imp and Syp are part of a much larger network of post-transcriptional regulation (Mittal et al., 2011). The RBPs whose mRNAs are bound by both Imp and Syp include *brat*, *elav*, *squid, pumilio* and *hephaestus.* These and many other RBP targets have been shown to have regulatory roles either in the nervous system or other tissues. If there is a network of RBP regulation, this could make interpretation of *imp* and *syp* mutant phenotypes more complex, as many other regulators would also be changed.

3.2.4 Imp and Syp bind genes with long 3' UTRs

RBP binding sites are often found in the untranslated regions of their target transcripts, as these regions can evolve without altering the encoded protein. Therefore, I examined the UTRs of the Imp and Syp bound mRNAs and found that many targets have extremely long 3' UTRs. The Imp target *mei-P26,* encoding a ubiquitin ligase, has the longest 3' UTR in the genome at an extraordinary 18.5 kb. *smooth*, an RBP and a target of both Imp and Syp, has an isoform with a 12.7 kb 3' UTR. Dr Lu Yang, in the Davis lab, has previously examined the 3' UTR of *pros* (a target of both Imp and Syp), which has a 15.5 kb 3' UTR.

Dr Aino Järvelin analysed the maximum 3' UTR lengths of all transcripts genome wide, and of the top 25% and top 10% most expressed genes in the larval brain (Figure 3.8). This analysis identified an enrichment in expression of genes with longer 3' UTRs in the brain. Almost all of the outlying genes with the longest 3' UTRs are highly expressed in the brain. Dr Aino Järvelin then examined the maximum 3' UTR lengths of the Imp and Syp targets and found a further enrichment for genes with long 3' UTRs. The targets included many of the genes with the longest 3' UTRs in the genome. Alternative polyadenylation allows production of isoforms with different length 3' UTRs (Di Giammartino et al., 2011). It has been previously reported that 3' UTRs are extended in neural tissues (Hilgers, 2011; Wang and Yi, 2014). This enrichment of long 3' UTRs may reflect the tight regulation in the brain, requiring longer regulatory sequences. These regulatory sequences are bound by RBPs such as Imp and Syp (Mayr, 2017).

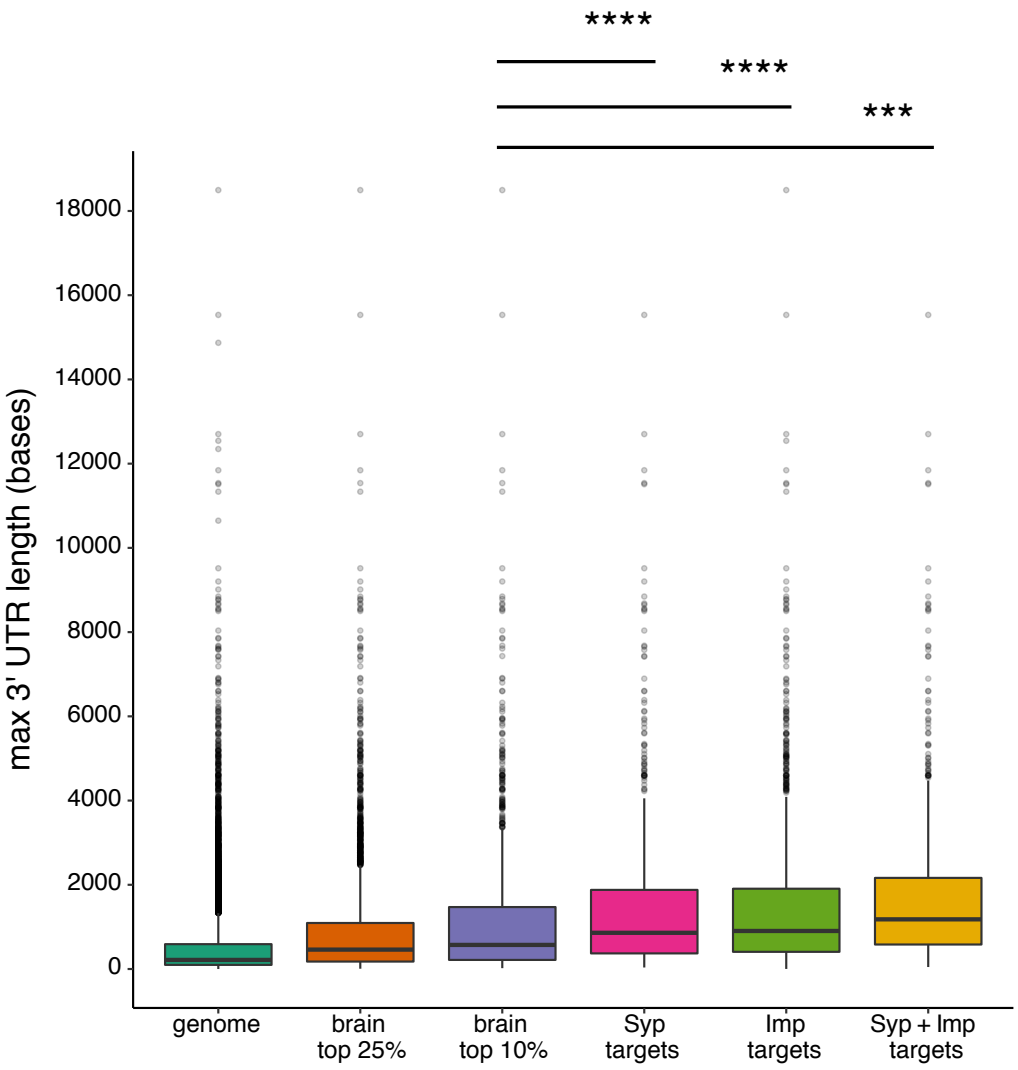


Figure 3.8 Imp and Syp bind genes with long 3' UTRs

Dr Aino Järvelin analysed maximum 3' UTR length across the genome. She then compared this to the top 25% and top 10% highest expressed genes in the brain (based on the *wild type* RNAseq data). The highest expressed genes in the brain have longer 3' UTRs than average. The Imp and Syp targets are also enriched for genes with longer 3' UTRs. Statistical significance was assessed by t test, compared to 'brain top 10%'. *** $p < 0.001$, **** $p < 0.0001$

3.3 ARE mRNA LEVELS OF SYP TARGETS ALTERED IN A *syp* MUTANT?

I then asked how the transcriptome of the brain changes when Syp is depleted. Targets of Imp or Syp, identified by RIPseq, might be regulated through their mRNA localisation, stability or translation. Targets might also be indirectly bound; found in the same complex as the RBP of interest but without direct binding or regulation. Both Imp and Syp have hundreds of mRNA targets and it is a difficult problem to identify targets which are meaningfully regulated by them. Therefore, I used RNAseq to compare the transcriptome in *wild type* and Syp depleted wL3 brains. This method can identify targets which might be regulated by mRNA stability, as their transcript level will be changed in the mutant.

3.3.1 RNAseq identified changes in mRNA levels in *syp* mutant

In order to examine the transcriptome changes in the *syp* mutant, differential expression analysis was performed comparing RNAseq from *wild type* and *syp* mutants. The *syp* mutant was a P element insertion, syp^{e00286} (Exelixis Collection at Harvard). I prepared triplicate RNAseq libraries from *syp* mutant brain lysates and sequenced them on the Ion Proton sequencer. Dr Aino Järvelin produced correlation plots, which show that the replicates are well correlated (Figure 3.9 A). *wild type* samples (the input samples from the Syp RIPseq experiment), were then compared to *syp* mutant brain samples.

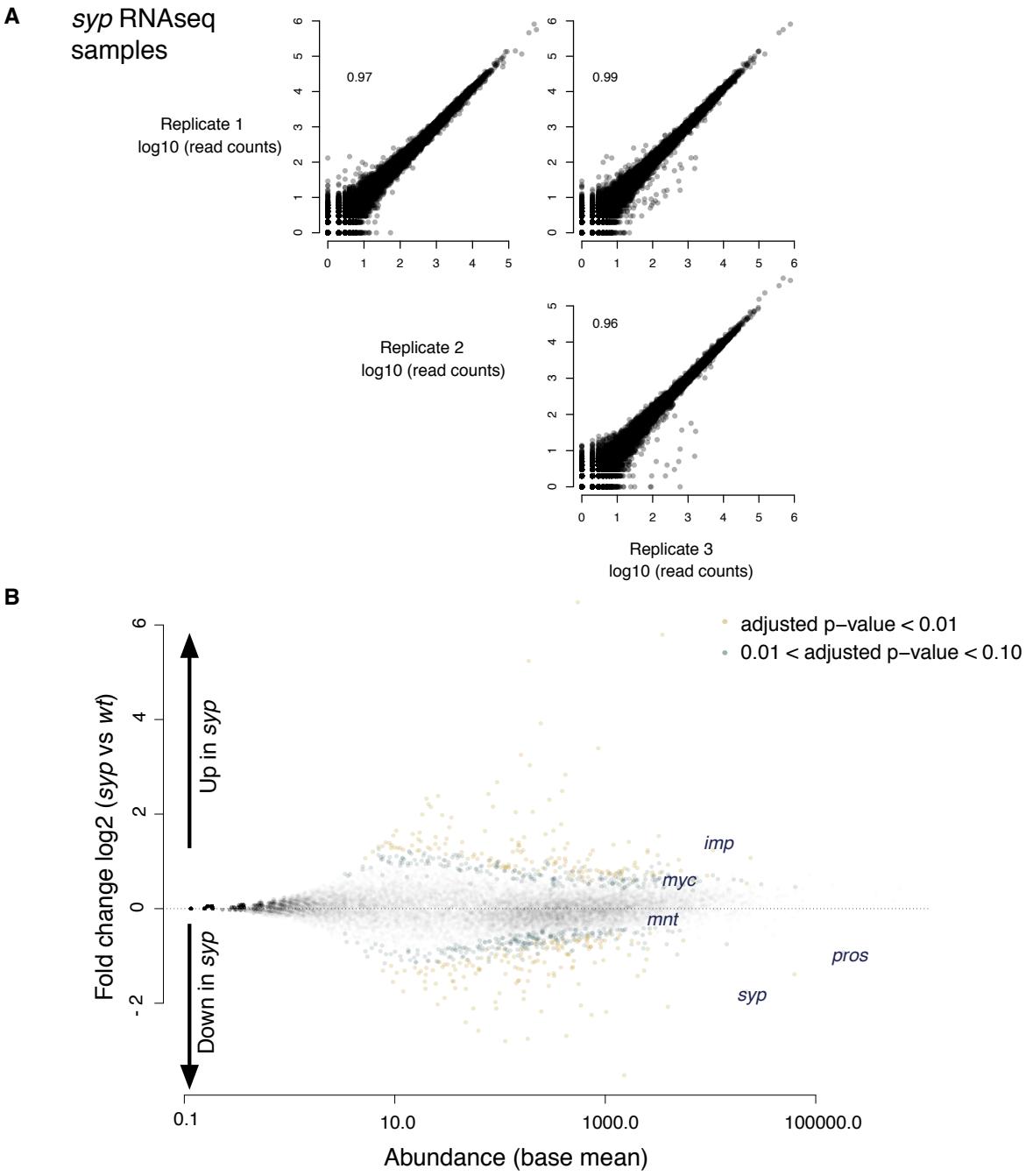


Figure 3.9 Changes in the transcriptome of *syp* mutant brains
A Dr Aino Järvelin produced plots to show the correlations between the triplicate repeats in the *syp* mutant RNAseq samples. The samples are very well correlated. The correlations were measured using the Pearson correlation, noted on each graph. **B** Differential expression analysis by Dr Aino Järvelin shows changes in transcript levels between the *wild type* and *syp* mutant brains. A roughly equal number of transcripts are upregulated and downregulated.

Dr Aino Järvelin performed differential expression analysis to identify changes in the *syp* mutant transcriptome. Changes in mRNA stability in a small number of cells within the brain will be diluted in the whole brain transcriptome. Therefore, in order to

identify as many changes as possible, a less stringent significance threshold of 0.05 was used, and no fold change threshold was imposed. 547 transcripts showed significant differences (adjp < 0.05) (Figure 3.9 B). 283 upregulated (Appendix Table E.1) and 264 of these were downregulated (Appendix Table E.2). As expected, *syp* mRNA is downregulated in the mutant, and *imp* mRNA is upregulated due to its derepression.

The changes in the transcriptome may be caused by altered post-transcriptional regulation due to the loss of Syp. However, they may also be indirect, transcriptional consequences downstream of changes in the levels or activity of TFs. Transcripts encoding TFs are altered (Table 3.3): *pros* and *dpn* are downregulated, and *zelda* and *taxi* are upregulated. The levels of transcripts encoding other RBPs is also changed in the *syp* mutant (Table 3.4): for example *imp*, *vasa* and *nanos* levels increase. I narrowed down examples of post-transcriptional regulation by specifically identifying changes in transcript levels of the Syp or Imp targets.

Table 3.3 TFs which change in the *syp* mutant
All TFs that are altered in the *syp* mutant, compared to *wild type* (adjp < 0.05).

Upregulated in *syp* mutant	log2FC	Downregulated in *syp* mutant	log2FC
CG17186	2.8124	*CG6654*	-2.2049
CG6470	1.2762	*dati*	-2.0966
CG18446	1.2601	*bab1*	-2.0660
sage	1.2129	*Eip78C*	-1.4408
CG3726	1.2093	*exp*	-1.3927
CG13458	1.1314	*CG43342*	-1.2586
rn	1.1110	*Blimp-1*	-1.2537
zld	1.0530	*CG9416*	-1.1572
CG2120	1.0064	*CG43343*	-1.1117
CG8301	0.9473	*Hr4*	-1.0936
tx	0.9331	*CG13617*	-1.0346
CG34367	0.8890	*bab2*	-1.0004
REPTOR	0.8876	*MP1*	-0.9758
dpy	0.8668	*pros*	-0.9479
RunxA	0.8541	*Sox14*	-0.8583
lov	0.8397	*PGRP-LC*	-0.8314
Ada2a	0.7704	*pdm2*	-0.7590
CG6701	0.7516	*gcm2*	-0.7521
shn	0.6793	*dpn*	-0.7503
CG43689	0.6570	*vri*	-0.7502
CG14441	0.6026	*slp1*	-0.7203
slou	0.5649	*Eip74EF*	-0.6916
psq	0.5648	*mip40*	-0.6799
tio	0.5483	*Sfxn2*	-0.6700
kn	0.5199	*Abd-B*	-0.6165
		tll	-0.5989
		CG45071	-0.5422

Table 3.4 RBPs which change in the *syp* mutant
All RBPs that are altered in the *syp* mutant, compared to *wild type* (adjp < 0.05).

Upregulated in *syp* mutant	log2FC	Downregulated in *syp* mutant	log2FC
RpS5b	1.5542	*Syp*	-1.7714
vas	1.4961	*tut*	-1.1441
Thor	1.4925	*CG10889*	-1.0374
Imp	1.2212	*Rrp4*	-0.8563
solo	0.9848	*eIF4B*	-0.7647
nos	0.7134	*Smn*	-0.7422
larp	0.6855	*mEFTs*	-0.7227
LanA	0.6795	*Srp19*	-0.7204
RNaseP:RNA	0.6733	*CG9344*	-0.7166
CG10384	0.6107	*CG2931*	-0.6370
CG31140	0.5744	*mdlc*	-0.6121
eIF3b	0.4834	*CG10948*	-0.4810
eEF1alpha1	0.4387		

3.3.2 Changes in target transcript levels in the *syp* mutant

Intersecting the changes in transcriptome in the *syp* mutant, with the mRNA targets of Syp, can begin to narrow down transcripts regulated by Syp. Of the 642 mRNA binding targets of Syp, 14 (2.2%) are upregulated in a *syp* mutant, and 27 (4.2%) are downregulated (Figure 3.10) (Table 3.5). This is a surprisingly low proportion of the targets, suggesting that mRNA stability is not a major regulatory mechanism of Syp. The unchanged targets might not be regulated by Syp, or might be regulated through their localisation or translation. It also likely that more subtle regulatory changes in a small number of cells are not picked up by this genome-wide method.

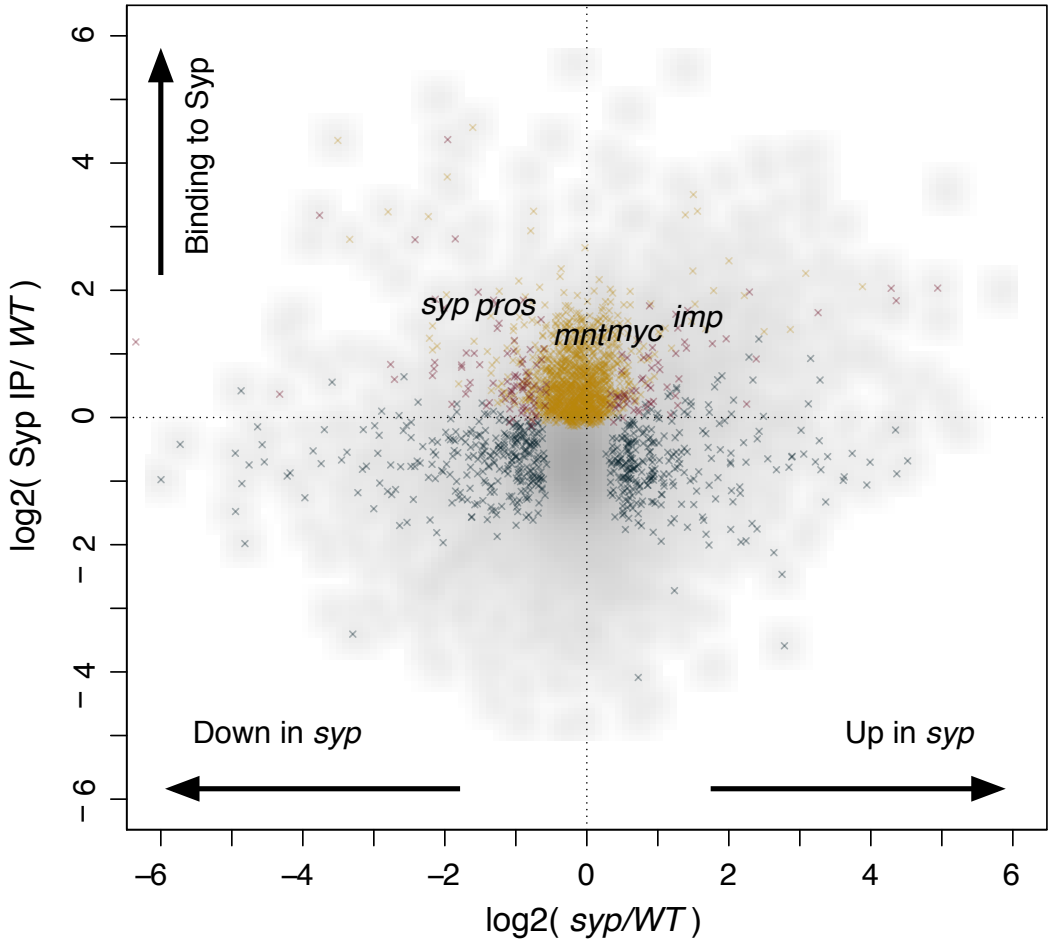


Figure 3.10 *syp* mutant data and overlap with targets
The changes in the *syp* mutant are co-visualised with their binding to Syp (Dr Aino Järvelin). All data points are shown in light grey, yellow crosses mark genes that are significantly IPd with Syp (padj < 0.1) but do not significantly change in the *syp* mutant. Green crosses mark genes that change significantly in RNAseq comparison to the *syp* mutant (padj < 0.10) but are not significantly IPd. Red crosses highlight genes that are significant in both comparisons.

Table 3.5 Syp targets changed in the *syp* mutant
All Syp targets (log2FC > 1, adjp < 0.01) which are altered in the *syp* mutant, compared to *wild type* (adjp < 0.05).

Syp targets Upregulated in *syp*	**log2FC**		**log2FC**
Thor	1.4925	*tx*	0.9331
Gs2	1.3325	*REPTOR*	0.8876
Imp	1.2212	*TpnC73F*	0.8635
CG13631	1.1452	*snoRNA:Psi18S-1377a*	0.8408
Rh50	1.0796	*Tsf1*	0.8158
CG32512	1.0095	*CG1673*	0.7819
Prm	0.9971	*fz2*	0.5768
Syp targets Downregulated in *syp*	**log2FC**		**log2FC**
Cpr49Ac	-2.1942	*cer*	-0.9020
bab1	-2.0660	*lft*	-0.8616
Syp	-1.7714	*CG6891*	-0.8593
CR44268	-1.7708	*Ilp6*	-0.8509
CG9192	-1.4630	*VepD*	-0.8354
Eip78C	-1.4408	*CG17124*	-0.7730
CR45242	-1.4130	*CG7860*	-0.7661
CR43283	-1.4096	*Cat*	-0.7242
pncr002:3R	-1.3301	*HIP-R*	-0.6969
Eip63F-1	-1.1565	*CG42240*	-0.6793
Eig71Ee	-1.1020	*CG42806*	-0.6530
CR43426	-1.0495	*CG2931*	-0.6370
CG31324	-0.9949	*Abd-B*	-0.6165
pros	-0.9479		

Imp protein is highly upregulated in the *syp* mutant and therefore its targets may also be dysregulated in the *syp* mutant. Therefore, I also examined which Imp targets are altered in the *syp* mutant. Of the 1109 Imp targets, 37 (3.3%) are upregulated in the

syp mutant, and 38 (3.4%) are downregulated (Table 3.6). Again this is a very small proportion of targets.

Table 3.6 Imp targets changed in the *syp* mutant
All Imp targets (log2FC > 1, adjp < 0.01) which are altered in the *syp* mutant, compared to *wild type* (adjp < 0.05).

Imp targets Upregulated in *syp*			
	log2FC		**log2FC**
Crg-1	1.9589	*CG31191*	0.7657
Gs2	1.3325	*Nlg3*	0.7557
CG33914	1.3179	*CG8910*	0.7538
CR44383	1.2901	*ImpL2*	0.7331
CG6470	1.2762	*GlcAT-P*	0.7297
CR42653	1.2753	*Col4a1*	0.7139
CG32650	1.2636	*ana*	0.7072
Imp	1.2212	*E(spl)m4-BFM*	0.7018
CG13631	1.1452	*Slob*	0.6584
CR45161	1.1284	*plum*	0.6531
Teh4	1.1265	*CG10384*	0.6107
CG8492	1.1180	*CG14441*	0.6026
Mur2B	1.0204	*CG43693*	0.5822
CG32512	1.0095	*CG31140*	0.5744
CG8301	0.9473	*kn*	0.5199
Arc1	0.9406	*CG13928*	0.5106
tx	0.9331	*CG17839*	0.4632
REPTOR	0.8876	*CG5065*	0.4311
CG13055	0.8468		
Imp targets Downregulated in *syp*			
	log2FC		**log2FC**
CG10936	-3.5438	*upd1*	-0.8750
dati	-2.0966	*ImpE1*	-0.8709
bab1	-2.0660	*CR45621*	-0.8645

Imp targets Upregulated in *syp*			
	log2FC		log2FC
CG6293	-1.8087	*Ift*	-0.8616
Syp	-1.7714	*CG6891*	-0.8593
Eip78C	-1.4408	*Ilp6*	-0.8509
CR45242	-1.4130	*VepD*	-0.8354
CR43283	-1.4096	*CG1463*	-0.8115
pncr002:3R	-1.3301	*CG17124*	-0.7730
Blimp-1	-1.2537	*CG14687*	-0.7556
CR44922	-1.1404	*Dh31-R*	-0.7073
St3	-1.0969	*Drep3*	-0.7014
Hr4	-1.0936	*CG17211*	-0.6997
CR43426	-1.0495	*HIP-R*	-0.6969
CG31324	-0.9949	*Eip74EF*	-0.6916
Lkr	-0.9741	*CG42240*	-0.6793
CG18467	-0.9549	*Abd-B*	-0.6165
pros	-0.9479	*SppL*	-0.5692
cer	-0.9020	*CG9003*	-0.5178

3.4 SELECTING TARGETS TO FOLLOW UP

Performing RIPseq of both Imp and Syp produced a huge list of potential targets for post-transcriptional regulation by these RBPs. Examining changes in the levels of these target transcripts in the *syp* mutant identified candidate genes which might be regulated at the level of mRNA stability. However, the brain is far from a homogenous mass of cells, and genes are highly likely to be regulated differently in different cell types. Regulatory processes in a small number of cells would likely be diluted in the RNAseq experiment. Therefore, there are opposing demands of identifying examples of post-transcriptional regulation in a high-throughput way, versus achieving cell type and spatio-temporal specificity.

Various genome-wide technologies are being adapted to provide improved spatio-temporal specificity and in the future this could be a very useful tool to further examine the Imp and Syp targets. For example, mRNA stability can be studied genome-wide using techniques such as pulse-chase with the uridine analog 4-thiouridine (4-sU) to label all newly synthesised mRNA and sequence to follow its life span (Mata and Wise, 2017). This 4-sU experiment can be made cell-type-specific using 4-thiouracil, by expressing the enzyme required for converting 4-thiouracil to 4-sU (uracil phosphoribosyltransferase) in specific cell types (Miller et al., 2009). This experiment could identify the targets with the most potential for post-transcriptional regulation. However, these methods are complex and time consuming to set up and optimise and so were beyond the scope of my thesis. Therefore, I explored microscopy techniques to investigate post-transcriptional regulation of individual genes.

3.4.1 Experimental rationale

I designed an approach to examine the regulation of each gene of interest, and its phenotype. I used immunofluorescence and smFISH to measure protein and mRNA levels in individual cells. I then used knockdown constructs to manipulate levels of Imp and Syp and quantitated the change in expression of the mRNA and protein.

I used smFISH as a quantitative measure of transcription and number of cytoplasmic mRNA transcripts. Briefly, for smFISH a collection of up to 48 short oligonucleotides are designed to hybridise along the mRNA of interest (Figure 3.11 A) (Femino et al., 1998). Each oligonucleotide probe is fluorescently labelled, resulting in a bright spot at each transcript with a low level of non-specific background binding signal. The number of cytoplasmic transcripts can then be counted. smFISH probes also bind to incomplete transcripts at the site of transcription. The intensity of these transcription

foci can be used to calculate the rate of transcription (higher transcription results in brighter transcription foci) (Bahar Halpern and Itzkovitz, 2016).

Observation of transcription, cytoplasmic mRNA and protein, provides insight into differences in regulation between cell types or mutants (Figure 3.11.B) (Yang et al., 2017b; Zenklusen, 2008). A discordance between mRNA and protein expression indicates post-transcriptional regulation. For example, if two cells have the same intensity of transcription foci but different levels of cytoplasmic mRNA, this suggests a difference in the transcript stability. If the cytoplasmic mRNA level of a gene is the same in two cells, but the level of protein is much higher in one, this suggests a higher rate of translation, or a lower rate of protein decay. There can also be more complex combinations of multiple levels of regulation. Comparison between *wild type*, *syp* knockdown and *imp* knockdown will indicate changes in the post-transcriptional regulation of the studied target.

I also needed to limit the biological scope of the analysis. The IF and smFISH staining are both done in whole dissected brains. However, the image acquisition and analysis is extremely time consuming and it is impractical to analyse the entire brain. I chose to focus on the type I NB lineages as these are the most numerous stem cells in the larval brain and have a very simple division hierarchy, with no intermediate amplifying progenitor cells. Type I NBs are also accessible for high quality imaging. Figure 3.12 A shows the type I NBs on the ventral side of the wL3 brain, as they will be imaged for the rest of this thesis. The type I NB is a large cell, surrounded by a cluster of its smaller progeny cells. I aimed to identify post-transcriptional regulatory events which explained the phenotypes of *imp* and *syp* in the type I NB lineages.

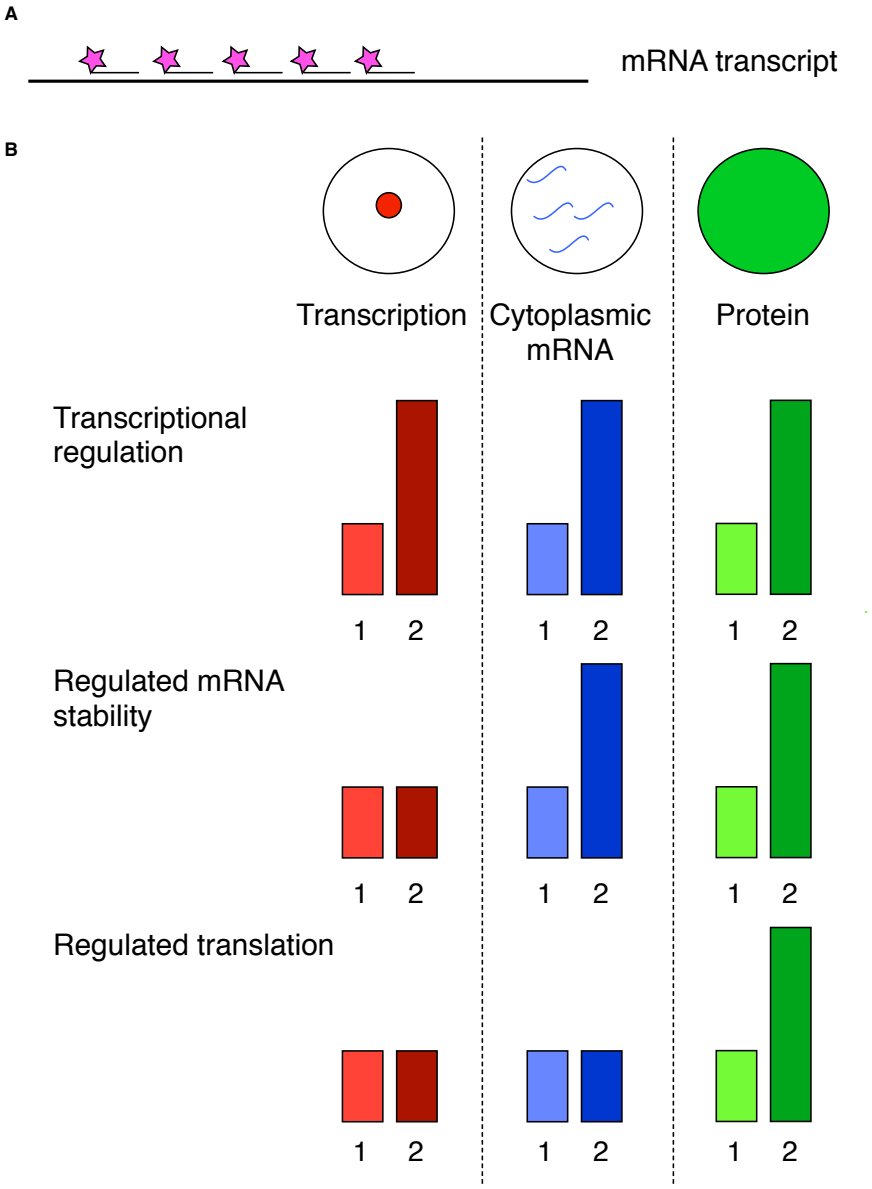


Figure 3.11 Diagram illustrating the microscopy experimental rationale
A In smFISH, up to 48 oligonucleotides are designed to tile a region of the transcript of interest. Each oligonucleotide is fluorescently labelled, producing good signal to noise ratio at each transcript so it can be counted. **B** Measurement of transcription rate, cytoplasmic mRNA and protein for a single gene provides information about differential regulation between two cell types or genotypes. Three examples are illustrated. Transcriptional regulation would be seen as different transcription foci intensities, leading to a change in cytoplasmic mRNA and then protein. Regulated mRNA stability would show similar transcription foci intensities but a change in the level of cytoplasmic mRNA and therefore protein. Finally, regulated translation would only show a difference in the level of protein, produced from the same amount of mRNA.

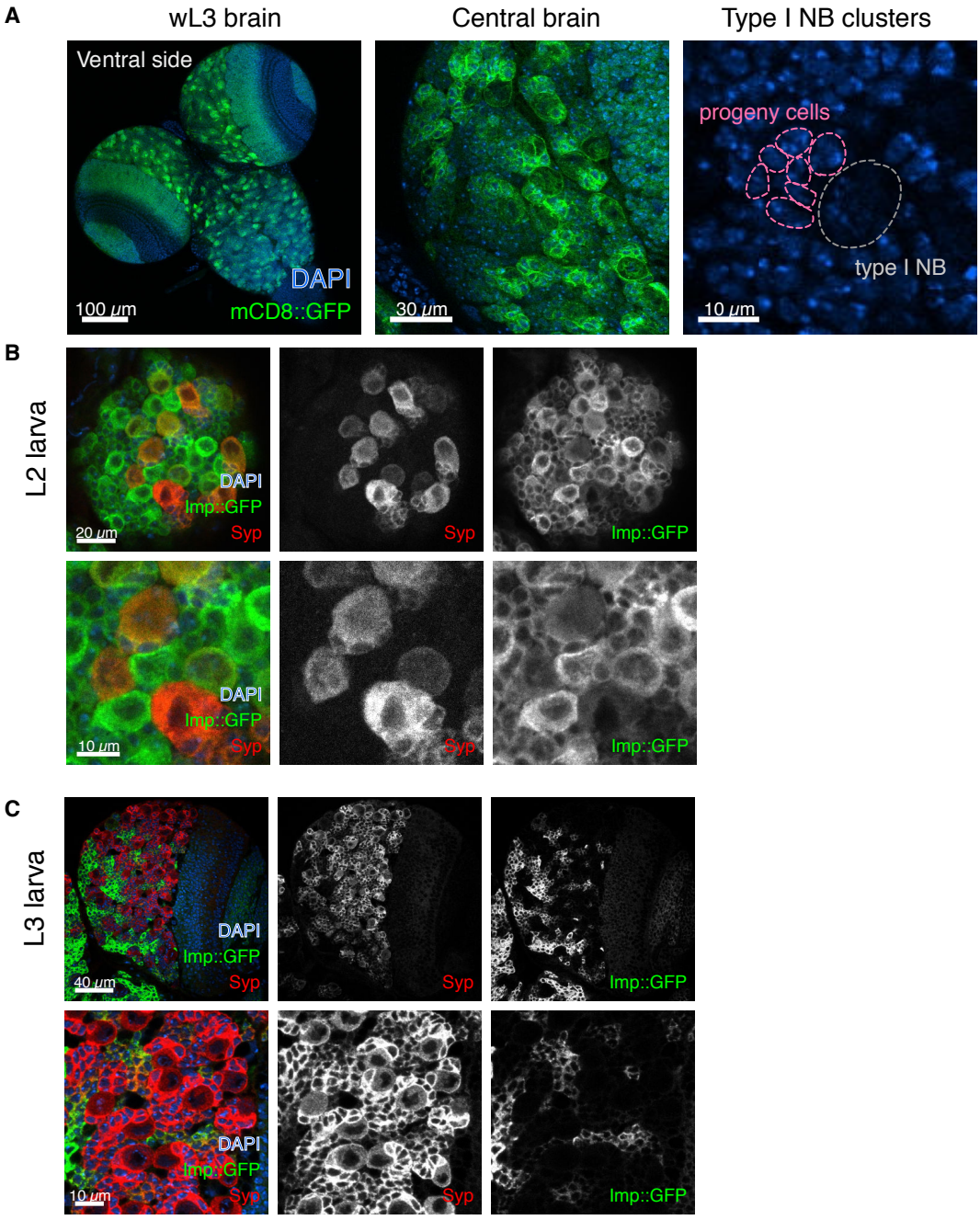


Figure 3.12 Imp and Syp expression

A Imaging the wL3 brains from the ventral side shows the type I NBs in the central brain (cell outlines shown with UAS-mCD8::GFP driven by insc-gal4). Increased magnification shows the large NB, surrounded by smaller progeny cells. Syp immunofluorescence staining in an *Imp::GFP* line shows expression of both RBPs in **B** L2 larval brains (36 h ALH) and **C** wL3 larval brains (wandering L3). In the L2 larva, **B**, both Syp and Imp are expressed in NBs. Higher Syp expression correlates with lower Imp expression. In the wL3 larval brain, **C**, Syp is expressed in type I NBs and their progeny, while Imp is absent from the NB and is expressed in mature neurons.

3.4.2 How do Imp and Syp behave in type I NBs?

Imp and Syp are expressed in opposing gradients in the MB NBs through larval development (Liu et al., 2015). This thesis focuses on the type I NBs in the central brain and therefore it was essential to understand the expression and regulation of Imp and Syp in these cells. IF staining for Syp was performed in an endogenously tagged *Imp::GFP* line (Toledano et al., 2012). This shows that both Imp and Syp are expressed in L2 NBs (Figure 3.12 B). At this stage, there is variation in levels of Imp and Syp between different NBs. NBs with higher Syp have lower levels of Imp, illustrating that different NBs have non-coordinated gradients of Imp and Syp. By the wL3 stage Syp is still found in the NB and progeny, but Imp is restricted to the older progeny cells and glial cells (Figure 3.12 C). Imp and Syp are both cytoplasmic in the NB and progeny cells.

I then examined how Imp and Syp regulate each other. In a *syp* mutant, Imp is highly upregulated in the type I NBs (Figure 3.13). This suggests that Syp represses Imp expression in the *wild type*. Imp and Syp levels can be more precisely manipulated using the GAL4/UAS system to drive overexpression or RNAi constructs in restricted cell types. The insc-GAL4 driver was used to drive UAS constructs in the NB and progeny (illustrated with UAS-mCD8::GFP in Figure 3.14 A).

Imp is undetectably low in *wild type* wL3 type I NBs, so Imp overexpression is the best tool to perturb Imp levels. Interestingly, Imp overexpression upregulates Imp levels in most progeny cells, but not the NB or GMCs (Figure 3.14 B). This might be because the high levels of Syp in these cells represses the Imp overexpression. This suggests that at the wL3 stage Syp represses Imp, but Imp cannot reciprocally repress Syp even if it is overexpressed. Syp is the dominant regulator.

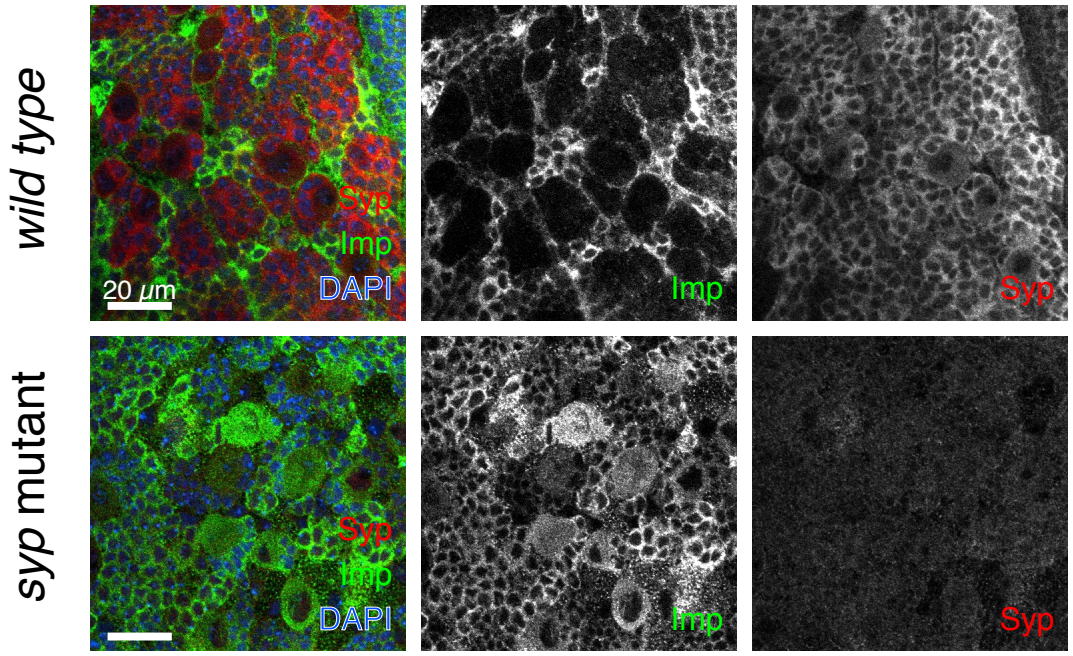


Figure 3.13 Syp represses Imp in type I NBs
Immunofluorescence against Imp and Syp in the wL3 brain, shows complete loss of Syp in the *syp* mutant. Imp is upregulated in the NB and early progeny cells in the *syp* mutant. This suggests that Syp represses Imp in the type I NB at the wL3 stage.

The mutual regulation of Imp by Syp makes it complicated to disentangle the regulatory effects of the two RBPs. Effects of Syp depletion may be directly due to the loss of Syp, or the consequent upregulation of Imp. A double knockdown of both Imp and Syp can distinguish these, as Imp is no longer be upregulated when Syp is removed (Figure 3.14 C).

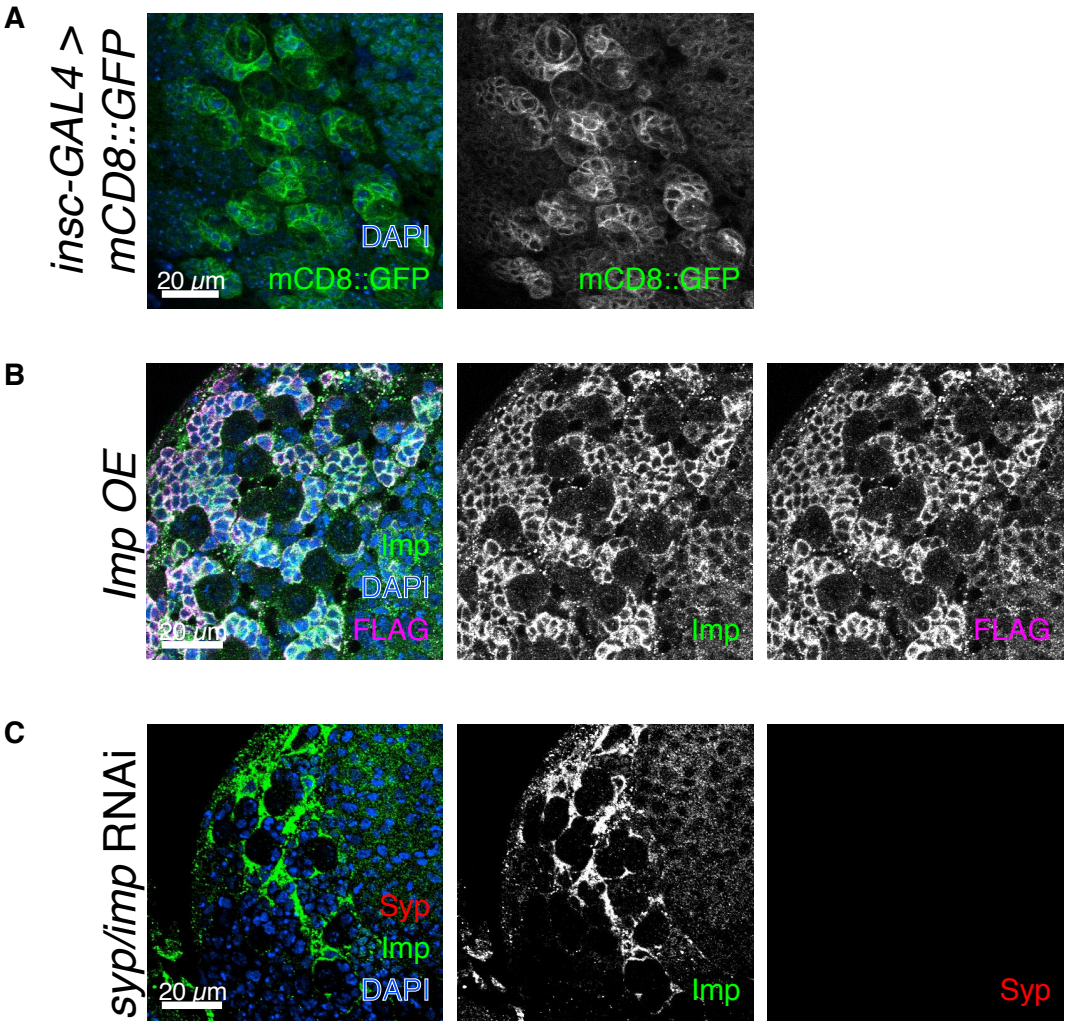


Figure 3.14 Manipulating Imp and Syp levels
A Insc-GAL4 driving the membrane bound UAS-mCD8::GFP shows the cells where insc-GAL4 acts. The UAS construct is expressed in the type I NBs and their progeny cells. **B** insc-GAL4 driving overexpression of a FLAG-tagged UAS-Imp construct, stained with anti-Imp and anti-FLAG immunofluorescence. Imp is upregulated in most progeny cells, but not in the NB or GMCs. **C** Double knockdown of Imp and Syp driven by insc-GAL4. Syp is lost, and there is no upregulation of Imp. Imp signal in the mature neurons and glial cells remains as insc-GAL4 does not drive the RNAi in these cells.

3.4.3 Phenotypes of *imp* and *syp* in type I NBs

I aimed to identify cases of post-transcriptional regulation by Imp and Syp in the type I NBs. I was specifically interested in the functional significance of this regulation, so I examined the phenotypes of Imp and Syp depletion in type I NBs. Dr Ching-Po Yang examined the role of Imp and Syp in NB termination, in a publication in which I am a co-author (Yang et al., 2017a). As discussed in section 1.5.3, Imp is responsible for

NB shrinkage, while Syp is required for the final symmetrical division. This phenotype can be assayed using Dpn staining in the pupa, in order to identify long-lived NBs which have not correctly terminated. We have also identified an enlarged brain in the *syp* mutant (Hailstone et al., 2018), so I asked whether Syp and Imp have phenotypes in type I NB behaviour in the larva. I developed assays to measure NB size, and division in the larva.

3.4.3.1 NB size

Dr Ching-Po Yang identified the role of Imp in regulating NB shrinkage in the pupa - overexpression of Imp prevents shrinkage (Yang et al., 2017a). This cell size effect is pronounced in the pupal stages, but it was not clear whether Imp regulates normal NB growth in the larva. I aimed to measure the effect of Imp and Syp on NB size in the larva. It is standard in the field to use diameter to measure NB size (Yang et al., 2017a). However, NBs are far from perfect spheres so volume is a much more accurate measurement of size and is likely to identify smaller differences in NB size between different strains. Therefore, I measured NB volume using phalloidin dye to stain the cortical actin (Figure 3.15 A). There is a significant increase in NB size in the *syp* knockdown, while *imp* and *syp* double knockdown has no change in NB size (Figure 3.15 B). This experiment shows that the increase in NB size in the *syp* RNAi is caused by the subsequent upregulation of Imp, as the phenotype is lost in the double knockdown. Therefore, Imp regulates NB size in the larval type I NBs.

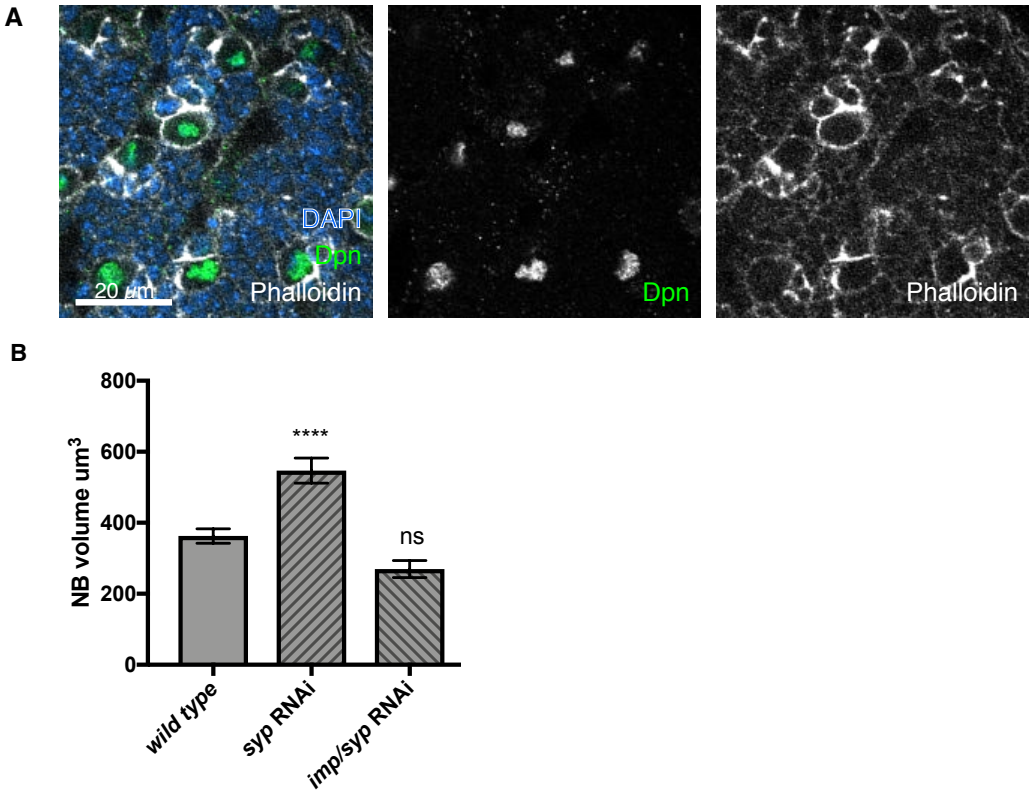


Figure 3.15 Imp regulates type I NB size in the larva
A Phalloidin dye was used to stain F-actin, clearly marking the perimeter of the NB. The NB is marked with Dpn. The phalloidin outline was used to measure the volume of the NB. **B** The volume of type I NBs was calculated. *syp* RNAi has significantly larger NB than *wild type*, while the *imp/syp* RNAi has no change in NB size from *wild type.* Measurements were taken from images of at least 9 different brains, in at least 3 technical replicates. *wild type* n = 20, *syp* RNAi n = 19, *imp/syp* RNAi n = 14. Significance was calculated using a One-way ANOVA and Dunnett's multiple comparisons test with comparison to the *wild type* n.s. not significant, **** $p < 0.0001$

3.4.3.2 Mitotic index

In order to examine the proliferation rate of the type I NBs when Imp and Syp levels were manipulated, I measured the mitotic index. Mitotic index is the proportion of cells in mitosis, measured in fixed samples using a phospho-histone 3 (pH3) staining (Figure 3.16 A). Histone 3 phosphorylation is tightly correlated with chromatin condensation during mitosis. Samples were costained with Dpn to mark NBs. The mitotic index is the number of Dpn +ve, PH3 +ve cells, divided by the total number of Dpn +ve cells. Assuming a constant length of mitosis, a higher mitotic index indicates a faster division rate.

The mitotic index of the *wild type* NBs was 0.18 (Figure 3.16 B). There were no significant differences in the different genotypes tested, except a significant increase in mitotic index up to 0.27 in the *imp* overexpression. This indicates an increased proliferation rate. Although the changes were not significant, there was also an increase to 0.24 in the *syp* RNAi, while *imp/syp* double knockdown was reduced to 0.14. Collectively, this suggests that elevated Imp promotes increased type I NB proliferation.

Manual counting of NBs to calculate the mitotic index is extremely time consuming and therefore n numbers in this experiment are low, reducing the statistical power. An automated counting method (such as QBrain/CytoCensus (Hailstone et al., 2018)) to identify NBs would allow collection of much larger n numbers and may show significance in small differences. The measurement of mitotic index to indicate changes in division rate assumes a constant length of mitosis. In most cases this is true, as most changes in cell cycle length come from shortening or lengthening of the Gap phases, but if there were changes in mitosis length, this method would not be valid. The method also measures a snapshot in time. This might be misleading if the NB divisions are coordinated. In my data I do not see evidence of any coordination of mitosis and this is supported by live imaging done in the lab (Hailstone et al., 2018).

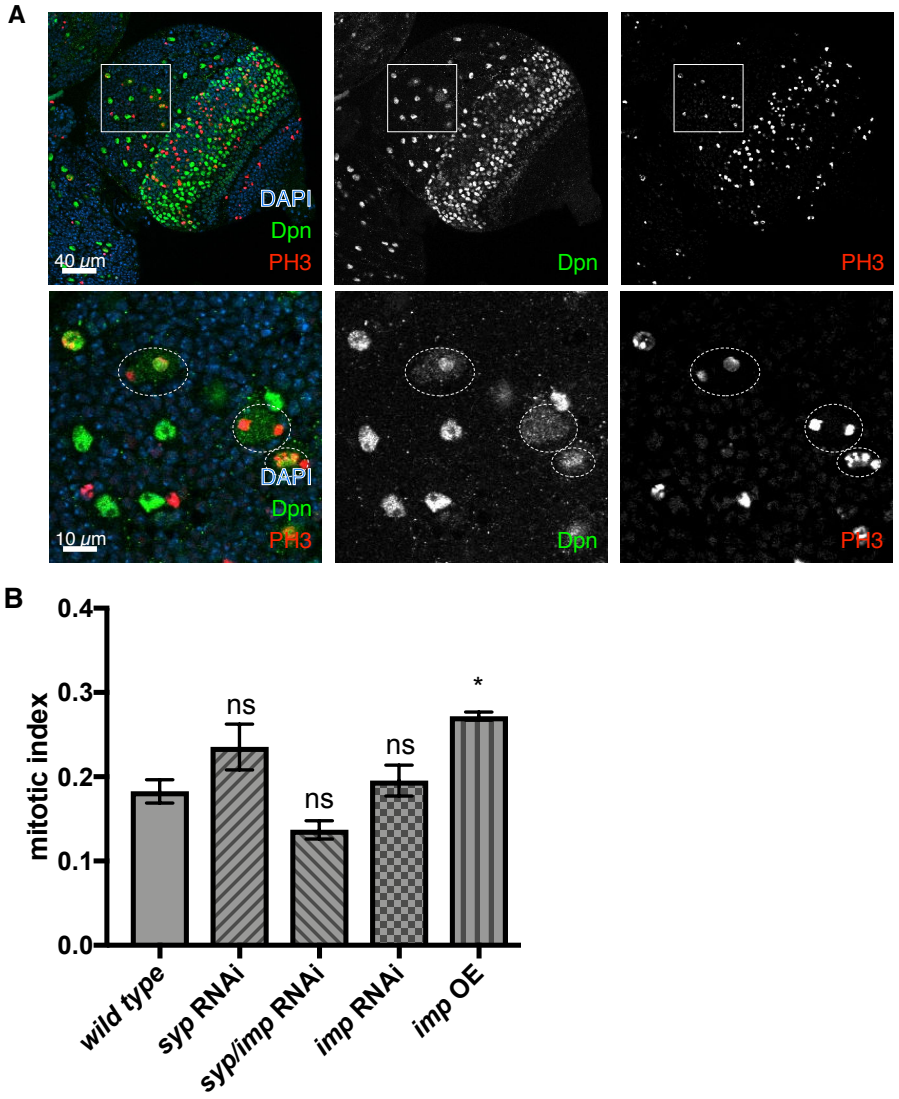


Figure 3.16 Imp overexpression increases NB mitotic index
A Co-staining of Dpn, marking NBs, and phospho-histone 3 (PH3), marking mitotic cells, in *wild type* larval brains. In the magnified view, white dotted lines mark NBs which are also positive for PH3, i.e. mitotic NBs. **B** The mitotic index is calculated as the number of Dpn +ve, PH3 +ve cells, divided by the total number of Dpn +ve cells. This is the proportion of cells in mitosis. The *wild type* mitotic index is 0.18. There is no significant difference in the *syp* RNAi, *syp/imp* RNAi or *imp* RNAi. The *imp* overexpression shows a significant increase in mitotic index. *wild type* n = 7, *syp* RNAi n = 9, *imp/syp* RNAi n = 5, *imp* RNAi n = 4, *imp* overexpression n = 5. Significance was calculated using a One-way ANOVA and Dunnett's multiple comparisons test with comparison to the *wild type* n.s. not significant, * $p < 0.05$

3.4.3.3 EdU labelling

I also explored a second approach to examine NB division rate. I used an S phase labelling method to count the number of progeny cells produced by each NB over a set period of time. wL3 larval brains were dissected and cultured in brain culture medium with 5-ethynyl-2-deoxyuridine (EdU) for 4 hr. Brains were then fixed and a Click chemistry kit (invitrogen) was used to visualise the labelled DNA (Figure 3.17 A). Every cell which has been through an S phase is labelled, therefore including all progeny cells from NB divisions during this time. The reported NB cell cycle duration is 90 minutes, so we would expect to see around 3 labelled progeny cells in four hours. In the *wild type* there was an average of 3.2 progeny per NB, which is approximately what was expected (Figure 3.17 B). The number of progeny was significantly increased in the *syp* mutant (4.2 progeny) and Imp overexpression (5.0 progeny). This supports the evidence from the mitotic index experiment that Imp elevation increases NB proliferation rate.

3.4.3.4 Live imaging

The best way to study the division rate of the type I NBs would be to image the divisions directly. Martin Hailstone in the Davis lab has optimised a protocol to continuously image dissected wL3 larval brains *ex vivo* (Hailstone et al., 2018). This allows direct visualisation of NB divisions and can therefore be used to calculate the division rate. This protocol has been further improved to reduce photo-toxicity, which was affecting the NB division rate. Preliminary results suggest that *syp* RNAi brains show faster NB divisions. When the new result has been validated, the technique will be applied to measure the NB division rates in Imp/Syp depleted brains as well as in depletions of any targets of interest.

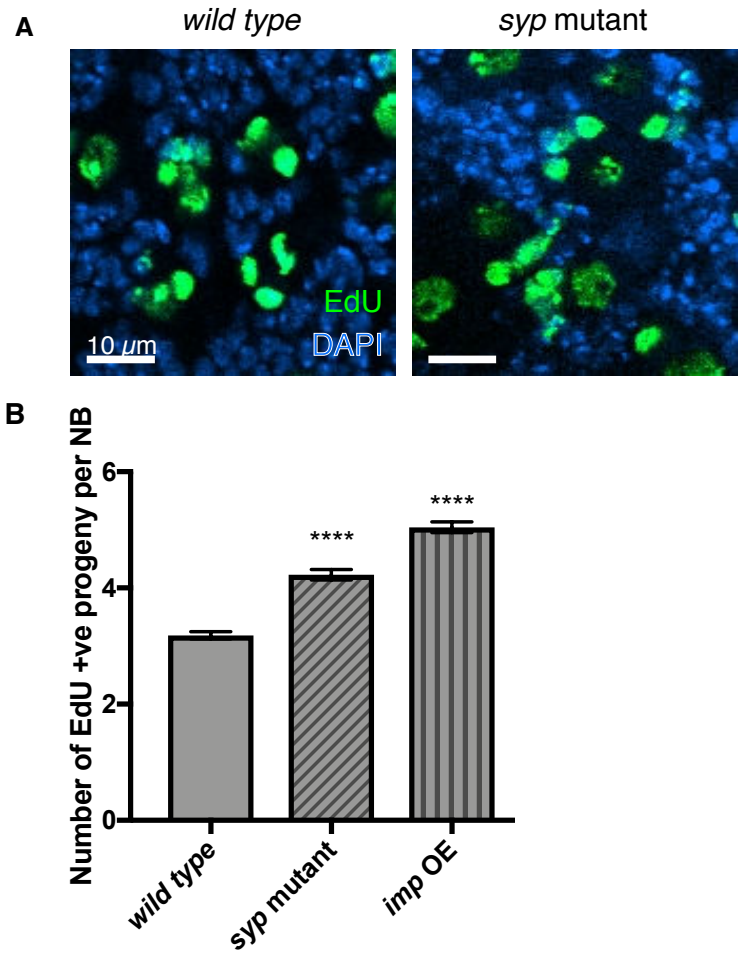


Figure 3.17 Imp overexpression increases rate of progeny production
A *wild type* larval brains were incubated with EdU for 4 hr, allowing incorporation of EdU into DNA during synthesis. Click chemistry was used to stain and visualise the EdU. All cells which underwent DNA synthesis in S phase are stained with EdU. For each NB the number of labelled progeny were counted, indicating the number of NB divisions within the 4 hr incubation period. **B** The average number of progeny cells labelled in the *wild type* was 3.2. The *syp* mutant showed an increase to 4.2, and the *imp* overexpression was even higher at 5.0. *wild type* n = 147, *syp* n = 66, *imp* OE n = 67. Significance was calculated using a One-way ANOVA and Dunnett's multiple comparisons test with comparison to the *wild type.* **** $p < 0.0001$.

3.4.4 Choosing targets to follow up

I aimed to identify examples of post-transcriptional regulation by Imp and Syp which play a key role in in neurogenesis, focusing on three phenotypes of Imp and Syp: NB size, proliferation and termination. The assays above were used to examine the roles of the targets of interest. I used a gene-by-gene approach, so I first selected genes to follow up. I was particularly interested in genes with human homologs, and those with

human disease links. For practical reasons, I selected targets with available tools such as RNAi or overexpression lines, and antibodies. I initially limited my inquiries to TFs, and used the literature to identify targets with a known role in NB regulation, or progeny fate.

I chose to follow up the Myc transcriptional complex (Chapter 4) and to develop the work of a previous DPhil student Dr Lu Yang on Prospero (Chapter 5). I also briefly examined the regulation of the Mediator complex, in collaboration with Dr Ching-Po Yang (section 4.5). Other targets are already being followed up by other members of the Davis lab, and further examples of post-transcriptional regulation have been identified.

3.5 CONCLUSION AND DISCUSSION

The RBPs Imp and Syp have been shown to characterise NB age through development (Liu et al., 2015). The relative levels of Imp and Syp determine the fate of progeny cells, and the termination of the NB divisions in the pupa (Yang et al., 2017a). RBPs act through post-transcriptional regulation of their cohort of target mRNAs, controlling their fate and altering the levels or localisation of the encoded proteins. Therefore, I aimed to identify the mRNA targets of Imp and Syp in order to understand their regulatory functions.

I used RIPseq in larval brain lysates, and Dr Aino Järvelin performed differential expression analysis to identify the mRNA targets of Imp and Syp. These targets are potentially post-transcriptionally regulated by Imp or Syp, and may be responsible for the phenotypes observed when Imp or Syp levels are manipulated. Both Imp and Syp have a large number of mRNA targets, and share a cohort of over 350 targets.

The targets are enriched for transcripts encoding TFs and RBPs, suggesting that Imp and Syp coordinate a complex regulatory network.

Analysis of the Imp and Syp targets, in collaboration with Dr Aino Järvelin, showed an enrichment of targets with long 3' UTRs. This might reflect a preference of Imp and Syp for binding to long 3' UTRs, or may be due to the increased probability of RBP binding sites in a longer 3' UTR. Comparing the targets of other RBPs in the brain could provide insight into whether this is a general phenomenon, or a specific preference of Imp and Syp. Furthermore, the current analysis does not examine whether the long 3' UTRs are actually expressed in the brain, or pulled down in the RIP experiments. Many transcripts have isoforms with different lengths of 3' UTRs, so different 3' UTR isoforms may be expressed in different cell types. It is known that transcripts express elongated 3' UTRs in neurons, mediated by Elav binding (Hilgers et al., 2012; Hilgers, 2011). Selective extension of the 3' UTR in specific cell types could alter the fate of the mRNA, due to the different binding of RBPs such as Imp and Syp. Therefore, understanding the isoforms bound by Imp and Syp could provide insight into their regulation, and this would be useful future analysis.

I performed RNAseq comparing the transcriptome of *wild type* and *syp* mutant larval brains. This experiment might determine if any targets are regulated at the level of mRNA stability, as their level in the transcriptome would be changed in the mutant. Surprisingly, relatively few Syp or Imp targets were significantly changed in the mutant. This may be because altered regulation in a small number of cells (e.g. NBs) was diluted in the whole brain transcriptome and therefore did not produce a statistically significant fold change. There are also gross differences between the *wild type* and *syp* mutant brains. This may mean the numbers of different cell types are changed, making direct effects of Syp or Imp binding difficult to distinguish.

Imp and Syp both have several hundred mRNA targets. An approximately equal number were upregulated and downregulated in the *syp* mutant. Therefore, it was not possible to make any single general conclusion about the mechanism of action of these RBPs. It is likely that the RIPseq targets include indirectly bound mRNAs, non-functionally bound mRNAs, and mRNAs which are regulated at the levels of mRNA stability, localisation and translation. There are genome-wide methods which could be pursued to identify post-transcriptional regulation, which will be considered in future to further understand the regulation of Imp and Syp. However, in this thesis I chose to select a few targets to examine in more detail.

I designed an approach to investigate both the regulation (using smFISH and IF) and function (using phenotype analysis) of the targets. This approach provides spatio-temporal specificity and a detailed understanding of key targets, but is extremely low throughput. I focused on the role of Imp and Syp in the type I NB lineage and specifically on the phenotypes of NB size, proliferation and termination. I then selected promising targets to follow up. Therefore, in the subsequent chapters I examine the regulation of the Myc transcriptional complex (Chapter 4) and the pro-differentiation TF, Prospero (Chapter 5). These examples are important to increase our understanding of key regulatory processes, but also illustrate the importance of post-transcriptional regulation in neurogenesis.

4.

MYC IS POST-TRANSCRIPTIONALLY REGULATED TO CONTROL NB SIZE

4.1 INTRODUCTION

In the previous Chapter, I identified the mRNA targets of Imp and Syp in the brain. I then designed an approach to study the regulation and function of individual targets, focusing on their roles in the type I NB. I was particularly interested in targets regulating NB size, proliferation and termination. Among these targets was *myc,* the *Drosophila* homolog of the human proto-oncogene *c-myc*. Myc is a transcription factor, and regulates cell growth and proliferation (Grandori et al., 2000) (discussed in more depth in section 1.2.3). Therefore, Myc could be the key target explaining the regulation of NB size and division rate by Imp and Syp. Imp has been shown to regulate NB shrinkage in the pupa (Yang et al., 2017a), and in the previous Chapter I showed that Imp regulates NB size and division rate in the larva. Multiple pathways of cell size regulation act via Myc, making it a very interesting target to examine further, in order to determine the basis of the Imp and Syp phenotypes.

I identified *myc* as a target of both Imp and Syp. *mnt*, another member of the Myc TF network, was also a target of both RBPs. In mammalian systems, Myc is a member of a group of bHLHZip TFs, also including Mnt, Mga and Mad (Grandori et al., 2000). Each of these TFs can form a heterodimer with Max (another bHLHZip TF), allowing DNA binding and transcriptional modulation (Blackwood and Eisenman, 1991). Each heterodimer binds to E-box binding sites, and activates or represses transcription of a set of genes, depending on the binding partner. This regulation occurs partly via the recruitment of histone deacetylases to alter the chromatin environment. Max is constitutively expressed and stable, but its activity depends on its binding partner. On the other hand, the partner TFs are unstable and have highly regulated expression. Tight regulation of partner availability determines which heterodimers are formed and therefore the effects on transcription. Myc and Mad have direct homologs in *Drosophila*, while the *Drosophila* Mnt has regions characteristic of both the mammalian Mad and Mnt. Both *myc* and *mnt* are targets of Imp and Syp in my RIPseq experiments. I hypothesised that the balance of regulation by Imp and Syp controls the levels of Myc and Mnt in the NB, determining the active heterodimers formed.

The Myc transcriptional network regulates cell division and growth and therefore could be responsible for the NB size and division phenotypes of Imp and Syp. In mouse, *c-myc* overexpression in NSCs leads to overproliferation, while *c-myc* knockdown in NSCs leads to a small brain (Swartling, 2012). *Drosophila* Myc (originally named Diminutive) was identified in a yeast two-hybrid screens using human Max as bait (Gallant et al., 1996). Human Myc rescues *Drosophila myc* mutants, suggesting that many functions are conserved (Benassayag et al., 2005). Mosaic analysis in the *Drosophila* wing disk showed that loss of Myc reduced cell size, while overexpression of Myc increased cell growth and size (Johnston et al.,

1999). Furthermore, in these experiments Myc overexpression promotes progression through the G1/S transition of the cell cycle in the wing disk, leading to a shortened G1 phase. However, this is insufficient to increase cell division rate when String (Stg, Cdc25), which controls the G2/M transition, is limiting. As in mammalian systems, *Drosophila* Mnt antagonises Myc activity. *mnt* mutants show phenotypes similar to Myc overexpression: larger adult flies and increased cell size (Loo et al., 2005). Myc must overcome the repressive effect of Mnt in order to activate genes for growth (Pierce et al., 2008).

I hypothesised that Imp and Syp bind and post-transcriptionally regulate *myc* and *mnt* in the NB. In developmental biology, Myc is generally thought to be regulated at the level of transcription: it is transcriptionally activated downstream of the TOR and PI3K/AKT signalling pathways (Hietakangas and Cohen, 2009). Myc and Mnt have not been implicated directly in regulation of the type I NB. However, the TOR and PI3K/AKT pathways are known to regulate nutrient-dependent NB growth and exit from quiescence in the early larva (Sousa-Nunes et al., 2011). It has been suggested that Myc is the downstream effector in NB exit from quiescence, leading to increased NB growth in the early larva (Hovhanyan et al., 2014). However, the transcriptional regulation of Myc may not be the whole story. Imp and Syp bind *myc* and *mnt,* and therefore these targets may also be post-transcriptionally regulated.

In Chapter 3, I presented RIPseq data showing that Syp and Imp bind to the mRNAs encoding both Myc and Mnt. However, pulldown in a RIPseq experiment does not mean there is a direct binding event *in vivo* in the NB, or that any binding event is functional. It is necessary to validate and explore the targets further on a gene-by-gene basis, both in the *wild type* and after depletion of the RBPs, Imp and Syp. In the current Chapter I ask: do Imp and Syp regulate Myc and Mnt in Type I NBs? Are Myc

and Mnt responsible for the phenotypes of *syp* and *imp*? I use smFISH and IF to quantitate the levels of *myc* transcripts and protein, and compare to Imp or Syp depleted brains. I then compare the phenotype of *syp* and *imp* depletion to *myc* overexpression using assays to measure cell size and division rate.

First, I examined the expression of Myc and Mnt in the *wild type* larval brain, and whether they show signs of post-transcriptional regulation. This is often seen as a discordance between the levels of transcription, mRNA and protein, suggesting regulation at intermediate stages. I then compared this expression to Imp and Syp depleted brains and found that Myc, but not Mnt, is regulated by Imp and Syp. I then used smFISH to count *myc* transcript numbers and to calculate *myc* transcription rate and mRNA half life in individual NBs, with manipulated levels of Imp or Syp. I used genetic methods to distinguish the effects of Imp and Syp, and found that elevated Imp stabilises *myc* mRNA, increasing Myc protein. This leads to increased NB size and cell division rate. I wanted to explore the mechanism of Imp regulation of *myc* in more detail so I then examined Imp binding data and used CRISPR technology to produce endogenous deletions at the *myc* locus to abolish Imp binding to the *myc* transcript.

4.1.1 Specific aims

1. To investigate the effect of Imp and Syp on Myc and Mnt regulation
2. To quantitate the effect of Imp and Syp on *myc* transcription rate and half life
3. To identify phenotypes of Myc dysregulation in NBs
4. To make CRISPR deletions at the *myc* locus to disrupt Imp binding

4.2 IS MYC OR MNT LEVEL REGULATED BY IMP/SYP?

myc and *mnt* mRNAs were identified as binding targets of both Imp and Syp in my RIPseq experiments. I aimed to understand the NB size and division phenotype of *imp* or *syp* knockdown, so I decided to focus on the Myc transcriptional network because of its involvement in cell size and cell cycle progression in other systems. If binding by Imp or Syp is functional, their depletion would be expected to alter either the expression level or localisation of Myc or Mnt protein, via regulation of their mRNA. To test these possibilities, I investigated Myc and Mnt expression using IF and smFISH.

4.2.1 Where are Myc and Mnt expressed?

I first wanted to understand how Myc and Mnt are expressed and regulated in different cell types in the *wild type* brain. I examined *myc* and *mnt* mRNA and protein expression in the *wild type* brain and looked for any discordance, a hallmark of post-transcriptional regulation (illustrated previously in Figure 3.11). To examine Myc protein distribution, I performed antibody staining against Myc in the larval wL3 brain (Figure 4.1 A). Consistent with previous publication (Betschinger et al., 2006), Myc protein was nuclear, and found only in the NB, which is specifically labelled with Dpn. The levels of Myc protein are very low in the NB, and the antibody showed fairly high levels of background in all cells of the brain.

Myc protein distribution might be regulated by the levels of *myc* mRNA in different cells. I designed smFISH probes against the *myc* intron and exon, to visualise cytoplasmic *myc* transcription foci and cytoplasmic transcripts (Figure 4.1 B). The

individual coding exons of *myc* were too short to allow a full 48 smFISH probe set. Therefore, I split the probes across both coding exons, which are adjacent to each other in the mature spliced mRNA. The smFISH showed that *myc* is transcribed in both NBs and progeny cells (Figure 4.1 C). There were relatively low levels of cytoplasmic *myc* mRNA in all of the cells. Interestingly, unlike the Myc protein, *myc* mRNA is not restricted to the NB. I conclude that *myc* is likely to be regulated post-transcriptionally, perhaps through translational repression in the progeny cells.

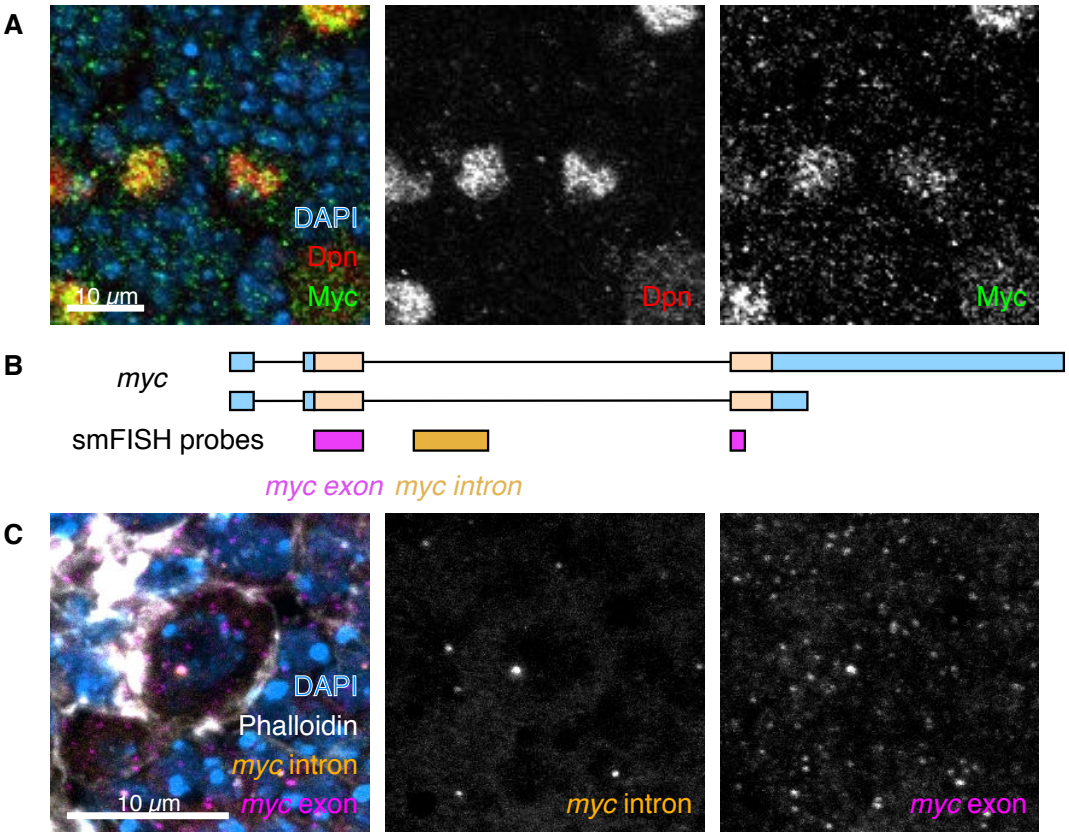


Figure 4.1 Myc protein, but not *myc* mRNA, is restricted to the NB
A IF shows Myc protein expression is restricted to the NBs, marked by Dpn. **B** smFISH probes were designed against the *myc* exons and intron. **C** smFISH against the *myc* intron and *myc* exon shows *myc* is transcribed in both the NB and progeny cells. There are fairly low levels of cytoplasmic mRNA in all cells of the NB lineage. The cell boundaries are marked using phalloidin.

I performed analagous experiments to examine the protein and mRNA expression of Mnt. I found that Mnt protein is nuclear, as expected, and is expressed in all cells of the type I NB lineage (Figure 4.2 A). I then designed smFISH probes against the Mnt

intron and exon. I found that *mnt* is expressed in all cells of the lineage (Figure 4.2 B). This suggests that Mnt is not differentially post-transcriptionally regulated within the tissue. Examining expression with manipulated RBP levels provides more insight into post-transcriptional regulation.

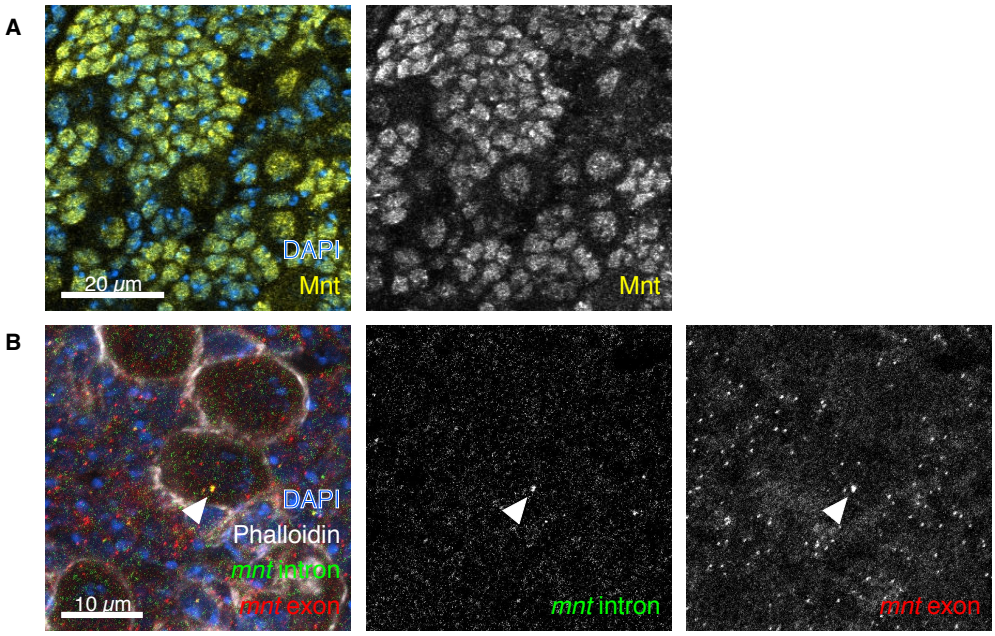


Figure 4.2 Mnt protein and mRNA is expressed in NBs and progeny
A IF shows Mnt protein is expressed in all cells of the type I lineage. **B** smFISH against the *mnt* exon and *mnt* intron shows *mnt* mRNA is also found in all both the NB and progeny cells. This does not indicate any differing post-transcriptional regulation.

4.2.2 Are Myc or Mnt levels regulated by Imp/Syp?

In Chapter 3, I present RIPseq data showing that *myc* and *mnt* mRNA are bound by both Imp and Syp, making these RBPs possible candidates for post-transcriptional regulation of Myc or Mnt level. In order to investigate potential regulation of Myc by Syp, I used IF to visualise Myc levels in *syp* mutants, with Dpn staining to mark NBs (Figure 4.3 A). This shows that Myc is increased in NBs in the *syp* mutant compared to *wild type* (quantitated in Figure 4.3 B), and this increase is restricted to the NBs. Loss of Syp in the NB leads to a derepression of Imp (as discussed in section 3.4), so the increase in Myc level in the *syp* mutant could be due to the loss of Syp or the consequent increase in Imp. As discussed in section 3.4.2, Imp overexpression is not

possible in the wL3 NB, likely due to repression by the high levels of Syp. Therefore, an Imp OE line cannot be directly compared to the genotypes shown here. Instead, I repeated the IF experiment in a *syp/imp* double RNAi knockdown. If the increase in Myc is simply due to the loss of Syp, the *syp/imp* double knockdown will also lead to an increase in Myc. However, if elevated Imp is responsible, the double knockdown will not show Myc upregulation. The IF experiment showed that Myc levels were similar to *wild type* in the *syp/imp* double knockdown flies (Figure 4.3 B). This suggests that Myc is increased in the NB via upregulation of Imp.

I used IF to examine Mnt levels in the *syp* mutant and found no difference to the *wild type* (Figure 4.3 C). This suggests that Mnt is not regulated by Imp and Syp. Therefore, I only continued to investigate the regulation of Myc.

Imp may regulate Myc in NBs at the level of transcription, mRNA stability or translation. In the previous section, I showed evidence that Myc may be translationally repressed in the progeny cells. Imp and Syp do not appear to be involved in this regulation, as Myc protein is restricted to the NB in all genotypes studied. Therefore, I focused on the regulation of Myc specifically in the NB, where the Imp upregulation leads to increased Myc levels.

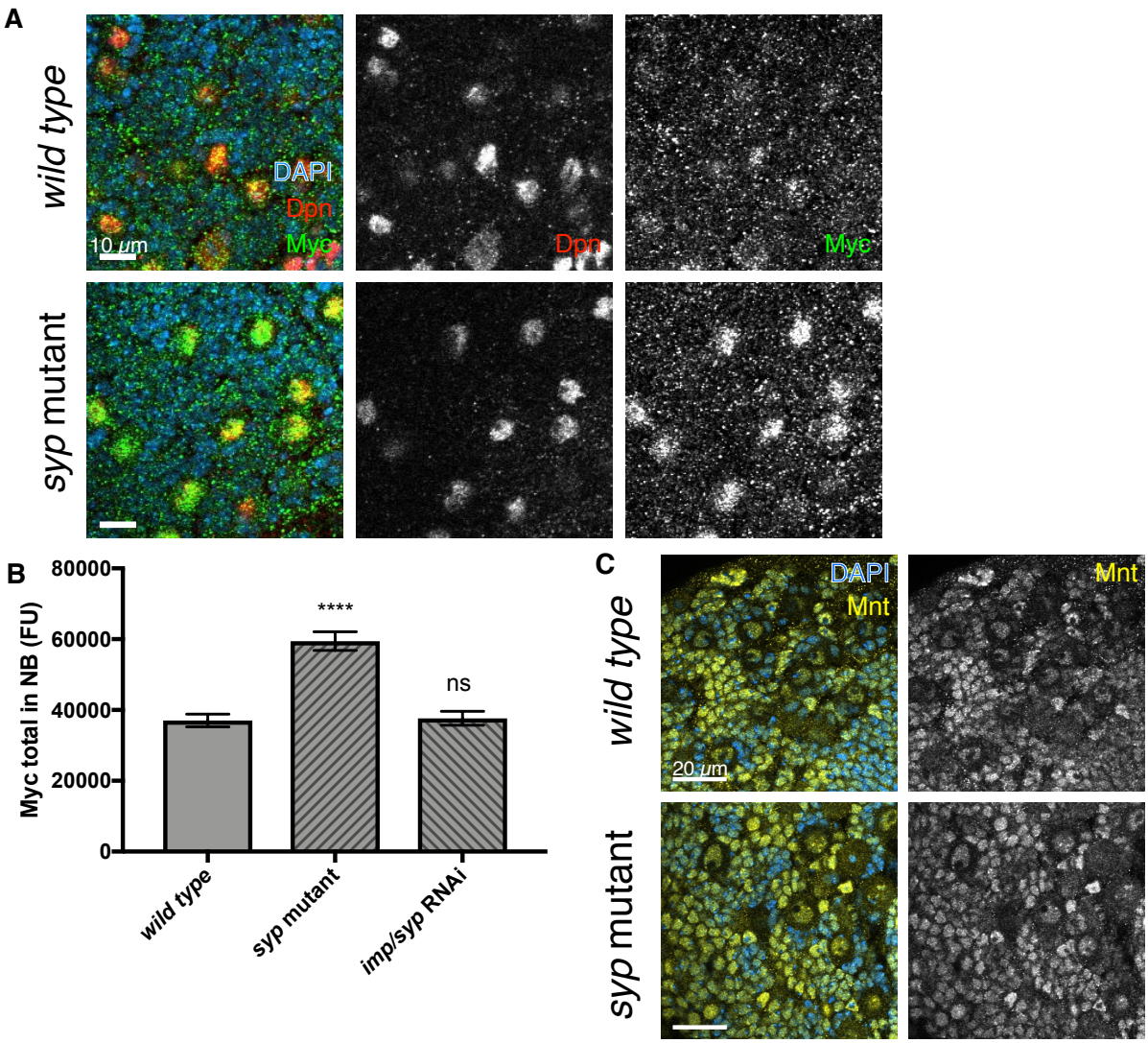


Figure 4.3 Myc, but not Mnt, level is regulated by Imp
A IF shows higher Myc levels in *syp* mutant NBs, compared to *wild type* NBs. NBs are marked with Dpn. **B** Quantitation of Myc protein level in type I NBs shows a significant increase in the *syp* mutant, but no change in a *imp/syp* double knockdown. FU: fluorescence units. Significance calculated using a one-way ANOVA and Dunnett's multiple comparisons test with comparison to the *wild type.* ns = not significant, **** $p < 0.0001$. **C** IF shows that Mnt level is unchanged in the *syp* mutant, suggesting that it is not regulated by Syp or Imp.

4.2.3 Which isoform of *myc* is expressed in NBs?

Myc levels are increased when Imp levels are elevated, suggesting that Imp regulates Myc. Transcript isoform choice can affect the regulatory processing of an mRNA species due to the differential inclusion of RBP binding sites. Therefore, I examined the annotated *myc* transcripts. The *myc* gene structure is fairly simple: there are two mRNA isoforms which differ only in their 3' UTR (Figure 4.4 A). Each

transcript has two identical coding exons totalling 2154 b, producing a 717 amino acid polypeptide. The *myc*^{short} isoform has a 699 b 3' UTR, while the *myc*^{long} isoform 3' UTR is 6385 b. This 3' UTR extension of almost 5.7 kb is likely to provide additional binding sites and regulatory elements.

In order to study *myc* isoform expression in NBs, I designed smFISH probes specifically against the *myc*^{long} isoform 3' UTR (position illustrated in Figure 4.4 A). Co-staining with smFISH probes against the common *myc* exon and *myc long* allowed an assessment of the isoform of transcripts present in the NB (Figure 4.4 B). The NB transcription focus is indicated with the white arrow, showing transcription in both channels (*myc* is on the X chromosome so in this male larva there is only a single site of transcription, for simplicity only male larvae were used for quantitations). All cytoplasmic smFISH spots in the exon channel also show signal in the *myc long* channel. This suggests that most, if not all, *myc* transcripts in the NB are the long isoform with 3' UTR extension.

I wanted to know which isoform of *myc* is bound by Imp. RIPseq does not give specific binding site information, but it can indicate which transcript isoforms are bound. Examining the Imp RIPseq data at the *myc* locus shows the alignment of reads (Figure 4.4 C). If Imp specifically bound to *myc*^{short}, there would be very few reads aligning to the *myc* extended 3' UTR, and there would be a significant drop in signal after the short 3' UTR. This drop is not seen and there are reads in the 3' UTR extension, which suggests that Imp binds to *myc*^{long}, possibly in addition to *myc*^{short}.

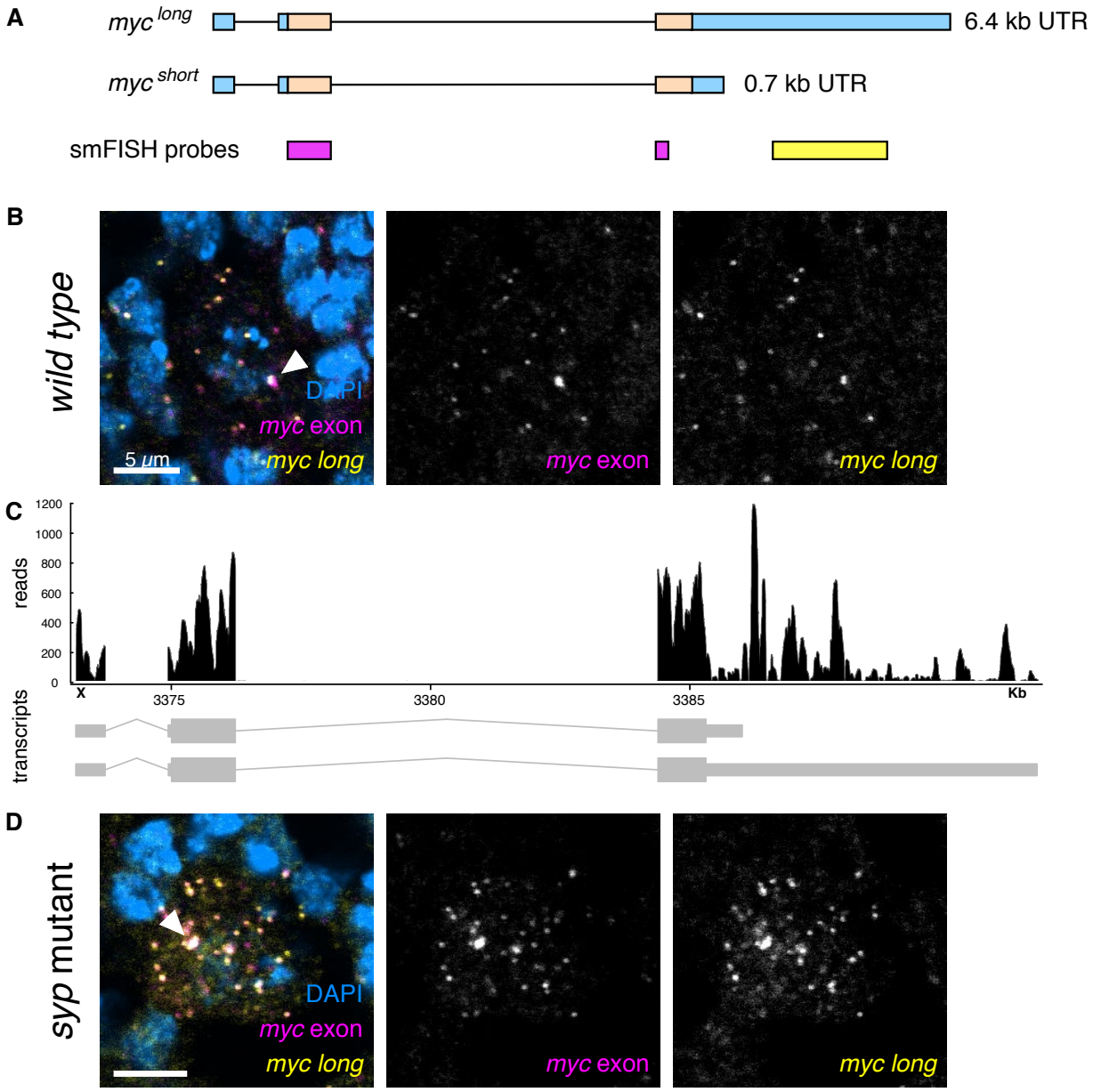


Figure 4.4 *myc*^{long} is expressed in NBs

A The transcript annotation of *myc* shows two isoforms with differing 3' UTR lengths. smFISH probes were designed marking either the common *myc* exon or the *myc*^{long} specific extended 3' UTR. **B** Costaining with *myc* exon and *myc long* probes, shows that all smFISH spots are positive for both probes. This suggests that all transcripts are *myc*^{long} in the *wild type* NB. The transcription focus is marked with a white arrow. **C** The Imp RIPseq experiment show that reads in the extended 3' UTR, suggesting that *myc*^{long} is pulled down by Imp (Dr Aino Järvelin). **D** Examining *myc* isoform expression with smFISH in the *syp* mutant, shows there is no isoform switch when Syp is depleted. All transcripts are positive for both *myc* exon and *myc long* probes, indicating that *myc*^{long} is predominant.

4.2.4 Is there an isoform switch in the *syp* mutant?

There are two isoforms of *myc* mRNA*,* differing in the length of their 3' UTRs. In *wild type* NBs, myc^{long} is the predominant isoform (section 4.2.3), but manipulating levels of Imp and Syp may induce an isoform switch or specifically stabilise myc^{short}. To test whether there was a change in isoform, I co-stained with smFISH probes against the common exon and *myc long* in the *syp* mutant (Figure 4.4 D). In the *syp* mutant, as in the *wild type*, all of the cytoplasmic *myc* transcripts are positive for both probes. This shows that there is no isoform switch in the mutant and myc^{long} is the expressed isoform in both genotypes. In this smFISH experiment I also observed a higher number of *myc* transcripts in the *syp* mutant, so I was interested to quantitate the levels of *myc* transcription and cytoplasmic mRNA.

4.3 IS MYC POST-TRANSCRIPTIONALLY REGULATED IN THE NB?

I have shown that elevated Imp increases Myc protein levels. This regulation of Myc could occur at the level of increased transcription, mRNA stability, translation, or protein stability. To distinguish between these possibilities, I used smFISH data to quantitate the rate of *myc* transcription and mRNA decay in individual cells. I compared these rates between genotypes to provide insight into the regulation of *myc.*

4.3.1. Measuring post-transcriptional regulation

In section 3.4.1, I illustrated how measurements of intron and exon smFISH probes, combined with IF, can provide information on the regulation of a gene (Figure 3.11). Quantitations using microscopy are advantageous as cells within a tissue can be measured individually. In contrast, traditional biochemical measurements from whole

brain lysates provide an average of all the cells in the brain, and therefore cell-type specific differences in regulation cannot be detected.

When imaged using confocal microscopy with sufficient resolution, smFISH allows detection of single molecules of mRNA which can be counted in the cytoplasm. smFISH probes designed against the intron of the gene mark the site of transcription. The intensity of these transcription foci can give a comparative measure of transcription rate. Alternatively, the average intensity of a single mRNA transcript can be used to calculate the number of transcripts at the transcription foci using a tool such as FISH-quant (Mueller et al., 2013).

smFISH data can also be used to calculate approximate transcription rates and decay rates for the gene (Bahar Halpern and Itzkovitz, 2016). Using an estimated rate of transcription elongation, and normalising for the position of the probe within the transcript, transcription rate can calculated from the number of transcripts at the transcription focus (see Materials and Methods 2.3.7). Assuming the cell is in a steady state, the rate of transcription of a gene is equal to the rate of decay and this can be used with the number of cytoplasmic transcripts, to calculate the half life of the transcript. This calculation takes into account any differences in transcription rate and so is the most direct method to compare mRNA stability between different genotypes or cell types. I used these methods to discover whether Imp increases *myc* transcription or mRNA stability, leading to increased Myc protein.

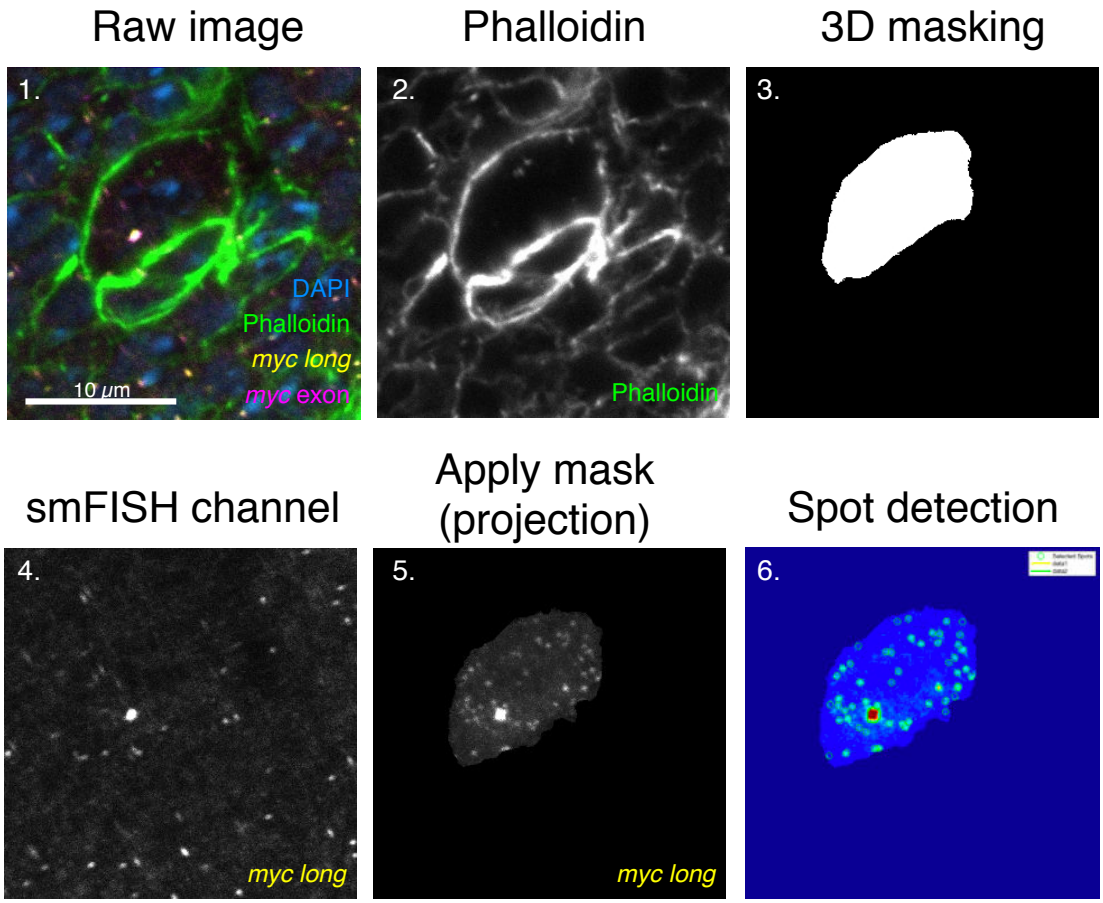


Figure 4.5 Workflow of transcript counting in NBs
The raw images for quantitation are four colours marking DNA (DAPI), cell boundaries (Phalloidin), and mRNA (smFISH for *myc* exon and *myc long*). The phalloidin channel is extracted to produce a 3D mask of the NB, using the FIJI plugin MorphoLibJ. This mask is then applied to the smFISH channel for quantitation. This removes all signal from outside the NB (image shown as a projection). FISHquant is then used to identify spots in this cell and measure the intensity of the outlined transcription focus.

4.3.2 Quantitating post-transcriptional regulation of *myc*

In Figure 4.4 D, there were more *myc* transcripts in the *syp* mutant than in the *wild type.* This could indicate regulation of *myc* via increased transcription or increased mRNA stability. I therefore used smFISH to calculate the *myc* transcription rate and mRNA half life in individual NBs. I used myc^{long} specific probes as this is the isoform observed in the NB, and using these isoform-specific probes removes the effect of any low levels of myc^{short} transcribed in the cell.

Larval brains were stained with *myc long* and *myc* exon smFISH probes and phalloidin-Alexa488 to mark actin and outline the cells. *myc exon* probes were used to allow better identification of the transcription foci as they are further 5', leading to a brighter signal (see section 5.2.2 for in depth explanation). NBs in mitosis were excluded from the analysis (identified by condensed chromatin in the DNA staining with DAPI). A workflow for spot counting is shown in Figure 4.5. I used phalloidin to mark the cortical actin of the NB and used this to create a mask to ensure only the transcripts within the cell were counted. I used FISHquant (Mueller et al., 2013), to count the smFISH spots and measure the number of transcripts at the transcription foci (see Materials and Methods 2.3.7 for details).

wild type, syp RNAi, and *imp/syp* double RNAi brains were stained and analysed. The raw numbers of mature and nascent transcripts were quantitated (Figure 4.6 A). The number of cytoplasmic *myc* transcripts was significantly increased in the *syp* knockdown NBs with no significant change in nascent transcript number (note that *myc* was not found to change in the *syp* mutant RNAseq experiment, Appendix E, perhaps because the regulation is in a small number of cells). This result suggests that an increase in mRNA stability rather than an increased level of transcription is responsible for the elevated Myc levels that I observed in the *syp* mutant. In the *imp* and *syp* double knockdown, the number of cytoplasmic transcripts returned to *wild type* levels, but the number of nascent transcripts is also reduced. In this case it is difficult to assess the contribution of the change in transcription and any change in mRNA stability. mRNA stability can be directly calculated from this data (as described in section 4.3.1) and takes differences in transcription rate into account. Therefore, this is the best method to understand the roles of transcription and mRNA stability.

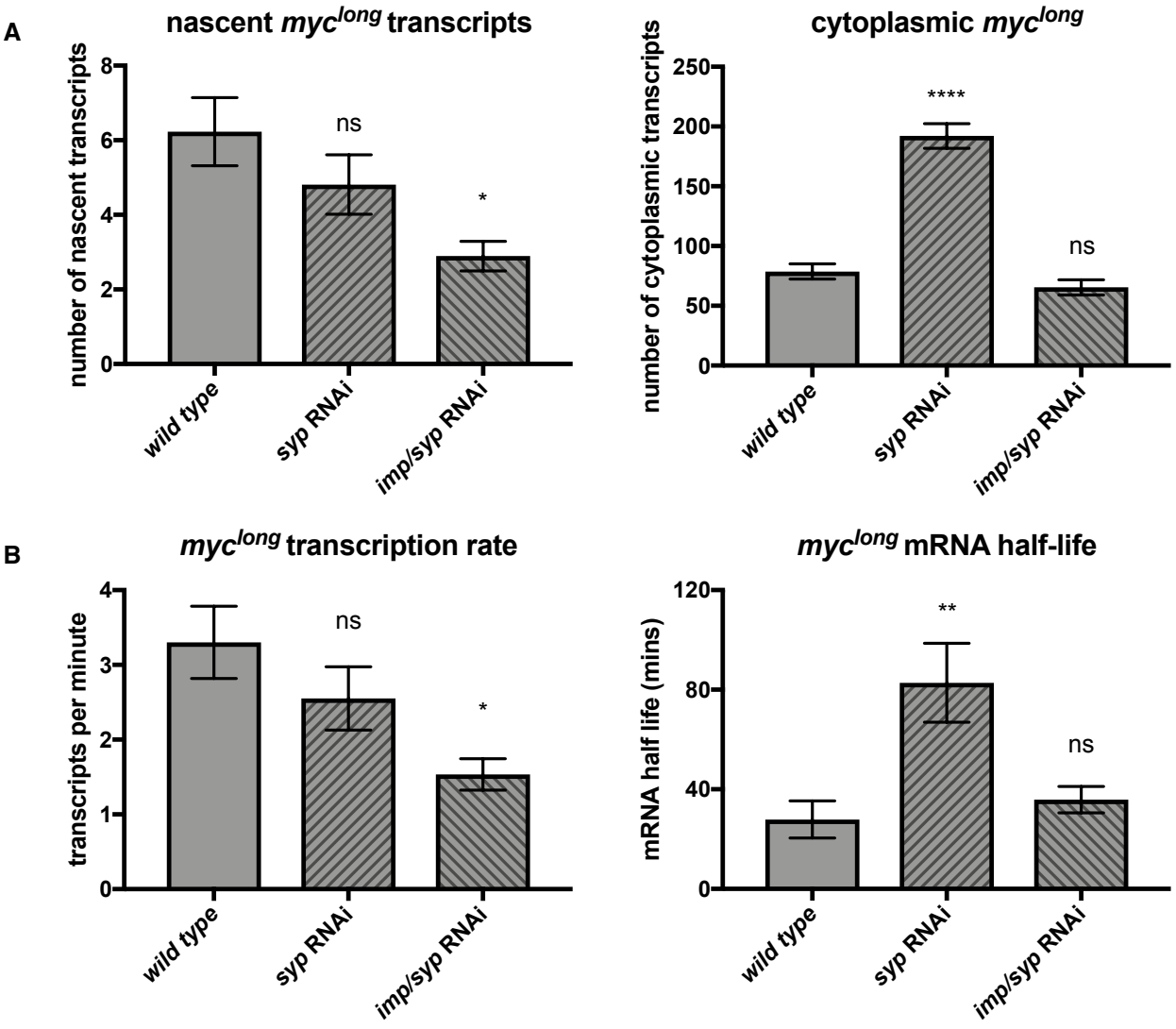


Figure 4.6 smFISH quantitation shows Imp regulates *myc*^{long} half life
A *myc*^{long} smFISH images were quantitated in type I NBs in *wild type*, *syp* RNAi and *imp/syp* RNAi brains. Cytoplasmic transcripts were counted, and the number of nascent transcripts was calculated from the intensity of the transcription foci. The *syp* RNAi had no change in nascent transcripts, but double the number of cytoplasmic *myc*^{long} transcripts. The *syp/imp* RNAi showed a significant reduction in nascent transcripts but no difference in cytoplasmic transcripts. **B** The transcript counts were used to calculate the transcription rate and half life of *myc*^{long} in each genotype. *syp* RNAi shows no change in transcription rate but a three-fold increase in *myc*^{long} half life. The *imp/syp* RNAi shows a significant reduction in transcription rate but no change in *myc*^{long} half life. *wild type* n = 20, *syp* RNAi n = 19, *imp/syp* RNAi n = 14. Significance was calculated using a One-way ANOVA and Dunnett's multiple comparisons test with comparison to the *wild type* * $p < 0.05$, ** $p < 0.01$, *** $p < 0.001$, **** $p < 0.0001$

I converted the raw transcript counts to transcription rates and mRNA half life estimates for each measured cell (Figure 4.6 B). I used an estimated transcription elongation rate of 1.5 kb per minute (Ardehali and Lis, 2009). These quantitations showed that loss of Syp has no significant effect on *myc*^{long} transcription rate, but increases the mRNA stability of *myc*^{long} 3-fold (*wild type = 27.9* mins*, syp* RNAi = 82.7 mins, p = 0.0014). Depleting both Imp and Syp shows a significant reduction in *myc*^{long} transcription, but no significant change in *myc*^{long} mRNA stability (*syp/imp* RNAi = 35.9 mins, p = 0.84). This shows that Imp increases *myc*^{long} mRNA stability. Imp and Syp may both contribute to regulation of *myc* transcription.

Together, this data suggests that Imp elevation increases *myc*^{long} mRNA stability, leading to an increase in Myc protein. There may be an additional role of transcriptional regulation but it is not clear whether this is directly regulated by either Imp or Syp.

4.3.3 Cycloheximide treatment stabilises *myc* mRNA in *wild type*

The work described above shows that *myc* mRNA is stabilised by Imp, but in the *wild type* wL3 brain Imp levels are extremely low in the NB. Therefore, *myc* mRNA is relatively unstable in the wL3 NB. Previous work in embryos used transcriptional inhibitors followed by *in situ* hybridisation to measure mRNA stability (Edgar and Datar, 1996). Therefore, I used a similar approach with smFISH in an effort to measure the rate of *myc* mRNA decay. However, despite trying several different transcription inhibitors and concentrations (actinomycin D, α-amanatin and DRB (5,6-dichloro-1-beta-D-ribofuranosylbenzimidazole)) I was unable to achieve reproducible transcriptional inhibition. Instead, I took the opposite approach, using the translation inhibitor cycloheximide (CHX) to freeze ribosomes onto the mRNA, stabilising it (Weir et al., 1988). smFISH was then used to visualise the stabilised mRNA (Figure 4.7).

Comparing the untreated and treated brains shows a large increase in signal in the *wild type* but no obvious difference in the *syp* mutant, a finding that was reproducible across biological and technical repeats. I interpret these results as indicating that *myc* is much more stable in the *syp* mutant than the *wild type*. Stabilising *myc* with CHX in *wild type* brains leads to *myc* mRNA signal being similar to the *syp* mutant. This is consistent with the data I presented in the previous section, namely that the half life of *myc* is shorter in the *wild type* compared to the *syp* knockdown.

The CHX experiment is limited in that it will only stabilise transcripts being translated, and there may be a feedback altering transcription rate when translation is blocked. Although the addition of such a harsh drug is very likely to alter the transcriptional behaviour of the cells in the brain, amongst other undesired effects, the experiment is useful in providing evidence supporting the smFISH calculations of half life. I conclude that that *myc* mRNA is unstable in the *wild type* NBs and is stabilised by the elevated levels of Imp present in the *syp* mutant.

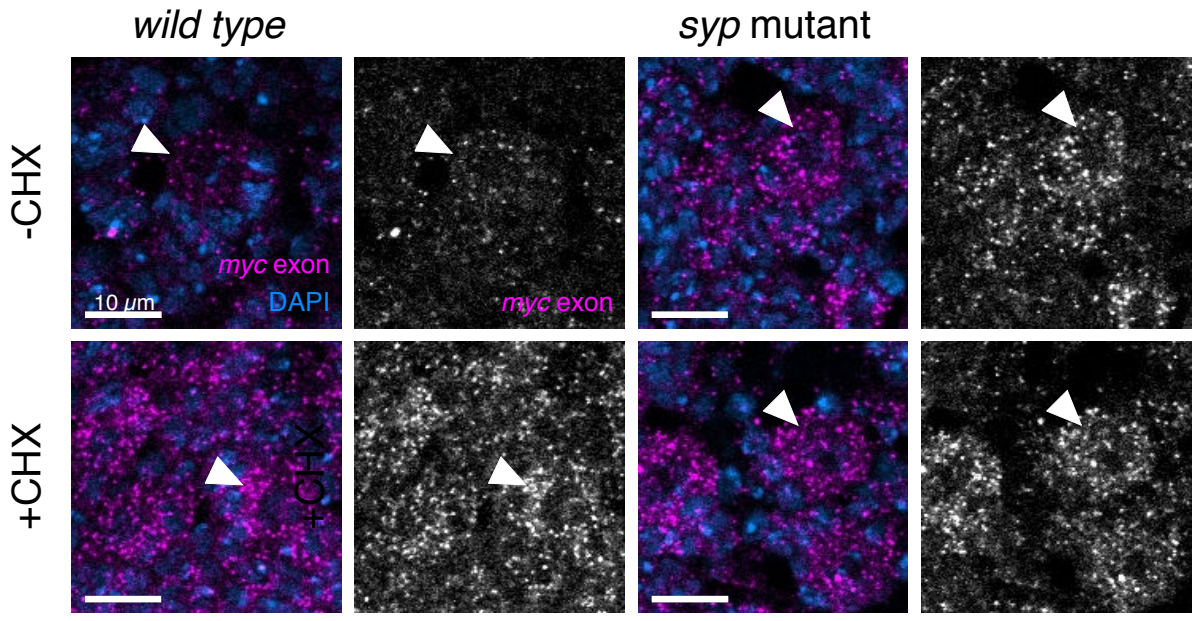


Figure 4.7 *myc* mRNA is unstable in *wild type* brains
Brains of *wild type* and *syp* mutant larvae were incubated for two hours in brain culture medium with or without 100 μM cycloheximide (CHX). Brains were then fixed and smFISH was performed against *myc* exon. CHX treatment increased *myc* exon signal in *wild type* much more than in the *syp* mutant. This suggests that *myc* is more unstable in the *wild type*. Example NB indicated with white arrow.

4.4 IS MYC ELEVATION RESPONSIBLE FOR THE PHENOTYPES OF IMP/SYP DYSREGULATION?

In the previous section I showed that elevated Imp levels causes an upregulation of Myc, through an increase in the transcript half life. The elevated levels of Myc could cause phenotypic changes in the type I NB, as Myc is known to regulate cell growth and proliferation. As discussed in Chapter 3 (section 3.4.4), elevated Imp increases NB size and proliferation rate. I applied the assays described in section 3.4.4, to examine the role of Myc in regulating NB size and proliferation. I used a *myc* overexpression construct driven by insc-gal4 in the type I NB and progeny (Figure 4.8 A). Myc is successfully upregulated in the NB and progeny cells. I then compared the NB size and proliferation rate to the *wild type* and Imp or Syp depleted measurements from Chapter 3.

I used the actin marker, phalloidin to measure NB volume. Overexpression of Myc shows an increase in NB size, as expected from other cell types (Figure 4.8 B). The increase in size is similar to the *syp* RNAi brains. Upregulation of Myc could be responsible for the phenotype of larger NBs caused by elevated Imp levels.

As well as increasing cell growth, Myc also promotes proliferation by promoting progression through the G1 phase into S phase (Johnston et al., 1999). This role characterises the function of Myc as an oncogene, promoting tumour cell division (Grandori et al., 2000). I measured the mitotic index of the type I NBs in the *myc* overexpression brains (Figure 4.8 C). There was no significant difference to *wild type*, though the average mitotic index was increased from 0.18 in *wild type* to 0.24 in the *myc* overexpression. As described in section 3.4.4, the small n numbers limits statistical power. Therefore, I also used the EdU staining assay which labels all progeny produced within a 4 hr incubation period (Figure 4.8 D). The number of

progeny significantly increased from 3.2 in the *wild type* to 4.3 in the *myc* overexpression. This indicates that the cell cycle is shortened when Myc is overexpressed.

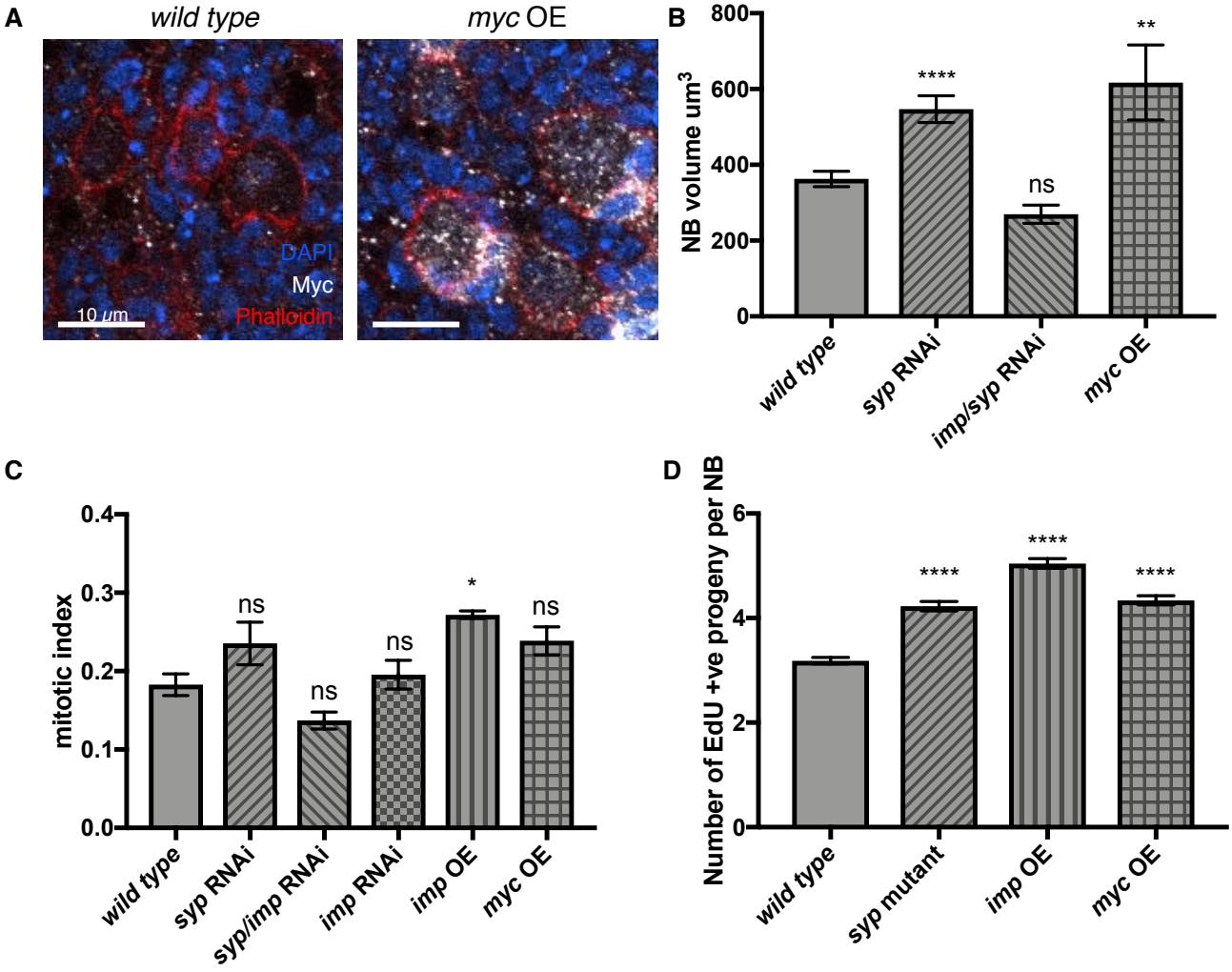


Figure 4.8 *myc* overexpression phenocopies Imp elevation
A *myc* overexpression with the insc-gal4 driver shows increased Myc protein in the type I NB and early progeny. Phenotype assays to measure NB size and proliferation rate were repeated in the *myc* overexpression brains (data from other genotypes repeated from Figure 3.15-17 for comparison). **B** NB volume measured using phalloidin staining shows significant increase in size in the *myc* overexpression. n = 4 **C** *myc* overexpression shows no change in mitotic index, measured from costaining of Dpn and PH3. n = 4 **D** Overexpression of Myc significantly increases the number of EdU labelled progeny in a four hour incubation. n = 68. Significance was calculated using a One-way ANOVA and Dunnett's multiple comparisons test with comparison to the *wild type* * $p < 0.05$, ** $p < 0.01$, *** $p < 0.001$, **** $p < 0.0001$

4.5 WHERE DOES IMP BIND TO *myc?*

In the previous sections I showed that elevated Imp levels stabilise *myc* mRNA in NBs and this leads to increased NB size and division rate. The best experiment to study the function of Imp regulation of *myc* would be to delete the specific Imp binding sites within the *myc* transcript. However, RIPseq does not give any binding site information. Furthermore, the method captures indirect interactions as well as direct binding, therefore Imp may act on *myc* via intermediate components. Understanding more about the interaction between *myc* and Imp is an essential step to uncovering the mechanism and function of *myc* regulation by Imp.

4.5.1 iCLIP analysis in S2 cells shows most binding in the extended 3' UTR

RIPseq identifies the mRNA targets of RBPs such as Imp, and suggested that Imp binds to myc^{long} (discussed in section 4.2.3). However, due to the lack of crosslinking, washes must be mild and therefore many indirect interactions are maintained. UV crosslinking allows more stringent washes to detect direct binding targets, and combining this with partial RNAse digestion can narrow down the region of the RNA bound by the RBP. The highest resolution of binding site identification is achieved using iCLIP (described in section 1.4.2). Performing iCLIP in tissues (such as the larval brain) is limited by the depth of UV crosslinking through tissue, and the difficulties in collecting sufficient material. Furthermore optimising the iCLIP protocol is complex and time-consuming. Therefore, in collaboration with Dr Aino Järvelin, I explored alternative published data sets.

Imp iCLIP has been performed in S2 cells, the most commonly used *Drosophila* cell line, derived from late embryonic *Drosophila* macrophages (Hansen et al., 2015). This study found most Imp binding in 3' UTRs, and a preference for CA-rich binding motifs. We hoped that this data set could provide insight into Imp binding sites in the

myc transcript. Of course, embryonic macrophages execute a very different function to larval NBs and therefore will have a different transcriptome and protein complement. Dr Aino Järvelin analysed S2 RNAseq data to examine the expression of *myc* and found that *myc* is expressed in S2 cells. However, the 3' UTR does not extend fully to the *myc*^{long} that is expressed in the brain (Figure 4.9 A)

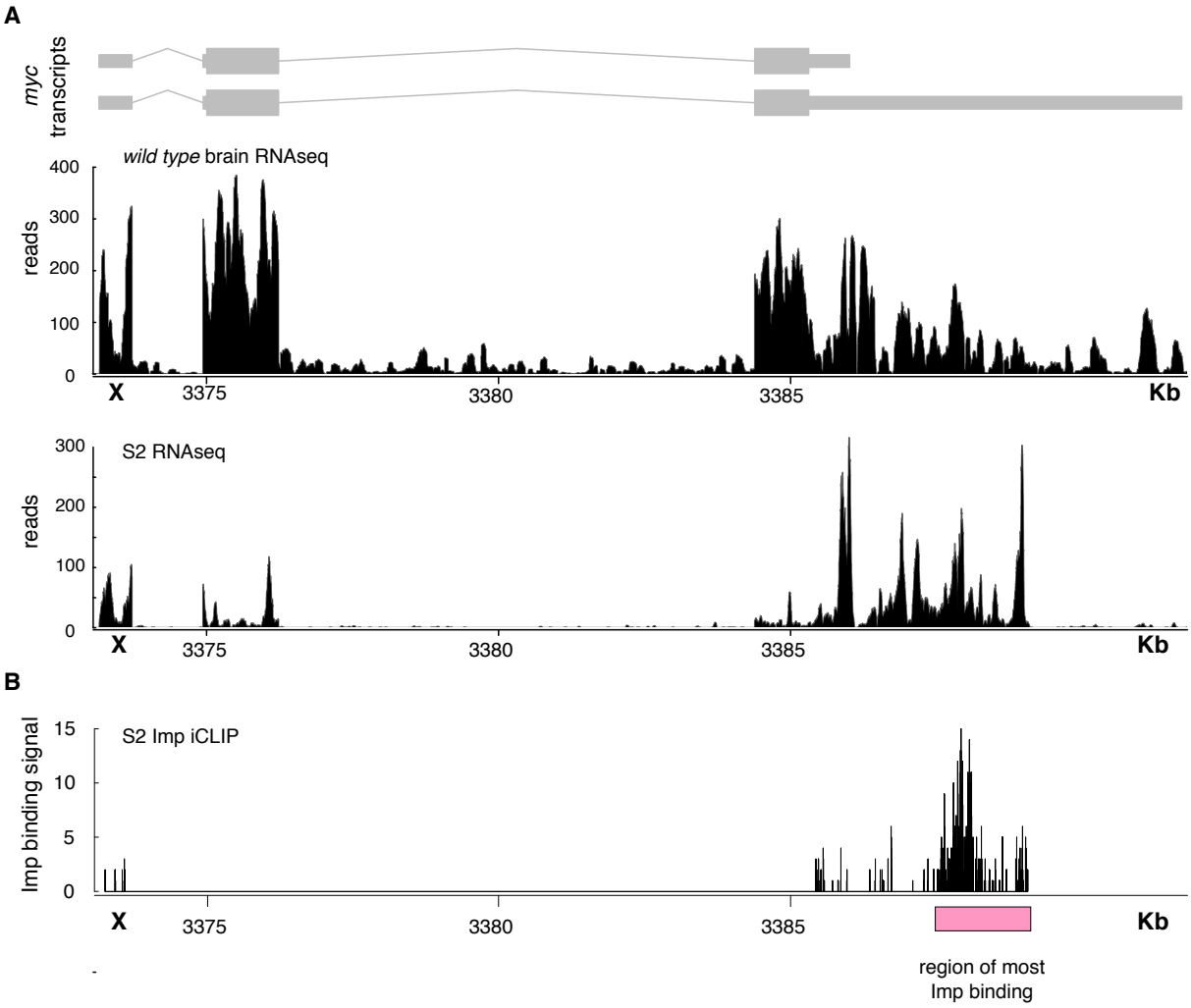


Figure 4.9 Imp binds *myc* in the 3' UTR extension
A Dr Aino Järvelin examined the coverage of the *myc* gene in the *wild type* brain RNAseq from this study, and previously published S2 RNAseq (Hansen et al., 2015). This shows that the full *myc* 3' UTR is expressed in the brain, but the most 3' end is not expressed in S2 cells. **B** Dr Aino Järvelin analysed previously published Imp iCLIP data in S2 cells (Hansen et al., 2015). There is no Imp binding signal in the *myc* coding exons. There are low levels of binding in the common 5' and 3' UTRs, but most Imp binding is observed in a region of the 3' UTR extension (marked).

Dr Aino Järvelin reanalysed the Imp iCLIP data set, to examine the Imp binding sites in the *myc* transcript (Figure 4.9 B). She showed that all binding was within the UTRs, with no binding signal found within the coding exons of *myc*. Most binding was within a region of the extended 3' UTR. Note that the full 3' UTR is not expressed in S2 cells so binding sites cannot be detected in that region. I could then use this identification of Imp binding regions to design endogenous deletions at the *myc* locus to prevent Imp binding.

4.5.2 Endogenous *myc* 3' UTR deletions

Imp stabilises the long 3' UTR isoform of *myc*, and iCLIP in S2 cells shows most Imp binding is within the 3' UTR extension. Does Imp stabilise *myc* via its 3' UTR extension? This question is best tested by measuring *myc* stability when the Imp binding sites within the *myc* 3' UTR extension are removed. However, the iCLIP data showed broad regions of Imp binding (Figure 4.9 B) and therefore mutating exact binding sites is not possible in this case. Therefore, I designed strategies to make three *myc* deletion lines removing the entire 3' UTR, the 3' UTR extension and the primary Imp binding region in the 3' UTR (highlighted in Figure 4.9 B).

In order to make precise deletions, a CRISPR/Cas9 strategy with homologous recombination (HR) repair was used (described further in Materials and Methods section 2.4). I designed guides (gRNAs) to direct Cas9 double-stranded DNA breaks at either end of the region to be deleted (Appendix Table C.3). To maximise the probability of a successful cut, three gRNAs were designed and cloned for each cut site. These were co-expressed using a plasmid which expresses gRNAs flanked by tRNAs allowing cleavage by the tRNA processing machinery to release each gRNA (Port and Bullock, 2016). A donor plasmid was then designed and produced to allow HR repair, with 1 kb homology arms flanking the deletion and containing a dsRED

marker (Figure 4.10 A). The double-stranded breaks produced by CRISPR Cas9 cleavage are repaired with the donor plasmid, inserting the dsRED marker. The marker allows rapid screening to identify positive flies, which are then used to make stocks. The dsRED marker is removed using the Cre-lox system and the final stock can then be validated by PCR and sequencing. The strategy simultaneously inserted an attP site, which may be used in future experiments to insert alternative 3' UTRs at the endogenous site.

The three deletion lines produced are illustrated in Figure 4.10 B. For each deletion gRNAs were designed and cloned, and a donor plasmid was produced containing homology arms specific to the deletion. These constructs were injected into embryos expressing Cas9 driven by *nanos* in the germline. Injections were performed by the University of Cambridge Department of Genetics Fly Facility. For each deletion, multiple positive stocks were produced and the dsRED marker was removed from the endogenous site. I screened the stocks by PCR spanning the deleted region and homology arms (to ensure the construct did not integrate at a different site), which will be followed by sequencing over the deletion. The final stocks were then balanced with a GFP balancer chromosome to allow selection of homozygous mutant larvae.

These deletion lines are a tool to examine the Imp regulation of *myc.* RIP-qPCR will be performed to ask whether Imp can pulldown *myc* with these regions deleted. The deletion lines will also be crossed into the *syp* mutant background. In this genotype Imp is upregulated and *myc* is stabilised, so I will ask whether *myc* can still be stabilised when the regions of its 3' UTR are removed. Furthermore, I will examine the NB size, to find out the extent to which the Imp NB size phenotype is due to the increase in Myc.

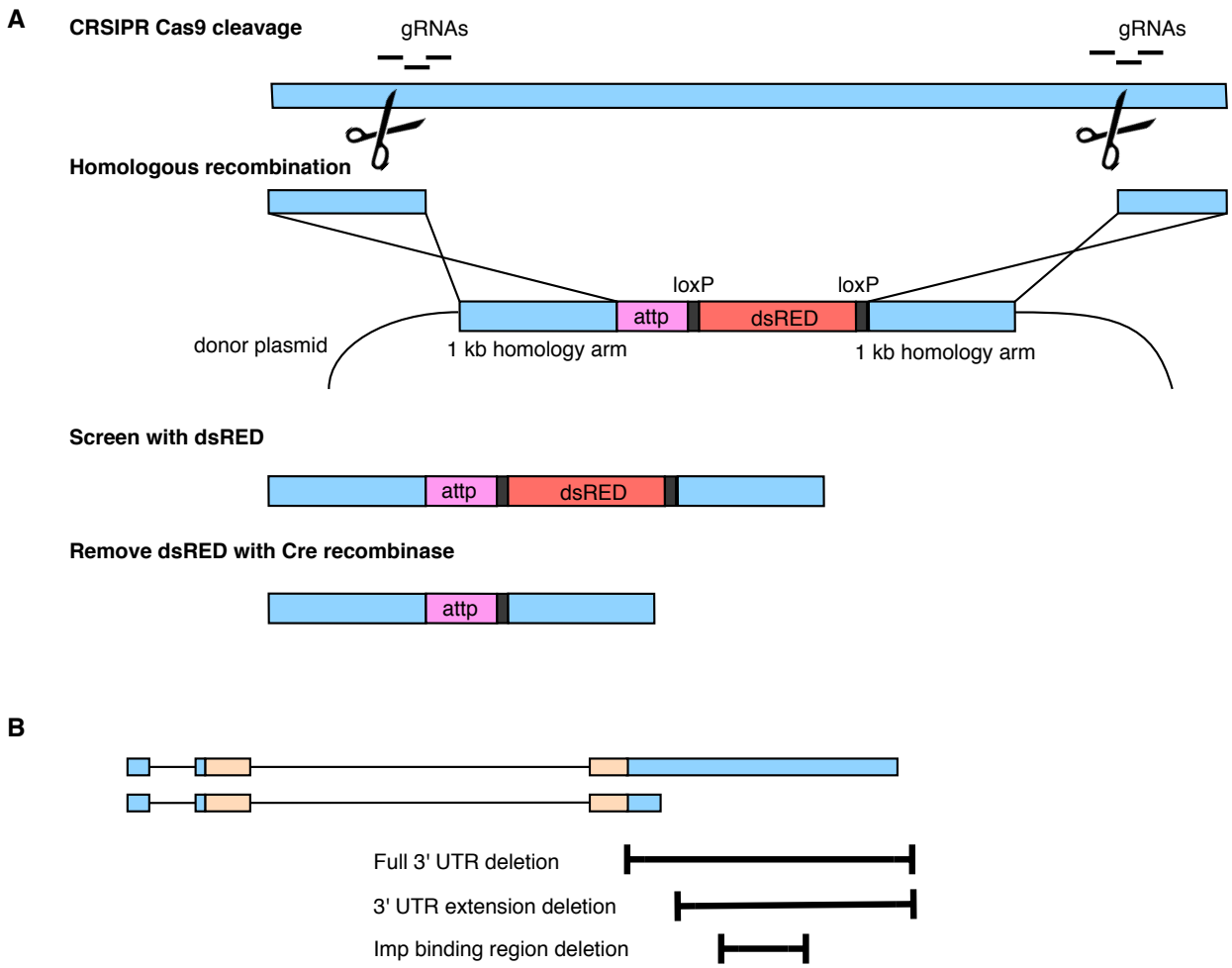


Figure 4.10 CRISPR homologous repair and deletion lines
A A CRISPR Cas9 strategy was designed to make double stranded DNA breaks at either end of the 3' UTR extension to remove 11.8 kb. A donor plasmid is constructed for homologous recombination repair with 1 kb homology arms, to insert an attP site and a fluorescent dsRED marker. Injected flies are screened for the deletion using the dsRED and then the marker is removed by Cre recombinase acting on the loxP sites flanking the marker. A balanced stock can then be made from the resulting line. **B** Three deletions lines were produced in the endogenous *myc* gene. These deletions removed the entire 3' UTR, the 3' UTR extension and the Imp binding region. In each case an attP site was inserted.

4.6 IMP AND NB SHRINKAGE IN THE PUPA

In parallel to the work described here, our collaborators Dr Ching-Po Yang and Dr Tzumin Lee examined the mechanism by which Imp regulates NB shrinkage in the pupa (Yang et al., 2017a). They hypothesised that Imp might suppress the Mediator complex, which has been previously shown to regulate pupal NB shrinkage (Homem et al., 2014). It has further been shown that NB shrinkage can be delayed by

overexpression of Med12 (Kohtalo, Kto), which is an inhibitory subunit of Mediator (Homem et al., 2014; Malik and Roeder, 2010). Dr Ching-Po Yang showed Med12 expression was elevated when Imp was overexpressed, and reduced when Imp was knocked down (Yang et al., 2017a). Therefore, we were interested to explore whether Imp binds to the mRNAs encoding any of the Mediator subunits, regulating the complex post-transcriptionally.

Eight Mediator complex components have been shown to be involved in NB shrinkage in the pupa (Homem et al., 2014). These are Med4, Med6, Med9, Med10, Med11, Med22, Med27 and Med31. In my Imp RIPseq data I found that Med31 and Med6 were enriched more than 2-fold over input, with a p value of less than 0.01. For publication, I validated these binding interactions by RIPqPCR (Figure 4.11) (Yang et al., 2017a). This method also showed significant differences to the control for *rp49, MED4, MED11* and *MED27.* However, these IPs pulled down less than 5% of the input so were considered to be too low to be likely biologically significant (note this boundary is subjective and depending on the experiment a lower threshold could be appropriate).

Interestingly, Med12 itself was not significantly pulled down with Imp. It may be indirectly regulated by Imp. Other components of the Mediator complex are bound by Imp so may be the regulatory links. Overexpression of Med12 in Imp-depleted MB NBs, only partially rescues the rapid shrinkage of the Imp-depleted MB NBs (Yang et al., 2017a). This suggests that Imp regulates NB shrinkage in part through inhibition of the Mediator complex, but that Imp also has additional regulatory roles, for example via *myc*.

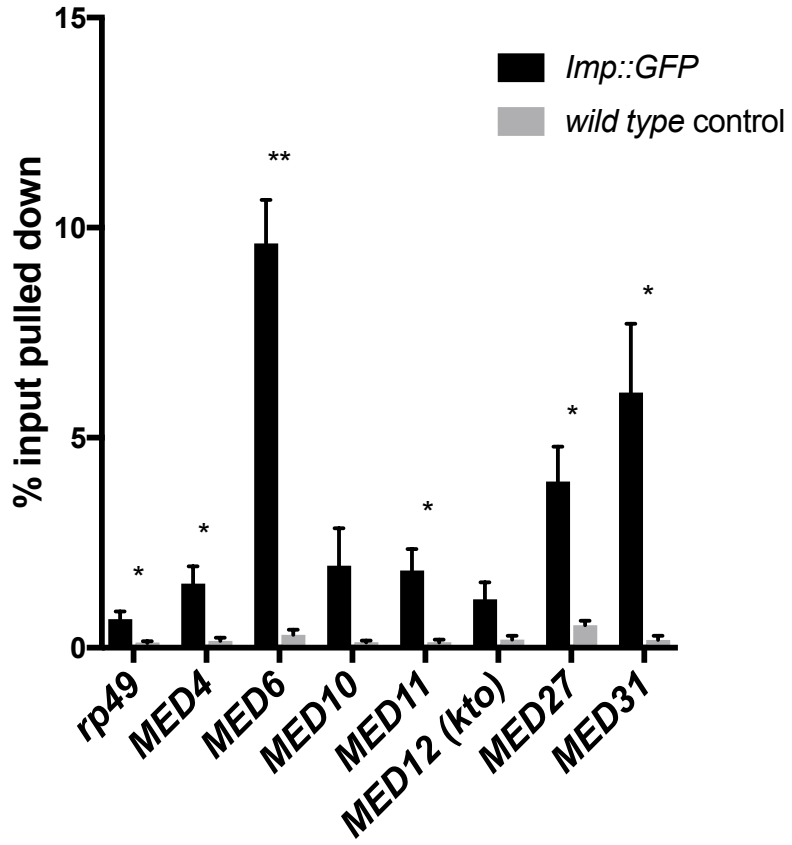


Figure 4.11 Imp binds to mRNAs encoding Mediator components.
I used qPCR to examine the binding of Imp to mRNAs encoding various Mediator complex components. I measured the % input pulldown with anti-GFP in the *Imp::GFP* line, compared to *wild type* brains. Statistical significance was calculated for each transcript between the *Imp::GFP* and the *wild type* control, using t-tests with correction for multiple comparisons using a False Discovery Rate allowance of 5%. * $q < 0.05$, ** $q < 0.01$, *** $q < 0.001$

4.7 CONCLUSION AND DISCUSSION

In this Chapter, I present evidence that Imp regulates *myc* mRNA half life, and suggest that this might be the key target responsible for the NB cell size and division phenotypes of Imp.

First, I examined Myc protein and mRNA expression in *wild type* type I NB lineages. I found that while Myc protein is restricted to the NB, its mRNA is expressed throughout the lineage. Manipulation of Imp and Syp levels did not affect this restriction of protein expression. Myc promotes growth and proliferation so must be downregulated in progeny cells to allow correct differentiation. Imp and Syp are not good candidates for this regulation as their levels vary through the developmental progression of the brain. Previously published indirect evidence suggests that Brat (one of the key cell fate determinants that is segregated to the GMC) might be responsible for translational repression of *myc* mRNA in progeny cells (Betschinger et al., 2006). The hypothesis was supported by Myc overexpression experiments, in which the authors found that Myc protein is not expressed in progeny cells unless Brat is knocked down. My direct observation of *myc* mRNA in progeny cells without protein expression, is stronger evidence of post-transcriptional regulation. In future, a temperature sensitive knockdown of Brat, followed by visualisation of Myc protein and mRNA could provide stronger evidence of the regulatory role of Brat.

I found that Imp elevation increased Myc protein levels in the type I NBs. Evidence from other cell types suggests that Myc is a likely candidate to regulate cell size in type I NBs. The cell size of type II NBs has been shown to be influenced by Myc levels, through Notch signalling (Song and Lu, 2011). I also examined Mnt expression and regulation, as it directly opposes Myc activity, and *mnt* is a target of both Imp and

Syp. However, I found that Mnt is constitutively expressed in the type I NB lineage, and there was no evidence of regulation by Imp and Syp.

Imp and Syp depletion does not affect *myc* regulation in the progeny cells, but does regulate Myc protein levels in the NB. I used smFISH to quantitate single transcripts of the predominant *myc^{long}* isoform in the NB, with knockdowns to deplete Syp and Imp levels. I used the single transcript counts to calculate *myc^{long}* transcription rate and half life in individual cells. This experiment showed that Imp upregulation increases *myc^{long}* half life. The absolute numbers should be interpreted with caution as they require several assumptions. The system must be treated as a steady state, but in a cell that divides every 90 minutes, this may not be a valid assumption. Furthermore, the transcriptional elongation rate is an estimate and may not be accurate in the NB. However, the values are certainly useful to understand differences between the genotypes, in this case showing an increase in half life between the *wild type* and *syp* knockdown, but not in the *imp/syp* double knockdown. I hypothesise that Imp binds to the otherwise unstable *myc* mRNA in the NB and this binding stabilises *myc* mRNA, increasing Myc protein.

I found that *myc* overexpression leads to an increase in type I NB size and division rate, suggesting it may be the key target responsible for the Imp phenotypes. Myc promotes cell growth through increasing ribosome biogenesis, leading to the observed increase in NB size. Myc is also thought to promote the G1 to S transition, but does not usually shorten the cell cycle as cdc25 is limiting (Johnston et al., 1999). The increase in division rate in the *myc* overexpression line may indicate that cdc25 is not limiting in the type I NBs. *myc* overexpression phenocopies Imp elevation (e.g. in the *syp* knockdown), which leads to *myc* mRNA stabilisation and increased Myc protein. However, a genetic epistasis experiment is required to conclusively show

that Myc upregulation is required for the NB size and proliferation phenotypes of Imp. A *myc/syp* double knockdown would lead to Imp upregulation without subsequent Myc upregulation. Repeating the phenotype assays in this line would allow examination of whether NB size and division rate are still increased. If they are not, we could conclude that regulation of Myc is responsible for the cell size and proliferation phenotypes of Imp.

I used RIPseq to show Imp and Syp binding to *myc* mRNA in the brain, but this experiment does not prove direct binding, or provide information on the binding sites within the transcript. Therefore, in collaboration with Dr Aino Järvelin, I examined iCLIP data in *Drosophila* S2 cells. This data suggests that Imp binds to *myc* primarily within its extended 3' UTR. S2 cells do not express the full length of myc^{long}, which may contain additional Imp binding regions. Furthermore, RBP binding can depend heavily on the context of other proteins present and therefore this may not accurately represent the Imp binding profile in NBs. However, this data was a good indication of likely Imp binding regions. I have produced endogenous deletions in the *myc* locus attempting to disrupt Imp binding. Studying these lines for their Imp binding and *myc* mRNA stability will provide essential functional and mechanistic insight into the regulatory process.

The finding of post-transcriptional regulation of Myc level is unexpected in this context, as most research has examined its transcriptional regulation. Myc is downstream of multiple signalling pathways including TOR and PI3K/Akt, which activate *myc* transcription. These signalling pathways respond to nutritional and systemic growth cues. However, NB growth also varies across developmental progression, with shrinkage in pupal NBs. Imp level declines in the NB through developmental time. The additional layer of *myc* mRNA stability regulation by Imp

may allow integration of systemic signalling with the intrinsic age of the cell. This would explain why all NBs do not respond simultaneously to the systemic signals triggered by feeding. At termination, the levels of Imp in each cell must have decreased sufficiently to reach a threshold where *myc* is no longer sufficiently stabilised and translated to promote cell growth. This produces a permissive state to allow the shrinkage required for NB termination. The potential role of *myc* stability is supported by the failure of previous attempts to prolong NB life in the pupa by manipulating common growth control pathways, which had no effect on NB size or termination (Homem et al., 2014). Knockdown of FOXO and overexpression of either PI3K or AKT did not prevent NB shrinkage. Myc is a key downstream effector of all of these pathways (Figure 1.4). I propose that Imp levels in the pupal type I NBs are too low to sufficiently stabilise *myc* mRNA, even when its transcription is increased by the activation of upstream signalling pathways.

I am also interested in the role of Imp in regulating *myc* earlier in development. Imp levels are highest in the NB in the early larva and decline through to the larval-pupal transition. I hypothesise that NB nuclear Myc levels, NB size and division rate may all decline through larval development as Imp levels are reduced. Preliminary live imaging by Martin Hailstone and Dr Richard Parton in the Davis Lab, suggests that larval NBs have a shorter cell cycle in L2 larvae. Further work is required to back up this hypothesis.

I examined Imp regulation of *myc* in the *Drosophila* NB, but the role of *c-myc* has also been highly studied in mammalian systems, because of its oncogenic role in cancers. *c-myc* levels are elevated in various human tumours including medulloblastomas and gliomas (Swartling, 2012). Furthermore, higher levels of c-myc are associated with more aggressive cancers. Therefore, c-myc is validated as a therapeutic target. In

mammalian systems, post-transcriptional regulation of *c-myc* by IGFBP family proteins (the human Imp homologs) has been previously observed and studied (described in section 1.5.1). Imp binds within the coding region of *c-myc,* protecting the transcript from endonucleolytic cleavage and decay (Bernstein et al., 1992). Experiments in human cell lines identified *c-myc* in untranslated mRNPs including IGF2BP1 and SYNCRIP (Weidensdorfer et al., 2009). Knockdown of IGF2BP1 increased the amount of *c-myc* in polysomes. *c-myc* contains rare codons, which slows translation and leaves the transcript vulnerable to endonucleases. The authors propose that IGF2BP1 associates with *c-myc* in cytoplasmic mRNPs, where it is protected from attack, and remains bound through the first round of translation until the correct tRNAs can be loaded. This protects the transcript from decay and regulated levels of IGF2BP1 may allow titration of the *c-myc* transcript depending on tRNA availability.

Interestingly, the mechanism of protection is not conserved in *Drosophila,* as our above analysis shows that Imp binding is seen in the 3' UTR of *myc* in *Drosophila*. However, the role of Imp in regulating *myc* through mRNA stability is conserved. In mammalian systems, the regulatory relationship between Imp and *c-myc* has been almost exclusively studied in the context of cancer. In the *Drosophila* NB, the stabilisation of *myc* by Imp plays a key role in stem cell size and division through development. Further examination will be required to discover whether the developmental function of *myc* regulation by Imp is conserved in mammalian neurogenesis.

Post-transcriptional regulation of *myc,* to control NB behaviour, is just one example of the roles of Imp and Syp in neurogenesis. In the following Chapter, I will describe how Syp regulates Pros, a key TF promoting neural differentiation.

5.

mRNA STABILITY REGULATES CELL-TYPE SPECIFIC EXPRESSION OF PROS

5.1 INTRODUCTION

Pros is a key transcription factor in neurogenesis, controlling the balance between NB division and progeny differentiation (Knoblich, 2008). Its expression must be tightly controlled in each cell, with spatio-temporal specificity to ensure the linear progression of neuronal differentiation. The function of Pros has been studied extensively (discussed in section 1.1.3), but its own regulation is less well understood. In Chapter 3, I showed that Syp and Imp both bind to *pros* mRNA. In this Chapter, I examine whether these RBPs regulate Pros at a post-transcriptional level.

Pros protein is produced in the NB and is asymmetrically segregated into the GMC, where it represses genes for proliferation and activates genes for differentiation. Loss-of-function *pros* mutants are embryonic lethal (Colonques et al., 2011). In the larval brain, *pros* mutant clones develop into undifferentiated tumours of uncontrolled cell division (Betschinger et al., 2006). This is caused by dysregulated self renewal in

both NBs and GMCs (Choksi et al., 2006; Colonques et al., 2011). In the *wild type* embryo, neurons switch off Pros expression in the process of differentiation, but in the larval neurons there is an upregulation of Pros. *pros* knockdown in post-mitotic larval neurons shows no phenotype, suggesting that once neurons have committed to differentiation, Pros is no longer required (Carney et al., 2013). Therefore, the function of Pros in larval neurons is currently unknown.

Pros is also required for correct NB termination in the pupa. Nuclear Pros is undetectable in NB nuclei at the larval/prepupal transition (Maurange et al., 2008). However, 24 hrs later there is a burst of Pros in the nuclei of many NBs in the interphase before their final division. Furthermore, inducing premature expression of Pros in NBs leads to early NB termination. Clones without Pros contain multiple NBs, and these persist beyond the normal termination point into adulthood (Maurange et al., 2008). This evidence suggests that termination of type I NBs is dependent on a nuclear burst of Pros. The *syp* mutant also has a defect in NB termination ((Yang et al., 2017a), discussed in section 1.5.3), so Pros is an interesting target to follow up.

pros was previously shown to be a target of Syp in whole larvae (McDermott et al., 2014) and Dr Lu Yang, a previous DPhil student in the Davis Lab, investigated its regulation by Syp. Dr Lu Yang used smFISH and IF to observe levels of *pros* transcription, mRNA and protein in cells of the NB lineage. She found that *pros* is stabilised by Syp in post-mitotic neurons, leading to the observed upregulation in Pros protein. Syp specifically stabilises an isoform of *pros* with a highly extended 3' UTR ($pros^{long}$), which is only transcribed in the mature progeny cells. The FlyBase annotation of *pros* shows three annotated 3' UTRs, ~1 kb, ~3 kb and ~15.5 kb. This alternative polyadenylation allows a huge variation in 3' UTR length, which may lead to the regulated inclusion or exclusion of binding sites for RBPs, so that these

different isoforms are regulated and processed very differently. The expression of the more stable *pros*^{long} isoform may allow Pros protein upregulation both in larval neurons and terminating pupal NBs.

Dr Lu Yang had to leave the Davis Lab before this work could be completed and published. Therefore, I took over this project. In the first section of this Chapter, I repeated the work of Dr Lu Yang, using multiplexed stains of mRNA and protein to produce improved images for publication. This is important as NB/progeny clusters develop differently in each brain so stains can only be directly compared in a single image. I also examined the role of Imp in *pros* regulation. I then aimed to understand the function of the Syp regulation of *pros*^{long} in larvae and pupae. I used clonal analysis to examine the function of Syp in larval neurons, but found no obvious differentiation defect. I then produced *Drosophila* lines, aiming to specifically remove endogenous *pros*^{long} using CRISPR/Cas9-mediated genome-editing technology. This work uncovered an even more complex regulatory system, including a novel isoform of *pros*.

5.1.1 Specific aims

1. To use multiplexed mRNA and protein imaging to study *pros* mRNA and protein levels in *wild type* and *syp* mutant brains
2. To study Pros function in larval neurons through clonal analysis.
3. To design and execute CRISPR-based strategies to dissect *pros* isoform function.

5.2 PROS IS POST-TRANSCRIPTIONALLY REGULATED BY SYP

5.2.1 Syp binds *pros* and is expressed in the same cells of the brain

In Chapter 3, RIPseq experiments showed that *pros* is an mRNA target of both Imp and Syp in the wandering L3 larval brain (section 3.2). I used IF to co-stain Syp and Pros protein in wL3 brains (Figure 5.1 A). Syp is observed in the NB, marked by Dpn, as well as the progeny cells in the cluster. Pros is observed at low levels in the NB but is upregulated in neurons as previously reported (Carney et al., 2013).

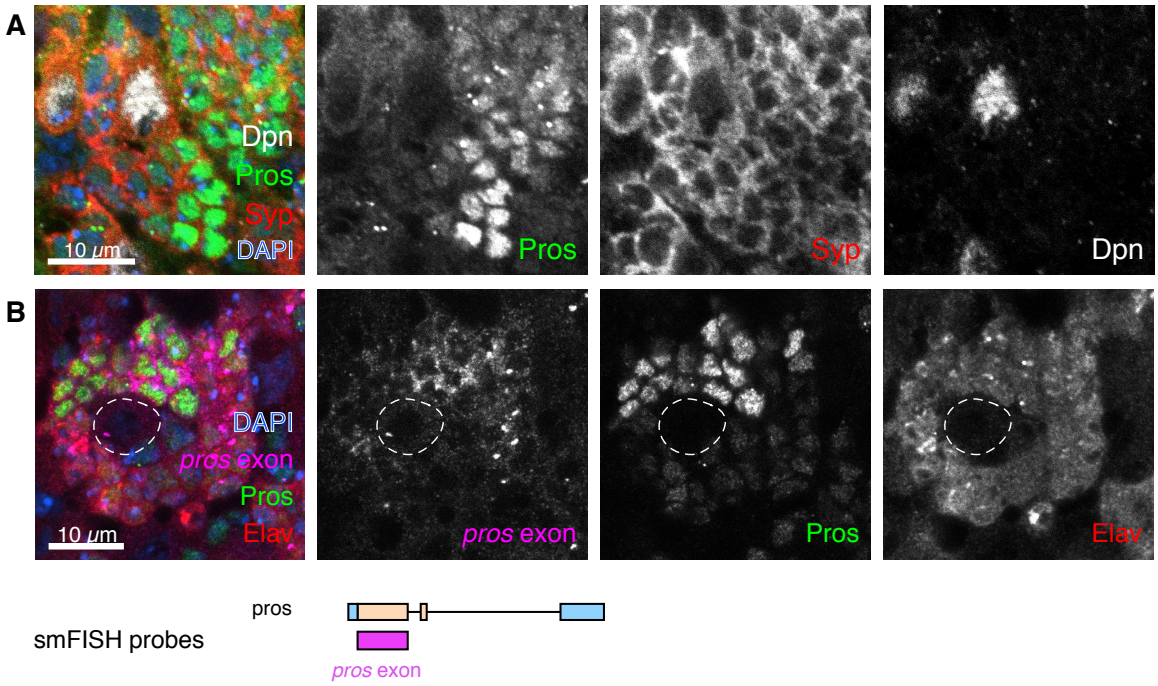


Figure 5.1 *pros* mRNA and protein are correlated in Syp expressing cells
A Syp is expressed in the cytoplasm of all cells of the Type I NB lineage, including cells expressing high levels of Pros. Pros is low in the NB and GMCs but upregulated in the post-mitotic neurons. Dpn staining marks the NB. **B** smFISH shows that *pros* mRNA is upregulated in post-mitotic neurons (marked with Elav), and this correlates with upregulated Pros protein. White dashed outline indicates the NB. Diagram shows the sequence targeted by the *pros* exon smFISH probes.

5.2.2 *pros* isoform choice determines protein level

Post-transcriptional regulation occurs at various stages of the mRNA lifespan so imaging the mRNA and protein of a particular gene together can indicate the level of regulation (as discussed in section 3.4.1). For example, different translation rates will alter the levels of protein in different cells, even if there are similar levels of mRNA. I used four colour staining with *pros* exon smFISH, anti-Pros antibody and anti-Elav antibody (marking differentiated neurons), to observe the expression of both Pros protein and mRNA in Type I NB lineages (Figure 5.1 B). Both Pros protein and mRNA are very low in the NB and early progeny cells but are hugely upregulated in neurons. Dr Lu Yang designed smFISH probes against the *pros* intron to mark transcription foci. I used four colour imaging to observe *pros* transcription, cytoplasmic mRNA and protein in the same brain, which shows that *pros* is transcribed in all cells of the lineage (Figure 5.2).

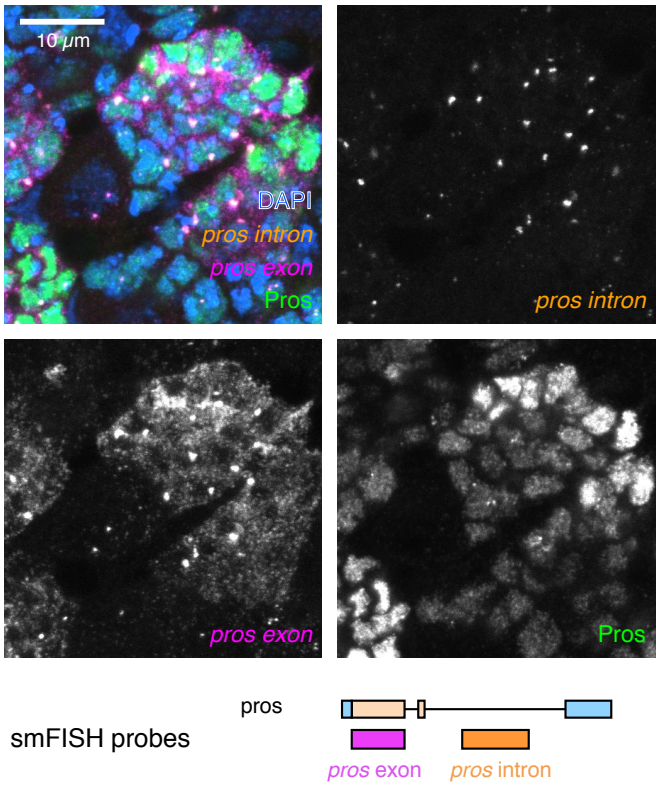


Figure 5.2 *pros* is transcribed in all cells in the Type I NB lineage
smFISH against the *pros* intron and *pros* exon (probe position illustrated in the diagram), with IF against Pros protein, shows that *pros* is transcribed in all cells of the Type I NB lineage (z projection of 5x 200 nm z stacks).

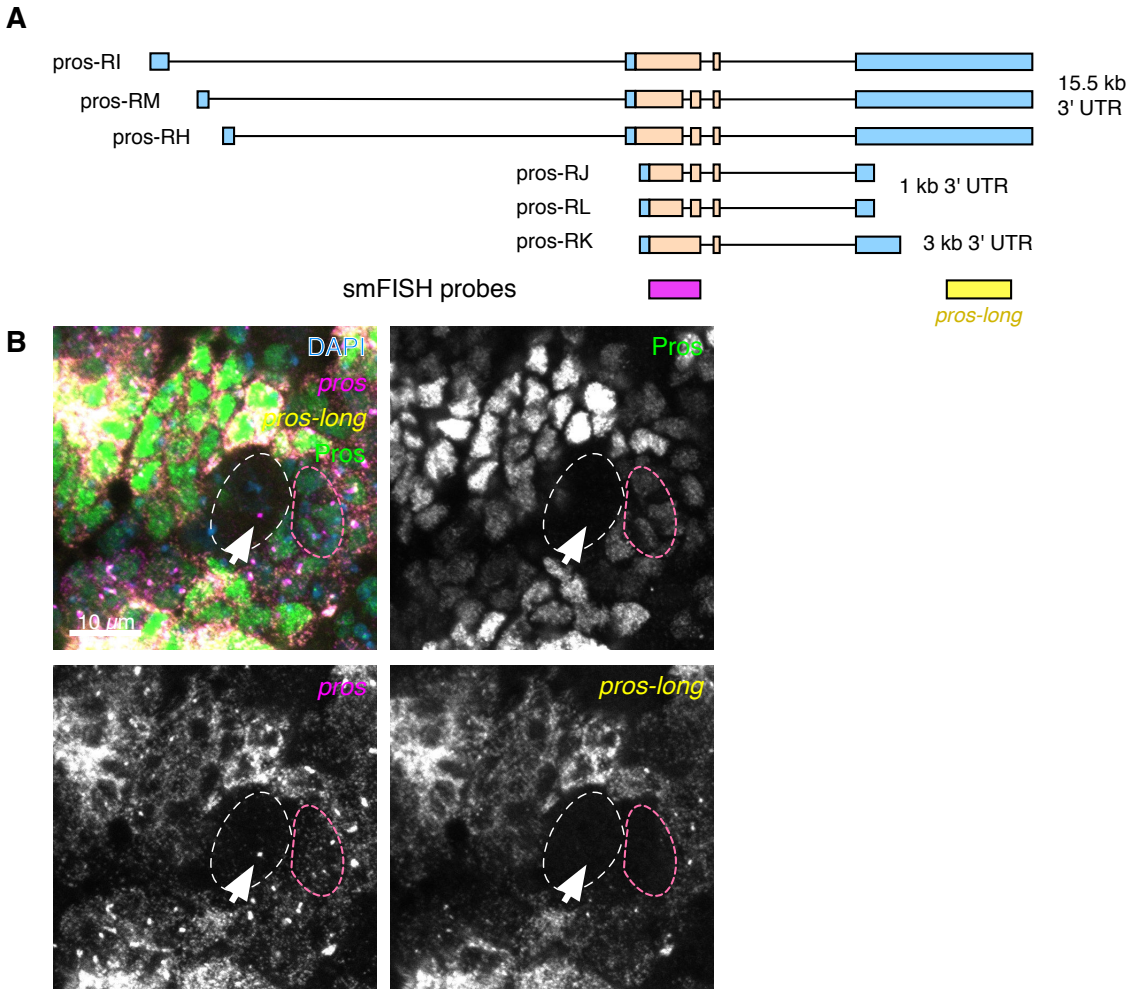


Figure 5.3 *pros* has a hugely extended 3' UTR
A FlyBase annotations show six *pros* isoforms with three different 3' UTR lengths. The *pros-long* smFISH probe was designed against the extended 3' UTR region. **B** *pros-long* signal is upregulated in post-mitotic neurons, correlating with increased *pros* exon and Pros protein signal. However, *pros-long* is not transcribed in the NB (white outline, transcription foci indicated with arrow) or early progeny (pink outline), where *pros* exon and Pros protein signal are much lower. (z projection of 3x 200 nm z stacks).

I explored *pros* isoform expression using smFISH probes against the extended 3' UTR region (labelling $pros^{long}$) (illustrated in Figure 5.3 A). Consistent with Dr Lu Yang's findings, *pros* and *pros-long* smFISH show very similar expression in post-mitotic neurons, indicating that most cytoplasmic *pros* in these cells includes the extended 3' UTR (Figure 5.3 B). However, there is no $pros^{long}$ signal in the NB (white outline) or young progeny (pink outline), including no $pros^{long}$ signal at the site of transcription (indicated in the NB with an arrow). This suggests that a short 3' UTR

isoform of *pros* (referred to hereafter as $pros^{short}$) is transcribed in NB and young progeny. There are low levels of nuclear Pros in the young progeny, where only $pros^{short}$ is expressed. In the older progeny there is a transcriptional switch to $pros^{long}$, correlating with the upregulation of Pros protein. The levels of cytoplasmic *pros* are much higher in the older progeny compared to the NB or young progeny. This could be because $pros^{long}$ is transcribed more highly than $pros^{short}$, or because $pros^{long}$ is more stable than $pros^{short}$.

In the previous Chapter, I demonstrated that the transcription rate and cytoplasmic half life of a transcript can be calculated from the number of nascent and cytoplasmic transcripts (section 4.3.2). However, the *pros* isoform switch makes it is very difficult to compare the *pros* transcription rates in the NB and progeny cells using smFISH. The position of the probe within the transcript determines the proportion of nascent transcripts which are labelled. This is accounted for with a positional weighting factor in the transcription rate calculations (Materials and Methods 2.3.7). If a probe is more 5', then more transcripts being produced at the transcription foci will include this sequence and the signal will be brighter. The large *pros* 3' UTR extension effectively shifts the exon probe more 5' within the transcript, so more transcripts at the site of transcription contain the probed sequence even at the same transcription rate.

Perhaps the transcription rates could be estimated using different weighting factors based on each isoform length. However, this calculation assumes that the isoform switch is immediate and complete. For my experiments I cannot distinguish whether $pros^{long}$ is expressed in addition to, or instead of $pros^{short}$. Therefore, I cannot compare the transcription rates in the NB and progeny cells. The level of cytoplasmic *pros* increases when the isoform switch occurs, but I cannot accurately assign the relative contributions of changes in transcription rate and *pros* mRNA stability.

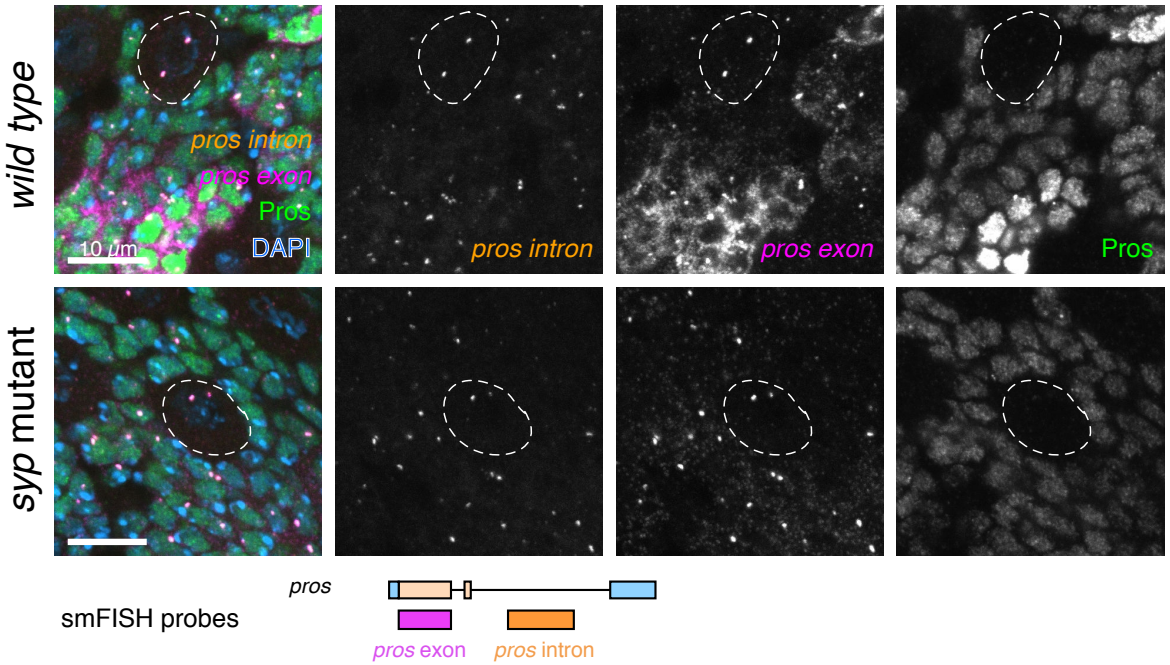


Figure 5.4 Syp regulates *pros* stability
A smFISH and IF staining in *syp* mutant shows downregulation of Pros protein and cytoplasmic *pros* mRNA. However, staining *pros* intron shows that *pros* transcription is unchanged between *wild type* and *syp* mutant. NB outlined in white. (z projection of 5x 200 nm z stacks).

5.2.3 Syp regulates *pros* mRNA stability

Dr Lu Yang found that both Pros protein and *pros* cytoplasmic mRNA levels in the post-mitotic neurons were very significantly reduced in the *syp* mutant. This is supported by my RNAseq experiment, which showed almost a two-fold *pros* reduction in the *syp* mutant compared to the *wild type* (section 3.3.1). However, she found that the signal from the intron smFISH probes was unchanged between *wild type* and the *syp* mutant. This indicates that *pros* mRNA stability is reduced in the *syp* mutant. I replicated this result in four colours to observe all stains in a single brain (Figure 5.4). This experiment shows that the upregulation of *pros* is lost in the *syp* mutant. However, low levels of *pros exon* signal remain in all of the progeny cells, at a similar level to the *wild type* young progeny. Similarly, the high levels of Pros in the mature neurons are reduced in the *syp* mutant, but lower levels of Pros remain. The

level of Pros in the *syp* mutant is similar to the Pros levels in the *wild type* young progeny.

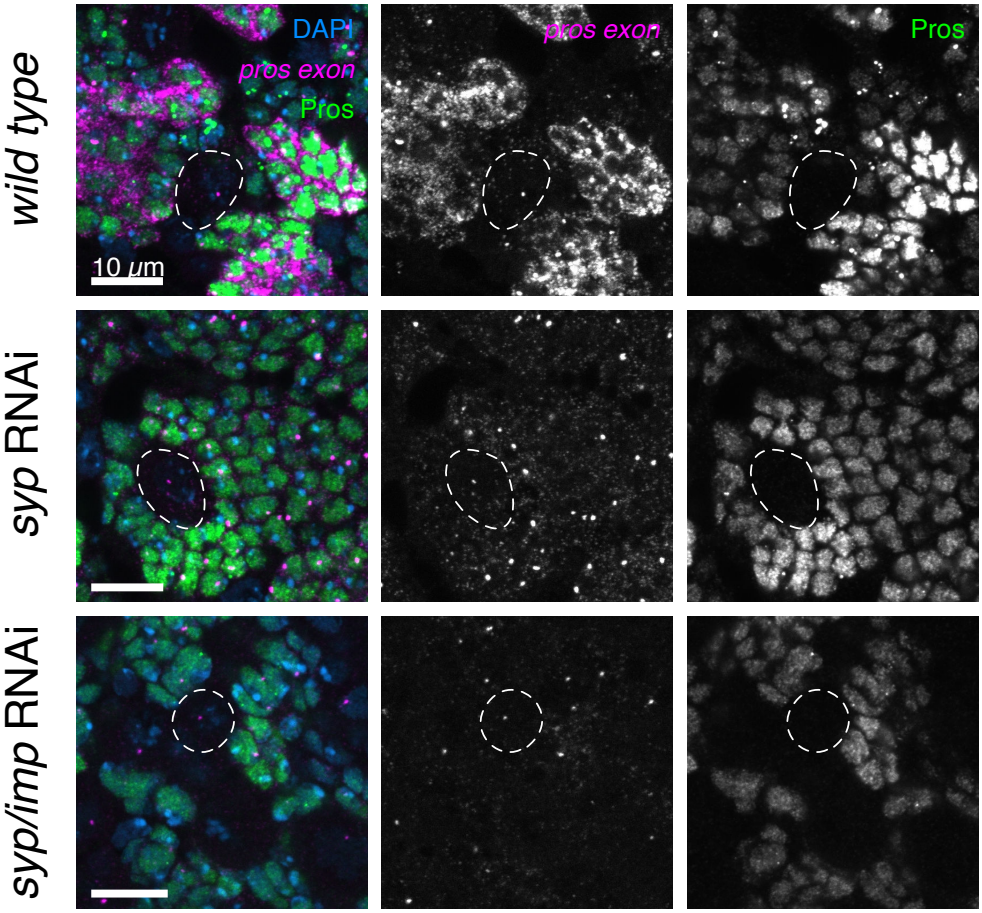


Figure 5.5 Imp does not contribute to Pros regulation
syp/imp double RNAi shows the same loss of *pros* mRNA and protein as the single *syp* RNAi. (z projection of 3x 200 nm z stacks). RNAi constructs are driven in NB and progeny by insc-Gal4.

The RIPseq data presented in Chapter 3 showed that *pros* is a binding target of Imp, as well as Syp. Therefore, I examined the regulation of *pros* by Imp. As discussed in section 3.4.1, the effects of the *syp* mutant may be due to the consequent increase in Imp levels, so an *imp/syp* double knockdown is needed to distinguish these effects. I examined the levels of *pros* mRNA and protein in an *imp/syp* RNAi line compared to the *wild type* and *syp* RNAi brains (RNAi constructs driven with *insc-gal4*) (Figure 5.5). Like the *syp* RNAi, the *imp/syp* RNAi brains show a reduction in *pros* mRNA and Pros protein. This shows that the *syp* phenotype is due to the loss of Syp and not the

upregulation of Imp. *pros* binding to Imp may be important in other cell types of the brain, or may be an indirect interaction.

5.2.4 *pros^{long}* is stabilised by Syp

pros^{long} is expressed specifically in mature progeny, where Syp is required to stabilise *pros.* In order to investigate whether Syp regulates *pros* in an isoform specific way, Dr Lu Yang used *pros-long UTR* smFISH in the *syp* mutant, and showed that *pros^{long}* is specifically lost in the *syp* mutant, with very few transcripts remaining. She designed a probe against the *pros^{long}* specific intron produced from the upstream TSSs, which are annotated to produce *pros^{long}*. A co-staining of *pros long intron* and *pros-long* in the *syp* mutant, showed that *pros^{long}* is still transcribed (Figure 5.6 A). The transcriptional switch to *pros^{long}* in the neurons is independent of Syp, but Syp specifically stabilises *pros^{long},* perhaps through binding sites in the long 3' UTR extension. This experiment also shows that the upstream TSSs are used to produce *pros^{long}* in post-mitotic neurons.

Close examination of the *syp* mutant RNAseq data (described in section 3.3, in collaboration with Dr Aino Järvelin) supports the specific loss of *pros^{long}*. The divergence of the *wild type* and *syp* mutant traces shows a significant reduction of reads from the 3' UTR extension in the *syp* mutant (Figure 5.6 B, C). The reduction in coverage occurs after the end of the 3 kb 3' UTR of *pros-RK.* This suggests that *pros^{long}* is specifically lost in the *syp* mutant. Figure 5.4 showed that low levels of Pros remain in the *syp* mutant, most likely translated from remaining *pros^{short}*.

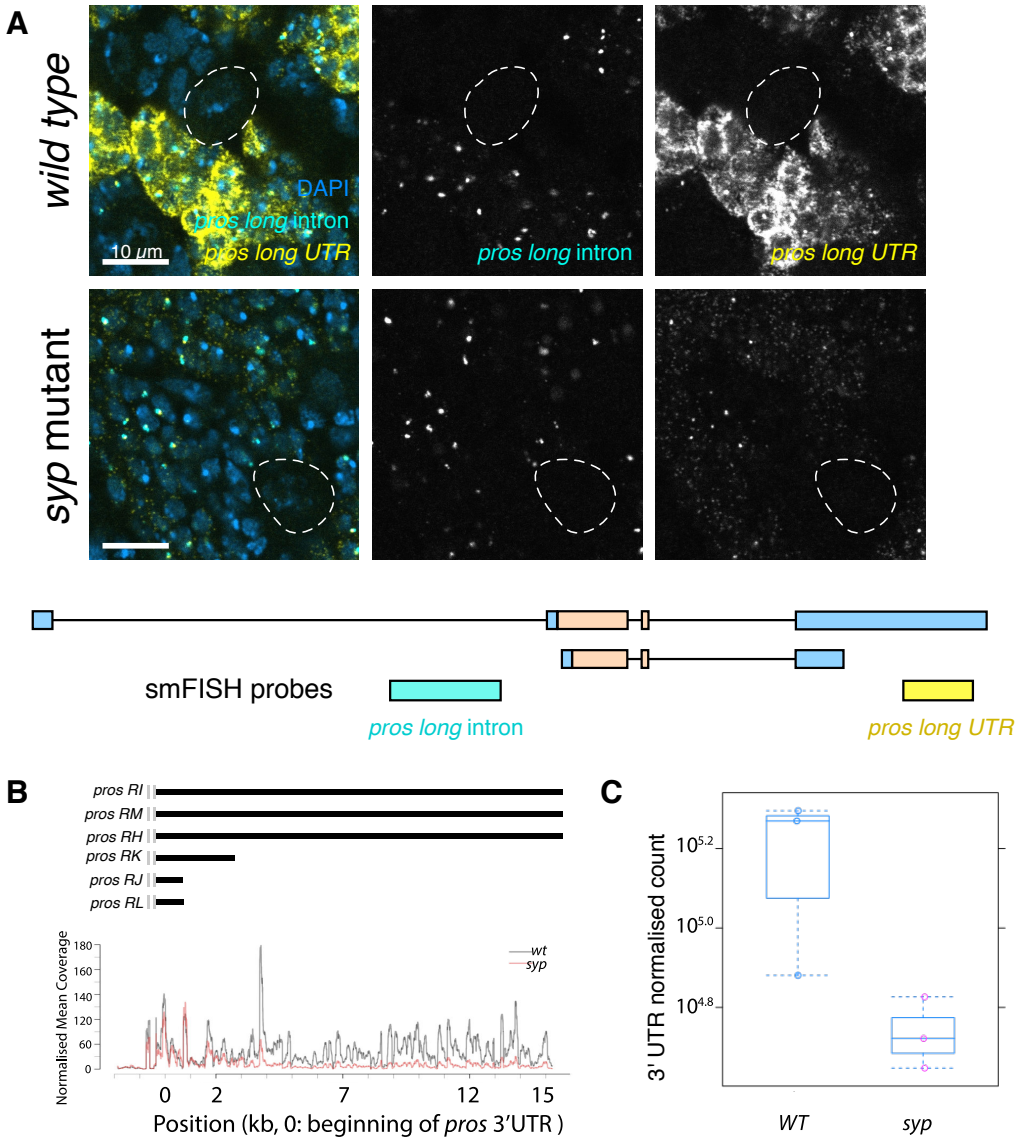


Figure 5.6 Syp specifically increases *pros*^{long} stability
A In the *syp* mutant, cytoplasmic *pros-long* signal is lost, but a *pros*^{long} specific upstream intron probe shows normal transcription in neurons. **B** RNAseq coverage in the *syp* mutant shows a loss of reads from the extended 3' UTR region of *pros* compared to the *wild type* (Dr Aino Järvelin). **C** A graphical depiction of the reduction in read count in the 3' UTR of *syp* mutant compared to *wild type* (Dr Aino Järvelin).

All together, this data supports a model in which *pros*^{short} is transcribed in the NB and young progeny, but is unstable and only produces low levels of Pros protein (Figure 5.7). In the older progeny, transcription of *pros*^{long} is switched on, and *pros*^{long} is stabilised by Syp, leading to an upregulation of Pros protein. When Syp is lost, low levels of Pros protein remain, likely translated from *pros*^{short}. The combination of both transcriptional and post-transcriptional contributions to the regulation of Pros levels

presumably reflects the importance of tight spatio-temporal control of this key transcription factor.

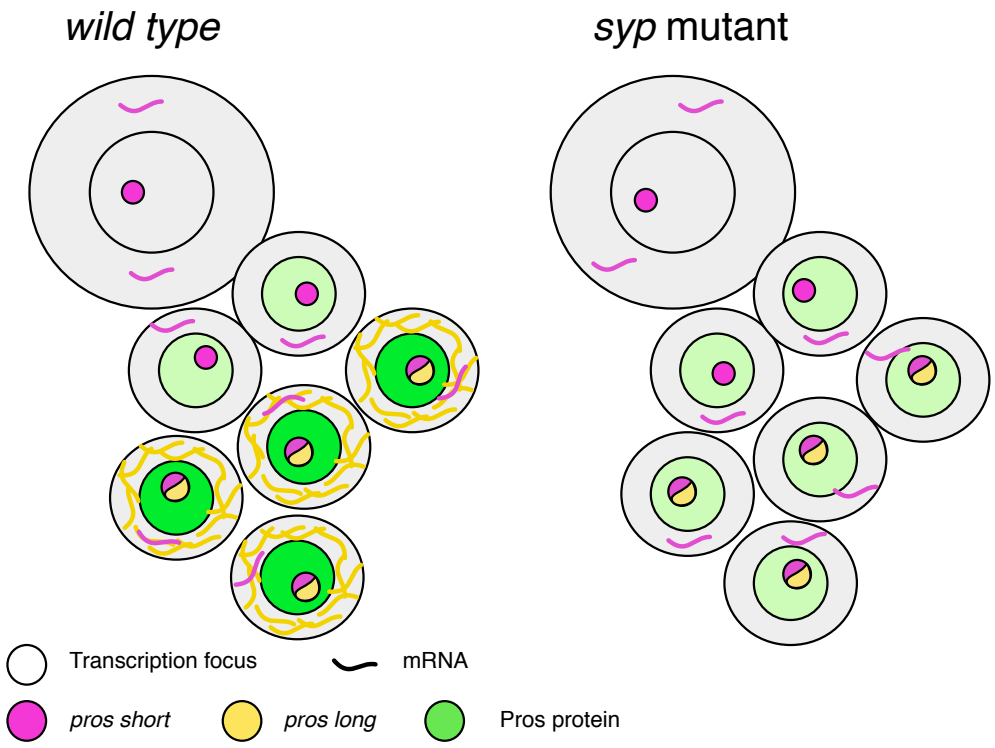


Figure 5.7 Model depicting Syp regulation of *pros*
pros^{short} is transcribed in the NB and young progeny then a transcriptional switch produces *pros*^{long} in post-mitotic neurons. *pros*^{long} is more stable and leads to upregulation of Pros protein. This increased mRNA stability is dependent on Syp so in a *syp* mutant cytoplasmic *pros*^{long} and Pros protein are significantly reduced, though transcription is unchanged.

5.3 WHAT IS THE FUNCTION OF PROS REGULATION BY SYP?

5.3.1 Clonal analysis shows normal exit from proliferation

Loss of Syp results in hugely decreased Pros level in the larval post-mitotic neurons. In order to examine the function of Syp regulation of *pros* in the larval brain, I performed clonal analysis in both *wild type* and *syp* mutant brains. In this strategy, single NB clones were marked with GFP so that a single cluster of progeny is labelled (Figure 5.8). This was achieved using a heat sensitive flippase to remove an FRT flanked STOP codon blocking mCD8::GFP expression. Each marked clone in both *wild type* and *syp* mutant contains a single Dpn positive NB and progeny which

mature to express the neuronal marker Elav. This shows that Syp does not affect normal exit from proliferation.

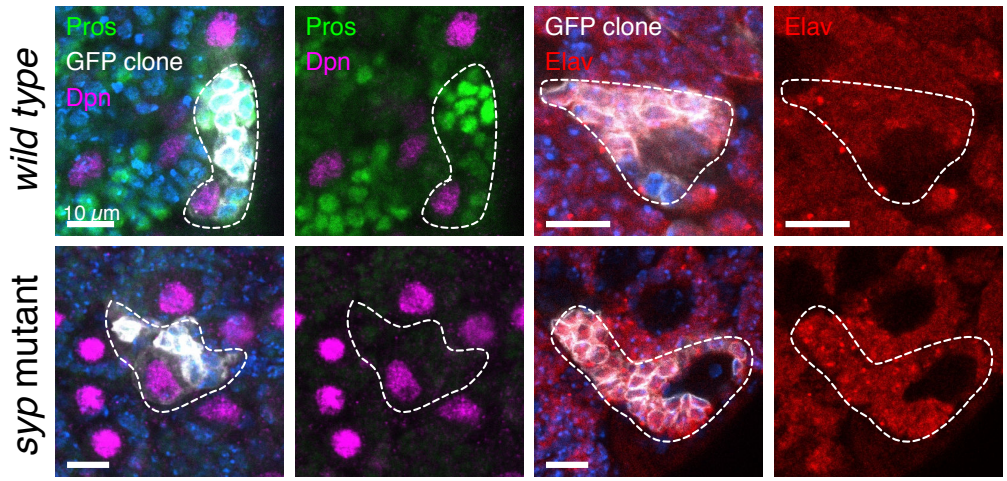


Figure 5.8 Clonal analysis shows normal GMC differentiation in *syp* mutant
Type I NB lineage clones are marked with mCD8::GFP (outlined with white trace) and stained with IF against Pros, Dpn (wt n = 7, *syp* n = 9) and Elav (wt n = 16, *syp* n = 4). Both *wild type* and *syp* mutant clones have a single Dpn expressing cell per clone and the progeny cells express Elav, marking a neuronal fate.

When Pros is lost from GMCs, a tumour forms (Betschinger et al., 2006; Choksi et al., 2006). However, I did not observe this in the *syp* mutant clones. This is consistent with published observations which show that *pros* knockdown in larval post-mitotic neurons does not trigger re-entry into the cell cycle (Carney et al., 2013). Furthermore, Pros staining in the *syp* mutant (Figure 5.4) showed that the low levels of Pros in the young progeny cells is not lost. Collectively, this suggests that Syp specifically regulates the production of the upregulated levels of Pros in mature neurons. Syp stabilises $pros^{long}$ in the mature progeny cells, while $pros^{short}$ in the NB and GMCs is unaffected. $pros^{short}$ is solely responsible for producing the Pros protein required in the NB and GMC for correct differentiation. $pros^{long}$ does not seem to have a role in exit from proliferation. In section 5.4 I will discuss the production of a *Drosophila* line with specific loss of $pros^{long}$ to distinguish its function more directly.

5.3.2 Syp is required for nuclear Pros in terminating NBs (Dr Lu Yang and Dr Ching-Po Yang)

Pros protein is also required for pupal NB termination as discussed in the Introduction (section 1.2.2). Furthermore, NB termination is compromised in *syp* RNAi flies (Yang et al., 2017a). In collaboration with Dr Lu Yang, Dr Ching-Po Yang and Dr Tzumin Lee hypothesised that Syp is required to allow Pros accumulation in the terminating NB. Dr Ching-Po Yang showed that Pros does not enter the nuclei of pupal NBs in the *syp* RNAi brain (Figure 5.9 A) (Yang et al., 2017a). He showed that transgenic Pros can terminate long-lived Syp depleted NBs, but that continuous Syp overexpression does not lead to early nuclear Pros accumulation or NB termination. This suggests that NB termination must be initiated in a Syp-independent step, before Syp is then required for Pros accumulation.

Syp stabilises $pros^{long}$ in larval post-mitotic neurons, so Dr Lu Yang hypothesised that the same mechanism allows Pros accumulation in the terminating NB. She used smFISH to stain for $pros^{long}$ expression in pupal NBs. She found that in NBs without nuclear Pros, $pros^{long}$ was not expressed, as in larval NBs (Figure 5.9 B). However, in NBs with nuclear Pros (i.e. terminating NBs), $pros^{long}$ was detected. Dr Lu Yang repeated the experiment in *syp* mutant pupal brains. She observed some NBs with $pros^{long}$ transcription foci but no cytoplasmic $pros^{long}$ or nuclear Pros (Figure 5.9 C). These are likely to be NBs in which termination has been initiated but cannot be executed without Syp stabilisation of $pros^{long}$.

Combined with Dr Ching-Po Yang's observations, these experiments suggest that NB termination is activated independently of Syp, and leads to a transcriptional switch from $pros^{short}$ to $pros^{long}$ in the terminating NB. Syp then stabilises $pros^{long}$ allowing accumulation of Pros, which enters the nucleus and leads to the terminal division.

The hypothesis can be tested by removal of *pros*^{long} expression, which would be expected to prevent normal NB termination, even in the presence of Syp.

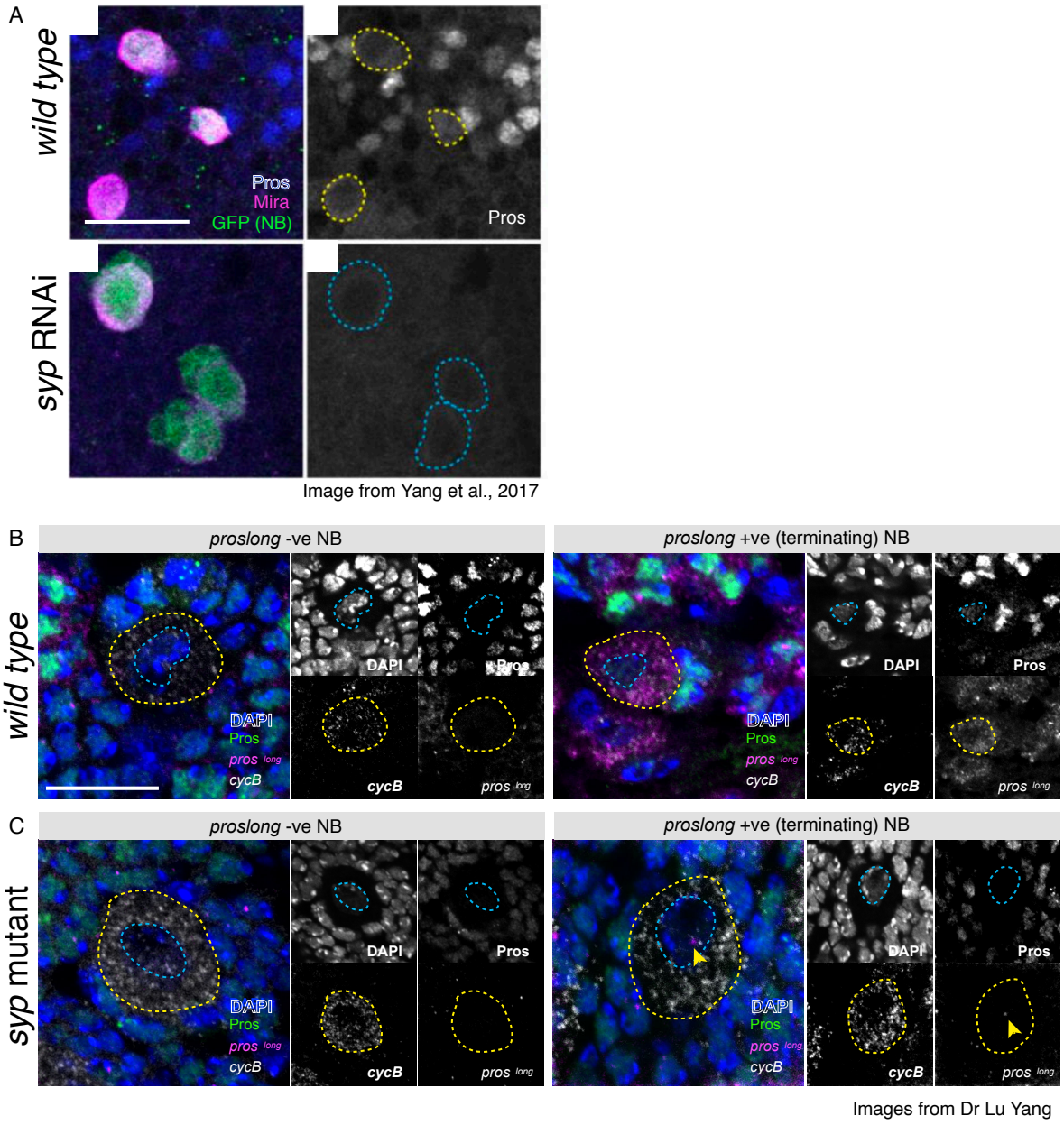


Figure 5.9 Syp stabilises *pros*^{long} in pupal NBs
A Syp is required for Pros accumulation in pupal NBs. Images from Yang *et al.,* 2017. At 24h APF nuclear Pros can be detected in some *wild type* NBs (marked with Mira), but not in *syp* RNAi, driven by *dpnEE-Gal4*. Scale bar: 10 um. **B-C** Images from Dr Lu Yang. **B** In most pupal NBs there is no nuclear Pros and no *pros*^{long} expression. However, in a low frequency of pupal NBs, nuclear Pros is observed and this correlates with cytoplasmic *pros*^{long} expression. **C** In *syp* mutant NBs nuclear Pros is never observed, but *pros*^{long} transcription foci are observed at a low frequency. In these cells cytoplasmic *pros*^{long} is not seen. Scale bar: 10 um.

5.4 CRISPR MUTANTS PROVIDE INSIGHT INTO PROS ISOFORM FUNCTIONS

Expression of *pros^{long}* is correlated with higher levels of Pros protein expression in larval neurons, as well as nuclear Pros protein in the terminating pupal NBs. This suggests that *pros^{long}* is the main contributor to Pros protein levels in these cells. *pros^{long}* is lost in the *syp* mutant, but many other Syp targets are also dysregulated, so it is not a good system to study the role of *pros^{long}* directly. The functional role of *pros^{long}* is best determined by specifically deleting this isoform, leaving the functions of *pros^{short}* intact. I pursued multiple strategies to remove *pros^{long}*, including nonsense mediated mRNA decay (NMD) and genomic deletions.

5.4.1 Removing *pros^{long}* through NMD

As discussed above, in FlyBase, *pros* is annotated to have six isoforms, three of which include the extended 15.5 kb 3' UTR. These are collectively referred to here as *pros^{long}*. All of these annotated *pros^{long}* isoforms contain an additional coding exon leading to an N-terminal 300 amino acid extension (Figure 5.10 A). Dr Lu Yang exploited this extension by designing a CRISPR/Cas9 strategy to produce a double stranded cut in this exon, leading to repair by non-homologous end joining (NHEJ). At a moderate frequency this leads to deletions causing a frame shift and resulting in a premature stop codon. This would produce a truncated Pros protein product and induce NMD of the *pros^{long}* transcripts. Dr Lu Yang produced a line (*pros-longSTOP*) with a 26 bp deletion, causing a frame shift which introduced a stop codon 80 bp further downstream (Figure 5.10 A, gRNA Appendix Table C.3, deletion Appendix C. 4). This would be expected to cause NMD decay and protein truncation.

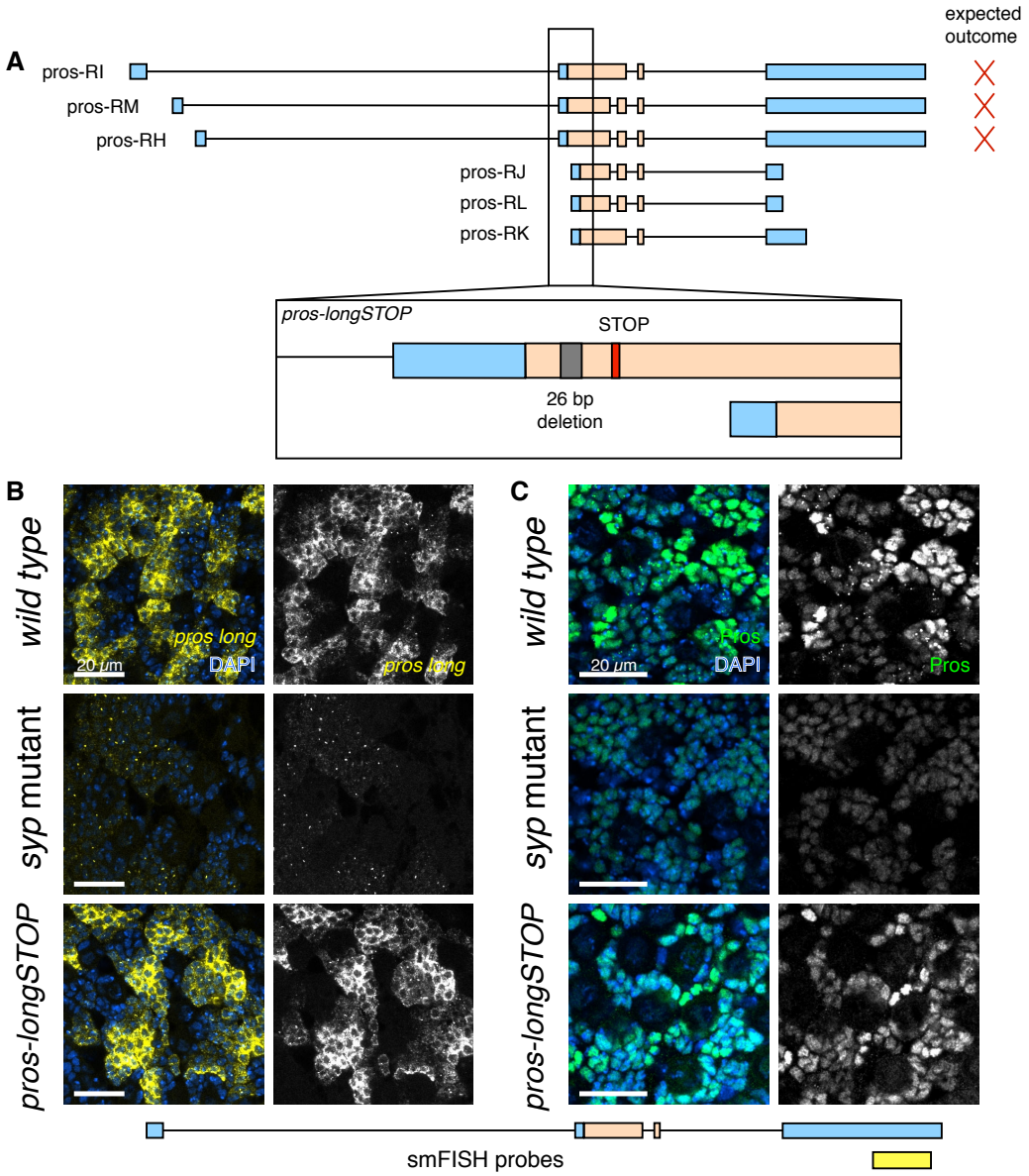


Figure 5.10 Introducing an NMD mutation does not remove *pros^{long}*
A Dr Lu Yang used CRISPR Cas9 to make a double stranded DNA break in the upstream coding sequence unique to the *pros^{long}* isoforms. Repair by non-homologous end joining resulted in small genomic deletions. *pros-longSTOP* has a 26 bp deletion, leading to a frame shift which introduces a premature stop codon 80 bp downstream. This should produce a truncated polypeptide and induce NMD of the *pros^{long}* mRNA isoforms. **B** The *pros-longSTOP* mutant was stained with *pros-long* smFISH and **C** Pros protein. Neither *pros^{long}* or Pros protein were significantly decreased.

I studied *pros-longSTOP* using smFISH and Pros antibody to examine the effect of the mutation. Unexpectedly, neither *pros*^{long} mRNA nor Pros protein were affected in the mutant (Figure 5.10 B). The anti-Pros antibody was designed against amino acids 1196-1320 of Pros, towards the C-terminus of the protein (Spana and Doe, 1995). This suggests that the full Pros protein is produced, and translation start site in the unique upstream exon in *pros*^{long} is not used. Pros protein is most likely produced only from the downstream AUG which is common to both *pros*^{long} and the *pros*^{short} isoforms. This would also prevent *pros*^{long} NMD in the *pros-longSTOP* line as the STOP codon is upstream of the translation start site. This experiment suggests that *pros*^{long} and *pros*^{short} produce the same Pros protein isoform, so the transcript isoform switch is not explained by a requirement to produce a functionally different Pros protein isoform.

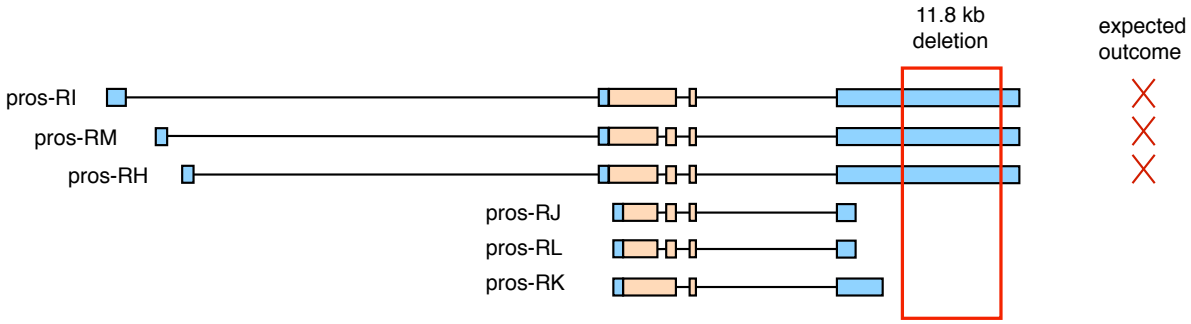


Figure 5.11 Deletion of the 3' UTR extension
Deletion of *pros*^{long} is necessary to study its function. Deletion of the genomic region encoding the *pros* 3' UTR extension would prevent it's inclusion in the *pros* transcripts. No positive deletion lines lines were recovered.

5.4.2 Using CRISPR to delete the *pros* 3' UTR extension

The most direct method to remove *pros*^{long} is to delete the 3' UTR extension (Figure 5.11). Dr Lu Yang designed gRNAs to use in a NHEJ strategy to delete the 3' UTR extension (Appendix Table C.3). Cuts were made 500 bp downstream of the short 3' UTR polyadenylation site, and 200 bp upstream of the long 3' UTR polyadenylation site. NHEJ repair events would lead to deletion of the intervening 11.8 kb sequence.

However, no positives were identified from this strategy, perhaps partially due to difficulties in PCR screening for these events.

As an alternative, I designed a homologous recombination (HR) repair strategy (Gratz et al., 2014) (described in Materials and Methods section 2.4 and section 4.5.2). This strategy re-used the gRNAs from the NHEJ experiment, but repaired the cuts with a homology construct including a dsRED marker for screening positive deletions. I produced the donor plasmid, with expert advice from Dr Francesca Robertson, and the constructs were injected at the University of Cambridge Department of Genetics Fly Facility.

The injected flies showed patches of dsRED expression both in the larvae and adults, suggesting successful integration of the donor construct. However, after three rounds of injection, no positive progeny flies were recovered. This could suggest that there were lethal off-target effects, or that the deletion itself had a dominant lethal phenotype (in the F1 generation, all deletions are kept over a balancer chromosome).

5.4.3 Deleting the *pros^{long}* promoters

Deleting the 3' UTR extension directly was an unsuccessful strategy, so the transcriptional start sites (TSSs) of the *pros^{long}* isoforms were targeted. In FlyBase the *pros^{long}* isoforms are annotated to originate from three different TSSs, upstream of the TSS of the *pros^{short}* isoforms (Figure 5.12 A). In section 5.2.4, I showed that the *pros-long intron* probe correlated with *pros^{long}* expression (Figure 5.6 A). Therefore, deletion of these three upstream TSSs would block transcription of *pros^{long}* without disrupting *pros^{short}*.

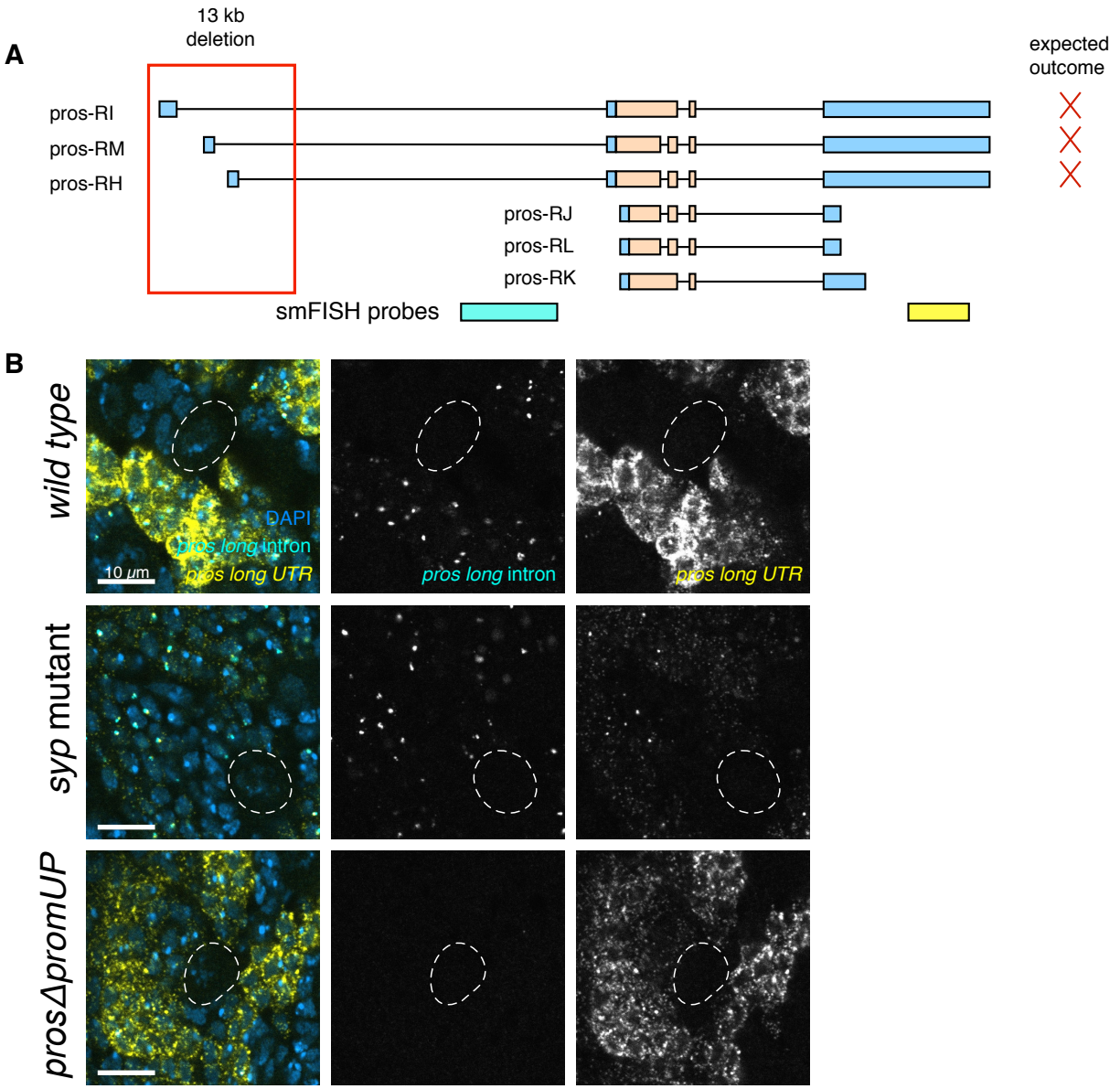


Figure 5.12 Deletion of the upstream TSSs does not remove all *pros-long* signal
A A CRISPR-Cas9 strategy was designed to delete the three upstream TSSs, which are annotated to produce *pros*^{long}. **B** Staining the *prosΔpromUP* line with *pros-long* intron and *pros-long* UTR smFISH probes showed that transcription from the upstream TSSs was abolished. However, low levels of signal from *pros-long* UTR remained. (*wild type* and *syp* mutant repeated from Figure 5.6).

I used an HR strategy with dsRED marker to produce this deletion in a similar way to the 3' UTR deletion. gRNAs designed by Dr Andrew Bassett were used to make two double stranded cuts, to delete ~13 kb spanning the three upstream *pros* TSSs (Figure 5.12 A, gRNAs Appendix Table C.3). I produced and validated a line with this deletion (*prosΔpromUP*) (Appendix C.4). I studied the *prosΔpromUP* line using smFISH (Figure 5.12 B). As expected, signal from the *pros*^{long} upstream intron was

lost, indicating that transcription from the upstream TSSs is abolished. Probes against the extended 3' UTR show a substantial decrease in transcript number, but not a complete loss of the *pros*^{long} isoform, as seen in the *syp* mutant. This shows that the extended 3' UTR is not necessarily produced from the upstream TSSs. The transcript in *prosΔpromUP* contains the 3' UTR extension, but originates from a downstream TSS. This is most likely due to transcriptional elongation from the downstream *pros*^{short} promoter. Alternatively there could be an further unannotated TSS, but TSS RAMPAGE (RNA Annotation and Mapping of Promoters for the Analysis of Gene Expression) data on FlyBase does not indicate additional TSSs. Finally, there could be activation of a cryptic TSS as a response to the deletion of the endogenous upstream TSSs.

I was interested to characterise the *pros* isoforms in *prosΔpromUP.* Costaining with *pros* exon and *pros-long* smFISH showed expression of the coding exon with the 3' UTR extension (Figure 5.13 A). I costained with anti-Pros IF, in order to examine Pros protein level. Surprisingly, despite the reduction in *pros-long* signal in *prosΔpromUP*, Pros protein was upregulated in neurons similarly to the *wild type* (Figure 5.13 A). I wanted to check whether the entire 3' UTR extension was expressed, so I designed smFISH probes at the far 5' and 3' ends of the *pros* 3' UTR and stained the *prosΔpromUP* line (Figure 5.13 B). This shows that the new *pros* isoform (hereafter referred to as *pros*^{mid}) contains the fully extended 3' UTR (estimated transcript structure illustrated in Figure 5.13 C). Although the levels of *pros*^{mid} in *prosΔpromUP* are lower than the *wild type* levels of *pros*^{long}, it is sufficient to produce Pros protein upregulation in neurons.

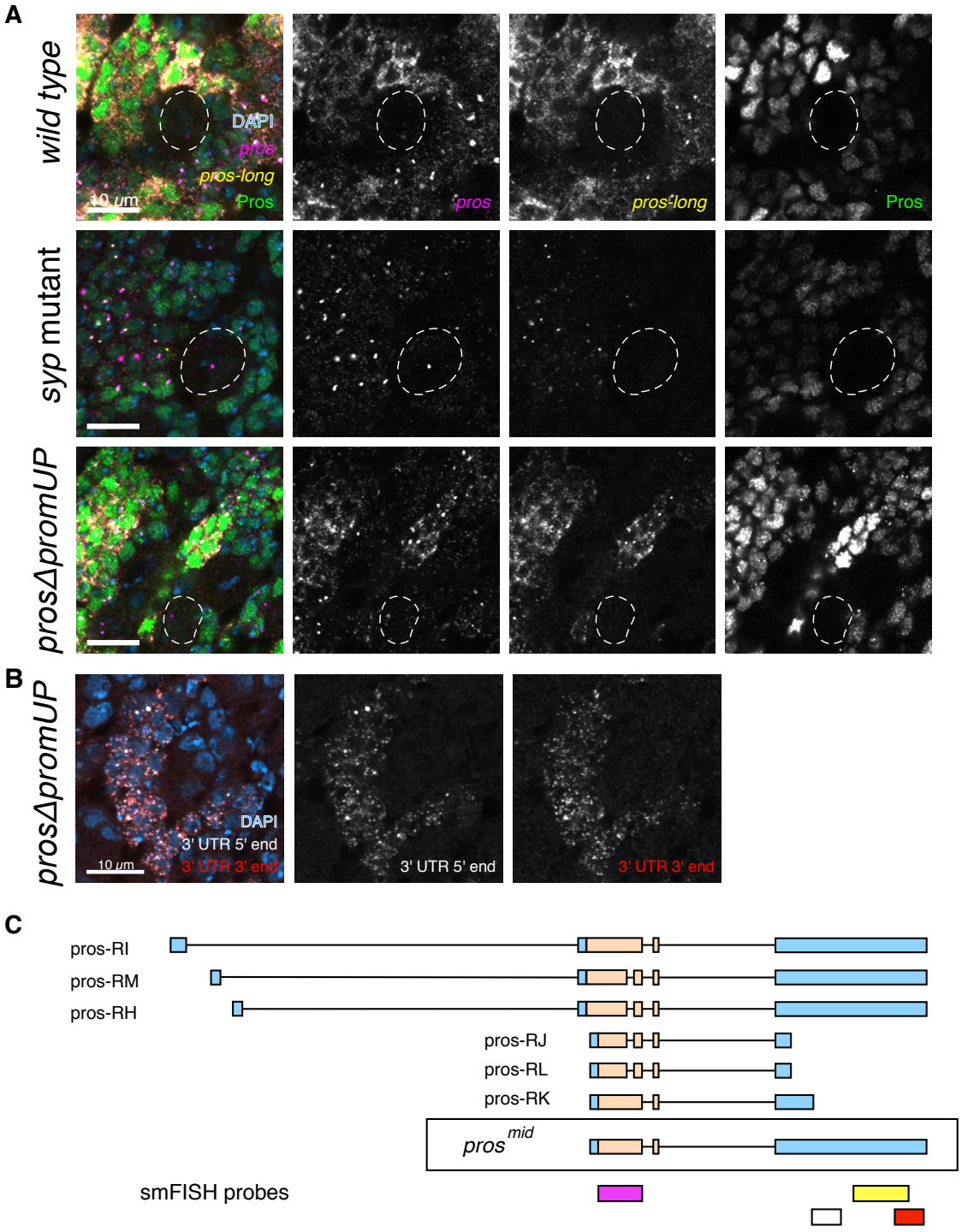


Figure 5.13 Deletion of the upstream TSSs reveals a new *pros* isoform
A Staining for *pros exon* smFISH shows that *prosΔpromUP* expresses a transcript including the coding exon as well as the extended 3' UTR. Pros protein staining shows that *prosΔpromUP* expresses *wild type* levels of Pros. **B** Staining with smFISH probes at the far 5' and 3' ends of the 3' UTR in the *prosΔpromUP* line shows that the novel transcript includes the full 3' UTR. **C** Annotation of the likely structure of the novel *pros* transcript, *pros*^{mid}.

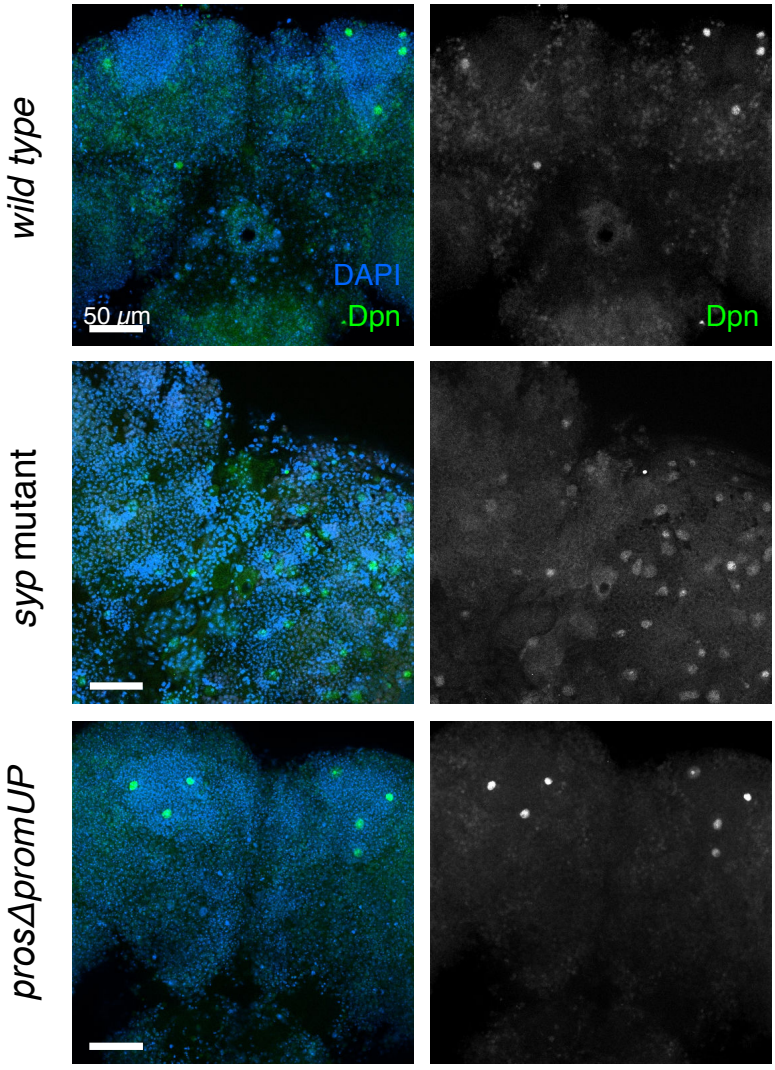


Figure 5.14 Pupal termination is unaffected by loss of upstream TSSs
Pupal brains were dissected at 48 hr after pupal formation (APF) and stained with Dpn to mark NBs. In the *wild type,* NBs have terminated at this stage, except the 8 long-lived MB NBs. In the *syp* mutant, many of the type I NBs do not terminate correctly and remain at 48 hr APF. In the *prosΔpromUP* line the NBs terminate as in the *wild type.* (z projection of 3x 500 nm z stacks).

Dr Lu Yang previously showed that terminating NBs express $pros^{long}$ (Figure 5.9). This suggested that there was a transcriptional switch from $pros^{short}$ to $pros^{long}$ at termination. Deletion of the upstream TSSs may prevent the transcriptional switch to the more stable isoform including the extended 3' UTR. This would block NB termination in *prosΔpromUP*, as seen in the *syp* mutant. I collected pupae at 48 hours APF and stained with Dpn to mark NBs (Figure 5.14). This showed that NBs terminate normally in *prosΔpromUP,* as only the four MB NBs were remaining in

each lobe (compared to the large number of persistent NBs in the *syp* mutant). This result suggests a redundancy in the *pros* isoform switch, which occurs both at the upstream TSS and by skipping the short polyadenylation sites. *pros^{mid}* presumably allows sufficient Pros expression in the pupal NB to permit termination.

Collectively *prosΔpromUP* indicates the presence of a third key *pros* isform, *pros^{mid},* which contributes most of the Pros protein upregulation in larval neurons. However, many questions remain. Is the transcript present and translated in the *wild type*? Do *pros^{long}* and *pros^{mid}* have distinct functional roles? Or is *pros^{mid}* upregulated in the *prosΔpromUP* mutant as a response to the lack of *pros^{long}*, to maintain the necessary levels of Pros protein? The upstream 5' UTR regions of *pros^{long}* are too short to design smFISH probes, and therefore it is not clear how much signal from the *pros-long* probes in the *wild type* is from *pros^{long}* versus *pros^{mid}*. Further experiments will be required to address these questions.

5.4.4 Ongoing strategies to delete the *pros* UTR extension

In 5.4.2, direct deletion of the *pros* 3' UTR extension was unsuccessful. However, this experiment is essential to identify the definitive function of the *pros* 3' UTR extension. Therefore, I explored alternative strategies to achieve this.

Firstly, I designed a construct to insert an attP site just downstream of the short polyA site (Figure 5.15 A). This strategy is similar to previous HR strategies discussed, but with a single CRISPR/Cas9 cut to allow insertion of the marker and attP site without deleting any genomic sequence. After producing the constructs for this approach, I have now identified positive lines, which will be validated after the submission of this thesis. This strategy will allow a second step to insert different sequences into this attP site through integration from a donor with an attB site. Initially, a strong SV40

terminator sequence will be inserted, which should block further elongation into the extended 3' UTR region. In the future, other sequences could also be inserted into this site, for example allowing inclusion of the extended 3' UTR with Syp binding sites mutated.

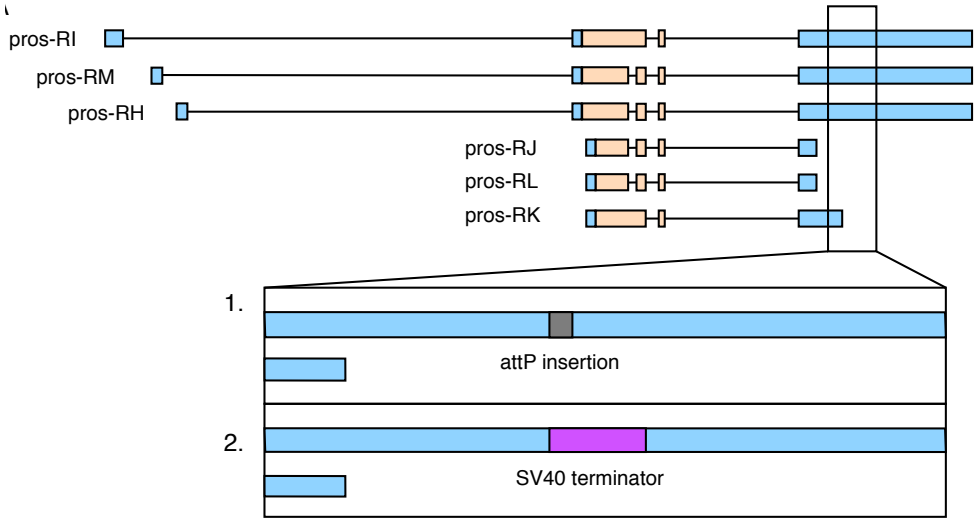


Figure 5.15 Ongoing strategies to study the *pros* extended 3' UTR
CRISPR Cas9 will be used to make one double stranded DNA break downstream of the short polyadenylation site. Homologous recombination will be used to insert an attP site, which can be used in a second step to insert sequences such as an SV40 terminator. This strategy will not delete any genomic DNA sequence.

I hope that this strategy will provide insight into the role of the *pros* extended 3' UTR, and its regulation by Syp.

5.5 CONCLUSION AND DISCUSSION

In this Chapter, I demonstrated that *pros* is regulated at the post-transcriptional level through Syp-dependent mRNA stability, and made progress to understanding the function of the different *pros* isoforms. This work validated and expanded upon the work of Dr Lu Yang. A switch in *pros* isoform, to include an extended 3' UTR, is tightly correlated with increased cytoplasmic *pros* mRNA, and a corresponding increase in Pros protein level. Syp specifically stabilises *pros*^{long}, and is required for the

upregulation of Pros protein. Therefore, it is hypothesised that the Syp stabilisation of *pros* mRNA through its extended 3' UTR leads to the upregulation of Pros protein.

The imaging data and clonal analysis in the *syp* mutant, show that Syp regulation of $pros^{long}$ does not play a role in the primary function of Pros: preventing reversion of GMCs to a stem cell fate. In the *syp* mutant, sufficient Pros remains to maintain a differentiated fate. However, the elevated levels of Pros in the post-mitotic progeny cells are significantly reduced and it is unclear what the functional consequence of this loss is, if any.

Both the molecular mechanism and function of Syp regulation of $pros^{long}$ have not been uncovered. Deletion of the *pros* extended 3' UTR is an essential experiment. It will show whether Syp stabilises $pros^{long}$ through its 3' UTR extension, as well as whether upregulated $pros^{long}$ is responsible for the Pros protein level increase in neurons and terminating pupal NBs. However, attempts to delete the 3' UTR extension were unsuccessful, perhaps due to a dominant lethal effect of either the deletion itself or off-targets. Deletion of such a large region may disrupt key enhancers of other genes. More speculatively, perhaps the long 3' UTR of *pros* is essential in order to mop up levels of other RBPs, and the loss of this function disrupts regulation of other genes. It is unclear why the 3' UTR is so huge, ~15 kb, which would intuitively seem very wasteful if it does not play a function.

The ongoing strategies planned and described in section 5.4.4 may provide the tools to study the role of the 3' UTR in more depth. However, although the attempts to delete $pros^{long}$ have so far been unsuccessful, they have uncovered further levels of complexity in the regulation of Pros. The NMD experiment in section 5.4.1 provided insight into the Pros protein isoforms. The annotated $pros^{long}$ isoforms include a 300

amino acid N terminal extension, which could alter protein function. However, inserting a frame shift and premature stop codon into this region did not truncate the protein or lead to NMD. This suggests that this exon is not translated, implying that *pros*^{long} and *pros*^{short} encode the same Pros protein isoform. This is important because it means that the switch in transcript isoform is not due to a requirement for a functionally different protein.

The *prosΔpromUP* line showed that the isoform switch to include the extended 3' UTR in the post-mitotic neurons may occur by skipping the *pros*^{short} polyA site, as well as through changing to an upstream TSS. It is unclear the extent to which these mechanisms contribute in the *wild type*. When the upstream TSSs are removed, elongation from a downstream TSS allows production of a much lower level of the extended 3' UTR isoform, *pros*^{mid}, but no difference in the amount of Pros protein. Collectively this data provides two possible hypotheses: 1. *pros*^{long} and *pros*^{mid} are both present in the *wild type,* but *pros*^{long} is translationally repressed, and the neuronal Pros protein upregulation comes from *pros*^{mid}. 2. Only *pros*^{long} is present and translated to produce the Pros protein upregulation in *wild type* neurons, but when the upstream TSS is removed, expression of *pros*^{mid} and increased translation compensate to allow *wild type* levels of Pros protein.

To distinguish these possibilities, it would be important to know if *pros*^{mid} is present in the *wild type*, or simply a response to the deletion mutant. This could be studied with Northern blots in the *wild type* and *prosΔpromUP* mutants, to look for changes in isoform expression. It is difficult to measure the relative levels of *pros*^{long} *and pros*^{mid} by smFISH because there is insufficient unique sequence to design smFISH probes. RNAseq data can indicate the levels of different isoforms using reads spanning exon junctions and relative levels of reads from unique and common exons. However,

where there are many combinations of alternative splicing, it is very difficult to assign the reads to the correct isoforms. An alternative sequencing technology such as long read RNAseq using Oxford Nanopore technology would circumvent this problem by sequencing the whole length of the mRNA (Byrne et al., 2017). However, the limiting step in this technology is currently the production of long enough cDNAs in the library preparation. Another option might be TIF-seq, which sequences the 5' and 3' ends of each transcript to help isoform identification (Pelechano et al., 2014).

Secondly, the level of translation of different isoforms could be measured. Polysome profiling, followed by sequencing, or ribosome profiling could be used to indicate if *pros*^{long} and *pros*^{mid} are translated, and if there are changes in isoform translation between the *wild type* and the *prosΔpromUP* mutant. These methods would depend on being able to measure reads from sequence that is unique to the different isoforms.

It would be interesting to examine the conservation of the post-transcriptional regulation of *pros.* The human homolog of Pros, PROX1, also functions in neurogenesis, particularly in the hippocampus (Stergiopoulos et al., 2014). PROX1 directs differentiation of progenitor cells to neurons *in vivo.* Furthermore, higher PROX1 expression in human neuroblastomas is associated with a more positive prognosis (Foskolou et al., 2013). Overexpression of PROX1 limits the proliferation of neuroblastoma cell lines. Therefore, understanding the regulation of PROX1 is of significant interest to cancer biologists. It will be very interesting to uncover if there is a role of isoform switching or post-transcriptional regulation of PROX1. Perhaps this could initially be examined with smFISH and IF experiments, analogous to those in this Chapter.

In conclusion, the regulation of Pros level involves a transcriptional isoform switch to exploit a change in Syp-dependent mRNA stability. The deletion lines described here have uncovered further layers of complexity and multiple layers of redundancy. However, the primary question of function remains unclear. The huge upregulation of *pros*^{long} and Pros protein in neurons would be unusually wasteful if it has no function, but this is still unknown. Specific isoform deletion is a necessary next step to understanding the regulation of Pros.

6.

DISCUSSION AND FUTURE PERSPECTIVES

Understanding the processes behind neurogenesis remains one of the great challenges of biology. A huge number and variety of neurons and non-neuronal cells are produced and form the vastly complex network that is the brain. This must be very tightly regulated in order to ensure functionality and avoid uncontrolled proliferation. The *Drosophila* model organism has been used with great success to uncover the principles of neurogenesis. Key regulators have been identified, many of which are conserved in mammalian systems. Most early work focused on identifying TFs and their downstream targets. This uncovered the TF cascade that governs progeny fate in the embryo, as well as TFs that control the balance between cell proliferation and differentiation, such as Pros. However, the regulation of the TFs themselves is less well understood and in some situations, such as larval progeny fate, responsible TFs have so far not been identified.

Post-transcriptional regulation, orchestrated by RBPs, allows precise temporal control of the protein complement within sub-cellular compartments, and flexibility to respond

rapidly to changing conditions. Intuitively, this additional layer of regulation could be critical to coordinate NB behaviour precisely throughout development. However, only a small number of examples of post-transcriptional regulation in neurogenesis have been uncovered. The extent of post-transcriptional regulation of NB activity was unknown. Therefore, in this thesis, I examined the contribution of post-transcriptional regulation in NB biology, specifically control of NB size, proliferation and termination.

A study aiming to find regulators of larval progeny fate identified two conserved RBPs, Imp and Syp, which are expressed in opposing gradients in NBs through development (Liu et al., 2015). These two RBPs regulate each other through reciprocal negative feedback to guide the progression of the gradients. The identification of Imp and Syp as regulators of progeny fate indicates a more significant role of post-transcriptional regulation in this system than previously appreciated. However, their mechanisms of action were poorly understood. A candidate approach identified Imp/Syp regulation of a key TF, Chinmo, which determines progeny fate in the MB (Liu et al., 2015). However, this candidate approach is limited by our prior knowledge in the literature, and does not give a broad insight into the action of Imp and Syp. I aimed to identify the mRNA targets of Imp and Syp with an unbiased, genome-wide approach, using RIPseq.

I performed RIPseq in collaboration with Dr Aino Järvelin to identify the mRNA targets of Imp and Syp (Chapter 3). Each RBP significantly IPed several hundred targets, including previously characterised targets and genes known to play important roles in various stages of neurogenesis. These are candidates which might be post-transcriptionally regulated by Imp or Syp through mRNA stability, localisation or translation. However, not all pulled down mRNAs are regulated, as some interactions are indirect. Therefore, I performed RNAseq in the *syp* mutant to identify targets with

altered transcript levels when Syp is removed and found a small number of candidates with significant changes. This method only identifies regulatory processes which affect mRNA level (e.g. transcription or mRNA stability), and furthermore measures an average of the whole brain, with no cell type specificity. I moved to a gene-by-gene microscopy strategy and used the lists of mRNA targets from the RIPseq experiment to choose targets to examine further. I particularly focused on conserved TFs with known phenotypes in neurogenesis, and genes with large 3' UTR extensions, which may allow for differential regulation. I characterised the phenotypes of *imp* and *syp* in regulating NB growth, division and termination, and then aimed to use the list of targets to understand the mechanism of this regulation.

Among the targets of Imp and Syp were the two key regulatory components of the Myc transcriptional network: Myc and Mnt. These TFs compete for binding to Max, forming heterodimers that antagonise each other in activity. The Myc transcriptional network has been shown to regulate cell growth and division in many different cell types, and is transcriptionally activated downstream of developmentally significant signalling pathways. Therefore, I asked whether Myc and Mnt are regulated by Imp or Syp, and whether a change in Myc or Mnt level explains the NB size and proliferation phenotypes of *imp* and *syp*. In Chapter 4, I showed that Myc level is increased in the *syp* mutant, but Mnt was unchanged, suggesting its level is not regulated by Imp or Syp. I then used smFISH and IF to quantitate the *myc* transcription rate and half life, showing that the *myc* half life was increased three-fold in the *syp* mutant, leading to increased Myc protein. I used a double Imp and Syp knockdown to show that Imp stabilises *myc.*

In order to understand the regulatory relationship between Imp and *myc*, I used previously published Imp iCLIP data performed in S2 cells (analysed by Dr Aino

Järvelin) to identify a region of most Imp binding in the *myc* 3' UTR extension. I produced CRISPR deletions in the endogenous *myc* locus to attempt to abolish Imp binding, but did not have time to characterise these lines in detail. After this thesis is submitted, these lines will be used to examine whether Imp stabilises *myc* via its long 3' UTR. I already showed that Myc overexpression phenocopies upregulated Imp in the increased NB size and proliferation rate. I therefore plan to do epistasis experiments with simultaneous manipulation of Imp and Myc levels, in order to test whether the NB growth and division phenotype of *imp* occurs due to dysregulation of Myc. The results of these experiments will strengthen our understanding of the role of Imp regulation of Myc.

pros was among the other Imp and Syp targets found in the RIPseq experiments. Pros is a key TF in ensuring the balance between proliferative character of the NB and the differentiation of the progeny cells. Its functional role has been highly studied, but its own regulation is poorly understood, especially in neurons and in the terminating NB. Dr Lu Yang, in the Davis lab, had previously shown that *pros* level is reduced in the *syp* mutant, through reduced mRNA stability, and that a long isoform of *pros* is specifically destabilised in the mutant. I continued this project in Chapter 5, aiming to identify the role of $pros^{long}$ and its regulation by Syp. I used clonal analysis to show that tumours are not formed in the *syp* mutant, which means that sufficient Pros remains in the absence of $pros^{long}$ to prevent reversion of progeny cells to a stem cell fate.

Syp is required for the terminal NB division (Yang et al., 2017a). We hypothesised that Syp may stabilise $pros^{long}$ in the pupal NB to allow termination. I used CRISPR/Cas9 technology to specifically remove $pros^{long,}$ in order to examine its function in the pupa, but I was unable to directly delete the extended 3' UTR region. Deletion of the

pros^{long}-specific promoter region uncovered a novel unannotated *pros* transcript, which may produce the majority of the Pros protein. I then designed alternative deletion strategies, which will be used in future to dissect the roles and regulation of the *pros* isoforms.

The work presented in this thesis examines two key examples of post-transcriptional regulation by Imp and Syp, and in identifying further targets, paves the way to uncover many more. Myc and Pros are both extremely well studied TFs, conserved in humans and involved in tumour formation and cancers. Understanding their regulation in *Drosophila* development may provide insight into human disease processes. Additionally, the lists of mRNA targets of Imp and Syp include many more genes that are well studied in neurogenesis. It is highly likely that many of these are post-transcriptionally regulated. Jeffrey Lee in the Davis lab is systematically examining these for indications of post-transcriptional regulation, using endogenously tagged proteins, smFISH and IF.

I successfully developed and executed an approach to identify and quantitate the post-transcriptional regulation of individual RBP bound targets. However, pinning down the exact functional roles of this regulation was much more difficult. Imp and Syp each have several hundred mRNA targets and therefore their complex phenotypes are certainly the result of dysregulation of a number of these different targets (and the downstream disruption). I focused on the targets encoding TFs, but Imp and Syp also bound a large number of transcripts encoding RBPs. This is indicative of a complex cross-regulatory network of RBPs, in which positive or negative feedback relationships minimise the effect of perturbations. However, a major disruption such as knockdown of a key RBP is likely to have knock-on effects

throughout the network. A single target approach is therefore extremely simplified, but is currently necessary for experimental as well as conceptual reasons.

This work also emphasised the importance of differential regulation of mRNA isoforms. Dissection of these processes, as in the case of *pros*, requires the production of tools, such as endogenous deletions, to examine their individual functions. Post-transcriptional regulation may be essential to fine-tune levels of key factors and therefore conventional all-or-nothing tools, such as overexpression and knockdown constructs, may not provide true insight into the real role of this regulation in development.

I did not examine the molecular mechanisms of Imp and Syp action in detail. I found that Imp promotes *myc* stability, and Syp stabilises $pros^{long}$, with indications that both of these processes depend on binding to the 3' UTR. However, I have not performed experiments to examine the mechanism of stabilisation. The RBP binding might protect the mRNA from the physical attack of the degradation machinery, or block the binding of alternative RBPs or microRNAs that recruit this machinery. Imp binding sites are enriched for AU-rich sequences (Hansen et al., 2015). AU-rich elements are commonly destabilising sequences that promote the recruitment of polyA shortening enzymes (Barreau et al., 2005). Imp binding of AU-rich sequences may block this recruitment and therefore prevent mRNA degradation. Imp or Syp binding could alternatively bring the specific mRNA to a protective RNP environment, where other RBPs prevent its degradation. Without experimental evidence, the molecular mechanisms can only be speculated.

This work has been done in *Drosophila* larval and pupal brains, which are a well-established model for stem cell development, but it would be very interesting to

examine whether the same principles are conserved in mammalian systems. Both Pros and Myc have important human homologs, which may be regulated in a similar manner. This could be tested, for example through smFISH in mouse brain sections. More generally, the post-transcriptional regulatory mechanisms described here may be found to regulate other candidate genes or processes in mammalian neurogenesis.

In conclusion, post-transcriptional regulation plays a significant role in NB biology, but must be considered as a partner of, rather than an alternative to, transcriptional regulation. The mRNA stability of *pros* is regulated by Syp, but is dependent on the isoform choice at the transcriptional level. Inclusion of the *pros* extended 3' UTR allows stabilisation by Syp. In the case of Myc, the developmental progression cue of Imp level stabilising *myc* mRNA is integrated with transcriptional activation downstream of systemic signals such as nutrient sensing. The layers of regulation allow coordination of multiple input signals resulting in tightly regulated stem cell growth and division. This thesis contributes to our understanding of neural development and raises future questions on the molecular mechanisms of neurogenesis.

Bibliography

Anders, S., Pyl, P.T., and Huber, W. (2015). Htseq--a Python Framework to Work with High-Throughput Sequencing Data. Bioinformatics *31*, 166-169.

Arama, E., Dickman, D., Kimchie, Z., SHearn, A., and Lev, Z. (2000). Mutations in the B-Propeller Domain of the Drosophila Brain Tumor (Brat) Protein Induce Neoplasm in the Larval Brain. Oncogene *19*, 3706-3716.

Ardehali, M.B., and Lis, J.T. (2009). Tracking Rates of Transcription and Splicing in Vivo. Nat Struct Mol Biol *16*, 1123-1124.

Awasaki, T., Kao, C.F., Lee, Y.J., Yang, C.P., Huang, Y., Pfeiffer, B.D., Luan, H., Jing, X., Huang, Y.F., He, Y.*, et al.* (2014). Making Drosophila Lineage-Restricted Drivers Via Patterned Recombination in Neuroblasts. Nat Neurosci *17*, 631-637.

Azevedo, F.A., Carvalho, L.R., Grinberg, L.T., Farfel, J.M., Ferretti, R.E., Leite, R.E., Jacob Filho, W., Lent, R., and Herculano-Houzel, S. (2009). Equal Numbers of Neuronal and Nonneuronal Cells Make the Human Brain an Isometrically Scaled-up Primate Brain. J Comp Neurol *513*, 532-541.

Bahar Halpern, K., and Itzkovitz, S. (2016). Single Molecule Approaches for Quantifying Transcription and Degradation Rates in Intact Mammalian Tissues. Methods *98*, 134-142.

Baltz, A.G., Munschauer, M., Schwanhausser, B., A., V., Murakawa, Y., Schueler, M., Youngs, N., Penfold-Brown, D., Drew, K., Milek, M.*, et al.* (2012). The Mrna-Bound Proteome and Its Global Occupancy Profile on Protein-Coding Transcripts. Mol Cell *46*, 674-690.

Bannai, H., Fukatsu, K., Mizutani, A., Natsume, T., Iemura, S., Ikegami, T., Inoue, T., and Mikoshiba, K. (2004). An Rna-Interacting Protein, Syncrip (Heterogeneous Nuclear Ribonuclear Protein Q1/Nsap1) Is a Component of Mrna Granule Transported with Inositol 1,4,5-Trisphosphate Receptor Type 1 Mrna in Neuronal Dendrites. J Biol Chem *279*, 53427-53434.

Barreau, C., Paillard, L., and Osborne, H.B. (2005). Au-Rich Elements and Associated Factors: Are There Unifying Principles? Nucleic Acids Res *33*, 7138-7150.

Bell, J.L., Wachter, K., Muhleck, B., Pazaitis, N., Kohn, M., Lederer, M., and Huttelmaier, S. (2013). Insulin-Like Growth Factor 2 Mrna-Binding Proteins (Igf2bps): Post-Transcriptional Drivers of Cancer Progression? Cell Mol Life Sci *70*, 2657-2675.

Bello, B., Reichert, H., and Hirth, F. (2006). The Brain Tumor Gene Negatively Regulates Neural Progenitor Cell Proliferation in the Larval Central Brain of Drosophila. Development *133*, 2639-2648.

Bello, B.C., Hirth, F., and Gould, A.P. (2003). A Pulse of the Drosophila Hox Protein Abdominal-a Schedules the End of Neural Proliferation Via Neuroblast Apoptosis. 37, 209-219.

Bello, B.C., Izergina, N., Caussinus, E., and Reichert, H. (2008). Amplification of Neural Stem Cell Proliferation by Intermediate Progenitor Cells in Drosophila Brain Development. Neural Dev *3*, 5.

Benassayag, C., Montero, L., Colombie, N., Gallant, P., Cribbs, D., and Morello, D. (2005). Human C-Myc Isoforms Differentially Regulate Cell Growth and Apoptosis in Drosophila Melanogaster. Mol Cell Biol *25*, 9897-9909.

Berdnik, D., Torok, T., Gonzalez-Gaitan, M., and Knoblich, J.A. (2002). The Endocytic Protein a-Adaptin Is Required for Numb-Mediated Asymmetric Cell Division in Drosophila. Developmental Cell *3*, 221-231.

Berger, C., Harzer, H., Burkard, T.R., Steinmann, J., van der Horst, S., Laurenson, A.S., Novatchkova, M., Reichert, H., and Knoblich, J.A. (2012). Facs Purification and Transcriptome Analysis of Drosophila Neural Stem Cells Reveals a Role for Klumpfuss in Self-Renewal. Cell Rep *2*, 407-418.

Bernstein, P.L., Herrick, D.J., Prokipcak, R.D., and Ross, J. (1992). Control of C-Myc Mrna Half-Life in Vitro by a Protein Capable of Binding to a Coding Region Stability Determinant. Genes & Development, *6*, 642-654.

Betschinger, J., Mechtler, K., and Knoblich, J.A. (2006). Asymmetric Segregation of the Tumor Suppressor Brat Regulates Self-Renewal in Drosophila Neural Stem Cells. Cell *124*, 1241-1253.

Blackwood, E.M., and Eisenman, R.N. (1991). Max: A Helic-Loop-Helix Zipper Protein That Forms a Sequence-Specific DNA-Binding Complex with Myc. Science *251*, 1211-1217.

Boylan, K.L., Mische, S., Li, M., Marques, G., Morin, X., Chia, W., and Hays, T.S. (2008). Motility Screen Identifies Drosophila Igf-Ii Mrna-Binding Protein--Zipcode-Binding Protein Acting in Oogenesis and Synaptogenesis. PLoS Genet *4*, e36.

Burgin, K.E., Waxham, M.N., Rickling, S., Westgate, S.A., Mobley, W.C., and Kelly, P.T. (1990). In Situ Hybridization Histochemistry of Ca2+/Calmodulin-Dependent Protein Kinase in Developing Rat Brain. The Journal of Neuroscience *6*.

Byrne, A., Beaudin, A.E., Olsen, H.E., Jain, M., Cole, C., Palmer, T., DuBois, R.M., Forsberg, E.C., Akeson, M., and Vollmers, C. (2017). Nanopore Long-Read Rnaseq Reveals Widespread Transcriptional Variation among the Surface Receptors of Individual B Cells. Nat Commun *8*, 16027.

Cajigas, I.J., Tushev, G., Will, T.J., tom Dieck, S., Fuerst, N., and Schuman, E.M. (2012). The Local Transcriptome in the Synaptic Neuropil Revealed by Deep Sequencing and High-Resolution Imaging. Neuron *74*, 453-466.

Carney, T.D., Struck, A.J., and Doe, C.Q. (2013). Midlife Crisis Encodes a Conserved Zinc-Finger Protein Required to Maintain Neuronal Differentiation in Drosophila. Development *140*, 4155-4164.

Castello, A., Fischer, B., Eichelbaum, K., Horos, R., Beckmann, B.M., Strein, C., Davey, N.E., Humphreys, D.T., Preiss, T., Steinmetz, L.M.*, et al.* (2012). Insights into Rna Biology from an Atlas of Mammalian Mrna-Binding Proteins. Cell *149*, 1393-1406.

Castello, A., Fischer, B., Frese, C.K., Horos, R., Alleaume, A.M., Foehr, S., Curk, T., Krijgsveld, J., and Hentze, M.W. (2016). Comprehensive Identification of Rna-Binding Domains in Human Cells. Mol Cell *63*, 696-710.

Ceron, J., Tejedor, F.J., and Moya, F. (2006). A Primary Cell Culture Of*drosophila*postembryonic Larval Neuroblasts to Study Cell Cycle and Asymmetric Division. EJCB *85*, 567-575.

Chell, J.M., and Brand, A.H. (2010). Nutrition-Responsive Glia Control Exit of Neural Stem Cells from Quiescence. Cell *143*, 1161-1173.

Cheng, L.Y., Bailey, A.P., Leevers, S.J., Ragan, T.J., Driscoll, P.C., and Gould, A.P. (2011). Anaplastic Lymphoma Kinase Spares Organ Growth During Nutrient Restriction in Drosophila. Cell *146*, 435-447.

Chia, W., Somers, W.G., and Wang, H. (2008). Drosophila Neuroblast Asymmetric Divisions: Cell Cycle Regulators, Asymmetric Protein Localization, and Tumorigenesis. J Cell Biol *180*, 267-272.

Choksi, S.P., Southall, T.D., Bossing, T., Edoff, K., de Wit, E., Fischer, B.E., van Steensel, B., Micklem, G., and Brand, A.H. (2006). Prospero Acts as a Binary Switch between Self-Renewal and Differentiation in Drosophila Neural Stem Cells. Dev Cell *11*, 775-789.

Colonques, J., Ceron, J., Reichert, H., and Tejedor, F.J. (2011). A Transient Expression of Prospero Promotes Cell Cycle Exit of Drosophila Postembryonic Neurons through the Regulation of Dacapo. PLoS One *6*, e19342.

Dai, N., Ji, F., Wright, J., Minichiello, L., Sadreyev, R., and Avruch, J. (2017). Igf2 Mrna Binding Protein-2 Is a Tumor Promoter That Drives Cancer Proliferation through Its Client Mrnas Igf2 and Hmga1. Elife *6*.

Di Giammartino, D.C., Nishida, K., and Manley, J.L. (2011). Mechanisms and Consequences of Alternative Polyadenylation. Mol Cell *43*, 853-866.

Dobin, A., Davis, C.A., Schlesinger, F., Drenkow, J., Zaleski, C., Jha, S., Batut, P., Chaisson, M., and Gingeras, T.R. (2013). Star: Ultrafast Universal Rna-Seq Aligner. Bioinformatics *29*, 15-21.

Doe, C.Q., and Goodman, C.S. (1985). Early Events in Insect Neurogeneis. Ii. The Role of Cell Interactions and Cell Lineage in the Determination of Neuronal Precursor Cells. Dev Biol *111*, 206-219.

Edgar, B.A., and Datar, S.A. (1996). Zygotic Degradation of Two Maternal Cdc25 Mrnas Terminates Drosophila Early Cell Cycle Program. Genes & Development, *10*, 1966-1977.

Eichler, K., Li, F., Litwin-Kumar, A., Park, Y., Andrade, I., Schneider-Mizell, C.M., Saumweber, T., Huser, A., Eschbach, C., Gerber, B*., et al.* (2017). The Complete Connectome of a Learning and Memory Centre in an Insect Brain. Nature *548*, 175-182.

Farina, K.L., Huttelmaier, S., Musunuru, K., Darnell, R., and Singer, R.H. (2003). Two Zbp1 Kh Domains Facilitate Beta-Actin Mrna Localization, Granule Formation, and Cytoskeletal Attachment. J Cell Biol *160*, 77-87.

Femino, A.M., Fay, F.S., Fogarty, K., and Singer, R.H. (1998). Visualization of Single Rna Transcripts in Situ. Science *280*.

Foskolou, I.P., Stellas, D., Rozani, I., Lavigne, M.D., and Politis, P.K. (2013). Prox1 Suppresses the Proliferation of Neuroblastoma Cells Via a Dual Action in P27-Kip1 and Cdc25a. Oncogene *32*, 947-960.

Fuse, N., Hisata, K., Katzen, A.L., and Matsuzaki, F. (2003). Heterotrimeric G Proteins Regulate Daughter Cell Size Asymmetry in Drosophila Neuroblast Divisions. Current Biology *13*, 947-954.

Gailite, I., Aerne, B.L., and Tapon, N. (2015). Differential Control of Yorkie Activity by Lkb1/Ampk and the Hippo/Warts Cascade in the Central Nervous System. Proc Natl Acad Sci U S A *112*, E5169-5178.

Gallant, P., Shiio, Y., Cheng, P.F., Parkhurst, A.M., and Eisenman, R.N. (1996). Myc and Max Homologs in Drosophila. Science *274*.

Geng, C., and Macdonald, P.M. (2006). Imp Associates with Squid and Hrp48 and Contributes to Localized Expression of Gurken in the Oocyte. Mol Cell Biol *26*, 9508-9516.

Grandori, C., Cowley, S.M., James, L.P., and Eisenman, R.N. (2000). The Myc/Max/Mad Network and the Transcriptional Control of Cell Behaviour. Annu Rev Cell Dev Biol *16*, 653-699.

Gratz, S.J., Ukken, F.P., Rubinstein, C.D., Thiede, G., Donohue, L.K., Cummings, A.M., and O'Connor-Giles, K.M. (2014). Highly Specific and Efficient Crispr/Cas9-Catalyzed Homology-Directed Repair in Drosophila. Genetics *196*, 961-971.

Gumy, L.F., Yeo, G.S., Tung, Y.C., Zivraj, K.H., Willis, D., Coppola, G., Lam, B.Y., Twiss, J.L., Holt, C.E., and Fawcett, J.W. (2011). Transcriptome Analysis of Embryonic and Adult Sensory Axons Reveals Changes in Mrna Repertoire Localization. RNA *17*, 85-98.

Hailstone, M., Yang, L., Waithe, D., Samuels, T.J., Arava, Y., Dobrzycki, T., Parton, R.M., and Davis, I. (2018). Brain Development: Machine Learning Analysis of Individual Stem Cells in Live 3d Tissue. bioRxiv.

Halstead, J.M., Lin, Y.Q., Durraine, L., Hamilton, R.S., Ball, G., Neely, G.G., Bellen, H.J., and Davis, I. (2014). Syncrip/Hnrnp Q Influences Synaptic Transmission and Regulates Bmp Signaling at the Drosophila Neuromuscular Synapse. Biol Open *3*, 839-849.

Hansen, H.T., Rasmussen, S.H., Adolph, S.K., Plass, M., Krogh, A., Sanford, J., Nielsen, F.C., and Christiansen, J. (2015). Drosophila Imp Iclip Identifies an Rna Assemblage Coordinating F-Actin Formation. Genome Biol *16*, 123.

Harris, R.M., Pfeiffer, B.D., Rubin, G.M., and Truman, J.W. (2015). Neuron Hemilineages Provide the Functional Ground Plan for the Drosophila Ventral Nervous System. Elife *4*.

Hartenstein, V., Rudloff, E., and Campos-Ortega, J.A. (1987). The Pattern of Proliferation of the Neuroblasts in the Wild-Type Embryo of Drosophila Melanogaster. Roux's Arch Dev Biol *196*, 473-485.

Hartenstein, V., and Wodarz, A. (2013). Initial Neurogenesis in Drosophila. Wiley Interdiscip Rev Dev Biol *2*, 701-721.

Havin, L., Git, A., Elisha, Z., Oberman, F., Yaniv, K., Schwartz, S.P., Standart, N., and Yisraeli, J.K. (1998). Rna-Binding Protein Conserved in Both Microtubule- and Microfilament-Based Rna Localization. Genes & Development, *12*.

Hentze, M.W., Castello, A., Schwarzl, T., and Preiss, T. (2018). A Brave New World of Rna-Binding Proteins. Nat Rev Mol Cell Biol.

Hermann, T., and Patel, D.J. (1999). Stitching Together Rna Tertiary Architectures. J Mol Biol *294*, 829-849.

Hermann, T., and Patel, D.J. (2000). Rna Bulges as Architectural and Recognition Motifs. Structure *8*.

Hietakangas, V., and Cohen, S.M. (2009). Regulation of Tissue Growth through Nutrient Sensing. Annu Rev Genet *43*, 389-410.

Hilgers, V., Lemke, S.B., and Levine, M. (2012). Elav Mediates 3' Utr Extension in the Drosophila Nervous System. Genes Dev *26*, 2259-2264.

Hilgers, V., Perry, M. W., Hendrix, D., Stark, A., Levine, M., Haley, B. (2011). Neural-Specific Elongation of 3' Utrs During Drosophila Development. Proceedings of the National Academy of Sciences of the United States of America, *108*, 15864-15869.

Hirata, J., Nakagoshi, H., Nabeshima, Y., Matsuzaki, F. (1995). Asymmetric Segregation of the Homeodomain Protein Prospero During Drosophila Development. Nature *377*, 627-630.

Hobor, F., Dallmann, A., Ball, N.J., Cicchini, C., Battistelli, C., Ogrodowicz, R.W., Christodoulou, E., Martin, S.R., Castello, A., Tripodi, M.*, et al.* (2018). A Cryptic Rna-Binding Domain Mediates Syncrip Recognition and Exosomal Partitioning of Mirna Targets. Nat Commun *9*, 831.

Holt, C.E., and Schuman, E.M. (2013). The Central Dogma Decentralized: New Perspectives on Rna Function and Local Translation in Neurons. Neuron *80*, 648-657.

Homem, C.C., and Knoblich, J.A. (2012). Drosophila Neuroblasts: A Model for Stem Cell Biology. Development *139*, 4297-4310.

Homem, C.C., Reichardt, I., Berger, C., Lendl, T., and Knoblich, J.A. (2013). Long-Term Live Cell Imaging and Automated 4d Analysis of Drosophila Neuroblast Lineages. PLoS One *8*.

Homem, C.C., Repic, M., and Knoblich, J.A. (2015). Proliferation Control in Neural Stem and Progenitor Cells. Nat Rev Neurosci *16*, 647-659.

Homem, C.C.F., Steinmann, V., Burkard, T.R., Jais, A., Esterbauer, H., and Knoblich, J.A. (2014). Ecdysone and Mediator Change Energy Metabolism to Terminate Proliferation in Drosophila Neural Stem Cells. Cell *158*, 874-888.

Horvitz, H.R., and Herskowitz, I. (1992). Mechanisms of Asymmetric Cell Division: Two Bs or Not Two Bs, That Is the Question. Cell *68*, 237-255.

Hovhanyan, A., Herter, E.K., Pfannstiel, J., Gallant, P., and T., R. (2014). Drosophila Mbm Is a Nucleolar Myc and Casein Kinase 2 Target Required for Ribosome Biogenesis and Cell Growth of Central Brain Neuroblasts. Molecular and Cellular Biology *34*, 1878-1891.

Hu, Y., Comjean, A., Perkins, L.A., Perrimon, N., and Mohr, S.E. (2015). Glad: An Online Database of Gene List Annotation for Drosophila. Journal of Genomics *3*, 75-81.

Huppertz, I., Attig, J., D'Ambrogio, A., Easton, L.E., Sibley, C.R., Sugimoto, Y., Tajnik, M., Konig, J., and Ule, J. (2014). Iclip: Protein-Rna Interactions at Nucleotide Resolution. Methods *65*, 274-287.

Ikeshima-Kataoka, H., Skeath, J. B., Nabeshima, Y., Doe, C. Q., Matsuzaki, F. (1997). Miranda Directs Prospero to a Daughter Cell During Drosophila Asymmetric Divisions. Nature *390*, 625-629.

Isshiki, T., Pearson, B., Holbrook, S., Doe, C. Q. (2001). Drosophila Neuroblasts Sequentially Express Transcription Factors Which Specify the Temporal Identity of Their Neuronal Progeny. Cell *106*, 511-521.

Johnston, L.A., Prober, D.A., Edgar, B.A., Eisenman, R.N., and Gallant, P. (1999). Drosophila Myc Regulates Cellular Growth During Development. Cell.

Jung, H., Yoon, B.C., and Holt, C.E. (2012). Axonal Mrna Localisation and Local Protein Synthesis in Nervous System Assembly, Maintenance and Repair. Nature Reviews Neuroscience *13*, 308-324.

Kaltschmidt, J.A., and Brand, A.H. (2002). Asymmetric Cell Division: Microtubule Dynamics and Spindle Asymmetry. Journal of Cell Science *115*, 2257-2264.

Keene, J.D. (2007). Rna Regulons: Coordination of Post-Transcriptional Events. Nat Rev Genet *8*, 533-543.

Knoblich, J.A. (2008). Mechanisms of Asymmetric Stem Cell Division. Cell *132*, 583-597.

Kohwi, M., and Doe, C.Q. (2013). Temporal Fate Specification and Neural Progenitor Competence During Development. Nat Rev Neurosci, *14*, 823-838.

Landskron, L., Steinmann, V., Bonnay, F., Burkard, T.R., Steinmann, J., Reichardt, I., Harzer, H., Laurenson, A.S., Reichert, H., and Knoblich, J.A. (2018). The Asymmetrically Segregating Lncrna Cherub Is Required for Transforming Stem Cells into Malignant Cells. Elife *7*.

Layalle, S., Arquier, N., and Leopold, P. (2008). The Tor Pathway Couples Nutrition and Developmental Timing in Drosophila. Dev Cell *15*, 568-577.

Legland, D., Arganda-Carreras, I., and Andrey, P. (2016). Morpholibj: Integrated Library and Plugins for Mathematical Morphology with Imagej. Bioinformatics *32*, 3532-3534.

Lelieveld, S.H., Reijnders, M.R., Pfundt, R., Yntema, H.G., Kamsteeg, E.J., de Vries, P., de Vries, B.B., Willemsen, M.H., Kleefstra, T., Lohner, K.*, et al.* (2016). Meta-Analysis of 2,104 Trios Provides Support for 10 New Genes for Intellectual Disability. Nat Neurosci *19*, 1194-1196.

Li, H., Handsaker, B., Wysoker, A., Fennell, T., Ruan, J., Homer, N., Marth, G., Abecasis, G., Durbin, R., and Genome Project Data Processing, S. (2009). The Sequence Alignment/Map Format and Samtools. Bioinformatics *25*, 2078-2079.

Li, P., Yang, X., Wasser, M., Cai, Y., and Chia, W. (1997). Inscuteable and Staufen Mediate Asymmetric Localization and Segregation of Prospero Rna During Drosophila Neuroblast Cell Divisions. Cell *90*, 437-447.

Li, X., Kazan, H., Lipshitz, H.D., and Morris, Q.D. (2014). Finding the Target Sites of Rna-Binding Proteins. Wiley Interdiscip Rev RNA *5*, 111-130.

Liu, Z., Yang, C.P., Sugino, K., Fu, C.C., Liu, L.Y., Yao, X., Lee, L.P., and Lee, T. (2015). Opposing Intrinsic Temporal Gradients Guide Neural Stem Cell Production of Varied Neuronal Fates. Science *350*, 317-320.

Lloyd, A.C. (2013). The Regulation of Cell Size. Cell *154*, 1194-1205.

Loo, L.W., Secombe, J., Little, J.T., Carlos, L.S., Yost, C., Cheng, P.F., Flynn, E.M., Edgar, B.A., and Eisenman, R.N. (2005). The Transcriptional Repressor Dmnt Is a Regulator of Growth in Drosophila Melanogaster. Mol Cell Biol *25*, 7078-7091.

Love, M.I., Huber, W., and Anders, S. (2014). Moderated Estimation of Fold Change and Dispersion for Rna-Seq Data with Deseq2. Genome Biol *15*, 550.

Malik, S., and Roeder, R.G. (2010). The Metazoan Mediator Co-Activator Complex as an Integrative Hub for Transcriptional Regulation. Nat Rev Genet *11*, 761-772.

Martin, M. (2011). Cutadapt Removes Adapter Sequences from High-Throughput Sequencing Reads. EMBnetjournal *17*.

Mata, J., and Wise, J.A. (2017). 4-Thiouridine Labeling to Analyze Mrna Turnover in Schizosaccharomyces Pombe. Cold Spring Harb Protoc *2017*, pdb prot091645.

Matsuzaki, H., Hiroaki, D., Hatta, M., Tanaka, K., and Fukamizu, A. (2003). Insulin-Induced Phosphorylation of Fkhr (Foxo1) Targets to Proteasomal Degradation. PNAS *100*, 11285-11290.

Maurange, C., Cheng, L., and Gould, A.P. (2008). Temporal Transcription Factors and Their Targets Schedule the End of Neural Proliferation in Drosophila. Cell *133*, 891-902.

Mayr, C. (2017). Regulation by 3'-Untranslated Regions. Annual Review of Genetics *51*, 171-194.

McDermott, S.M., Meignin, C., Rappsilber, J., and Davis, I. (2012). Drosophila Syncrip Binds the Gurken Mrna Localisation Signal and Regulates Localised Transcripts During Axis Specification. Biol Open *1*, 488-497.

McDermott, S.M., Yang, L., Halstead, J.M., Hamilton, R.S., Meignin, C., and Davis, I. (2014). Drosophila Syncrip Modulates the Expression of Mrnas Encoding Key Synaptic Proteins Required for Morphology at the Neuromuscular Junction. RNA *20*, 1593-1606.

Medioni, C., Ramialison, M., Ephrussi, A., and Besse, F. (2014). Imp Promotes Axonal Remodeling by Regulating Profilin Mrna During Brain Development. Curr Biol *24*, 793-800.

Melzer, J., Kraft, K.F., Urbach, R., and Raabe, T. (2013). The P21-Activated Kinase Mbt Is a Component of the Apical Protein Complex in Central Brain Neuroblasts and Controls Cell Proliferation. Development *140*, 1871-1881.

Mili, S., and Steitz, J.A. (2004). Evidence for Reassociation of Rna-Binding Proteins after Cell Lysis: Implications for the Interpretation of Immunoprecipitation Analyses. RNA *10*, 1692-1694.

Miller, M.R., Robinson, K.J., Cleary, M.D., and Doe, C.Q. (2009). Tu-Tagging: Cell Type-Specific Rna Isolation from Intact Complex Tissues. Nat Methods *6*, 439-441.

Misra, M., Edmund, H., Ennis, D., Schlueter, M.A., Marot, J.E., Tambasco, J., Barlow, I., Sigurbjornsdottir, S., Mathew, R., Valles, A.M.*, et al.* (2016). A Genome-Wide Screen for Dendritically Localized Rnas Identifies Genes Required for Dendrite Morphogenesis. G3 (Bethesda) *6*, 2397-2405.

Mittal, N., Scherrer, T., Gerber, A.P., and Janga, S.C. (2011). Interplay between Posttranscriptional and Posttranslational Interactions of Rna-Binding Proteins. J Mol Biol *409*, 466-479.

Mohr, C., and Hartmann, B. (2014). Alternative Splicing in Drosophila Neuronal Development. J Neurogenet *28*, 199-215.

Mueller, F., Senecal, A., Tantale, K., Marie-Nelly, H., Ly, N., Collin, O., Basyuk, E., Bertrand, E., Darzacq, X., and Zimmer, C. (2013). Fish-Quant: Automatic Counting of Transcripts in 3d Fish Images. Nat Methods *10*, 277-278.

Munro, T.P., Kwon, S., Schnapp, B.J., and St Johnston, D. (2006). A Repeated Imp-Binding Motif Controls Oskar Mrna Translation and Anchoring Independently of Drosophila Melanogaster Imp. J Cell Biol *172*, 577-588.

Narbonne-Reveau, K., Lanet, E., Dillard, C., Foppolo, S., Chen, C.H., Parrinello, H., Rialle, S., Sokol, N.S., and Maurange, C. (2016). Neural Stem Cell-Encoded Temporal Patterning Delineates an Early Window of Malignant Susceptibility in Drosophila. Elife *5*.

Neto-Silva, R.M., de Beco, S., and Johnston, L.A. (2010). Evidence for a Growth Stabilizing Regulatory Feedback Mechanism between Myc and Yorkie, the Drosophila Homolog of Yap. Dev Cell *19*, 507-520.

Neumuller, R.A., Richter, C., Fischer, A., Novatchkova, M., Neumuller, K.G., and Knoblich, J.A. (2011). Genome-Wide Analysis of Self-Renewal in Drosophila Neural Stem Cells by Transgenic Rnai. Cell Stem Cell *8*, 580-593.

Pandey, U.B., and Nichols, C.D. (2011). Human Disease Models in Drosophila Melanogaster and the Role of the Fly in Therapeutic Drug Discovery. Pharmacol Rev *63*, 411-436.

Pascale, A., Amadio, M., and Quattrone, A. (2008). Defining a Neuron: Neuronal Elav Proteins. Cell Mol Life Sci *65*, 128-140.

Pelechano, V., Wei, W., Jakob, P., and Steinmetz, L.M. (2014). Genome-Wide Identification of Transcript Start and End Sites by Transcript Isoform Sequencing. Nature Protocols *9*, 1740-1759.

Phanstiel, D.H., Boyle, A.P., Araya, C.L., and Snyder, M.P. (2014). Sushi.R: Flexible, Quantitative and Integrative Genomic Visualizations for Publication-Quality Multi-Panel Figures. Bioinformatics *30*, 2808-2810.

Pierce, S.B., Yost, C., Anderson, S.A.R., Flynn, E.M., Delrow, J., and Eisenman, R.N. (2008). Drosophila Growth and Development in the Absence of Dmyc and Dmnt. Dev Biol *315*, 303-316.

Poon, C.L., Mitchell, K.A., Kondo, S., Cheng, L.Y., and Harvey, K.F. (2016). The Hippo Pathway Regulates Neuroblasts and Brain Size in Drosophila Melanogaster. Curr Biol *26*, 1034-1042.

Port, F., and Bullock, S.L. (2016). Augmenting Crispr Applications in Drosophila with Trna-Flanked Sgrnas. Nat Methods *13*, 852-854.

Port, F., Chen, H.M., Lee, T., and Bullock, S.L. (2014). Optimized Crispr/Cas Tools for Efficient Germline and Somatic Genome Engineering in Drosophila. Proc Natl Acad Sci U S A *111*, E2967-2976.

Prokipcak, R.D., Herrick, D.J., and Ross, J. (1994). Purification and Properties of a Protein That Binds to the C-Terminal Coding Region of Human C-Myc Mrna. The Journal of Biological Chemistry *269*, 9261-9269.

Quinlan, A.R., and Hall, I.M. (2010). Bedtools: A Flexible Suite of Utilities for Comparing Genomic Features. Bioinformatics *26*, 841-842.

Rebollo, E., Roldan, M., and Gonzalez, C. (2009). Spindle Alignment Is Achieved without Rotation after the First Cell Cycle in Drosophila Embryonic Neuroblasts. Development *136*, 3393-3397.

Reichardt, I., Bonnay, F., Steinmann, V., Loedige, I., Burkard, T.R., Meister, G., and Knoblich, J.A. (2018). The Tumor Suppressor Brat Controls Neuronal Stem Cell Lineages by Inhibiting Deadpan and Zelda. EMBO Rep *19*, 102-117.

Ren, Q., Yang, C.P., Liu, Z., Sugino, K., Mok, K., He, Y., Ito, M., Nern, A., Otsuna, H., and Lee, T. (2017). Stem Cell-Intrinsic, Seven-up-Triggered Temporal Factor Gradients Diversify Intermediate Neural Progenitors. Curr Biol *27*, 1303-1313.

Rothberg, J.M., Hinz, W., Rearick, T.M., Schultz, J., Mileski, W., Davey, M., Leamon, J.H., Johnson, K., Milgrew, M.J., Edwards, M.*, et al.* (2011). An Integrated Semiconductor Device Enabling Non-Optical Genome Sequencing. Nature *475*, 348-352.

San-Juan, B.P., and Baonza, A. (2011). The Bhlh Factor Deadpan Is a Direct Target of Notch Signaling and Regulates Neuroblast Self-Renewal in Drosophila. Dev Biol *352*, 70-82.

Shaw, R.J., Kosmatka, M., Bardeesy, N., Hurley, R.L., Witters, L.A., DePinho, R.A., and Cantley, L.C. (2004). The Tumor Suppressor Lkb1 Kinase Directly Activates Amp-Activated Kinase and Regulates Apoptosis in Response to Energy Stress. Proc Natl Acad Sci U S A *101*, 3329-3335.

Shen, Q., Wang, Y., Dimos, J.T., Fasano, C.A., Phoenix, T.N., Lemischka, I.R., Ivanova, N.B., Stifani, S., Morrisey, E.E., and Temple, S. (2006). The Timing of Cortical Neurogenesis Is Encoded within Lineages of Individual Progenitor Cells. Nat Neurosci *9*, 743-751.

Siegrist, S.E., Haque, N.S., Chen, C.H., Hay, B.A., and Hariharan, I.K. (2010). Inactivation of Both Foxo and Reaper Promotes Long-Term Adult Neurogenesis in Drosophila. Curr Biol *20*, 643-648.

Skeath, J.B., and Thor, S. (2003). Genetic Control of Drosophila Nerve Cord Development. Current Opinion in Neurobiology *13*, 8-15.

Song, Y., and Lu, B. (2011). Regulation of Cell Growth by Notch Signaling and Its Differential Requirement in Normal Vs. Tumor-Forming Stem Cells in Drosophila. Genes Dev *25*, 2644-2658.

Sousa-Nunes, R., Yee, L.L., and Gould, A.P. (2011). Fat Cells Reactivate Quiescent Neuroblasts Via Tor and Glial Insulin Relays in Drosophila. Nature *471*, 508-512.

Spana, E.P., and Doe, C.Q. (1995). The Prospero Transcription Factor Is Asymmetrically Localized to the Cell Cortex During Neuroblast Mitosis in Drosophila. Development, *121*, 3187-3195.

Stergiopoulos, A., Elkouris, M., and Politis, P.K. (2014). Prospero-Related Homeobox 1 (Prox1) at the Crossroads of Diverse Pathways During Adult Neural Fate Specification. Front Cell Neurosci *8*, 454.

Stocker, H. (2011). Growth Control: Myc and Yorkie Get Connected. Curr Biol *21*, R37-39.

Suzuki, A., and Ohno, S. (2006). The Par-Apkc System: Lessons in Polarity. Journal of Cell Science *119*, 979-987.

Svitkin, Y.V., Yanagiya, A., Karetnikov, A.E., Alain, T., Fabian, M.R., Khoutorsky, A., Perreault, S., Topisirovic, I., and Sonenberg, N. (2013). Control of Translation and Mirna-Dependent Repression by a Novel Poly(a) Binding Protein, Hnrnp-Q. PLoS Biol *11*, e1001564.

Swartling, F.J. (2012). Myc Proteins in Brain Tumor Development and Maintenance. Ups J Med Sci *117*, 122-131.

Syed, M.H., Mark, B., and Doe, C.Q. (2017a). Playing Well with Others: Extrinsic Cues Regulate Neural Progenitor Temporal Identity to Generate Neuronal Diversity. Trends Genet *33*, 933-942.

Syed, M.H., Mark, B., and Doe, C.Q. (2017b). Steroid Hormone Induction of Temporal Gene Expression in Drosophila Brain Neuroblasts Generates Neuronal and Glial Diversity. Elife *6*.

Takemura, S.Y., Aso, Y., Hige, T., Wong, A., Lu, Z., Xu, C.S., Rivlin, P.K., Hess, H.F., Zhao, T., Parag , T.*, et al.* (2017). A Connectome of a Learning and Memory Center in the Adult Drosophila Brain. eLife *6*.

Teleman, A.A., Hietakangas, V., Sayadian, A.C., and Cohen, S.M. (2008). Nutritional Control of Protein Biosynthetic Capacity by Insulin Via Myc in Drosophila. Cell Metab *7*, 21-32.

Toledano, H., D'Alterio, C., Czech, B., Levine, E., and Jones, D.L. (2012). The Let-7-Imp Axis Regulates Ageing of the Drosophila Testis Stem-Cell Niche. Nature *485*, 605-610.

Truman, J.W., and Bate, M. (1987). Spatial and Temporal Patterns of Neurogenesis in the Central Nervous System of Drosophila Melanogaster. Dev Biol *125*, 145-157.

Turner, J.J., Ewald, J.C., and Skotheim, J.M. (2012). Cell Size Control in Yeast. Curr Biol *22*, 350-359.

van Riggelen, J., Yetil, A., and Felsher, D.W. (2010). Myc as a Regulator of Ribosome Biogenesis and Protein Synthesis. Nature Reviews Cancer *10*.

Wang, H., Ouyang, Y., Somers, W.G., Chia, W., and Lu, B. (2007). Polo Inhibits Progenitor Self-Renewal and Regulates Numb Asymmetry by Phosphorylating Pon. Nature *449*, 96-100.

Wang, L., and Yi, R. (2014). 3'utrs Take a Long Shot in the Brain. Bioessays *36*, 39-45.

Weidensdorfer, D., Stohr, N., Baude, A., Lederer, M., Kohn, M., Schierhorn, A., Buchmeier, S., Wahle, E., and Huttelmaier, S. (2009). Control of C-Myc Mrna Stability by Igf2bp1-Associated Cytoplasmic Rnps. RNA *15*, 104-115.

Weigmann, K., and Lehner, C.F. (1995). Cell Fate Specification by Even-Skipped Expression in the Drosophila Nervous System Is Coupled to Cell Cycle Progression. Development *121*, 3713-3721.

Weir, M.P., Edgar, B.A., Kornberg, T., and Schubiger, G. (1988). Spatial Regulation of Engrailed Expression in the Drosophila Embryo. Genes & Development, *2*, 1194-1203.

Wheeler, E.C., Van Nostrand, E.L., and Yeo, G.W. (2018). Advances and Challenges in the Detection of Transcriptome-Wide Protein-Rna Interactions. Wiley Interdiscip Rev RNA *9*.

Wodarz, A., and Nathke, I. (2007). Cell Polarity in Development and Cancer. Nat Cell Bio *9*.

Yang, C.P., Fu, C.C., Sugino, K., Liu, Z., Ren, Q., Liu, L.Y., Yao, X., Lee, L.P., and Lee, T. (2016). Transcriptomes of Lineage-Specific Drosophila Neuroblasts Profiled by Genetic Targeting and Robotic Sorting. Development *143*, 411-421.

Yang, C.P., Samuels, T.J., Huang, Y., Yang, L., Ish-Horowicz, D., Davis, I., and Lee, T. (2017a). Imp and Syp Rna-Binding Proteins Govern Decommissioning of Drosophila Neural Stem Cells. Development *144*, 3454-3464.

Yang, L., Titlow, J., Ennis, D., Smith, C., Mitchell, J., Young, F.L., Waddell, S., Ish-Horowicz, D., and Davis, I. (2017b). Single Molecule Fluorescence in Situ Hybridisation for Quantitating Post-Transcriptional Regulation in Drosophila Brains. Methods *126*, 166-176.

Zacharioudaki, E., Housden, B.E., Garinis, G., Stojnic, R., Delidakis, C., and Bray, S.J. (2016). Genes Implicated in Stem Cell Identity and Temporal Programme Are Directly Targeted by Notch in Neuroblast Tumours. Development *143*, 219-231.

Zenklusen, D., Larson, D.R., Singer, R.H. (2008). Single-Rna Counting Reveals Alternative Modes of Gene Expression in Yeast. Nature structural & molecular biology *15*, 1263-1271.

Zhu, S., Lin, S., Kao, C.F., Awasaki, T., Chiang, A.S., and Lee, T. (2006). Gradients of the Drosophila Chinmo Btb-Zinc Finger Protein Govern Neuronal Temporal Identity. Cell *127*, 409-422.

Zhu, S., Lin, S., Kao, C.-F., Awasaki, T., Chiang, A.-S., Lee, T. (2006). Gradients of the Drosophila Chinmo Btb-Zinc Nger Protein Govern Neuronal Temporal Identity. Cell *127*, 409-422.

Zhu, S., Wildonger, J., Barshow, S., Younger, S., Huang, Y., and Lee, T. (2012). The Bhlh Repressor Deadpan Regulates the Self-Renewal and Specification of Drosophila Larval Neural Stem Cells Independently of Notch. PLoS One *7*, e46724.

Zivraj, K.H., Tung, Y.C., Piper, M., Gumy, L., Fawcett, J.W., Yeo, G.S., and Holt, C.E. (2010). Subcellular Profiling Reveals Distinct and Developmentally Regulated Repertoire of Growth Cone Mrnas. J Neurosci *30*, 15464-15478.

Appendix

A. qPCR primers

Gene	Forward	Reverse
rp49	GCTAAGCTGTCGCACAAA	TCCGGTGGGCAGCATGTG
dlg1	ATCCGCATAATAATGTAAACTACGACAGAA	ACTCATTATATAGGTTTAAATCAACG
ase	CTGGAAGAAAGGGTTTGCCT	TCTTCTGGGATCTTCTCCCG
cas	GGCCACCCAAGAAAATCC	GACTCGTCTTCGACTTTCAGG
stc	GGAGCCTTTGGACTGAACC	CATGGCCTGCGAGTAAAAAT
par6	TCTAATCGAGGTGAAATCGAAGTT	TCTGCTCCGCCTCATTTC
ey	GCTTGGGAAATTCGGGATAG	ATACACGGTTTATTGAGGACACAC
wor	GCTCAAGAAGCGTCCGATAAT	AAGTCCACTGGTCCTTCATCA
imp	CACCATCAGGACGATCACACA	ACTTCCAGGATGCGCTTACAG
chinmo	GCATCGCCACAGTCCAGT	ACTGGTGGCATTTCCATTTC
pros	TATGCACGACAAGCTGTCACC	CGACCACGAAGCGGAAATTC
elav	TCACACCGAGCGAAATTG	CATTAGCTGTGCCTGTGTGTC
klu	CTCGGCCACCGTCTAAATC	TGGGATTCTTCCTCGCTATC
chic	CTGCATGAAGACAACACAAGC	CAAGTTTCTCTACCACGGAAGC
syp	TATGTGCGAAATCTTACCCAGGA	CGTTCCACTTTTCCGTATTGCTC
myc	CGGCAGCGATAGCATAAAAT	ACCTCGTCGGTAAGACTGTGA
Eip93F	CGATGTGAAGTCCGTCAGAG	GATTTCCGGGCATCTAGCTT
mamo	CCATCAGAGCCCATAAGGTG	CAAAACGGACGTCCTTCAAT
MED4	ATTTCGCAAAATGCTGGAAC	GCAGCTTCTGGATCTCACG
MED6	ATCCCAACAAGGGCTACACG	TCATCCTTCGCTGAGTTGGC
MED10	CAGATCCGCATAATCGTAAGC	CCGGTCACCAAGCTGTTAAT
MED11	TGGAATCGAAGCTGTCCGAG	TTTGGAGCACTTTGGCGGAT
MED12 (kto)	AACACTCCAGAGCAGCTTGAC	CAGCCAGTGAGGATCCAGTT
MED27	TCCTTCAACAACGATCCAGAC	CGAAGGGACGAAAAATTCTG
MED31	CGGAAAGGGTAAGACTGCTATC	AAAAATCCACGCTGTGCAA

B. smFISH probe sequences

myc exon - Quasar 670

ATGGCCCTTTACCGCTCTGATCCGTATTCCATAATGGACGACCAACTTTTTTCAAATATTTCAATATTCGATATGGATAA
TGATCTGTACGATATGGACAAACTCCTTTCGTCGTCCACCATTCAGAGTGATCTCGAGAAGATCGAGGACATGGAAAGTG

TATTTCAAGACTATGACTTAGAGGAGGATATGAAGCCAGAGATCCGCAACATCGACTGCATGTGGCCGGCGATGTCCAGC
TGTTTGACCAGCGGTAACGGTAATGGAATAGAGAGCGGAAACAGTGCAGCCTCGTCGTACAGCGAAACCGGTGCCGTATC
CCTGGCGATGGTTTCCGGCTCTACGAATCTCTACAGCGCGTATCAACGATCGCAGACGACAGATAACACCCAGTCAAATC
AACAGCATGTCGTCAACAGTGCCGAGAACATGCCGGTGATCATCAAGAAGGAGCTCGCAGATCTGGACTACACGGTCTGT
CAGAAGCGCCTCCGTTTGAGCGGCGGTGACAAGAAGTCACAGATCCAGGACGAGGTCCATTTAATACCGCCCGGCGGAAG
TTTGCTCCGCAAGCGGAACAACCAGGACATTATCCGCAAATCGGGCGAATTGAGCGGCAGCGATAGCATAAAATACCAGA
GACCAGACACACCTCACAGTCTTACCGACGAGGTGGCCGCCTCAGAGTTTAGACATAACGTCGACTTGCGTGCCTGCGTG
ATGGGCAGCAATAATATCTCGCTGACCGGCAATGATAGCGATGTCAACTACATTAAGCAAATCAGCAGGGAGCTTCAGAA
TACCGGCAAGGATCCGTTGCCGGTGCGTTACATCCCGCCGATCAACGATGTCCTCGATGTGCTCAACCAGCATTCCAATT
CGACGGGTGGCCAACAGCAGTTGAACCAACAGCAACTGGACGAGCAACAACAGGCCATCGATATAGCCACTGGACGCAAC
ACAGTGGATTCTCCGCCGACGACCGGCTCTGATAGTGACTCCGATGACGGTGAACCCCTCAACTTTGACCTGCGCCATCA
TCGCACTAGCAAAAGCGGCAGCAATGCCAGCATCACCACCAACAACAACAACAGCAACAACAAAAACAACAAATTGAAGA
ACAACAGCAACGGCATGCTGCACATGATGCACATCACCGATCACAGCTACACGCGCTGCAACGATATGGTGGACGATGGT
CCCAATTTGGAGACCCCCTCAGATTCCGATGAGGAAATCGATGTCGTTTCATATACGGACAAGAAGCTACCCACAAATCC
CTCGTGCCACTTGATGGGCGCCCTACAGTTCCAGATGGCCCATAAGATCTCGATTGATCACATGAAGCAAAAACCGCGCT
ACAATAACTTCAATCTGCCGTACACACCGGCCAGCAGCAGTCCAGTGAAATCGGTGGCCAACTCGCGTTATCCATCACCG
TCGAGCACACCGTATCAGAACTGCTCCTCCGCTTCGCCGTCCTACTCGCCGCTATCCGTGGACTCTTCAAATGTCAGCTC
GAGCAGCTCCAGTTCCAGTTCGCAGTCAAGCTTCACCACCTCCAGTTCGAACAAGGGACGCAAACGATCCAGTCTGAAGG

myc intron - Quasar 570

AGAGGGAAACTACATTAAAAAAAAGTCCAGCTAGAATACGTGTTTTTCATATCTATATTTTTATAGTACTCCTACCTACT
TGTTTTATTTGTGCCGGCGAGTTCAATGTCTGGCTCTCTTTCTCTCTTTTTGGCGCGCAAATCGTTATCCATTGAGCAAC
CCTCGCAAGCTTACGTCACGTCAATCATCTTGATTTTTACTACGTCTTACGCTACAACTACAACTGCGCATGCAACTACG
TGTGCATTTTCTACTACAATGACTACTACAACTACAACTACTACTACTACTACGCTATGGAGCCGGTGTGGGCGTAAGCT
TTTTGCCGCCGCTCATTAAAAAAAAATATATGGTAAATAATAGCGGGAAATCAAGAAGGGGCTAGAGGTGGGGCAATGCAA
GGGATAAATTAAACTTGGATTATAAAATATTTACCAATAAAGCAAAAAGCAAGAGCAACAGCAAGAGCAAGAGCAAAAGC
ATTTAACTCGTGTTTCTGCTCCCGCTTTTTCTCTCTCGCTCGCCTGTCTTTAGTTTCTCTCTTGCAATTTGCCGAGTGCA
GTTAAACCGAGAAATTGCAGTAACAACAAGTTTGTTTTGTACGTTTGTTTTGGTTTATATGCTTTGCTTTTTTCTGCGCT
CTGCTTTTTGGGTGTTGTCTGCTTTTGCGTTTTGCGTGCTTTTTTTTTTGTGTGTTTTATGCTTTTGCTTCTACCGCAAC
GAACGGAACGCAAAAAATGTCAAAAAAGAAAATGTGCAATATGTAAAATGCTTACCATAAATTGAGGAAAACCCACACAC
GCGTGTGTATGAATTTTAATTACTCAGAATCAGAAAGACAAATTTACGTAGAATTGCTAGTATTTTATGATCGTTTGGCA
AAATGGAATTCTGAAGCGTTATCATCATCTTAGTTTGGTGACGAAATCGCATCATAATTTTCCACTGCTAATTTGGCAAA
CTAAAAGCTTGACACAAGTGGCTCGAGATTAGTTCTTTCTATTCTTTTTGCGTGCGCGATTCTTGTTGGAAGCAGATATG
GGAATAGCAGAAGAAACGTAAAAAGAAATCAGGTGCGTGCCGCAGATTAGCAAATCTTTGCCCTCTTGCTCGCACGCGAA
ACTCGTGAGGCTTGCGAGAGGGAGATGGCGCTCTTCGAACACACGCACTTGTATCAATATCAATTCTTTTCTTTCCTTTA
TTGTGGAGGGGGGTTGCTTTCTTTATCGCTATGCTGCAGTCTTCTAATTAGTATAAAAGCTTACGTGAGCGAGCGAGACG
GGGCGCGTCACGTGCGAGCGAGAGCGGCGGTTGGCAACAACGCACGAAATTCGGCACATAGATAAGGTTCACGGGGGAG
TGAGCGAGAGACTAGAGGCCACATGCCTATGATGTTGGCGCCTCTATAAAAGTGCGTACACACACACACACACATACATGA
CTGGCTGTGTACGTATAATATGTATATGTATTTACCTTTGGCAGTGCGTGCTGGTTTTTGGCATTTCGCACCTTGCGACT
GTGTGTGTGTGTGTGCGTTTGTGGGTTTGGAAAAATGTTAATGAACTGAACCAAGGTCAGCCATTCGCCGGAAAAAAAAG
TGCGTAGAAACCGAAAATTAGTGGTGTGGGGGTGCGGCACAGAAAAAAAAAAAAAAAAAAACGTATGGCCAAGTCATGTT
GGCTAAAACAATATTTCCTATTTTGGCCTCTTCGCTTTACACTTTCGATCTCAGCAGCTCTTCTGGGCTCTCTTGTGGCC
TTTTAGAAGAAGACAACAATCGAAAGTATAGAGACATGTAAACAACATTAAATGAAATTAAATAACGCCCAAGAAGAAAG
AAGAAACTGTATGAAAAAGTAGTGGATAATAATAATACGAAAACCCCAAAGACTAGAACATAAATAGTTGTCGATTGTTG

myc 3’ UTR - Quasar 570

AGCAAGAAAATTTCTATAGTGTAGGGCGCGAGACGTTTCAACGAAAATTTTTTTCTATGTGAGTTCTAGGCTAATGCTGC
CTACTAAACCTATACCCAGATATACATATAATTCTTATATTTTTGTTTACCTAGTAGCTTAACGTTCGAACACATGAAAT
ATTTTTTACCTTATACATTTCTTTAAGTACGCCGCCGCAAAAACTTTTGAAAAACTACCTACTTAACTCTTCATTTTTGT
AATAAAAAGAAAAAAAAACAACAAACAAACAACAACAACTATAAAACAATTGTTAAATGGAAAATAATGATATATATCTA
TCTACGTGGACAAACAATTAAAGAGTATATTTTTTGTATTGTTTCGACCAAAAAATGTGTACACACTGTAAATAGCAATC
TCGTTAAATAATAGTTACACACGCCTACAAAATAGCGAACCCAAAACCCAAGAAATGGAATTATTTTTATAGAAAACAAA
AAAACCCGGAGAGAAAACACAAAGCAATAGACTTAAGCGAATTGTACAACGCGAAACGAAAACAAAACTTCAATAAACCA
ACAAAAACACACACACTTATATATATATACATATATATATGTATATATACATATACAAAACCACACACGAATGCACCTAT
TTTCCTATAGTACATACAACCAGAAATAGTTAAACGAAAAAACCATGTTTTCTTTCAATAATTTCAACAAACAAAACCGT
ACAAATTTACAAGAAACAAAAATACGAAAAGCAAACCTTTTCTTTGTTTGGTCCTTTTATTAATTTATTAACGAAACAAC
AAATTCAAGTGAAAGGGCATTTTTAAACATAATTTTTCATTGTAAAAAAAACAAAATATATACACTAAAACTATGACCAA
AACCAAAATCCTCGCAAACAAAACAAAAAAATATTAAATTTTTTTCTTTTAAAATATATTTATAACAAAAAACAAAACAA
AAGTTTTTAAGTTTAAATATATTTTTATGATTATCAAATTTTTTATATTATATACACACACACAAACTACTATTTGAATT
AGTTGTTAAAAAATTTATATTATTAAAACAACACATTATTTGAAGACAAATAACATAAAAAAAAAACTATGTAAAAAAAA
ATCTGAAAAACTCATGAAATGAAAGCAAAAAACTGTTAAAGCCGTACGGAAAATATGAAACTATAGACGAACATGCTTGA
ATTATTACATGTATATTTAAATTAATTTTTTTTTTTAGTCATAAACGTATGCAAAAAACGTATACGTTTATGGCTATGCA
TTTGAAATCCCTATTTTTGATTTGATGACAAAAGAAGATATGAAAATTCTGTTTACTTTGGTTATTGCTTATTAAATATG
TGTAAAAATTGCAAAATAATATAGATATATCTGGCAAAACAAGCTAAACAACTATATTAATATATTATCTAATAAATTTT

AACTCGTTATGTAGTTACCTATTAATGAAAAACAAATTAAAAGCAAAAAAAATGAGAAAAGTAAACACAATAAATTACAT
TTTATGTACCTTCTACATATATAAACTAAATATATTACACAGAACACACACACTTATATATAAACACACACACACACACA
CACACTACTATATATAGAAACCGTTTAAATATTTTTTTTTTTCAAAATTTCTGATAATGGAATTATATATACATTATACAA
TAAAAATACTTCACCAACAAATTACTTTTGATTTTGTTTTTATTTTTACGCTTGATTCCTTTTCGTTTAATATATGGATG
CAATTATTGAAGCTTCCCAGATCTTTCAATTGGCACAAGGATTTCCTCTTGTTATTTGCGTTTTCGTATTCGAATATTCA
AATATTCGAATATGCAATTTTGTTGCACATTTTTTCTGGACGCCCTGTTTTATTTTATTTACTTTCAGCGACTTTCAAAA
CCCCAAGTGTGTTTCATCCGAGTTGTTTATATTTGTTTTACTTTAGAAAATCGTATTGTGTCTCACAATAAGCTGGCTAA
AAAAAAACAGCTTTTCCTTTTTTGGAATTTGGTACTATCCAACTTGTGCTTCACTTTCATTTTCCAACCGCGCCGAGTAT
CAAATTCGCAGTGAATCATTCGAGTGAGTAAGTGATTCACATTTGTGGGTGGTGGGAAAATTGCTTTTGTCGCCGTTTCT
AATCTAGCAGTTCAACGTATTTTTTCTCGTTGCCTGGTTGCGCTGCCTCGCTCATTTGCCCACCAGACAAATTAAGTTAA
TTCAATAAGAGTTGTTGCTCACTATTGTTGTTGTTGTTTTACCGGCAAATTTTTTGTTTTTAATGAAATCAAAGCGACAA
CAACGACAGCCGAGAAGCCGGTTGGGATACAGTCAGCGACATGACGACAATAACAACGATCACAACGATAGCCATATAAT
ATAACATTTTATTTATATGTACGTGTTTTGTTTTCGTTGATTTTTGCTGGTTTATTATTTTACTACAATCATTCAGTTAC
GGTTTCGTTGGTTGAATTTTTTTCTTTTAATTTTTACTCGAAACTTTCGGAAGAAACCAAAACGAAATAGGCGATGCTCT
TATTTGAATGTACAATATATTATTTAAACAGTGTGTGTTGTATAGTGTTTTATGCGTGTTCTATGAAAAGTGTTGTTAAT
TGTTTGGATATATTTTTTAAGCATCACATAAAGTTTTCTGTTGGGTCGTTTAAGTTTAAAAGTTTAAAATGGAGAGCTAA
AACAGATGAATTAAACTTAATTTGCAGTTTATTATGACAGTGGGGATACCGCGTTAAATAGAAAGGGTACACGAATGGCA
GAAGTAGCCGGCAAATTCACACACACACACACACACACAGCGGGCCAAGCAAAACAGAGACAACGAAATTGGGGTGCACA

mnt exon - Quasar 570

TTTGTAAACAATATTTGAAACCAAAACCATTTTCAAAAACTTTTAACAATCATTTAAGTAACAACAAATACGAAGGATTCAACCAA
AATTTATACAAAAAATAAGAACTGAACCAATTCTCAACACCAATTCAACAACTATTTCAACAAATAACTGTAAACGTGTCGCGAC
TCAAAGCTCCTCCCGCTATCCTGCTCTCTCGCGTAAACTCGTCGCCATCGTCTTTTTCCGTTGTGGTGTACGATTTTGGTGTT
TTTTCTCCAAAATATATATATTTATTGTTCTACGCGTTCGTCGTCCTTGTCCCGTGCGTGAGACCTTGTCCTCGTGTGCGTCTG
TGTGTGTGCGTGTGCGAGAAGAGGAGTGCGGTAGTTTGTGTATGCTATGTCAGGGATCGGGGGCATTGGGGTGCTCCTCG
AGGCGGCTCAATTTCTTGAGCAGCATGAGAAGCTCCCGCAGGCGGGAGGCGGCGGCGGTAGCGCCCTGGGCGTGGGCG
TGGCACTGCCTCAACAGCAGCAGCAGACGGTGCACTGCAAGAGCACTCCATTATCAACAACAACAATAGCAGCCAGCACAA
TAGAAATAGCAGCAGTAGCAGTAACGGGATTATTGCAACGCCACCGTTCACGAACGGAAATGGCAACGGTACCGTCGGCGT
CGGTAACGCGAGCGCCATTTTCAACGTTAGCGTCAATGCGAACGGGAACGGTCTGAGCAACGGTCACAGCAGTCCGCGCA
GTCAATTAGCCGCCGCAGCCACTGCCCACGATTACGAGTATAGCGCCGCCGGAGTTGCCAATGGACACAGCGAAGGTCGC
CCCCACGTCTCGGCAGCCAGGGATCAGCAGGACCATCCGCAGCATCAGCAACATGCCAACCATATGCAGATCCAGCAGCAT
TACGGCTATATGAGGAGTAACATTGGCGGCGTGATCTATGGCTTGCACAAGGACTCTGCCGACTCTGCGGCATCCTCGGCAT
GTGGAGCGGGAGCGGGAGCAGCAGCGGTGGGCATGAGCATTGCCTCCTCGGCGCCAGCGGCGGGATCTCAGCTATCGGC
GCATCATCACACGGGACACGGAGGCCGCAGGCGCACCACCAGTTCCAATAGTAATGGAGCGGGCACCCGGGAGGTGCAC
AACAAGCTGGAAAAGGAGCGACGCGCCCAGCTGAAGGAGTGCTATGACCTGCTCAAAAAGGTGCTGCCCATGGGTGACGA
GGACCGAAAGAAAACATCAAACTTGACAATACTTGACACGGCCCACAAATATGTCAATTCCTTGAGTCATGAAGTTTGCGAGC
AGGAGGCGAAGATAGAGAAACTGGCCAAGCAGAAGATCGAGCTGCAGAAGCGGCTAAAGCAACTGAGCTTAAGGAGGGAA
TCGCCGCCCACCGATCAGCAAATCATTCCACAGGCCGACAAAGCAGTTTGTCTGGCAACAACAGCCACAACAGCACCACCA
ACGGCGGCCAGTGGCCACAATGGAACCACAATTCTATTCGATGCAGGCAACGCCTGTGCCACTGGGCAGCTAACAACTGTG
ATAAACAAAACTAATGGAGGAGCAACCGCAGCAGCCAGCAGCAAACACAATGGCAACCACACAGGAGGTGCAACAACCACA
CTGACTCCGGCCATGGGCATCATGACAATTAAAAATGGCAATGGCAGCAACGGCAACATGCTGGCAATCTCACCAACGGGA
GGCCACAATCATCAGTTGCACCAGCACCACAACGGCAGCCCAGCGGGCAGTCCATCGGGAATAGGAGCCACAACTGGAGC
CACCATCACACGTGGCTCGCCAACGCCATCGACTCCATCGCCGTCGCCCAGCTCCTCGTCCAGTGGCGTCTCGTTGTCGA
CCTCATTTATGGGCGGCTCCTCATCATCGTCCTCATCCTCCTCATCATCATCATCTTCCAGTTCGTCGTCCAGTTCTTCGTCG
CCCACGCAACAACAGCAGATAATCACGCCCACGGCCACAGCCCGTAGTGTTGGCCTAAAATTCCATGGCGGTGCGGGCGC
TGCTGTGCCAGCTGGCGGAGGTTCAGTGAATGGGTTCCATCAGGCCGATAAGGATCGCAATTACACTTTCCTGAGGCTCAG
TGCTGGGACAACGGCACAGTAA

mnt intron - Quasar 670

CCGACTTACCAAAGTCTCAAACGACCAATTCTTATCACTCATCATTAACATACATCACATTCATCCAAACTGTTACTACTCTGCT
GCCCACTACTGTGCGAGCATCGTCTAACACTCTTCTCTGGTGCAACACCATCAGCTGCTTAGGTCTGCTGTTAACTGTTGTT
GGGCTCTCTCGTCAGGCGACAAAAGTTTCCAAAAGGAAAAGGAAATAGTGTCGAGAAAAATCAAACTAGCTTAGTCGCTTTC
TTAGCTCTAGTGCGTTGCTAATTGGCACTTTGCTTGCATGTGTGTATGCAAATATATAAAATATTGGTGATAAAAAATATCGCAGA
TAACGTTGCTCAATTTTGAACTTGATTGATTATAATAGCAAGGTGTAGCCAAATGCTCGATTGCAGGCGATAACCTTTAATAAAC
TTGTATACATGCATACATACACACAAATATAGATAAAGAGTTATTCCCACATAGAAGACGAACCAGACACCTATGGAAAGTAAAC
TAATCGTCATTTAAAATAATATTTATACCGAGATATTTGATAGTAAACAACAGCCACTCGAAGCAGACACTTTGGTCGCCTTTAC
GAAACGAAACCGTTTGTGCTCTCTTTCTCCATTTGCTTTTGCTGCATTTAAACTTGTTTTGACCTTGTTTGCGACGTCGACTG
CATTTTGCGTGGGCGTGCACTGTACCAAAAAAAGTTAAAATTAAATACAAACCCCAAAAGACAACAACAGCACGGTGCTCTTT
GTCTCTCTTTCTCTCTCCTGCGCTCTCATTTTGGCACAGGTTGCAAGCGTGGCAAGCAGCAGGTTCTGTTATATTTTTAGCTC
GCTGCTGGCTGCGACGTCAGCGTCGACGCTGGCTTCGCTGTCCAATTGGCATGTGCTAAATTGCCATGCTGCGTTTTTGTTT
TTGCCTCTCTTTGTTTTTGTTGCCTTGACTATCGGAAACAAAATTTGCAACGTCAAAAATACAGTGAAAATAATGAAAGTCTAA
GTTCAATATTTAAATTCAGACAATGTCATAGTTTCAATTAGATGTTAGCTGTTCAATTGATACTATCTCAAAGATGCATTACATACA
TATATGAAAAAAACCAAACAGATCGAATTGAAAATGAAGAAATATATATAGAAATGTAAAGAATTATGTCCTAAATAGGGTGAAAA
ATGAAATGCGGGGGAGAAATTGTGTTAAAATAATAATTTATGTGCCTCTTTGGGCACTGTGTTTTGAATTTCTGTATTTCTTTTC
TTTTGCTTTTTGCTGTGCTCATTTCGGTTTTTGGTTTTTCTCTTTTTTTTTGTCAACATATGTGTAGTTTGTTGTTCATCTTGACT
ACTTTTTTACATTTTTTTTGCGTTGTTATTTTTTCTTTGTCTTTTTTTCGCTTTTGTCATGCGCTCGCTTCGTTCGTATATTTTCGC

ACGTACGCTTGTACTTGTTGCTGTTGTTGTTTGGGGTCACGTCATGTGCTGGTTCTCTCTCGCCCCGTCTCTTTTGCGTT
AGTCATAGTATGGTCCGCCAAATAAGAGAGAGAGTTCCACGTGAGCCGTTTCTCTTTGAGCTCATTTCTCTTCAATCGTTCTC
TCTTTTCCACTGGCACTCTCTTCCGGCTGCTGGTGTAAAACAAAGTCAATGAACTTTGTACGCATTTTTTGTTATTGTTGTTTT
TGTTTTTGGCCTGCCTTTTTCCGTGCCCATTTCGTATTATTATTTGGCCTTTCTTTAAGGCTTATATGTTTTTTGTTTTCATCACA
CTTACAAATTGTATTATTTGTACGGCGTGTATCTTGGCGTTGCATGTGTAATATTTAGACAGCTGACTCTGTTGTTTAGCCTCTC
TCTTCGGCGTCTCCTCGTTTCCTAGTTCCGGTTTCTGCTTTTCTTTTCCTTGTTTTGTTTTAT

pros exon - Quasar 570

ATGAGTAGCGCTGCCGCGGCTGCTGCGGGTGCCGCTGGTGGAGGAGCCCTGTTCCAACCACAATCGGTCAGCACGGCCA
ATAGCAGTAGTAGTAACAATAACAATTCAAGCACACCGGCTGCTCTTGCCACCCATTCGCCCACGAGCAACTCACCAGTTTC
GGGCGCCAGTTCGGCATCGTCCTTGTTGACGGCCGCCTTTGGCAACCTGTTTGGTGGCTCCTCGGCCAAGATGCTGAACG
AGCTGTTTGGCCGCCAGATGAAGCAGGCCCAGGACGCAACGAGTGGCCTGCCCCAGAGTTTGGACAACGCCATGCTGGC
CGCCGCCATGGAGACGGCCACCAGTGCCGAGCTGTTGATCGGCAGCCTCAATTCCACGTCCAAGTTGCTGCAGCAGCAGC
ACAATAACAACAGCATTGCTCCCGCCAATAGCACGCCCATGAGCAATGGCACAAATGCATCGATCTCGCCGGGATCGGCCCA
CAGTTCCAGTCACTCGCATCAGGGAGTCTCGCCCAAAGGAAGTCGCAGGGTGTCGGCCTGCAGTGATCGCTCCTTGGAGG
CGGCAGCTGCTGATGTTGCTGGTGGCTCGCCGCCACGAGCGGCATCGGTGAGCTCGCTGAACGGAGGAGCCAGCAGTGG
GGAGCAGCACCAGTCTCAGTTGCAACACGACCTGGTGGCACATCACATGCTGCGCAATATACTGCAGGGCAAGAAGGAGCT
GATGCAACTGGATCAGGAGCTGCGCACCGCCATGCAGCAGCAGCAACAGCAGCTGCAGGAGAAGGAGCAACTGCACTCCA
AGCTTAACAATAATAATAACAACAATATTGCTGCCACCGCCAACAACAATAACAACACCACAATGGAGAGTATCAATCTGATCG
ACGATTCGGAAATGGCTGACATCAAGATCAAGAGTGAGCCCCAGACGGCTCCGCAGCCACAGCAATCGCCGCACGGAAGC
AGCCACAGCAGCCGAAGTGGGAGCGGCAGTGGGAGCCACAGCAGCATGGCCAGCGATGGCAGCCTGCGACGCAAGTCCT
CCGACTCCCTGGACAGCCACGGGGCGCAGGACGATGCGCAGGACGAGGAAGATGCTGCGCCCACTGGCCAGAGATCCGA
GAGCAGGGCTCCGGAGGAGCCACAGCTGCCCACCAAAAAAGAATCCGTGGACGATATGCTTGACGAGGTGGAGCTCCTGG
GTCTGCACTCCCGCGGATCCGATATGGATAGCCTGGCCTCGCCCAGTCACTCGGACATGATGCTGCTGGACAAGGACGATG
TCCTGGACGAGGACGACGACGATGATTGCGTGGAGCAGAAAACATCCGGCAGCGGATGTCTCAAGAAACCCGGCATGGAC
TTGAAGCGCGCTCGCGTCGAGAACATCGTGTCGGGAATGCGATGCAGTCCATCCTCCGGATTAGCGCAGGCAGGACAACT
GCAGGTAAATGGTTGTAAGAAGCGCAAGCTCTACCAGCCCCAGCAACACGCCATGGAGCGTTATGTGGCCGCCGCAGCTG
GTCTGAATTTCGGCCTCAATCTGCAGAGCATGATGCTCGACCAGGAGGACAGTGAGTCCAATGAGCTGGAGTCCCCGCAAA
TCCAACAGAAGCGTGTGGAGAAAAATGCGCTCAAGTCCCAGCTGCGATCCATGCAGGAGCAGCTCGCGGAGATGCAGCAG
AAATATGTGCAGCTGTGCTCGCGCATGGAGCAGGAATCCGAGTGCCAGGAACTTGACCAGGACCAGGATGTGGAACAAGAA
CAAGAGCCGGACAATGGCAGCAGTGATCATATCGAGCTGTCGCCCTCGCCCACTTTGACCGGAGATGGTGACGTTAGTCCC
AACCACAAGGAGGAAACTGGGCAGGAACGACCTGGTTCCAGCTCACCCTCACCATCGCCCCTAAAACCCAAGACATCGCT
GGGCGAGAGCAGCGACTCAGGCGCTAACATGCTATCCCAGATGATGAGCAAGATGATGTCCGGCAAGCTGCACAATCCACT
GGTGGGTGTGGGTCATCCCGCCCTGCCTCAAGGATTTCCTCCACTGCTCCAGCACATGGGCGACATGTCGCACGCAGCCG
CCATGTACCAGCAGTTCTTCTTCGAGCAGGAGGCGCGCATGGCCAAGGAAGCCGCCGAGCAGCAGCAGCAACAGCAGCAA
CAGCAACAACAGCAGCAGCAGCAACAGCAGCAGGAGCAACAGCGCCGCTTCGAGCAGGAGCAACAAGAGCAGCAGCGAC
GCAAGGAGGAGCAGCAACAGCAGATCCAGCGCCAGCAGCAGCATCTGCAACAGCTGCAGCAACAGCAAATGGAGCAGCAA
CATGTGGCCACTGCCGCCCCCAGGCCGCAGATGCACCACCCAGCGCCCGCCCGCCTGCCCACACGAATGGGCGGTGCTG
CTGGCCACACGGCCCTCAAGTCCGAACTGTCGGAAAAGTTCCAAATGCTGCGCGCCAACAACAATAGCTCAATGATGCGCA
TGTCGGGCACGGACCTGGAGGGACTGGCCGATGTGCTCAAGTCCGAGATCACCACCTCGCTGTCCGCTCTGGTGGACACC
ATTGTGACCCGCTTCGTCCACCAACGGCGGCTGTTCAGCAAGCAAGCGGACTCCGTGACCGCGGCTGCCGAGCAGCTGA
ACAAGGACCTGCTGCTGGCTTCGCAGATCCTCGACCGGAAGTCACCGCGCACCAAGGTGGCGGACAGGCCCCAGAACGG
ACCCACGCCCGCAACACAATCA

pros intron - Quasar 670

GTAAGTTGAGCAATTAACAATTCCAGACCTAGTTCTAGATCTAGACGTAAGACAATATGTATTAACCATTCAGCAGCAGCATTCA
TATTTATGATTTCGTTACGTCGCGCTTGAGTTTTTGAACTTTTAAGTTTTGTGGGCGTTAGTCGGGGGCTTTTGTTACAAATTG
ATTGCCCAAATTCGAGACTGCCACCTATCGAAACCCTCGACTTGCACTCAAGAAGTAGTCGCAGGACATGCAACACCATTCG
GCTGTCATTCCGCGCCTCCAACTGTCAGTCCGTGAAATTGCGCAAGAAGTTGCCAAAAAGAGCAGAAAGACAACGACTACG
GAAAAACGACAGCTGCCAGATAGTCCGTGGTGTGGGTAAATTCGGATATACGGTTATTCCGTGGAAGGAGTGGGCTGTTCTC
AATGGAACAGAGCCAAAGTGAAGTGAGGTAGGCCCGCATGCAGTCGCCGTGATTTGCGCGCCAAATCCGGGCCGCATCTG
TCCGCCCCGAAGTGAATACCATACCGAAGGAAAACAGAGAACCGAGCTGAAAACAGAGCGTGGCACAAGGTCTCACCTGGA
TTTATAACTTGCAACCCTCTTTCATCGTCGGCTTAGCAGCTGCCCGTCTCCGATTTGTCTAAGACATGCGCAACGTCTTAAGG
AATTGTCCGCAAGACACCCTAAGAAATTCCCCTACCTGCGCACAAGCGAACAGCACAAAAGACAACAAATCAAGACCCGGC
GGCGCGGGGTTTGTTCGGAATTTCTTATGGGGGTTGCTACCCTTGCGCGATGTGCCCTAACCCTACTTTGCATGGGAATCGG
GGAGTTGGCATCTTGTCTTTGCCTTCGACGACTTCGGCGACTTCTTGGGCGAGAGGTTAAAATGGGTGGGAATATTTTCTGA
TTTCCTAACTGGTACTCGATTGTTTGTTTCCGTTTTTTTTTTTTTTTTTTTTGCTTTTGGATCTTAGGGGTAGTTGGGATGTAAC
GGTTTTCTTTGCGTTTCTTTCTCATGCTGAGTTGCTAAGTTTGATTTTAGTTTTCATTGTTCTCGGGAAAATGCTTTTCCTCTTA
ATCGTTTTCCCCCTAAATTAACCTAGGTGTAAAATCCCAAATAAGAAGACTTTACTCGTTGAGTTTTTGTAAGAAACTGGTTTTA
TTTGGAAATATCTTCGGTTTAAATAGGTGACATGAGAATCGCATCTTAAAGTAAATGGCCTACGCAGAGGCCTACGTAAATAGT
CCCCGCCTTATCGAGGTCCCACGCTCGGGCACATCTGCCTATCTTGAGCGGCGAGGACCTTATCTGTGGTCTCCCACTAAG
GGACTATTTTAGGAGGCGGGGAACGATCTCAAGTGACTGACTCATGTAGTGTGCACTTAAATTACATGTTTTTGAGCAATGCA
CCCATGTCGCCTTAGATAACAAAATCCTAAATATAATTTATCGCTCTCGATTCATTTACATAAGATATGAACGGAGCCCAAAATTG
TAAGTCTTTAAATATATTCGTGTTCATGTGTGAACATTCTGCCAAAGGGCCAGCAAAGCTGAGATGTACATTAGTATATTAGTTG
CATTTATAACAGTAGTGGACTGTATTTATTTGATATATGTTCATTTATTTTGCAACTAAGATTTCAATGGGCCTAGTTTTTCTGGCT
TTTAATTTTATTGGATTACAATTATGGTTTATATTATTTTTAATTCAACAATTTGTACTCAATTAACTTATTTTAAACATTTTGCTTTTT

CTATGTAGAAGTACATTTTCTATTAGTGGACTGTATATTTTTATTTGTTATATTATTTTATTGTTTATTTACTATTGATATTTATAGTAC
TGGCAACGGACCTGCAAAGGTTATTGCTTGCATTCTTTGTTGCACAGCACATTTCCGTATGAAATATATTATTAATACTATCATTA
GTATTAAAGCAATAATTAATCCAGCATGTCCGGAAATATGATGGAAATGTAAATCTTTCAATTTTTGATGGTTCTCTTTCATAAATT
TAATTTCATTATTCAATCGTTCAAATTCCTCAGTATGATTTAATATTGATAGTTTCAGCGGATCCCAAATAATCTTCGGCACTCCA
CTAACTTCTCCTATATAAGGTGTTGATAATAATTCTTCACTTTCGGACTGAATGTTATGGTGGGCAACTAGAATTTTATCGTCGG
TTCTTGCCGTACAATATGGCGCAATGCTTAAAACTCCTTGCTGAGGCAAATCAAACAATTCAATTTGAGAGCCAGTACATTGCA
GACGGACTTTTGAATTCGCAGGAACCTTAAACAACCAACTACTTTTCTTTTCTAACTCTACCCAGTAACTTTTAGAGTCGACTA
CTGTTTTATAGATGCAGTTCGCCGCTTTATCTGGCTTTAGAGGCTGAATCTCACATGCATTATCATTCGCTGAATTCCAGGGCC
AACTTCCTTTGCATATTCTCTTATTTAGTTGCCATTTCTGACATTGATTTAATGTGGCTTCCGTCATTATGTGATAGGAATCTATC
TCAAAATTATAAATTAAATATTCGGACGTTGTATGCACCATTATTATCCGATCTTCATTTCGAATTGGCACCGGAATAAGCCTGAA
CAATTTGGATGGATGCCTGCTAAACAGAGGCACCTTTGCACTAATGATCAATTTATCGTCGATGAATAAACCCCTGGCTGTTAA
CAGTGTATACACCTCCTTAAGTTCCGTACCTGACCGTTTTCCTGGAATTACTAGGTTCTCTGAAAGACTCTGCTGAATTTTGGC
AATTTCTTTTTTAAGCTGATTTGGCCTGAGAATATTTGTATTTAGCCTACCGTGATTAATATCAATCAACAGGCTTATAATGCCTG
CTTGAATTTTTTCGCCTTCTTCAATCAATGAGTGTAGCTGTTTCGTAATCATAAAGAATTTTATTGATTCCTTATAAACATAATAAT
TTTCTTTAAGAACTTCTGTCATGTTCTCAATTCTTATTTGCATACTTCTAAAATTGGAGTTAACATCTTCTGTTGTTCTCTTTAATA
GATTAGAAGTTGAATCAACCACAGATGTTTGTTTTTGAATTAGTTTATCAAGGTTGTTCTGGTTATCTAACAAATTCTTCATATTT
TCTTCTAATTGCTCTCTATCATCTTCATCCATTATACCAAATAAAATATGATACAAGGAACCCATAAATTCGAAAGGAGCACGCTT
GCTTCTAGATCTAGACTGCATCATAAACAATTTATTGTTTTCTTCAAGTTCCGATAACTGACTTTGCATATTATCTAAGACTAGAC
TACATTGCTCTTCAAAGCTATGAAGTCTTTCGCAAACTTTCCTCATACTTTGTATAAGCGCATTACCCTTTGTTAACATTTTAAAA
TATGGATCCATTTTATAATAGATAACCAAATTCCAAGAAGTACTCACAATCTCAACATCTCCTAGCGGGTCTAGATATATTGCTGA
GGTTTTATTTATTTTGTCTATAGAATATCTTGGTGCTATATCTTTAGGTAATGCGCTAGAAACTTGACAACTTAACACAAACAACA
ACATTGCCATAATGATTCCGATCTTGGACATTCCCGATGTCGCTCTAGTTCGTCTTTTTGGCTCTTGGTCAGCCTCATTTTTGT
CAACAGACTTTATTCCTTCCAAGGGACAAATTTTAGTAATGGGTCTAGTGATATATCCTTCCTGCATCTTTACTTTAGCCACTCG
GACCTTATCATCATTCCCCTTATGCACCTTTTCCACCTTTCCTAAAGGCCATCTTGCAGGATGACAATTCTCATCCTTTAATAAA
ACTATTTGCCCTTCTTCTATATTAGGAATTTCCTTTTTCCATTTATTCCTTTGCTGGAGCGTATGCAAATATTCACTTTTCCACTTA
ACCCAGAAATCTTTCTTCATTTTTTGGATAAGTCTCCACCTATCCAAATTTCCGATTTTTTCATCTTCCATTGGTTCGACTATTTC
TAAAGGTGGTCTTCCAATTAAAAAATGACCTGGTGTTAAAACTTCTTGTTGGTCCTTCTCACTAACTATAGTGTATAATGGCCTT
GAATTTAAGCATGCTTCTATTTGACATAAAAGAGTTGACATTTCTTCATAAGTCAAAATAGTGTCGCCGATTATACGCTTTAAATG
GTATTTCATTGACTTAACTCCAGCTTCCCAAATACCTCCGAAGTGAGGTCCTGCCGGGGGAATAAAATGCCAATCAATCCTGT
CCTTTTCAAGCTGCGCTGCAATCGTTATATTTTCTTGTATTGCATTAAATAACTCTTGATCTAATTTTCTTGCAGCTCCTACAAAA
TTTGTTCCGTTGTCTGAATAGATATTGGAACATTTTCCCCGTCTAGCAATAAATCTTCTGAGTGCTGCTAAAAATGCGTCTGAA
GTTAGATCGCTTACCATTTCTAAGTGTATGGCTTTGGTGGCCATGCAAACGAATACAGCAACGTATCCTTTAAATGTTTTTTGG
CCACGATTTTTTGAACATTTAACATAATAAGGACCTGCGTAATCTATTCCAGTATTAAGAAACGGGAATGTCATCGTCACTCTAT
ATTTTGGCAAGTTACCCATTATTTGCTGAGCTGTATTTTGTTTATACCTTGCACACGTTACACATTCTCTTAAATACTTTTTCAAC
GAATTTTTCAACCCGAAAATCCAATACTTTCTTTGGATATAGTTTCGCATTAGGTTTATCCCTCCATGCAATGTTTCCTTATGAG
CATTTTTTATTAATAAGCTTGTTAGGTGGCATTTTTCTAAAATGATTGGATGTTTAACATTAAATTCTGCATTGGAATTTTGCAATC
TTCCTCCAACTCTTAGAACCCCATCCTTGTCCAAAAATGGATTCAATGACAATATTTTATTATTTGTCTTGATTTCCTTTTTGATT
TTAAGGCACTTTATCTCTTGCCTAAACTGGTATTCTTGTTGTTTCTTAATAACAACTGTTTCCGCTATTCTTATCTCCTTTACTGA
AATAATTGATGAATAGGCTTTATTTCTTGTTTTCATCTGCACGAATCTATTTATGTATGCTATTATACGTATAAGTTTTTCTATACTG
GAATACCTTTCTATTAATTCGTAAATAGGATCATCTATTTTGTCATTTAATACCGTATTTATTAAGACAGGTTCTTCTACAGACTGC
TGCCGAGGCCAAAGTTCTTTTGGGTCTGCTAGCCATTTCGGACCTTTCCACCAAAAATCACAGTTGATCAACTGGTTAGAATC
CACTCCCCTGGATGCTAAATCTGCTGGATTATCCTCTGACTTAACATGATTCCATTCAGTATTTTTTAATTTCCGAATGTCATCC
GTTCTTCTTTTTATAAATTTGATCTTACTTTGACCACTGTTAATCCATGCTAAGGTAATCGTGGAATCACTCCAAGCATAGATCTC
CATTATATTGTCAATTGATCCTTTTAGTCTTTGGATTAATTCACTAAGCAGGTGAGCTGCACACAGCTCGAGTTTGGGAATTGT
CTTCCTATTTTTTATAGGGTTGACTCTACTTTTGCTAGCTATTATATTAACATGAGGTCCTACTTTAGCATAGACTACTGCAGCAT
ATGCTTTTTCGGAGGCGTCCGCAAATCCGTGAATCTGAATGACTGAAGAACTGTTTGAATTAATCCACCTTGGGATTCGAATA
TTCTCTAACAATAATAAATTTTCTTTATATTTTTCCCAATAATTTTTATCTTCTATGGATAATTCCTGATCCCATTCACTTTTATTTAT
CCAAAGTTTTTGAATAAAAAGTTTTCCTGAAACCGTGACTGGTGCCAACCATCCTAACGGATCAAATATTTTTGCTAGCGTTGA
TAACACAACGCGCTTATTTATATTTTTTGATTCATCATTACAATTTACGCTGAACTTAAATAAATCCTTTTGAGGTTCCCATTTTAG
TCCTAAAGTTTTAACACATTCATTTTCGATAATATTGAGAACCTTATTGTCCCCTGTGTCCTCCACAGTGGTTAATATTTTGGAAT
TGTTGGAAATCCATTTCCTTAAGTTGAATCCAACTTTCTGCAATTCATGGGGAATTAATGTTATTAATTTATTAGCTTCTTCTACC
GAATCAGCTCCAGTCATTAGGTCATCCATATAGAAATCATTCCTAATTATTGCACTAATAACTTGGTTTTTACATTTATCTGCAATA
TCTACCAGAACCCTGGTAGCCAAATATGGTGCAGATGCAGTTCCGTAAGTGACTGTGGTTAATTTATATGTTTTAATTTTTTCTT
TTGGAGAATTTCTCCATAAAATATATTGATATTTTTGATCATTATTATCTATTTTAATTTGTCGGTACATCTTTTCAATGTCTGCCGA
AACAACAAATTCCCATTTTCTCCATTTAATAATAATGTCAAAAATATCTTTTTGAACTCGTGGCCCAACCCACATTATGTCGTTCA
AACTTTTGTTATTCGTAGTTTTTGCTGAAGCATCAAAAACTACTCTCAATTTGGTCGTAAGGCTTGAATCTCTAATCACTGCCTG
GTGCGGTAAAAAATATTTGCCTTCATCACTCACTTCAATCATGTGTCCTAAATCCATGTATTCATTCATGAATTTAGTGTAGTCAA
CCTTAAGTTTTTCATTTCTTTTTAGTTTTTTCTCCAGATTCATGTAACGAGCTATCGCTTGTTTCTTTGAATCTCCTAAGGTGACA
TCCTCCTTGAATGGAATTGACACAATGTATCGCCCATCTGAATCTTTTTTTGTCGTTTTGATAAATTTATTTTCACAGATTTCAGA
CTCGATATCATCTTTTTCTTCTTCTTCCACTTCCCAGTAGCGATCTAACTCTTTTATTTCTATTGTTGTGGCTACAATGGTTTCTT
TTCCTTTGGATTTTTTACATCCAGAAACTATCCACCCGAAATCAGTTTTTTGCCCAAGGAGACCGTCTATTTTTATAACTCCATT
TTGCAGAATGTGAGTATATACGTCTGCTCCAATGATTAAATCAATGCGACCCGGTTTATTAAAATCGGGGTCGGCTAATTTAAA
GTTCTTCCATTTTTTCTGATCAACATTAATCGTGTTGACTGGAAGTGCCTTCATAAGTTTTGGGAGAATAATTGCTTCAATTTCT
AAATTTTTCGGAGAATTTCTTATCGAAATAACCGCTTTGTGCTTGGAGATGCACGTTCCTGTGGAAGATACTCCACTTATTTCA
GTATGAGACCGAAATTTTTTCAATTTTAGAATCTGTGCAGACTCTTCTGAAATAATTGTGCTTTGAGAGCCACTATCAATCAATG
CTCTTAATTGTTCAAAGCCTCCATACCTCGACTTTACTTGAATCAAGGCCGTGGCCAACAAGGCTTGACCTGTTGTTCTACAC
GTATTCACTTTTTCTGGATTATGACCTGCAAAGTGAAGTAACGTGTGGTGAGGTTTACGACAAGTCGAACAAAGCTGCTCGCT
TATACATTTTTTACCGAACGGATGCCTCAGACATCTTAGGCAAATCCCATTTTTTCTTACCCAGTCAGACCGTTCTGCTGGATT
CATTATTTTAAATTTATGGCATTGAATTAAATAATGCCCTGGTAGTTTGCAATATGCACAATTGTCACTATAATTTTTATTCTTGTTA

TTATTAATCATTTTCTTTACAGGTTTTACTTCCTGTGAGAATGATGATATAGAATTGAGCCTTTGCTCTAAAAAGTCCATGACATC
AGAAAGTGCCTGTATTTCTTTTGTCTTTTTAACATGGCTTTCATATAAATTGAGTGATTCTTTATTGAATTTCCGAAGAATTATGT
GAGCGAAAATTGCATCCACATCTTCTGGTAATTGTGCCTTTAATTTTATAATATAAATTGACTCGTTAATCGTGTCAATAAATGTC
TTTATTTGCTTATTGGATTCTAAATTTAAATTTGGCATATCCATAAGCCTATTCATATGATCTG

pros UTR-long - Quasar 670

GCGTTATGGGAAATTGAGCAATACTTGAGTTCTGAACAATAGTGCCGGTAACATTTATACTATAAGTGAAACTATATAAATAGAC
ATATATATATAAAATACATACTCTAGACGTCGTAATCCGTATTTCAGCATAGCTAACAAATGTTCTAAATGTACACTGAGTAATGAA
AATCCGGAACCCAAGCAACAAACCAAAAAACAAAAATGCAGATAAGTCAGTCAGGTGAGTGAAAGAAGATAGAGGGTATTCG
CTTGTGCAGCATTTTTCGAGCGGTACATGCAGATCGAATATTACCTGGTATTGGCCGAGTGACCCAACAAAACCCCCAAGTAG
CCCCGCCCCTCCCAGCACACGAACCACACACTCAACCACATTACGATCCACAACCTTATAAATATATATAACTTATTACTTATAT
AAGGACATAAACTCAAAGCAAGCAAAACAAAATTATAATAAAATACAAATACAAGATAATGGTAGTTGCTATTTTAAATATGTATTA
CAAAACCAAGAAAAATGCAAAAAAAAAATAACAAAGAAAACCAAACAAAACAAACTAAATTAAATCGAATGTCAGTCAAAATAA
AATGATCTTCAGCGCAAGCAGCAAAAGTCTCTAGTAAATGTTAAGCAGGAACCAAAAGCCAACCTGAGCAACAACAACAGCA
GCAGCAGAAACCGATTCAGAAGCAAAGCAAAAGCAAATCAGTCAGACACACCTATATATTACCTTAATATATATATAACGCAGTT
TGTTCCAAGCCAAAATCAGTACATGAAACTATATGATATTTGTATGCTTTTTTACTCACACCATATAAGCCAAGTGGAAATTGGTA
CAGATCAGATCAGATCGGCAGGACCTATTCGCCAGGATACTCCGCCGCCTTTAGGTTTAATTTACGCACTCAGACACGCAGA
CACAGACACACTCGAAAAAAAAAAACAAAATGAACAGAGATACTACGAAACTGAATGTCAGCATAGGTATAATCGTAACGAGAA
TCAACTAAAATTTATACTCATAGTTTAGCAGTCGCCGTAATTGATTTATATTTTGTCAGCCACACGAAGCAGAATCAAACCGACA
GACGAGACGAACTCAACTAAGCTAGATACAGATACAGATACAGATACAAAGAATATCCAAAAGATACATTAAATATAACTCAACA
ACAGCCACCTAGAACAAGAGAACAACAACCACAGTAACTACAACAACTTAATGCCGTTCAGCCAACAACAACATCAACCAGA
ACAACAATCGAGCAGGATCAGTTCACAGATGCAGCAGCTTACTTATAGTTTTTTCAGGATAATAAAGATAAAGATACATACACCA
TCTAAGCATACTTATAGCCAAGCCCAGCCCAAAAACAAAAAACGGAACTCCAGACCACAATCAAAAGCAGAAACAGGTACAG
ATTTCAGAGCAGGATCAGAGAAGGAATGAGGAGGATGAGAAAACATTTCAATCAAGTGCTAGCATTTCGAAGAACGTTTTAAC
ATTTCGGCTTAGAAATACGTAGAGAAAAATTACAACTTTCGGCTCAAAAGCAACGCGCTGCATTTTGCAAAAGAAACCCAACA
AGAATGAGAACTCTTGCACACATGCAAGACTAAAACGAACACCTAAATGAAGTAAAACACTCTCGGCTAAGACTTTGGCGTG
AATTTCGGAAAATAAATATAGAAAAAACTCAGACGAACGTTTTGATACAGACGATAATTCAGATTGCGACATCAGAACTATAATG
AAACCAAATGTGACCAAAGACGCGGTGCAAGCGGCCCAGTAGTTTTCCAGATACTTTCAACACTCGCAGACCCACAAAAAAA
TCATGTTTAGGTATAAGTGTAAAATTATATACAATATAAACGTATTTCGGTAATGTTCCTAATAAACATATGACACACATTCGCTCA
CAGACAGACTTGTGCGCATATATGCATAGGCATATTCAAAAAGTATATATGTGCGAATAAATTGCAGTTTCGGCCACACAGTAAA
AATTCAGCATTTAACCGTTTGGCAAAGTAAATTAGCGGGTATAACAAAAACTAGGAAACAAAAATTGGTCTGCGAGCTCGATTA
AGCTGGAAAAATTGAAAACTGGACTGCTTGCAGAAAACATTAGAACATGTAAAATGAAATTAACTTAATTGTTTACAGGCAGCA
TTCTATGAGAAGATTACATTCAGATCGTTTAGATAATCTTATTTCCCGTTGAAAAGCAGACAAGATCAGTGCTTTTCAATCAATG
ACAACGCGTTTAAAAGCCCAAAAAAAAGGAAAAGAAAATCATGCAAGTACGAAACAAATCACGAAATGAACTAAATTAAAAAC
CTCTCGGCCATGTTTGGATAATTCTCTCTCGGTGTAAACATTCAGGACAAATTTACAAAAAAAAACCACAAAAAAAAAACAAAA
ACCAAAAAGAAAAGAAAACTTTAGGATTAAAAAAAAGGGAAAAATACGAATTCAAAATCCAAAAATTATACGCAAAATTACTGAA
TTTTGGAACACAAAATTACGTAACAAAAACTTAAGATGTAAGCGAAAGCAGCAAAGAGCTGCATTTCGGAAAGCAGTAGACGA
AGCAGTGTAGTCGAAGCAGGGAAGTAAGCAGTAGAGAAAGCAGCCTAAAACCAGAACGGGAAAATGGAAAACGGAAAACTT
TGAAAGAAATTTTGAAAACGTGTTGGAAAAATATCAGAAAAAGTACAAGCTTATTTTAAGCACCTTCGCGCCTTATCTTTAAGAA
CGTAAATAAATCGATGCAAAAATGAGAAAAAGTAACCGAAACAAAGCGATAACAAAACACAAACTTAAATTAAAATAAATTTAAT
ACGAAAACATTGTACATTTAGAAAATACGAGCAAAATTGAGCAAAGTTTCGATACATCTCCGGGTAGTTAACCTTATCTAAGCTT
AAGTTCGATTCGAACCGGTTAAATTCGGGCTCGGATACTGCAGAAAGCACCTTTAGTTTTCCCTCAGTTCGGGTTTTATGAAA
AACTCAGTCCTAAATTGTATACACAAGCAAGGAAAGGATAATACGAAAAAGCAGTAGGTGAAAAAGCTGAAAAGAACATGACT
AGTCGACAACCAAGGCAGTGGCAGGAACTAATTGGAAAAATCAGTTCCGGTCCCCGCTGACAATTGAAACCGAATAAACAAC
AAACAAAATTCCAAAACATTGCAGCAGCAGACTTCAAAATTATAAAGAGATAAATAAAAAAAAAGCCAACCAAATTAACAAAATT
CATAACTGCGGTTCGGAGCACATAGGGAAAAGTGTATGAAAGGTATGATAAAAATATAAATCCAAAAAGCTAATGCGAAGATTG
AAAGAAAAAGTAAACTTTTGTGTTCCCCAAATCTCTGTAAATGTTTAGATGTATGAAAGAAAACCAGTCGAGGACACTACTTGA
GTTGAGTTAGGTTTTGGTGGGGCTGAGACCGACTTCAAAATAAGATGTGTATGTAAAAATCAAACTAAAATGAATACTATAAAT
GTAACGCTATGAATCCTAACCCCATTGCCCGAGATTTAGTTTTAAAACTTGATAAGTATCTATTACCTTGACCACTATCCACCAG
CTTATATTCGTGTATGTAACCCCCATTTTATTGTTTTTTGAGATTTGCCAACGATCGATCAAGCGTGATTCCTTTTACGCTCTTG
AGTTCCTTCCCCAAGAAACCACATCCAAAGAGATCCATTGGGATTTGTGCACCGGGCCAAGGAGTGGGCAGTTCTCAAGCC
TCGAAAATAAACCCAAACTGCCCGGCCCAGTGGCCAGAACATCGGCATTGTTATGGGTCGGGCAACTCCAGGACATCCAGA
TCCGTTTCGCACCATAGCACTCAAGGCAATACAAACAACCGGCGGCTAGAGAGAAGCAAAATGAAAAGAAAAGCAGAAGAC
AAGGCAAAGGACAAGTTTCGAACCAAGGATTTCGGTAACATTTCGAACGCAACTTTCGGCAGAGTTTCGAACAACTTTGGAT
TAGGCTTTTGTTGTTAATTTGTTTTTTTGCGACCACGTCTCCATAGCACTCGAGCAACATGCAATATGCAACAGCAACATGCAA
CAGCAACACACAACACAAGCAGCAAGCAGCAAGCGGCAACGTGATACACGAGTTGAGCAAGTGAAAAGCAATTTTTGAAAT
GGGGCCACAACGTCCGATCTAAAGTGCCTTCAAGTAACAATGAAAACAAAAGAAAACAAAAAGAAAATACCAAAACTAAAAAC
TGTTAATTTTTTATGTAACTAAAACCAACGCGGAGGATGAAATTATAACACAAAAATTGTATAAAGAAATTAAACGTGTAAAAAGT
ATAAAAATTTAAACAAAAACTAAGCGATGACGATGGTGAACGCGAAAGCGGAAACGTAAACGTAGAGAAAGGGCTCCAAATA
GACCGGAAATTAAGCAAAAACCATAACTGCTTCATTCTTTGGCCTGGTCACACCGTCTCTCCGAAGGAACTCACGCATATGG
GCTAAAAATGCAAAGGAAAATCGATCGCAAATCTCTTAGAAGCCATCTTAAACATTTACTTTCGCATCCTTCCCTAGCAAAAAG
TTGTAATTGACTACCTAATTAAGCGGAAAAAATATGTATGTATTTAGTTTTAGTATGTAAGCGAATGGAAATTCACATAAAACTCG
ATTTAGACGAACATAATGTATGGGAAAATTAATTATTTAGACTAGCGAAAGCAGCAACAAAGGTTTGGATATAGACACCCCGAG
TATACCCCCTATACCCCATACCCCATACATACGCCTATAGCGCTGAGTTGCTCATCTATCAATGTACTTAAAACCACAAGAACAC
AGCCACACTGACACTTGCATGTACTATGCTACATTTAATTTAGATTTAGATGCGAATAACTAAGTATTCAACTCAAAGTTATTCGA
AGAACGATACGAGATGAACTGCGAACGGCATACTGAAGAGGTGGCAATTAGATATAGAGCGAACTATATTTAAGGACTCGGAA
CTAGCGACTCTCAGAAAATGAAAATGAAACGCGAGTGCGCAGCGACACAGGATCGCAGATAAACTATAAGACTTTCCAGAAA
CGAAGGGGGAAACCTGTCGTTTCCCACTTTTGTGCTTTTTCCTACCCCTGACACACACACTGCAGACATACACCTACCGTAG

ATCTTGAGTTGGCAGCATCGTAATCGTTTTTTTAGTCGACGATGGGAAAGAACTAGCAAAAATTAGCAAAATTTAAAATTGATTA
TGTGACACACAACACACCTTCCACACACTCACACACACACAGATACTCCATGTATATAAGTATGTATATTCCTTTGAGCTGAAC
ATTGTATAACCGAACGATTACGATACCACAAACAAACACAGCGACACAACGACCTTAGCCATCAGAATACAAGGACACACCGA
GGTGTGTAAAGGGTTCTTTGCTTACAACTTTTCAAACGAATTAAACCGTTTCGGCCAACCTTTAGGATTGACAAAAGATCGAC
TTGAGGAACACAGCCCCGCCCACTCTGCTCCGAAATTCAATGAGCGGGGGGGCGGGA

pros long-specific intron - Quasar 570

AACACACTGAAACCGGCCAAAGAGCCCGGAGTGAAGAACTGTAGAAGGAAACGCAAATAAATGAATTGCACTTTTCCTTTGC
TCGAATTTTCTTCTGGCGCCCCGTTTCAATGGGCCGCGCCTCAATGGCAGTGGAAAAACTTTGCATATTGTGTTTATTCTATG
CCCGCGGAGATAAAGAGCTCCAAGCTTCGAGCCAGGTGGAAGTCGCAGGCGGAGGCAGAGGCAGGCTTTAATTAAGCGGG
TCCAAGTCGCAGTCCGTTGGCATTATGCCCAGATAATGGCAAGGCCGAGCTGGAAAAAAAAGGGGCCAACGAGGGGCGAT
GGGCGTAGATGTGGGCGGGGGAAGACAGATATGAAATGCAAATTATGCGGCGAATTGTGTGCTCATTAATTAAAATTGAACCA
AACTGAGGCAAGAACTCGGCCTGAGAAAGAATGCTCAACCATCAAAGCACCAGCAGCATCATTAGAGCCCGTCCAGCTTAA
CCAGCCAAATCCTCCATCCTGAATACTCAATCCACCATCCTCAATCCTCCTGCCCAAGGATCTCTCTCTCACTGTCCACGCCA
CTGCACTTTGAGGTGAACACTCAAAAGTTTTTCCCGCCACGGATGGGGGGCGAAAATTTGAGAGAAATATTATACATATATTTA
TTACTTGTGGTCGGGGGTCTGAGTCAAAATGCAAATCTTGCAGATTTTTAATTTCTTTTCAACGAAAATTTTATTTTCTGTTTGC
ATTTCTTGTTGTTCGCCCAGGACGTTGGCAGGACCAACCCTTTTTTATTTGCCATCCTGCCAAGGATACTGATGCCCCCCCC
CTCCTCACCACGCCCCCCTTTCGCCACTCCTCTCGAGATGGCGTGCTGCTTTTAAGCTTTATTATTATGTATTATAGATTCATTT
TATGCACTTTTTAACTTTTTTTTCTGACGTCTCAGGGCTTGAGACTCTCCAGACCGACAGCCCAAAATGAAATGCGTTTTGCC
TTAGCGGATAATGAGAATTGTGTTCTCAGCTTATCAGAAGTCATGTACACACTTTCTTAATAACTGTTTATAATAAGCAGAAAATT
TCCTATTAAGTTATATATAAAGTGAATAATCTACATATACATTAATTGGCTAGATAATGAAAATAATTGATACTTTTCAAAATATTGAA
AGTGACTAAGTGTAATGATATGCTCGATGCTCTTTAGCAGTTAGGGTATTCAATAACTTCTTGGACTGGGCAATGCTGCTGCAG
CCAGACGTCGAATGTCCTTGGCAGAGCCACCCTTCTGTTCGCGAGATCCCGCAGTGTGGGTTGTCTTCTGGTTGCATTGCC
ACAAGTTGCTGCTCGAGATACCCACCCAGAAGGACACGGCTCCTTTCGATGCCGCCTCCTTGTTCTTGTGCAGTGCCTTTC
AAGACTTTTTGCCAGCCTTTCTTGGCAACATTTGGGGGCGGCTTTTGGGGTTGCATCTCTGTGAGATACATTCGCGTAATGAA
TTCGGCCCGAGGGTGGCGACAATGAACTTGCCTGCATTCGCCGCACCACACCTCCCATCCGCCCCGCAAACATGTTAGGC
CGTTGACATGTCAGGGCGAAGTATTCCGAATATTACTTGCAAGGCTCGCTGGTTAAAGGAAACCCTGAGCCAAAAAACGTAG
GAGAACTTCACGCATTGCTTGCCAGGAAGCCAGGACATCGAGAGGGGGAGGAAAGCGGGTTCGTTTTCGGCCAGCTGGGA
ACCGAAACTGCCGATTCATGTAAAGCTATGCCGGAAAGCGCCTTGAAGCAGAACCAAAGGAAACTATAGGAAACAATTTCTAT
GCATTTGCATGCCGATCGCCAGAGCGCAGATCGCAGAGATCACGGAAAGCGGAGGAAAAGGCGAGGGTGCGCTTTTCACA
CGGTTCGCGCGGAGGAAAAGACCCAAGGGTCGGTCATAATTTTTAATAATTTCCTTTGCTTAAATAGTTTTTCCTTTGGCATAA
CAAATTCCCACCGCCGACGCAGCAGTGGGCAATTGAAGTGTTAGATGCAAAGATCCAATTGCCCGCAAGTGGCTGTAGAAC
AACACAGATACGCACAAGATAACTTGATTGCACTAATTTGACTGCTGCACCCGAAGAGCTCGCTATATATATGTACATATATGTA
TGCATTGTTCCCATGGCGGACTAGTTTCATAGTTCCGCATCGGACAGTTCCCAGTTCCTTCTTCGAAATGCAGCCCAAGTTG
AGGTCTCAACTGGTCTGCTGGGGGTTGCTTCAATCAACTTCTGACAAGAAGTGTTAAATCTGCACTCGCTGCAATTGCAGCT
GGAGGCCGCTTTATTAGAATATCCGGCAGCTTAGGCCGCAGACAGCCTGTCTGCAGCAGCAGCACCATTACCATTATCACTAT
CTGCCCTGGTCCACATTGTCATAATTCATAAATCAACTAATTCTGGAGTCGTTGGGCCAGCACAACGACAGAAACAAATAGCT
TCCCCCCCACCCAAAAAAAATACAAAAAAAGTACACAAATCTGTGACGAAGACACTCGTTTTGAGTCGAAAAGTTCTCAGGC
CTGGCGAAGTCAGGAAGACGAAACAATTAAAGGGTTTCGAGTTGCCTTAATGAACCGCAGCCAGACAAAAGGTCAAAGACA
AGACCATCATCGTCAGCGCAAACAAAGGCCTAGATGGCCCAAAACCAAAGGCAAACAAAGGTGTGTCCCCACACACACACA
CACTAAAACAAAAGCGAAAGGGAGAAGACGTCACGGCGGTTGCCTGCACTTCCTGGCAAGGAACAGAAGGCAGAGGCTAC
AAGACGCCGCTGGGTTTCAATTACCAGGGTCCAAGGCCCAAGTCACAAGTCCCAAGATTTCTCCCCGCTCCAAGATGAGTG
ACCTCCCTTAATTGAGCGTGAAGGGCTGCAATACTTTGACACCTTTATGACACGGACATGGACTTCGACAGCGCCATCAACA
TTGCATTGACATCGAAATGGATATATGGACGGTAGACATGGACGACTATACGGACGATGGACGTTGGACAGTGGCAACCCCC
TAAGACAGACGGAACCGAACTGGCCGGTGGACGACACTAATGAACATTAATGTTCGTATTGTGTAATGTCGCGACTTTAATGT
AAAGTGCAATGAAGCAATGCAAGGCCAGGGGGTAGTGCATCCACCGGATGCACTCATTAAGTGCTGCAGCCTTTGACTTGC
AGACCCGAAAGAACTGGACGCAAATGTGAGCTGAGTTATGATGCCAGCTGACGAGCTGTCAGAAGCGTCATCCACCGCGGA
GGAGGTGGACTCAATGGGTTGGGCTGCGTTGGATTGCTGGCATGGGGGGTTACTGCCGACTGGCCGGCAAGTGGTTGTTA
AGTCTGATTCACGGCTCGATTCGGAAATCAGCGGGCAGCACGTGTTCCCCTGCACTCTGCAGCCTGCTCTTACCCTTTGATC
TGACCAGGGGACATTCGGCATGGTAGGGGCTTCTCTTGCCCCACCGATCCGTCCCAAGCCCCCACTTGATTTTCCTTCGCC
CTGCGAAAACCATTTTCCACAAATTTAATTCCATTAATGTCGCAGCAGCGGCAGTGTCGTTAGCTCATCCTTTGGCCCTCCTT
TCACTGCTCGCGCTCCTCCAGCGGCCCTTCAAAGGTTCTTCAAATGTCAAGCGGAGGCAGGCCAGGATTCTCCAGCAACTA
AATTATCATAATGAATCTCGCAACTACTTGAGTTTTGTTTGCCCAAGCGGCAACTCAACTCGGTCCGAGGAGGGTTAAGCGAT
GGCTCTACTCCTAACGATTTTTTAATTGAAACTGTCACTTGTCGAGGAGCCAAGGATGGCCAGAATTCAACCAAAGAGGGTG
GACAGTCGCAAGAACTCTGGCTCCTAACCTCTCCGCCTGAAGTAGTTTCCATTGCAATTACGAAGGAATTAAATGCTGCTGCA
GGAAGATGAGACCGACCCACAAATCGCATCAAAAGTTTTCCAAGAATTTCATCTCCGATGCATAAATCAACTATTGTCCCTGC
ACCACAGACATGGCCATTGTTTGATTAAGAAAATCTTTTCCATTTAATCCAAACACAACGAGCTGGTTGAGAAGGAGGAGCCA
GCTGGAACAATGGGAATTGAATTTTATGCTTTACAAGATTTTATTGCGACTTTTCGACTCGACGCCTCAGCTCGATTCCCAGCT
CCCCAATCATGCACTTCGCTCTGAAAACGAAAGCGAAAACGAATCGCAGTCCGCCTTTATTAGCAGCAAATTTCATTATTCAA
GTCAATTTGCCTCGGAGATGCCTCGAAAACTTGCTCGATAGTGACCCCCCACTTGGCTGGGCTCTTTGCATGGGTTCAATTG
AATTAAATGCAATCAATTTGTTGATACGCAGATGAATTTAAACAAATTTAGCCCGAGAGTGTGCGGCGAGCGAGGCCAGCTGG
ATGACTCAGCCGCTTTCGTTGTCCGGAGCCCAGGGTCCCATGTCCCATCGGTTAGTCACTCCGGCGGGGCAAACGACACC
CAAGTGCCGTCCAAGGCTCTGGACATGCAATCAGAGTTGCCCCAAGCCCCTTTCTGCTCCCTCGGATCCTCTGGTAACTAC
AAAAAAAAAAAAAAAAAAAAAAAACGAAGCACAAGATAGACTAAAAGGGAGTCCTGTGTACAACCTCTAATTATCTCAAGCCAT
GACATGAAGTCATTTCTCCCATATACCCATGTATCCTATTAATGCCAGCGCTCACGCTGAAATTGAAACTTCAAATATTTGTGCG
CGGCTCAAGGACTCGCCGTACTCGCCGGTAGGACTCGGCCATGTGTGTGTAATTTCCTTAATAACCGCCAGCCTATCGCATT
AACATATCTCGCATTTGTCATAAAAATAAGTCAACCACCGGCACCACCCACCCACCAACGTATAACCACTCACAAAATGGCCC
AGCTGGTCTCCGCGGAGGAGGCGTTTTGTCAAGGAAAACTATAACCCCCCTCCCCCCCACCACAACATCACGTGGGCGGA

AGGTGGAATGCGAAGGAAGGAAGTGTTTATGCCTGCTCATGTGCGTCTCGTAATGACTCCCGGCTAAATGGACACATTACGC
GGCGGACACACGAAAAATTGAATTATTTAAGCAAGTTTTTGGAGGCGTCCGCATTTGAAGCCAAACGATGTTGCGTGTCAAA
GTTCATACCTTACTCTAATTCCCAAGCTCAGCTCCACACCCACTTCTTGAACGGGACTAAGAAATACGTTACAAAAGCCAGTG
GCAGCCGGCCCAGAAAATAAGCTGGAAAAACCTAGATGGTGTGAGTGCAGCGAATGCCTTAAAGTTCCACTTGGTGACTTTT
GAGACGCCGTTTACGCTCTATGCTCATACAGCACACGTCAGACCCAGGACACAGCCCAAAAACCCATACACCCATCGTAGTC
ACTGAAAAGGAAAAAACCCTGAACCCTAAGGAAATGTAACGGCCGACGATCGACGACAGTTGGTTTCCCAGAGCGTCTTCA
AGACGATCGAGGGGGTGACTTATGCGGAAAAGGCACCCGACATCTGCCAGCTGGACGGGTAGGCAGCGGATCTACCTCTG
ATTGCAACGTTAATAATGCACCGACAGAGGGTTACTGCCACGCACCAAAGCGGATGTTAAGGGGGAAATCAGTGTGGGGAG
GCACTGCTACGTGGAACTTTCATCGCTTGGCGGGACTGTACTCAAATTAGTTAGGGAGCGAGTGCAAAAAGCACTTACGATT
AAGAGCCGGAGGAGCAGGAGCTGTGTGCGGGTGGAGATGGATGGGGCAAGTATCATTTGGCTAACGCTTGAAATTGGCTT
CGTGACGCTTATCGCGATCAATAAATAATATACGAGCAGCTCTAGACAGAGACGGGTAGCAACGGATAGATAGATACACGAAC
GACATCGAGGCGGAAAACAAAAAGTATCTGCCAGATACATTTGAGTAATTTGCGTCGTTAGTGCCGGAAAGAGAGGCAAAAT
AATAATAATAAAAGAAAGTACGCTTGATTACAATGAAAATGTTTTTAATGCCCAAGCTCCTCTCTTCCCTCCTCACCACCCACTA
TACACCCACACACAGAGACAGAGAAAGATATCTGCATAGATAGGCGAAGCAAAAGGACACACGTTAGGCATGCATTTTTCCC
CCATTTTCCTTTCTTTTTTGTCGATATCAAAAGCGCGATAAGCACTAGACACGAATGTGGGCAAGTGGGCTGGAGTGGCAGG
GAGTGGGTGGCAGGTGCAGGTGCAGGCTTGCAGGTTGGACAAAAGCCCGACGGCGGGCGGCAGACGGATGTGGAAAAG
CCTCAAAGTCGAACGCGACCAGCGACAACGACCACTGTCCAAACAAAAGTCGGAAAAATGAGCAATGGGAGCCGACTTGG
CCACATATGGCCATTTTCTGGCCATTTCCATTGCGTGCCTGGTCGGAATACTAGTATACGTATCCGTATCTGTATCTCGCCGTG
CTCGTGTCCATATCCGTAGTATCCTAGGCTGCAATGTACGGCAGTGTGTGCTATCTAATCAAGCGCCGAAAGACAATAAAAGC
CAACAACGCAGCCACGACAAACAGCGACCACAAAATGTGCTTATGTCTGAAAATAACAGCAGGACAAGACCATCAAGTTTCG
TGGAGACCAATAGGATACCCAGGAATATCTGGAGTTGTCCGTGAAATATGAACCCATATTTGAATTTGGTATGATTTGAGCTCT
TTTTATGAATAAGTTTCAGAGTTTAGATTTGCCAAGTACAATTACCCAAATGGAACCATAATTTCAATATTTTTCGATTGCGACCA
ATTCATGTCCAACCACATCCTTAACCTAATTGAAAGTATCCCGTTTAACCAAAAATCACGGAGAATTCCGGGCAACCTACTTCT
GTGCGGCTAAGTGCAGCGGGAAAACCTTGCCGGGCAGCACTCGAAAGTATCGCACGGATGTCGTATCTATGGACCGCCATA
TGGCGAGCAAACGGCGATATCTGTGAGAGTGTTTCCATGTACGAGTGACTGTATCTTATCTGGCAGTTGGGGTATTAGCCAA
GAAGCGTGCACCCCATACTCCAGCTCTGGGCTTCGAAATCCAGCAGTGGCCATAACAATAACTGAGACTGGGCTGACATCAT
AATAATTCGAGTTAACTGCATCGCCATCCCGACCGAGAGACCTTTTGGCAAGTTCGGAGGAAACTTTTCGCATAAAATCCCTG
TTGGAGACAGCGCACTGGAGAAGGCAGAGAAGGACATTTTCTTTTAGCACAATTCGCTTCACAAAGTTGCTGCCAATTCTGG
TGGAAACTACTGCCAACAAACTTTGCAGCAACATAATTTTAATGGTCTTGTGGCTGGATTAGAGCTAGCAAGCTGCAACTGCA
TTGCCAATGAATGCCAAAACAAGTTGAAAGGTGTTCCTGAACTTTATTGATGTCGTCGGGCGACTTCGGGCGACTTCCGCAC
CACCCGTTAGACAAATGGGTAATGCTATCAGGTAAAAATCGGTTCCCGACTGGATGAATGTCAAATGCCACCACCACCAGCA
CGCCCCTCGGTTCCGTCTGCCTGGGCTCGCTTCTTCGCCTCCTCGATTCCTTCTGCCTCTGCCCCTGCTCCTCATCATCGT
CCTCCGCCTCCTCCTCCACCTCCTCCCTTCAGCGATCCCCAGCGTGTGCGCACGCGCATTGAGGCATAGACGAGCGAGTC
CAGGTGTGCTCTGATCATCGTCCGCCGCTCGTGGCTTCAAGTACGTGCCATAAACACAGTCCGCACACTCAAAAAAAAAAAT
TGTTGAAAATGTTGAAAGTCTCATCATTATGAAAAACCCATATCTAACCCGTCTGAAAATATAAAACTTCTGTGTAAACTTACATT
AATTTACATTAATTTTAGGATATGCAGTAAATGAATATGTTAATCAAGCTTACTTTTTAAACTTTTTCATTTTTCAATAGTTGTATAA
CCCTTAAAATTAATA

pros UTR-long 5’ end - Quasar 570

GCATTTAGATTAAGTACAGCAGCAGGAAACCAGACGAGAACCGGAAATGGACGATGGACATCCATCCGGACGAAGCAA
CCAATCAGCGACCCGTGTGGCCAGTGCTGGTCAACAGACCAACATCGAGTTCACCGCACAGAAAATCCAAACTTAAACCATT
AATGCACACTGCACGCAAACCGATAACGAAAACAAATCGATCAAATGATCGAGGCAGACGATGGGAAGCGAGATCGAGATG
GAAGGCGAGATAAGTATATACCTACTACACGTAAACCAATTACCAAATATAAAAGCAGATGCAGCCATATGCAATTTTAACTAGA
TTTTAAAAGCATTAATACCGCAGAATACCAAGCAAACCAAAAGAAAATTACCCCAAAACATACCGATTACTGATTACTGAATGAA
AAACAAAACCGATAACAGAAATTGATCAGATTTGTACATAGCGACATTTAAATACAACTACGTACACGTAATTAAAATATTACTAC
AGTCTAAGCATAAGCGACCCCCAAAGAACCCACTCAGAGCCCCTGAAAAGGACATTCTGGCCAAGGCCAGGACGATATTCA
CTCACAGCCTTACTGCATTGAAAATGCTCGCATTGCGATTACCATTAGGAGGGAAGAACGAAGGGAAGAAGGAGTAGGGGAT
TGAGATAGGAGATGTGCCAAAACCAAATCGGTATATATATCAAGCAGATCCCCTTTGGCAAGCCCACACACGCACAAAACACT
GAAAAGAAAATCAGTCAAACTAAACACGTAGGGTACATACTCCATGGTAAATCAAAGCAAATCTATTCGTAACTTCAACTTCAG
AGTAACCATAAGTTAATTAAACATCCTTGGTTTGGAAAACATCTGATCACAAGACAGAAAGGACGAAGTAAAATAAAATACACAT
AAATTTGCAGTTTTGGTATACATGAAAATGAAAAATGAAACGAAAAATCTTTTTAACGATGAAATATTTCCAAAAAAAAAAGGAA
ACAATTGCGTTTTTTTTAGTAGCAAGCGCGATTCTCAAAATTCCCAATAACTTTTGGCCAAAAATCGAGTCACCGAACAATAAAC
AAAAACCGTTTGGATGTAACATTTTTATCACTTATTTGGCGTAGGAAGAATCAGAGAGAAGAGTGTAGAAGAGGAGTGTATGA
AGATTAAGCCGTGGCGCATCCAAATGCACCACATCTTTCTTTAAAACAAACTGCAATAGAGCAGCACACAGTGCGTATACTTT
CGGCATGCACTGTGTGCCTGCACCAATGGACTTAGTTAAACAATCAAAATTCCTGCAATCATTGCAACAGCAACCAGTATTAC
TAACATTTTTCAGTTGATCAATCAGGAATCAATTTACGCATCCTTATTTGTGAAGTTTATGAAGAAGAGGTTAAAACTTTTGGCT
TATGACGTAAACCCAACTTTTCGGCCGCAATGAACATTGCCCATGGAAATTCTAAATTCGAATTGATATATATACAACAACATCA
AAAAGCACATGAGAAAGTATAAAAATATAAAGAAAATGTTGCATAAACCCCTAAACAAAAACGATAACCAAA\

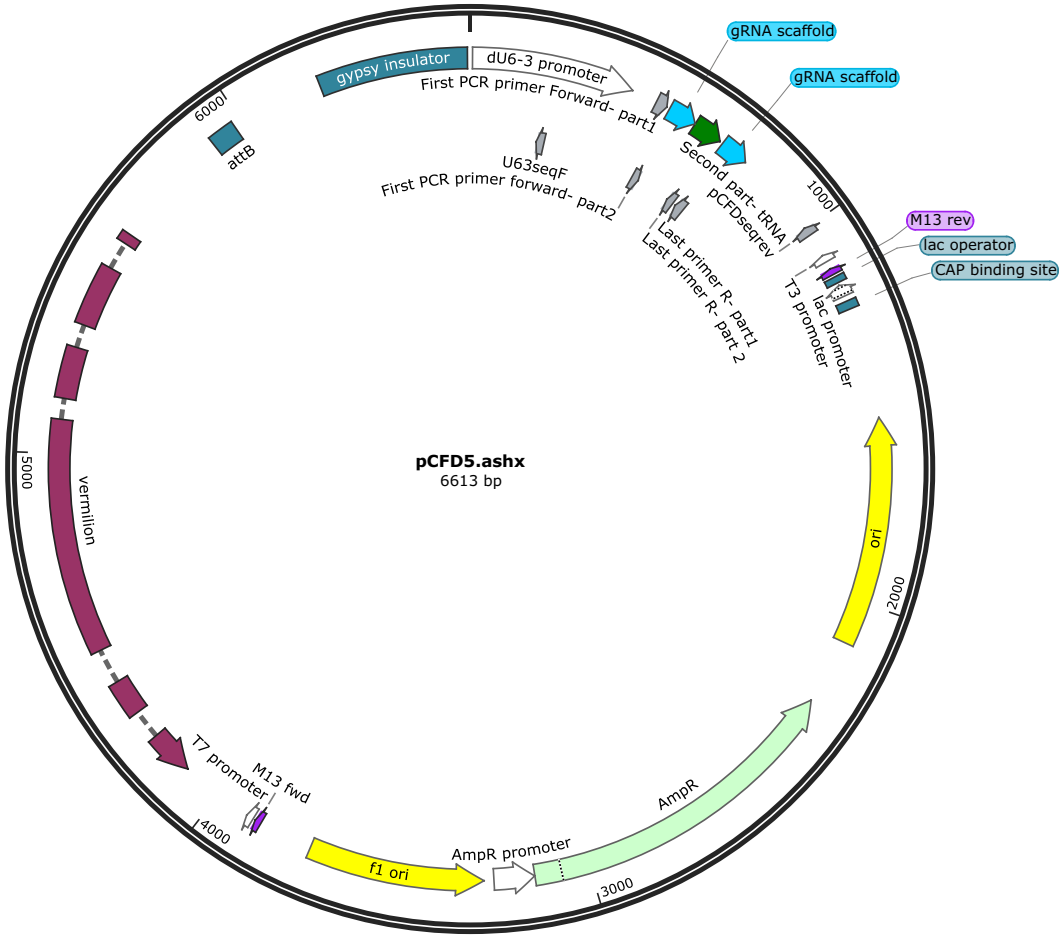
pros UTR-long 3’ end - Quasar 670

ACATCCAAAGAGATCCATTGGGATTTGTGCACCGGGCCAAGGAGTGGGCAGTTCTCAAGCCTCGAAAATAAACCCAAACTG
CCCGGCCCAGTGGCCAGAACATCGGCATTGTTATGGGTCGGGCAACTCCAGGACATCCAGATCCGTTTCGCACCATAGCAC
TCAAGGCAATACAAACAACCGGCGGCTAGAGAGAAGCAAAATGAAAAGAAAAGCAGAAGACAAGGCAAAGGACAAGTTTCG
AACCAAGGATTTCGGTAACATTTCGAACGCAACTTTCGGCAGAGTTTCGAACAACTTTGGATTAGGCTTTTGTTGTTAATTTGT
TTTTTTGCGACCACGTCTCCATAGCACTCGAGCAACATGCAATATGCAACAGCAACATGCAACAGCAACACACAACACAAGC
AGCAAGCAGCAAGCGGCAACGTGATACACGAGTTGAGCAAGTGAAAAGCAATTTTTGAAATGGGGCCACAACGTCCGATCT

AAAGTGCCTTCAAGTAACAATGAAAACAAAAGAAAACAAAAAGAAAATACCAAAACTAAAAACTGTTAATTTTTTATGTAACTAA
AACCAACGCGGAGGATGAAATTATAACACAAAAATTGTATAAAGAAATTAAACGTGTAAAAAGTATAAAAATTTAAACAAAAACT
AAGCGATGACGATGGTGAACGCGAAAGCGGAAACGTAAACGTAGAGAAAGGGCTCCAAATAGACCGGAAATTAAGCAAAAA
CCATAACTGCTTCATTCTTTGGCCTGGTCACACCGTCTCTCCGAAGGAACTCACGCATATGGGCTAAAAATGCAAAGGAAAAT
CGATCGCAAATCTCTTAGAAGCCATCTTAAACATTTACTTTCGCATCCTTCCCTAGCAAAAAGTTGTAATTGACTACCTAATTAA
GCGGAAAAAATATGTATGTATTTAGTTTTAGTATGTAAGCGAATGGAAATTCACATAAAACTCGATTTAGACGAACATAATGTATG
GGAAAATTAATTATTTAGACTAGCGAAAGCAGCAACAAAGGTTTGGATATAGACACCCCGAGTATACCCCCTATACCCCATACC
CCATACATACGCCTATAGCGCTGAGTTGCTCATCTATCAATGTACTTAAAACCACAAGAACACAGCCACACTGACACTTGCATG
TACTATGCTACATTTAATTTAGATTTAGATGCGAATAACTAAGTATTCAACTCAAAGTTATTCGAAGAACGATACGAGATGAACTG
CGAACGGCATACTGAAGAGGTGGCAATTAGATATAGAGCGAACTATATTTAAGGACTCGGAACTAGCGACTCTCAGAAAATGA
AAATGAAACGCGAGTGCGCAGCGACACAGGATCGCAGATAAACTATAAGACTTTCCAGAAACGAAGGGGGAAACCTGTCGT
TTCCCACTTTTGTGCTTTTTCCTACCCCTGACACACACACTGCAGACATACACCTACCGTAGATCTTGAGTTGGCAGCATCGT
AATCGTTTTTTTAGTCGACGATGGGAAAGAACTAGCAAAAATTAGCAAAATTTAAAATTGATTATGTGACACACAACACACCTTC
CACACACTCACACACACACAGATACTCCATGTATATAAGTATGTATATTCCTTTGAGCTGAACATTGTATAACCGAACGATTACG
ATACCACAAACAAACACAGCGACACAACGACCTTAGCCATCAGAATACAAGGACACACCGAGGTGTGTAAAGGGTTCTTTGC
TTACAACTTTTCAAACGAATTAAACCGTTTCGGCCAACCTTTAGGATTGACAAAAGATCGACTTGAGGAACACAGCCCCGCCC
ACTCTGCTCCGAAATTCAATGAGCGGGGGGGCGGGAGAATGCATCGTTTCGGTTGATGGATGCA

C. CRISPR/Cas9 Deletions

C.1 pCFD5 (guide cloning)



C.2 pDsRED-attP vector 51019 (homology template cloning)

pDsRed-attP was a gift from Melissa Harrison & Kate O'Connor-Giles & Jill Wildonger (Addgene plasmid # 51019 ; http://n2t.net/addgene:51019 ; RRID:Addgene_51019)

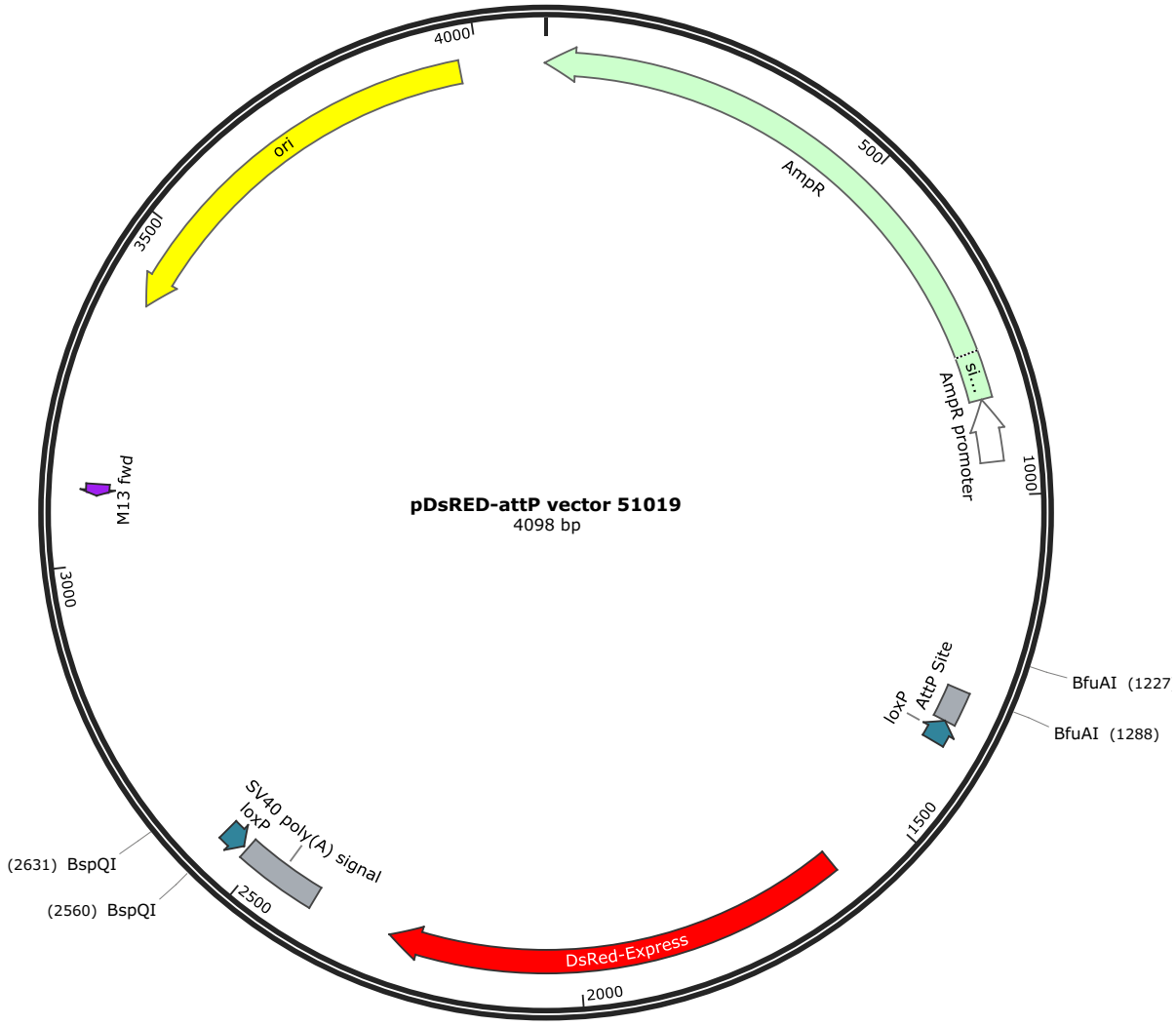


Table C.3 gRNAs

***pros* deletion lines**	**gRNA**
pros-longSTOP	GTGTGACCGTTGCTGCTCGG_CGG
***prosΔpromUP* (upstream)**	TTCCTACTAACTCATGCACA_TGG
***prosΔpromUP* (downstream)**	GTTGGGCTACTAGAACTACA_AGG
***prosΔUTR* (upstream)**	TTTAGTGAGATGTGTGAAGG_TGG
***prosΔUTR* (downstream)**	ACTAAAAATGTGTAATGGAA_TGG

***myc* UTR deletion lines**	**gRNAs**		
Full deletion upstream	ATACTATCGGCTTAAAG CGG_CGG	ATAGTGTTGTCTCATAC TAT_CGG	CTCATACTATCGGCTTA AAG_CGG
Extension deletion upstream	ACGATGATTTAATTCGA CCT_TGG	GTTAATAAACTAGCGAA CCA_AGG	
Imp binding upstream	AATTTGAATGAGATCG GGGG_AGG	GACCAGAATTTGAATG AGATCGG	CAGAATTTGAATGAGAT CGG_GGG
Imp binding downstream	TTGTGCCAATTGAAAG ATCT_GGG	AGCTTCCCAGATCTTT CAAT_TGG	CTTGTGCCAATTGAAA GATC_TGG
Full deletion downstream	TATCAGCCGTTGATTAA CCG_AGG	TTGTTAAATTCTGCCTG CCT_CGG	AGCCGTTGATTAACCG AGGC_AGG

C.4 Deleted sequence

pros-longSTOP

Deleted sequence: TCAACACCAGCAACCACCGCCGAGCA

prosΔpromUP

Deleted sequence:

GCATGAGTTAGTAGGAATTTATGCTGGCTCTATTATTGTTGCTCTTGTTGTCGCGGATCCTTTTTGGCGGGGTATGAGTGCGG
ACGACGCTCTACATTTTTTTCAGCTGCAGTTTTCTTTGCTGGATATTTTAATGCCAACTCTGACGATATACCAATACCAGTGCCA
ATAACCAACACCCATAAATGGCGGCAAAATAAAATAGGAAAAAAATGTGTGTTGCATTCGCGCAGGGGCAACATAGAAAACTT
TTACGTTTCGCTTAGGGTTTTGCTTTATTTTTTGCTTTCAGGTTTCCCTCTTCTTTTTTTGCGATTTTCATTTTGTTGCTTTGGCA
TTGCAAATGAAAACGAAAAAATTGCATTTTCCCCGCATATGGATGTGTGTGAGAAGCACGAAATCAAAACAAAACATGGCCAC
ATGGCGGGTCCTGTCGGCTGGTGGGTGTGCGGATGGGATGTATGGATGCATGGACGGATGGGGCACATGAACAGTGCACA
GCCAGGAGCAACAGCTCCCACAGCTGCCACACTACCTCCCTGCAGATGTATCTGTATCTGCGAAATGGTATGGTCCATCTGG
CGGGAAAAGGGGCTGGGTTTTAGGTACACTTAGGCTCGATAGCTGCAGTTTTTCGCCACCCAGTCAGCGAAACAGACCACC
ACGCAGTTGCCCAGTCCAAAAACCACCTCATCAGTCGTTTGGGGGTTTGGGTGTTCCATACTTTTTGGCGTTGTTTGATTTTT
AGGCGCAGCAAAATGCGTTTTGCTCTTGATTGAAAGTGTGAAGAGTGTGGGGCAGCATGCCAGCGTGTGTGTGTGCGATAT
GTGCATTGTCCGTGTCCTTCTCGCAGTGTGCATGTATTGGCGAGGACGCCGCTGCCGCTGTCGTCGCGCTTTGTTTTGATTT
TTCGCGACTGAGCGCGCGTTGCTGTCTGTTTCTCTCTGTGTTTTTGGATTTGTCCAGCAATGCATATGTGCGCCCACTGTTCT
AGTGGGTGTGTGTGTGTGTTTGTGGTTGTGTGCGAGGTTTGCATGTATATGTACACTAGCAGCTAGGAGCGGCGCTGACGT
CGCAGTCGCAGCAATTTTTTGCGCCAAAGCCAAACCAAAAAGGACGAGGACAATTCGGTTGGCGCTGCAGCTGCGACGTA
GCCGCGGAATTTTTTTGCGCGTTTCGCGCCCGGCCAGCGGCCACTTTCATCCGTATCCACGTATCCAAGTATCCACATCCGC
ATCATCCTACTCCATCAGCGTTAGCATCAGCGGCCGAGGGGCTGGCGTCCCTCATAATCAACGCGCTGCAGCGACGACGCC
ATCGACATCGACAGCGGCTCTGGCTTTGGCTTTGGCTCTGTGACTCTGGGGCCCGTCATCGTTAGCAATTTTTGCCAGGACA
TTGCAACAGAAAACTGCTAAACGCGAAACAAGTTGCGGCGCTTTTTTCTGCTCCTCGGGTTCTCGCTGTCTCCCTGTCCTG
GCCTGTCCTGAATCGAACTGAGCCGTGCTGCCAGGATCAGGCAGCAGCAGGCAGCAGACAGCAGGCAAGGCACATCAGTA
GGCAGTGCAAGGCAGGCAGGCAGGCAGTCGGCAGGCAGGTCGCCACTTCTCGCAGACTTCTTCGCATCTGCATAAATCAA
ACCCAGAGGCAGTAGCAGAAGCAGTTAGCCACCCCAAGAAAAAACTCTACAACAGAAAAATACCGAAAAACAAAAGAAAAAC
AAACAAACAAATAGAAATAGAAAAGAGAGACATCGAAGCAGAGAAACGATAGGAGAACGAAAAAAAGTGCCAAGTGAATGTG

AAAGTGAAAGTGTGTGCAAAATGACTTGAAGTGCAAGACTAGACACCTATGTACGTACCACCTACACCACCCAGCCTGGAAC
ACACTACGTATACGCAATGCGGCCCAGGCGCTCATACGCCCCGTTGGCCCGCCAGCCCTTCGAACTAAGACTCGGGCTGG
GGCTCGAACAGCCATCGCTCGCCATGCCGTCTTGAGTGCAAAAAATTACCCGCCAAAAACCCAAAAACACACACGGCCGGC
TTGCGCCAAAGACAATGTAAGCGCCGGCACTAGAATGTAGAGCAGTTTTTTCTTCATTTCCCAAAACTAACTAACAAAACCAG
CCAGCCAACAACAAATAACAAAATAGACAAAGTTACATTTTTACCAATATCGATAATATTAATCACTTGATAATCAGCGCCAGTCA
AACGCAACATTTCGTTCGTAAACAACAACTACAACTAGCCACAACAAAGCAAGTCAAAGCCAAGAAGCAACCAAATAAGCAG
GCAATACCAGTCAGTCCGTAACGTCAGCAGCAGAAACCAACGAAAAACCAAAATAATAAAGTAAAACGATTGAGTAACTCCAG
TTTCAGTACCGCACCGATTCCGATTTGAGCAAAAATTCAAGCGTCTGAATTTGATTTCGATATCGTCTGGCCCGTTCCGTCTT
CAAGTCTCGGCCAAAGGTTCGTCATCGTCCCGACACACTCTCAGTTTCTACAAATTCAGACGTAGATCCTTAGTTAATTCACC
TTTTGTATTGTGCATTTCGGCAAGCAAATATTTTGGAAAGGATCCCCAGAGAACAAAAAAAAAAAAAAGGCGAAGAAGAGCAGA
AGTCAACACTCGAAATCGAAAACTACGAAATTACCTGAAAATTTTTAAACAACCAAAAAGTCTATGAATGCAACAAAAATTACAC
GCTAAATTTTACAAGTGCAAAATTTTCTTATAATAATTTATCAAAAAAATAAAAATAAATTTACAAAAAAAAAAAAAAATTAAAAAAGA
AGCATAAAAAAACGGAACTTAGTGAGAAAATTAATCAAAGTTTAGAGAGAACATTAAATGCAAACGGAATATCAAAAATTGTTGT
GATGTGATATTTTTTCGATGTACTTTTATTTGAGGGTAAGTAAAGATCACTATCAAAAATTCATTTTTCAACCATTACTCCATTCTT
TTCATCAATCATTGACTCATTGGGGTTTATTTATCTTTTCAGAATTATAGAATTTAGATAGAGAAATAAGGGAAATAAATACATTCG
AAGCGTATATTTTAAGATCTAGGTAATTTAAAGATGTTCTGATTAAGAAAAGTATCTATTATGGGATGCTTGATCATAAGAAAATG
ATTAACAGTGAGCATTTAACTACTGATCATTTTTGGAAGAGAACGAGAAGAGAACGACATTTAAGACAAATAGTAAATGGATAAT
ATGAGTGTGAAACATTGAGCAGTATTGATTTTCATTAGAAAAATTAGGAAAAGGTTCATTCTTTAATTATAATGTTATCATCTAAG
TTAAAATCAATTCAAAGATATACTCTTTTTAAGGCACAAAATCTATTTCACCAACGAAAGAAAGCAGGGCAGTCAAATTTTAGTA
ACTTAGCTAAACAGCATGTTTATTTCAAAGCGCCAAAATAATAACCATATTAATTGCTACAAGTAAATATTTAAGAGGAAATGTCT
CCTTTGGAGTTCCTTAGTTCAGTGGGTCTGAAGATCGCAGAAGTCTTTCTCCGCGATTGAGCTCGGCACTTCCTCCCAAAGT
TCTTCGTGTCCTGTCGTCGGGTGACGGCGTTCAGCTGCAGCAGCAACATGCAACAGCATCGTGTTGCTGGTGTGCACGCG
GCTCTCCCCAGCAGCAGCAGGTTTAGTTGTAGTTGTAGACTTTTTGCTTTTCTACATCCTCACACACATACAGGCACACAAAC
GCACACAGCAACAAACACGAGTGCAAGACGCGAAGTTTTGGAGGCATGCACATAATGTAAACAAGGACATGCGCAATGCAC
CGCGCTGGCTTTCCCCGCTTCCACAACAGGAGAAGTGCATTGCAGGCAATGCAATTGCCAACTAGAAGATAGCAGCAGCCA
AAGGGGCAGTGGGTGGCTGGGCAGGATTTTGGTCGCTTTTGGGGGGGGGGGGGGTGTGGTATTGGCGATGGGGTGTTGC
TGGGTGGCTGCTTCATTTACCAACGGCTGCACTAGTAAATAGCAGATGGCAGCGAAGTCGGCGTCGGCATCGCTGTCGACG
CCAACTTGCCACAGTTTAGATGGGAAAAAAGGAAAACTCCAAAGAGCCAGAGAGAAAGACAGAGTGAGGGAGAGAGAGCG
AGCGAGAGTGGGTGAGAAAGAGAGAGCGAGGGCTGCGCAACGAGAGTGGCGAGTGCAGCCGAAAGGATGCAATGCTGCA
AGGCAATTGCACTCCAGGACTCTCACACACACACTTACGCACACAAACGCATCCGCAAGCAGCTAGACTGAGGCGGTTGCT
TCTTTTTTGGTTGTGTTGTCTCTTTTCGGCTTATTTTTAGAAGTCCTTTGCCCCCTCGCCGGCGCACATCCCACCCCAGCCCC
CTTGGCTGCATTTTATTTACTTGACCAGGCCTCGGAAATTTACATGGCCAGCCGTGGGAGGGGGTTGCAGTATCCACAGCAG
TAGCAGCAGCTGTTCCTGGAGCCCCAGCACGTGCAGCAAGCAACTGCCCTTCAGCCGCCCAGCCGCCCAGCCACCCAGC
CACCCAGCTGCCTGCGTGATTTGTGCGTTGCCAGGATGCTGATGCTGATGATGATGGCGATGGCGATGATGAGGCATCTCG
TAATGATCTGGGGCCGGGAAAAAAGGGAGCAGGAGGCGGTGGTGCAGCTGCATTTCCTTGCCAGCAACGCCGTGCGTGGT
TGGTCGGCTCGAAAAAGGGTCGGCGGCACTGATGGGGGTTGGGCTGTGATGGGCTGGCTGGATGGATCGAAGTGTGGGC
GCGTAGACATTGCGTAGAGTTGGAGCCAATTTTTTTCTATTTCTTGATGGGCAACCTGGTCCGACCGCCTACATCACCCATTC
CACCGCCCCCTTTTTGGACCGCGCTTCATTCGCACATCGAGTGGTCAAAGTACATAGATACCCCATGCCCATGTGTCATGTG
TGTGTGTGTGTGCTTTTTGCGCGCGCGAACTTTGGCCAAAGGAAAAAAACTTAAACAGAGATGCTTTTACATACGGAGGGGG
GGTTTTTTCGGATGGCTCGCTGCATTTTGCGCGTCTGTAGCTTTTTTTGGCGGCCGTCGATGATGGGGTGCGAAGGGTTGG
GGCGCGTGGTGTGTTCCCCGGCCTGGTGGAGGCCATGTACGCGTCGTCGTTTGCTAAAGTCCGTGTCCGTGTCGCGATGA
CGGAACGCCGAACGAACTGAACGCAACGCAACGCAACGCATCGCATCGCATCTATCGGCATCGGAAGGCATCGGCCGGGC
ACCGCAGTTGGCATACGGCTTTTGGACGTCTTTTGAGTAGAACATTGCTTTTTTATATTCTCGGCTCGACGCACCGCACCGAG
CAAAAGAAGTAACGCCAACGCCGCGTAACGATAGCTGCCGCTCCAGCGAGGAGCCGCAGAGTTGGTCCAAGTCGTCGACG
GTTCGGTTCAGTTTCGGACTTGCTTATTTTCTAAAAAATCCAGCAACCAGCAACTAGCACACACACACGCCGTCGAGTGGAG
TGGCGTGGAGTGAGGCCGCATTATTATATATAAAATATATATATTGCATATATATATACGGTATAGAATATAGATATATATATATAAAT
GGGTGCAAAGTGCGCGCGCGTTTGCCGCCCCCAAGTCAACCGCCCATGCCTCTCAATCCGCTGAGGGGCTGAGGTTCAGT
TGCAGTTCGAGTGCCGTCAAATACTATTTATATACAATAAATGAAATAAAATATATACAAATATATATAAATATATATATATATGTCT
AAAAATATATGTATCCGGTCGCGAGTATCCTTTCGTGTGCGTTCGTGTGTGTGCGTGTGTGTGTGTGCGTCAGCGGGTGTGT
GTTACAATAACAGCTTCGATTGAAAGCAAACAACGAAATTCTAATGCAATCATCTGATTTTTTTGACATATCCAATTGATTATTAA
ACACTCCGCCGCTGCCCCCATAAAGACCAAAATTTAAAACGCTCCATTAAACCAAAACGTTTTGCTGACATCTTGAACCCAAA
GATCCAGCCTCGATTGAAACAGTCCAGTCAACGGCGTCCACTCGTCTGCGTCGTCGTCTGCTGGCATCTAACTTCAGAAAA
CCAAAATTCATAAGATGCTAGTCCCAAGAGAACTGAATCATCCCATGATCGAGATGCTATTTAACTATTAATATTTGCAACGGGA
AACCCGCAAAAAGTCCACTGACTGACCTCTCATGTTTGCACACACTCTGATCCTGGTGCAATCCGACCGATACTGCAAGGCA
CTGCAACCGTTCGAAAAGCCGCCAGATTTTCATAGCGATCCTCTGGAGCGGCTGTCTCAGCTTTTCCGGCTGGACTTGTCG
CACCGTTACGCGTTCCCGGCGACGGCGACGCAGACAACGATGCTAGAGTGGCCAACGAACTGCCCTACAGGACTCACCAG
GATCCTTGGGATCAGCCAGGTCATAGCCGTGGACACGAGAGAAAATCTGAACACCGTCATGGATAAATAACATCAGTAAATTG
TCCTGTACGTGATCGAAAATCGCACATGTCCCATGCTAAAAACCCCCAATGCACTTGACCATCATAATATCATATATCATTCATA
TGTAGTTAGTTCATAGTGTGATATTCATTTATATTTTCAATTAGACGCTGAGTATAACCAACATTTGAGATTATGTTATGAATTTGA
ATCCCCTCAAAACATAACAAACTTGTTGTGTATAAAAACGTTTTATTCTGAAGGACATTAAATTTAGTGTTATAAAATGTCAAAAT
TAAGGACATTCTTTTAAGCTCAAAATTATTTTATATTGGGTGTGGAAAATTTAAAAATGAAAATATTCTTCCATATTTTCTTAATAGA
TAGATTCAAGTTAGATATTCATATTCATTTCATAGCTTTAACTATTATTTTCATTTTCTCTCCCGTTCTCAACCGCTTTGTTCCCAT
AAGCTGAACTACTTGTTAGCTTCATTTGAGTATCTCTCTAGCTTTAGCACGTGTTAGCTCGCTTAAACATAAAAAGACTATATTA
AAATGGGGGCAAATGTGTAGCAAGTCGAGTTATTAAATGACACAAGCTTAGAGTCCTTTCCCCAGCGAAAGTACCGACGGCA
ACTCTGAGTGGTTTCTTGTCAGCAATCTGAAAGTAGGGTTCAGATTTTCGAGTATCTTGTGGAATGCATTTTGAACATTGGGG
AATCTTCAGTAGAGGAGAATGTTCTGAGAAAGTCATTTTAGACGTGTGGGAGGGATGCTCTTTTTGCCATTCTCCCCTCACTA
ACACCGGCCTAACCAGGCTCACACACACATTCACACAACACACCCCCTGCCCATTCTCCATTTTGTTAAGCTGCCCCAACTG
GCAGCGACGTCGACGTTGGCAGCGCTGCTTGCCCCTCCATGAACGAGTATTTGAAATGCGCACTAGCTCTAGCTCAAATGG
CTTATGTGTCTGTGTGGGCTCCCCTCCGTTGTGGCGTTGTGTGCGTGTGTGGGAGAGTATCCGGCTTCGGGTGGGTGGGC

AATTCAGGAAGTCCTGGCAGCGCTGCCGCTGATTTTATTTGCAAAGCCCCACTGTGTGTGTTTTTGCCGTTGCCTTTGGCTT
TGCAATGCCTCCCTGGGATATATCCTCCTCCCCCCGGACATTCGCGTATTTTTTCGCGGCTGCGGCGGGCAAACATTTTTTG
CTGCCAATACACATACTAGCGCACTCACACCCATACACACACACACACACACACACACTGGCTGGGGCAGAGAGCCGCGGC
AACGACAACGCAACGACAACGACACCGTCAGCGGTCGTCCTCGGCCTATTCGCGGCGAAATAATTTTTCGCATTTTTAGTAC
AAAGCTTCACATCAACGTCGTCGTACAAACAAATTTTTATTTTCGGATTTTTCAATTACGTTTTCATTTATTTTTAAGTATTAAGTT
TGCGTGCACTCAAAAAAAAAAAAAAAAACCAAAAACAAAAAGCAACTAAATCAGCAACTAAAACTCGAACAAAATCATAAGGA
AATTCATATCCAGAAAACAGTTGATAGATCGTGTGTCCAAACATCGAAATCAAAAGCAAAAAAGCAAAAAGGAAACTCATTCAG
ACCAAAAAGAATCGAACCACATTTACCGGCTTCCAAAAAACGATTCTCAAGTGTTTTTTCGCCGTATCTCCAAAAGTCTCGAC
TAAACTCTCAACCGGCAGGAACTCTCGACGATTCTCAGTTTGTTATATGTTTCAACTTGTTTGCCCTCCCACAACACAATATCA
TCAGTCCATTTTAGTTCTTTAAAATATCAAAAAACGAATAGCGAATGATATTTGAAAAGCAAAGATTACGAACAAAGTCGCGAAC
AAATTGAAAACAAAAAACAAAAAAACACTAGACGAACAAGGACACAAGTTACAAAATTCAAATGTAAAATCAAAAGTACAAAGC
AAAAAGATTGTTGGCAACATTTTTATAAGTATATATATACGTATTATTATGATTTGTATATATTTTTTATACGAACTCAAAACTACAGAG
TCCAAAACTCAATTTTGATACGCAGAATTGCTCATGTGATGCTCCGAATCCTCCGACGGGTAAGCAAATAGTGTGCGTTATCTT
CTCCCGATTAGAAGACGCTGGCGGCAGAGCGAAAGAGTAGGGGCGACAGAAAGAGAGGGAGAGAGAGTGAGAGAGAAGT
GAAGAGAAAGGGGCTCTATTCTCGGACTTCTCCTTTCGAAAGTGTCTGAACCGGCAATACGAAGACTGCCAGCCGCAGGCT
TCGGGTCTTCGTGCCTTCGTGTCTGATTTTCGGCTGCTTCGTGTCCTGCTGCTTTCTAATTGCGTTCTCTCTCTGCCGGCGT
CTGTGTGCGTATGTCTGAGTGTGCCAGTGTGAGTGTGTGCGACTGTGAGTGCATTACATTATCCTGAGGCAGCGGCTACACC
TACACCTACGCAGCAGCTTCGGCATCCGACTTCCGATTCCGAATCCGCTCCGATTGCGACTCGGCAAGGACCTCAGCTTGC
TGCGGCCGCTGCCTGCCTGCTTCTTCTCTTCTAGTCCTTCTTAAGCTACGCGCGCGTACGGTCGTACCACCCGCCCGCCCG
CCGCTCATCCCGCTCATCGTCCCGTTCGTGGCCGCTCGTTTTGGCCATCGGCTCCTCCTTGGAGCGCTTCTTCGTGCAGGT
ATGCGTGCGATTGTGTGTGTGAGCAGGCGCACACTTACTTGCACTTACTGCGTGTAGGAAATTATCTGCTCCCTCTGTCGCT
GCCGGCGTCGCCTAATACATATATAAATAATATATATTATTATACGGGATATACATATATTTAAAAGCGACGACGCTCGTGTATATA
GAAAAGGCAGCTCGTTATCGCAGATGCCTGGATAAGGGATGCCAGGGAGTAGGGAGAAGGACCGCCTGCTTGCAAGAAAG
TGTAGCACACTTATGTGGGCAGGCGTTGACTGAAGCAGCAGCAATAGCAGCAATAGCAGCGGCGGCAGCTGAGACGGAAA
CGGAAACGGAGTCCGAATCCTCGACTTCGACTTCGACTGAGGCAGCGCCTTGGTCTTCTGCCACTTTACTTTCGCAGTCTA
GAATACAAAATTCAGTACGTTTCCAGTCACGCGCGCTGGCAGAAGTTTTGCTTGCGTATGTCTTCTATCGACGACGTCGACG
AACGCCGCCTCGAATTGTGTAAAAATTCCAATCGCTCCACATAAATTATTAAAATAAAATAATAATAAAATATTAACAAAACAAAA
AAAAAACCAAAAAAAAAAAAAAAGTGTAGCGTGCATTAGCTGTGTGTCTGAGTTGAAGCATCAATTCAAATCAGTTTCAAATCAA
TCAAATCTAATAAAATATATTTATTTTAAATAAAATAAATAATAAATTTAAATTAAATAAATAAATAAATTGCATTATCACATAAACTAG
AAATAACTATTTAAAGCCTAGTTCAGCCAGCTCAATCGTCTCGCCCATCGAACCCAGTCACAGATCCTCCTCAATTAGCTCAG
GTGTCGCTGTCTTGTGGTACGTGCAACTTGCGGCGCGTTTATTCGCTGCCTTCTTTCGCGATTAGCCAACCAAAGGGCCACA
CACACTCTCCACAGAATGTGTAAAAAAAAATCGAAAAAATACTAAACAAAAAAACCATCGAACACACCAACACACACGCAATG
GGGCGCCACTTGCTGCTGTTGCTGCGGCATTGGTGGCCACATTGCGCATACGACATGTTAGCCCGCAATTATCCTGCCTGC
GCATTGGCAGGCGTCGCGTCTTGGCTTTGATGGGGAAAAACTTGGCAGGAAATTATCTAAAGCTCCCAAGGCAGCCAGAGA
CTCAGATTCGCCGCAGCCCCGCTCAACTTAGTCAGCAACTCTTCACAGACACTCGCACTCACACACACATACCAACAAGCA
GGAGGCTATACTTATACTTATATAGTTGAGATACAGCGAGTCGTGTCTAATTTTATATAAATACTCTCACACAGACGCTGGCACA
CTCGGAGCCGAATATAAAAGCATTGGGGCTTCGTTTCTTGAAAGACATTTGATCGTCTTGGCTGGCAGCGACTGCAGCGCAG
CAAAAGCGGTCAGTTAGGAGGTGGTTTGTCCTTAGTCAGTTGGTCACTCAGCTGGGGAACAAGAACAGCGCAATCAGCATT
AGTCAGTAATCAGTTATCAGTTACCAGTTACCAGTTCAAGTCCACACTTTGATGATGGTACGTGCCAGGTTGGGGGATGATGA
GAGCCTCTCAGAAGGATGTTTTAAATAAATAACTCGCTAAAACCGTGACAAAGTGAGACGAAATTTTACGACTGTGAAAAAAA
AAACACAAATATATCAACTCGGAAAATAAATGTTGTGAATTCAAACAGTGCTACAAATAATACCAATAAATGACTAAATATGAAAT
AAATCAATTAAACATGTTTTAAAATTAAATAGATATTTGTATTATCTTTATATTTAATTTTAAGTTGTTACTTTCAGTAATGATCTTTA
CTGTCTCTTAAATTGTTTTATGTCTGTATTATTTTATGATGTTATTTACTGTGTAAAGATTTCTATATGTACTTCTTTAATACCATTTA
AAGAAAAAGAAAATTTCTGAGAATAATGGATTTTTATTCTATTATTTTTGTAATCTTCGAACTTAAATTTTAATAAATATATTATATTT
CTTCATGAACAGAATATCGAAATTTAGCTAAAAATAAAAACAAAGCCATAAAACAAAACACAAAAAAAGTCTTACAAAATAAATAA
GAAAGCAAAAATGATCGAAATTCTAAATTAAACTTGTAAAATCGAAAGCGCTGCGGCAACAAACCTTTGGAAAACCCTTTCGA
AAGAAACGAATAAAATAACTAATATATGCGAAATAACTACAACCAAATAACCGGAAATGCTCTGAAACAGTGAAAAGTGTGGCA
TAGTTTTCGGTGTGCCGCGAAATGAAGTGACAACAAAAGTAGCCAGCCGTGTGGCGGTGCCTTAAAAATAAAATGATAAATGA
TTCCGTTAGCGACTAAAGAAAAGTTACAAAAATTAGTGACCCCCGATGACCCCACTCCCCACGGCCCCCGTTGACCGCAGC
GCTAGAGTGAATTGTGTTCGCCTCTCCCCAAGTCCCAAACGAAATTTACCCCCTGAAAGCAAAAAGTCTGTGCACAGCGACT
CGGCCAGAGATATGAGTCGTCCTCATCCGAATTCCGAAATGCATCACCAGCGACCGGAGCGGTCAGCGGCCAACTCCCGC
CCGCTCCTGCTCCTGCTCCTGGCAGCGGTACAGTTCCGCTCATCGGGAGCGACTGGCGCTGCCGCCGCTCCTGCCGCCA
GCTGCCAACGCTGAACACACGGCCGCCATGAAGCGGTGCGATCCTCTGAAGCGGCTCGATTCGCACTTGCCACTCGCCAC
TGGCCACTGGCATTGTAACTTAAATTAAGGGTAAAATATCGCAAATGGTATTGGTGCAAAAAAAAAAAAAAAAACAAAACAAACC
AAACAAACAATGAAAACAAACCAAAAATCTATGAACATTTCATCCCAACTCGAACCGAACATTCAAGAAAAGCTTATAGGTTGC
GTTTATACAAATTAGTATAGTAAATTTAGGTAATTGAGGGCGCAGATAAAATATAGAGAAGCTGCAAGTTTTTACATATTTTAAATT
CATTATTTATTTATAATTTAAGATAGAAATGGAATGGATTGTGATATATTTTTATAACAAATACTGACATATATGTTTAATGATGTGAA
TTATTTGTAATAATTCTGAAGCTAAAAGTAAAATATAGATTTTATTTTTTAATATTTGTTATTGTAGCTTTTATTATTTATTTTGTTTTC
GCTTGCAGCTTGTGACTTGCAAACCCATTCAATTACTGATAAATAATATGATAAATATATAAAAAAAAAACGCCAAATAGCTCGC
ACTCCAGTTGAGTTAGCTTTTCGACAGAAAAAGAATTCTTAAGACATAGGGCTTGTGAATACCCCCATTGAAAATTCTTCACAA
CATTTTCAGCCTACCATCTGAATCAATTGACCAGATTACTAATCTCACATTTACGTTGCGCCCTGTGCCATCGTCTGCTTTTTTA
CTTGCAGGTTACACCATATCGAGAAGTTATCCAATGAGAAAGCCGCTTAAATTTTGGTAAGTCAACTCCAGTTCATCCTCTTAC
TTTAAGTCTGGGTCCAGTCTTCGTCTAATGAAACGCCTTTGTGCTCGAGTGGACTTCATTTTTTAATTAGAAAGTCAACACACA
CACACACACACACACTCGCACGGGGGTGGGGCGAAGTATCCTTAATCGAAAAGTGCTGCCATATGGAGAGGCGCCTTTGTG
AGCTGCAGGACTCTGCAACCCCCGCCCGCTTGTTTGCCTTTGTTTATTTGTGTGCTACTTAAGATGAAATGGCAAAGAAAACT
GACAGAGATGGTTGTTGGGCTACTAGAACT

D. RIPseq target tables

Table D.1 Syp RIPseq targets

geneID	geneName	log2FoldChange	padj	RNA-binding protein	TF/DNA binding	Imp target
FBgn0283548	mir-9381	3.0315	2.40021E-10	FALSE	FALSE	FALSE
FBgn0262972	CR43283	2.9723	1.13529E-17	FALSE	FALSE	**TRUE**
FBgn0267910	MRE16	2.8632	7.54860E-19	FALSE	FALSE	FALSE
FBgn0036467	CG12310	2.6654	7.17307E-14	FALSE	FALSE	FALSE
FBgn0034512	CG18067	2.6380	1.03293E-05	FALSE	FALSE	FALSE
FBgn0052039	CG32039	2.5632	1.87891E-31	FALSE	FALSE	**TRUE**
FBgn0036468	CG13461	2.5019	2.88662E-05	FALSE	FALSE	FALSE
FBgn0263762	CG43679	2.4967	1.47776E-05	FALSE	FALSE	FALSE
FBgn0266261	CG44956	2.4811	1.69049E-05	FALSE	FALSE	FALSE
FBgn0040565	CG7606	2.4591	4.00148E-05	FALSE	FALSE	FALSE
FBgn0010295	ng3	2.4213	2.07586E-10	FALSE	FALSE	FALSE
FBgn0026197	noe	2.4163	3.01315E-09	FALSE	FALSE	**TRUE**
FBgn0022959	yps	2.4162	1.89955E-22	**TRUE**	**TRUE**	**TRUE**
FBgn0063127	pncr002:3R	2.4049	5.56306E-28	FALSE	FALSE	**TRUE**
FBgn0031097	obst-A	2.3943	9.52711E-09	FALSE	FALSE	**TRUE**
FBgn0003374	Sgs4	2.3381	4.34560E-05	FALSE	FALSE	FALSE
FBgn0266936	CR45387	2.3148	2.78690E-09	FALSE	FALSE	**TRUE**
FBgn0051451	CR31451	2.3072	1.64260E-12	FALSE	FALSE	**TRUE**
FBgn0036940	obst-J	2.2904	6.09475E-04	FALSE	FALSE	FALSE
FBgn0033683	CG18343	2.2764	2.91996E-25	FALSE	FALSE	**TRUE**
FBgn0038646	CG7715	2.2653	2.37938E-04	FALSE	FALSE	FALSE
FBgn0029715	CG11444	2.2646	8.51576E-13	FALSE	FALSE	**TRUE**
FBgn0030183	CG15309	2.2591	1.87891E-31	FALSE	FALSE	**TRUE**
FBgn0027556	CG4928	2.2386	3.42743E-10	FALSE	FALSE	**TRUE**
FBgn0019661	roX1	2.2368	3.55838E-18	FALSE	FALSE	**TRUE**
FBgn0038826	Syp	2.2137	4.65566E-15	**TRUE**	FALSE	**TRUE**
FBgn0004636	Rap1	2.2110	5.28644E-27	FALSE	FALSE	**TRUE**
FBgn0036599	CG13044	2.2105	2.68805E-09	FALSE	FALSE	FALSE
FBgn0034443	cer	2.1838	4.12841E-16	FALSE	FALSE	**TRUE**
FBgn0050009	CR30009	2.1729	5.72657E-16	FALSE	FALSE	**TRUE**
FBgn0026250	eIF1A	2.1486	3.41436E-27	**TRUE**	FALSE	**TRUE**
FBgn0052672	Atg8a	2.1427	1.38199E-11	FALSE	FALSE	**TRUE**
FBgn0022355	Tsf1	2.1217	1.00262E-10	FALSE	FALSE	FALSE
FBgn0003372	Sgs1	2.1138	4.54179E-05	FALSE	FALSE	FALSE
FBgn0031857	LUBEL	2.1124	1.53964E-09	FALSE	FALSE	FALSE
FBgn0027339	jim	2.0996	3.55038E-10	FALSE	**TRUE**	**TRUE**
FBgn0016660	H15	2.0986	8.77891E-16	FALSE	**TRUE**	**TRUE**
FBgn0025809	Paf-AHalpha	2.0966	1.99816E-17	FALSE	FALSE	**TRUE**

geneID	geneName	log2FoldChange	padj	RNA-binding protein	TF/DNA binding	Imp target
FBgn0032899	CG9338	2.0956	3.60062E-11	FALSE	FALSE	FALSE
FBgn0004595	pros	2.0768	1.90869E-08	FALSE	FALSE	**TRUE**
FBgn0082598	akirin	2.0529	1.35370E-18	FALSE	FALSE	**TRUE**
FBgn0035772	Sh3beta	2.0522	7.53690E-29	FALSE	FALSE	**TRUE**
FBgn0003377	Sgs7	2.0499	2.59942E-04	FALSE	FALSE	FALSE
FBgn0014011	Rac2	2.0316	6.28412E-21	FALSE	FALSE	FALSE
FBgn0010638	Sec61beta	2.0170	1.92314E-25	FALSE	FALSE	**TRUE**
FBgn0015229	glec	2.0033	2.86103E-14	FALSE	FALSE	**TRUE**
FBgn0010228	HmgZ	2.0030	6.73199E-21	FALSE	**TRUE**	**TRUE**
FBgn0260747	Chchd2	2.0025	7.69997E-20	FALSE	FALSE	FALSE
FBgn0285926	Imp	1.9971	1.81264E-09	**TRUE**	FALSE	**TRUE**
FBgn0021895	ytr	1.9927	8.95853E-21	**TRUE**	FALSE	**TRUE**
FBgn0035737	Cpr65Ec	1.9823	3.05950E-07	FALSE	FALSE	FALSE
FBgn0028699	Rh50	1.9734	1.84792E-09	FALSE	FALSE	FALSE
FBgn0037636	CG9821	1.9720	1.03010E-08	FALSE	FALSE	**TRUE**
FBgn0259950	CG42460	1.9698	1.30574E-04	FALSE	FALSE	FALSE
FBgn0000046	Act87E	1.9636	5.49397E-10	FALSE	FALSE	FALSE
FBgn0000308	chic	1.9619	1.70014E-23	FALSE	FALSE	**TRUE**
FBgn0041094	scyl	1.9527	9.18962E-17	FALSE	FALSE	**TRUE**
FBgn0267253	CG32700	1.9501	3.38623E-13	FALSE	**TRUE**	**TRUE**
FBgn0015320	Ubc2	1.9495	3.89103E-26	FALSE	FALSE	**TRUE**
FBgn0035816	CG13685	1.9487	7.32262E-16	FALSE	FALSE	**TRUE**
FBgn0052428	CG32428	1.9440	9.18962E-17	FALSE	FALSE	**TRUE**
FBgn0030502	tth	1.9393	8.32263E-15	FALSE	FALSE	FALSE
FBgn0086675	fne	1.9380	1.00847E-12	**TRUE**	FALSE	**TRUE**
FBgn0036165	chrb	1.9368	1.40462E-12	FALSE	FALSE	**TRUE**
FBgn0000173	ben	1.9347	1.12701E-28	FALSE	FALSE	**TRUE**
FBgn0001320	kni	1.9040	3.68224E-07	FALSE	**TRUE**	FALSE
FBgn0053265	Muc68E	1.9026	1.75783E-03	FALSE	FALSE	FALSE
FBgn0038294	Mf	1.9021	5.33580E-08	FALSE	FALSE	**TRUE**
FBgn0086680	vvl	1.8994	1.51586E-12	FALSE	**TRUE**	**TRUE**
FBgn0030897	Frq1	1.8973	4.26614E-14	FALSE	FALSE	**TRUE**
FBgn0036362	CG10725	1.8918	2.78423E-03	FALSE	FALSE	FALSE
FBgn0019660	roX2	1.8907	6.64692E-10	FALSE	FALSE	FALSE
FBgn0259168	mnb	1.8899	1.08287E-17	FALSE	FALSE	**TRUE**
FBgn0261963	mid	1.8873	9.26263E-12	FALSE	**TRUE**	FALSE
FBgn0030806	CG13001	1.8866	7.75116E-15	FALSE	FALSE	FALSE
FBgn0038332	CG6136	1.8845	1.08279E-09	FALSE	FALSE	FALSE
FBgn0266937	CR45388	1.8822	7.87995E-10	FALSE	FALSE	**TRUE**
FBgn0263352	Unr	1.8776	3.27349E-18	**TRUE**	**TRUE**	**TRUE**
FBgn0004396	CrebA	1.8773	2.63324E-09	FALSE	**TRUE**	**TRUE**
FBgn0051324	CG31324	1.8749	9.65571E-13	FALSE	FALSE	**TRUE**

geneID	geneName	log2FoldChange	padj	RNA-binding protein	TF/DNA binding	Imp target
FBgn0035993	Nf-YA	1.8742	9.00239E-14	FALSE	**TRUE**	**TRUE**
FBgn0040958	Peritrophin-15b	1.8726	2.10913E-03	FALSE	FALSE	FALSE
FBgn0003463	sog	1.8670	9.44381E-13	FALSE	FALSE	**TRUE**
FBgn0030066	CG1885	1.8472	3.19212E-14	FALSE	FALSE	FALSE
FBgn0262734	eIF4H1	1.8419	2.10246E-19	**TRUE**	FALSE	**TRUE**
FBgn0024330	MED6	1.8417	1.80673E-12	FALSE	**TRUE**	**TRUE**
FBgn0023526	CG2865	1.8407	7.25067E-11	FALSE	FALSE	**TRUE**
FBgn0038645	CG7714	1.8367	2.97017E-03	FALSE	FALSE	FALSE
FBgn0014163	fax	1.8356	3.80777E-24	FALSE	FALSE	**TRUE**
FBgn0026160	tna	1.8253	1.06773E-12	FALSE	**TRUE**	**TRUE**
FBgn0013334	Sap47	1.8245	4.14262E-16	FALSE	FALSE	**TRUE**
FBgn0003373	Sgs3	1.8244	3.16455E-04	FALSE	FALSE	FALSE
FBgn0034231	APC10	1.8238	1.20566E-11	FALSE	FALSE	FALSE
FBgn0031751	CG9016	1.8233	4.45765E-10	FALSE	FALSE	**TRUE**
FBgn0030763	CG9782	1.8185	1.58678E-07	FALSE	FALSE	**TRUE**
FBgn0263504	CR43493	1.8159	2.61648E-03	FALSE	FALSE	FALSE
FBgn0011481	Ssdp	1.8156	3.70202E-17	FALSE	**TRUE**	**TRUE**
FBgn0014184	Oda	1.8140	4.82399E-12	FALSE	FALSE	**TRUE**
FBgn0023215	Mnt	1.8122	5.34666E-11	FALSE	**TRUE**	**TRUE**
FBgn0031453	Bacc	1.8097	1.16060E-18	FALSE	FALSE	**TRUE**
FBgn0032495	CG16820	1.8051	4.14918E-04	FALSE	FALSE	FALSE
FBgn0032230	lft	1.8045	8.55714E-09	FALSE	FALSE	**TRUE**
FBgn0031277	CG13947	1.8040	1.15892E-03	FALSE	FALSE	FALSE
FBgn0034435	fest	1.7943	1.65249E-03	FALSE	FALSE	**TRUE**
FBgn0011837	Tis11	1.7929	3.80739E-11	**TRUE**	FALSE	**TRUE**
FBgn0264489	CG43897	1.7911	3.74088E-07	FALSE	FALSE	**TRUE**
FBgn0028743	Dhit	1.7861	5.10939E-13	FALSE	FALSE	**TRUE**
FBgn0037645	CG11966	1.7839	2.30430E-03	FALSE	FALSE	FALSE
FBgn0013981	His4r	1.7830	2.70901E-09	FALSE	FALSE	**TRUE**
FBgn0014388	sty	1.7817	3.67538E-12	FALSE	FALSE	**TRUE**
FBgn0035397	CG11486	1.7813	1.40463E-12	FALSE	FALSE	**TRUE**
FBgn0000625	eyg	1.7802	1.17603E-04	FALSE	**TRUE**	FALSE
FBgn0035593	CG4603	1.7745	2.17415E-17	FALSE	FALSE	**TRUE**
FBgn0040153	l(1)G0469	1.7730	2.45789E-16	FALSE	FALSE	**TRUE**
FBgn0011824	CG4038	1.7685	3.24390E-17	**TRUE**	FALSE	FALSE
FBgn0040959	Peritrophin-15a	1.7671	1.16492E-03	FALSE	FALSE	FALSE
FBgn0264490	Eip93F	1.7668	2.03943E-07	FALSE	**TRUE**	**TRUE**
FBgn0036126	Irbp18	1.7525	1.43207E-06	FALSE	**TRUE**	FALSE
FBgn0086758	chinmo	1.7514	1.15495E-05	FALSE	FALSE	**TRUE**
FBgn0040066	wds	1.7504	4.09353E-18	FALSE	FALSE	**TRUE**
FBgn0058469	CR40469	1.7459	5.41095E-05	FALSE	FALSE	FALSE

geneID	geneName	log2FoldChange	padj	RNA-binding protein	TF/DNA binding	Imp target
FBgn0004592	Eig71Ee	1.7425	4.22060E-03	FALSE	FALSE	FALSE
FBgn0038100	Paip2	1.7403	2.25145E-10	FALSE	FALSE	**TRUE**
FBgn0026144	CBP	1.7368	4.01507E-06	FALSE	FALSE	**TRUE**
FBgn0262954	Rpb12	1.7324	1.34520E-12	FALSE	FALSE	**TRUE**
FBgn0031049	Sec61gamma	1.7293	5.67692E-13	FALSE	FALSE	**TRUE**
FBgn0011760	ctp	1.7278	1.11361E-20	FALSE	FALSE	**TRUE**
FBgn0029687	Vap33	1.7219	5.33816E-18	FALSE	FALSE	**TRUE**
FBgn0004921	Ggamma1	1.7139	2.30284E-18	FALSE	FALSE	**TRUE**
FBgn0011817	nmo	1.7136	2.84392E-08	FALSE	FALSE	**TRUE**
FBgn0038654	CG14298	1.7118	4.72562E-03	FALSE	FALSE	FALSE
FBgn0037181	CG11370	1.7089	6.64682E-07	FALSE	FALSE	FALSE
FBgn0003129	Poxm	1.7084	8.04955E-03	FALSE	**TRUE**	FALSE
FBgn0000253	Cam	1.7079	5.97743E-20	FALSE	FALSE	**TRUE**
FBgn0265356	tn	1.7010	5.66223E-06	FALSE	**TRUE**	FALSE
FBgn0003149	Prm	1.7000	1.54675E-05	FALSE	FALSE	FALSE
FBgn0001105	Gbeta13F	1.6993	1.21570E-17	FALSE	FALSE	**TRUE**
FBgn0037614	TMEM216	1.6948	9.31876E-09	FALSE	FALSE	**TRUE**
FBgn0024244	drm	1.6932	7.14458E-07	FALSE	**TRUE**	**TRUE**
FBgn0020238	14-3-3epsilon	1.6926	1.41527E-16	FALSE	FALSE	**TRUE**
FBgn0260642	Antp	1.6917	5.56331E-12	FALSE	**TRUE**	**TRUE**
FBgn0265297	pAbp	1.6915	3.46207E-10	**TRUE**	FALSE	**TRUE**
FBgn0001235	hth	1.6881	5.44462E-10	FALSE	**TRUE**	**TRUE**
FBgn0029894	CG14440	1.6876	3.54627E-09	FALSE	FALSE	**TRUE**
FBgn0267912	CanA-14F	1.6842	3.54668E-07	FALSE	FALSE	**TRUE**
FBgn0262656	Myc	1.6821	9.92063E-07	FALSE	**TRUE**	**TRUE**
FBgn0034860	CG9812	1.6808	1.84822E-03	FALSE	FALSE	FALSE
FBgn0261552	ps	1.6731	1.13581E-06	**TRUE**	FALSE	**TRUE**
FBgn0032304	CG17134	1.6683	6.69515E-03	FALSE	FALSE	FALSE
FBgn0032297	CG17124	1.6671	1.01144E-10	FALSE	FALSE	**TRUE**
FBgn0000273	Pka-C1	1.6632	1.95794E-13	FALSE	FALSE	**TRUE**
FBgn0083991	CG34155	1.6612	5.04334E-13	FALSE	FALSE	**TRUE**
FBgn0003053	peb	1.6592	4.89977E-08	FALSE	FALSE	FALSE
FBgn0250819	CG33521	1.6510	2.44494E-05	FALSE	FALSE	FALSE
FBgn0014010	Rab5	1.6479	1.55858E-13	FALSE	FALSE	**TRUE**
FBgn0260400	elav	1.6457	1.02544E-08	**TRUE**	FALSE	**TRUE**
FBgn0022238	lolal	1.6444	7.22310E-14	FALSE	FALSE	**TRUE**
FBgn0017572	Mo25	1.6361	7.42206E-16	FALSE	FALSE	**TRUE**
FBgn0003410	sina	1.6329	1.25271E-15	FALSE	FALSE	**TRUE**
FBgn0264834	CR44042	1.6321	3.19555E-04	FALSE	FALSE	FALSE
FBgn0035719	tow	1.6264	5.20286E-09	FALSE	FALSE	**TRUE**
FBgn0031632	CG15628	1.6232	3.55776E-12	FALSE	FALSE	**TRUE**
FBgn0047114	CG31142	1.6209	5.97159E-05	FALSE	FALSE	FALSE

geneID	geneName	log2FoldChange	padj	RNA-binding protein	TF/DNA binding	Imp target
FBgn0040393	CG14265	1.6166	1.89117E-04	FALSE	FALSE	FALSE
FBgn0035469	CG14977	1.6152	9.35492E-08	FALSE	FALSE	**TRUE**
FBgn0266446	CG45076	1.6151	1.83684E-03	FALSE	FALSE	**TRUE**
FBgn0038523	CG7587	1.6116	9.55818E-03	FALSE	FALSE	FALSE
FBgn0033968	hui	1.6114	4.87020E-07	FALSE	FALSE	FALSE
FBgn0031736	CG11030	1.6102	6.40469E-10	FALSE	FALSE	**TRUE**
FBgn0266549	CR45102	1.6102	7.46737E-09	FALSE	FALSE	**TRUE**
FBgn0024941	RSG7	1.6089	4.87807E-07	FALSE	FALSE	**TRUE**
FBgn0029996	UbcE2H	1.6058	1.89688E-14	FALSE	FALSE	**TRUE**
FBgn0036428	Gbs-70E	1.6052	2.34618E-10	FALSE	FALSE	**TRUE**
FBgn0266072	CR44825	1.6037	1.13957E-03	FALSE	FALSE	FALSE
FBgn0022893	Df31	1.6006	3.01315E-09	FALSE	**TRUE**	**TRUE**
FBgn0035501	CG1299	1.5999	1.47527E-06	FALSE	FALSE	FALSE
FBgn0015946	grim	1.5959	8.39443E-07	FALSE	FALSE	**TRUE**
FBgn0036030	CG6767	1.5917	9.72144E-10	FALSE	FALSE	**TRUE**
FBgn0263396	sqd	1.5830	9.48185E-09	**TRUE**	**TRUE**	**TRUE**
FBgn0266410	CG45050	1.5822	9.99544E-12	FALSE	**TRUE**	**TRUE**
FBgn0052198	CG32198	1.5816	4.21490E-04	FALSE	FALSE	FALSE
FBgn0040859	CR32658	1.5816	9.26005E-03	FALSE	FALSE	FALSE
FBgn0004907	14-3-3zeta	1.5803	6.49025E-12	FALSE	**TRUE**	**TRUE**
FBgn0003525	stg	1.5797	1.68448E-08	FALSE	FALSE	**TRUE**
FBgn0037468	CG1943	1.5788	1.49021E-10	FALSE	FALSE	**TRUE**
FBgn0010113	hdc	1.5717	1.29376E-05	FALSE	FALSE	**TRUE**
FBgn0040718	CG15353	1.5625	1.84083E-03	FALSE	FALSE	**TRUE**
FBgn0036661	CG9705	1.5606	8.05999E-13	**TRUE**	**TRUE**	**TRUE**
FBgn0261560	Thor	1.5595	1.20015E-05	**TRUE**	FALSE	FALSE
FBgn0040007	RpL38	1.5544	1.31644E-18	FALSE	FALSE	FALSE
FBgn0266521	stai	1.5533	5.64423E-10	FALSE	FALSE	FALSE
FBgn0000459	disco	1.5494	1.94719E-07	FALSE	**TRUE**	**TRUE**
FBgn0038114	CG11670	1.5492	8.58158E-07	FALSE	FALSE	FALSE
FBgn0263773	fok	1.5489	1.60157E-09	FALSE	FALSE	**TRUE**
FBgn0010415	Sdc	1.5474	7.38350E-12	FALSE	FALSE	**TRUE**
FBgn0024183	vig	1.5454	8.52350E-10	**TRUE**	FALSE	FALSE
FBgn0035542	DOR	1.5439	1.81491E-11	FALSE	FALSE	FALSE
FBgn0011766	E2f1	1.5411	5.18956E-08	FALSE	**TRUE**	**TRUE**
FBgn0263511	Vsx1	1.5410	8.50259E-13	FALSE	FALSE	**TRUE**
FBgn0036576	CG5151	1.5409	5.80371E-06	FALSE	FALSE	**TRUE**
FBgn0030973	CG7332	1.5363	4.81478E-14	FALSE	FALSE	**TRUE**
FBgn0002772	Mlc1	1.5358	9.87105E-04	FALSE	FALSE	**TRUE**
FBgn0037697	GstZ2	1.5356	2.84133E-10	FALSE	FALSE	**TRUE**
FBgn0039078	CG4374	1.5335	1.77181E-05	FALSE	**TRUE**	FALSE
FBgn0000259	CkIIbeta	1.5297	2.02574E-09	FALSE	FALSE	**TRUE**

geneID	geneName	log2FoldChange	padj	RNA-binding protein	TF/DNA binding	Imp target
FBgn0265254	CR44268	1.5285	5.85246E-05	FALSE	FALSE	FALSE
FBgn0037676	CG8861	1.5259	1.00817E-08	FALSE	FALSE	FALSE
FBgn0003447	sn	1.5253	1.11607E-06	FALSE	FALSE	**TRUE**
FBgn0031909	CG5181	1.5244	1.23230E-10	FALSE	FALSE	FALSE
FBgn0040600	CG13631	1.5215	4.67219E-05	FALSE	FALSE	**TRUE**
FBgn0044047	Ilp6	1.5205	2.41602E-16	FALSE	FALSE	**TRUE**
FBgn0035020	CG13585	1.5193	1.02544E-08	FALSE	FALSE	**TRUE**
FBgn0001145	Gs2	1.5182	2.31959E-07	FALSE	FALSE	**TRUE**
FBgn0036090	CG8009	1.5165	1.55452E-09	FALSE	FALSE	**TRUE**
FBgn0000015	Abd-B	1.5147	2.97557E-10	FALSE	**TRUE**	**TRUE**
FBgn0033274	CG14757	1.5122	4.49909E-03	FALSE	FALSE	**TRUE**
FBgn0029778	RhoGAP5A	1.5113	1.06051E-15	FALSE	FALSE	**TRUE**
FBgn0003378	Sgs8	1.5076	9.37366E-03	FALSE	FALSE	FALSE
FBgn0032731	Swip-1	1.5036	8.10207E-09	FALSE	FALSE	FALSE
FBgn0262886	CR43241	1.4972	1.66154E-06	FALSE	FALSE	FALSE
FBgn0000412	D1	1.4965	7.56219E-10	FALSE	**TRUE**	**TRUE**
FBgn0003997	hid	1.4937	1.10432E-06	FALSE	FALSE	**TRUE**
FBgn0036264	CG11529	1.4918	4.00991E-03	FALSE	FALSE	FALSE
FBgn0005655	PCNA	1.4907	2.36847E-08	FALSE	FALSE	**TRUE**
FBgn0030529	Clic	1.4823	9.61768E-07	FALSE	FALSE	FALSE
FBgn0004838	Hrb27C	1.4775	4.47423E-07	**TRUE**	FALSE	**TRUE**
FBgn0030955	CG6891	1.4737	3.45345E-09	FALSE	FALSE	**TRUE**
FBgn0025800	Smox	1.4727	1.61879E-08	FALSE	**TRUE**	FALSE
FBgn0063498	GstE2	1.4727	2.68325E-04	FALSE	FALSE	**TRUE**
FBgn0004880	scrt	1.4717	1.13143E-05	FALSE	**TRUE**	**TRUE**
FBgn0000489	Pka-C3	1.4715	1.00266E-06	FALSE	FALSE	**TRUE**
FBgn0004910	Eip63F-1	1.4682	8.01204E-08	FALSE	FALSE	FALSE
FBgn0004646	ogre	1.4673	1.55819E-12	FALSE	FALSE	**TRUE**
FBgn0030693	CG8974	1.4668	7.22608E-10	FALSE	FALSE	FALSE
FBgn0026190	PH4alphaMP	1.4664	5.60585E-04	FALSE	FALSE	FALSE
FBgn0035016	CG4612	1.4636	1.81663E-09	**TRUE**	FALSE	**TRUE**
FBgn0032635	CG15141	1.4630	1.13738E-05	FALSE	**TRUE**	FALSE
FBgn0263019	CR43314	1.4629	1.43654E-03	FALSE	FALSE	FALSE
FBgn0003435	sm	1.4615	1.07732E-05	**TRUE**	FALSE	**TRUE**
FBgn0004865	Eip78C	1.4577	4.78672E-11	FALSE	FALSE	FALSE
FBgn0085391	trv	1.4553	2.86841E-08	**TRUE**	FALSE	**TRUE**
FBgn0263380	CR43432	1.4519	3.73047E-03	FALSE	FALSE	FALSE
FBgn0016694	Pdp1	1.4509	5.29441E-05	FALSE	**TRUE**	**TRUE**
FBgn0004858	elB	1.4487	6.70947E-12	FALSE	FALSE	**TRUE**
FBgn0030400	CG11138	1.4436	2.00543E-09	FALSE	FALSE	**TRUE**
FBgn0264001	bru3	1.4385	7.79899E-06	**TRUE**	FALSE	**TRUE**
FBgn0003975	vg	1.4353	9.13094E-09	FALSE	**TRUE**	**TRUE**

geneID	geneName	log2FoldChange	padj	RNA-binding protein	TF/DNA binding	Imp target
FBgn0052544	CG32544	1.4327	1.01330E-10	FALSE	FALSE	**TRUE**
FBgn0001168	h	1.4322	3.79913E-05	FALSE	**TRUE**	**TRUE**
FBgn0263106	DnaJ-1	1.4302	2.05437E-05	FALSE	FALSE	FALSE
FBgn0030654	CG15643	1.4290	3.51921E-08	FALSE	FALSE	FALSE
FBgn0039754	CG9747	1.4281	4.13510E-04	FALSE	FALSE	FALSE
FBgn0000560	eg	1.4263	2.04767E-03	FALSE	**TRUE**	FALSE
FBgn0051781	CR31781	1.4248	4.75719E-09	FALSE	FALSE	**TRUE**
FBgn0028408	Drep2	1.4204	6.42419E-08	FALSE	FALSE	**TRUE**
FBgn0260484	HIP	1.4191	6.03269E-12	FALSE	FALSE	FALSE
FBgn0029666	CG10803	1.4179	3.03680E-08	**TRUE**	FALSE	**TRUE**
FBgn0019972	Drice	1.4143	2.23244E-04	FALSE	FALSE	FALSE
FBgn0000546	EcR	1.4127	9.86273E-07	FALSE	**TRUE**	FALSE
FBgn0051221	CG31221	1.4121	5.29722E-07	FALSE	FALSE	**TRUE**
FBgn0029911	CG14435	1.4114	6.90777E-11	FALSE	FALSE	**TRUE**
FBgn0036670	CG13029	1.4104	1.17624E-04	FALSE	FALSE	FALSE
FBgn0039380	CG5890	1.4102	1.56487E-07	FALSE	FALSE	**TRUE**
FBgn0261549	rdgA	1.4100	2.09691E-04	FALSE	FALSE	**TRUE**
FBgn0041191	Rheb	1.4091	3.03723E-05	FALSE	FALSE	**TRUE**
FBgn0026411	Lim1	1.4082	5.33580E-08	FALSE	**TRUE**	**TRUE**
FBgn0001197	His2Av	1.4072	1.27699E-10	FALSE	FALSE	**TRUE**
FBgn0030559	CG13404	1.4067	2.26828E-09	FALSE	FALSE	**TRUE**
FBgn0011305	Rsf1	1.4063	1.64260E-12	**TRUE**	FALSE	FALSE
FBgn0031011	CG8034	1.4060	1.13439E-11	FALSE	FALSE	**TRUE**
FBgn0026084	cib	1.4035	3.85505E-11	FALSE	FALSE	**TRUE**
FBgn0000261	Cat	1.4020	6.01870E-12	FALSE	FALSE	FALSE
FBgn0267033	mamo	1.3989	6.53983E-04	FALSE	**TRUE**	**TRUE**
FBgn0264922	smt3	1.3976	1.44486E-15	FALSE	FALSE	**TRUE**
FBgn0283471	wupA	1.3964	2.42866E-03	FALSE	FALSE	**TRUE**
FBgn0004177	mts	1.3954	5.18956E-08	FALSE	FALSE	**TRUE**
FBgn0038126	CG8483	1.3936	3.61638E-04	FALSE	FALSE	**TRUE**
FBgn0014857	His3.3A	1.3898	3.77397E-09	FALSE	FALSE	FALSE
FBgn0030114	CG17754	1.3804	5.77017E-08	FALSE	FALSE	**TRUE**
FBgn0036746	Crtc	1.3799	5.84010E-08	FALSE	FALSE	**TRUE**
FBgn0264488	CG43896	1.3787	3.93340E-03	FALSE	FALSE	FALSE
FBgn0010341	Cdc42	1.3676	1.74430E-10	FALSE	FALSE	**TRUE**
FBgn0003944	Ubx	1.3636	1.52218E-05	FALSE	**TRUE**	FALSE
FBgn0039858	CycG	1.3619	1.13243E-05	FALSE	FALSE	**TRUE**
FBgn0035495	CG14989	1.3592	7.68441E-06	FALSE	FALSE	**TRUE**
FBgn0086665	snoRNA:Psi18S-1377a	1.3583	1.30007E-05	FALSE	FALSE	FALSE
FBgn0000028	acj6	1.3582	9.49825E-05	FALSE	**TRUE**	**TRUE**
FBgn0028836	CSN7	1.3582	1.06421E-05	FALSE	FALSE	FALSE
FBgn0038080	CG12279	1.3575	2.31959E-07	FALSE	FALSE	FALSE

geneID	geneName	log2FoldChange	padj	RNA-binding protein	TF/DNA binding	Imp target
FBgn0000479	dnc	1.3574	1.51633E-04	FALSE	FALSE	**TRUE**
FBgn0032429	CG5446	1.3551	5.44462E-10	FALSE	FALSE	FALSE
FBgn0026415	Idgf4	1.3534	1.92893E-05	FALSE	FALSE	FALSE
FBgn0262631	CR43148	1.3528	3.15860E-03	FALSE	FALSE	FALSE
FBgn0036111	Aps	1.3527	2.81708E-09	FALSE	FALSE	**TRUE**
FBgn0259143	CG42258	1.3515	6.45066E-09	FALSE	FALSE	**TRUE**
FBgn0044020	Roc2	1.3504	5.18956E-08	FALSE	FALSE	FALSE
FBgn0005648	Pabp2	1.3504	9.99544E-12	**TRUE**	FALSE	**TRUE**
FBgn0035481	CG12605	1.3476	3.87439E-05	FALSE	**TRUE**	**TRUE**
FBgn0023214	edl	1.3475	2.67898E-07	FALSE	**TRUE**	**TRUE**
FBgn0085229	CG34200	1.3473	8.95105E-07	FALSE	FALSE	FALSE
FBgn0015778	rin	1.3443	2.90173E-09	**TRUE**	FALSE	**TRUE**
FBgn0036918	Pfdn6	1.3428	5.84216E-06	FALSE	FALSE	FALSE
FBgn0041188	Atx2	1.3378	5.88176E-07	FALSE	FALSE	**TRUE**
FBgn0028397	Tob	1.3373	1.73115E-04	FALSE	FALSE	**TRUE**
FBgn0032900	CG14401	1.3355	8.78735E-03	FALSE	FALSE	FALSE
FBgn0040020	MED21	1.3350	2.15529E-04	FALSE	FALSE	**TRUE**
FBgn0264491	how	1.3343	6.07486E-08	**TRUE**	FALSE	**TRUE**
FBgn0032200	CG5676	1.3289	2.14168E-03	FALSE	FALSE	FALSE
FBgn0061515	endos	1.3282	1.70902E-08	FALSE	FALSE	**TRUE**
FBgn0264078	Flo2	1.3278	2.07586E-10	FALSE	FALSE	**TRUE**
FBgn0029939	CG9650	1.3261	3.26472E-05	FALSE	**TRUE**	FALSE
FBgn0033624	CG12384	1.3257	1.90869E-08	FALSE	FALSE	FALSE
FBgn0035725	Mis12	1.3160	1.19862E-03	FALSE	FALSE	FALSE
FBgn0033691	CG8860	1.3138	4.37192E-05	FALSE	FALSE	FALSE
FBgn0263118	tx	1.3131	2.10263E-03	FALSE	FALSE	**TRUE**
FBgn0013343	Syx1A	1.3123	1.34695E-04	FALSE	FALSE	**TRUE**
FBgn0032284	CG7294	1.3110	7.53809E-03	FALSE	FALSE	FALSE
FBgn0033551	CG7222	1.3110	3.85536E-06	FALSE	FALSE	**TRUE**
FBgn0033446	CG1648	1.3089	1.75207E-05	FALSE	FALSE	FALSE
FBgn0265276	l(3)neo38	1.3071	8.55774E-09	FALSE	**TRUE**	**TRUE**
FBgn0001994	crp	1.3017	5.49397E-10	FALSE	FALSE	**TRUE**
FBgn0031992	CG8498	1.2998	1.22165E-06	FALSE	FALSE	FALSE
FBgn0037016	CG13252	1.2994	1.61610E-09	FALSE	FALSE	**TRUE**
FBgn0036538	CG15715	1.2990	7.53494E-08	FALSE	**TRUE**	**TRUE**
FBgn0032482	Pect	1.2971	7.31839E-08	FALSE	FALSE	FALSE
FBgn0036537	CG18081	1.2964	2.36755E-06	FALSE	FALSE	**TRUE**
FBgn0262512	Vha14-1	1.2925	2.81052E-09	FALSE	FALSE	FALSE
FBgn0035285	CG12025	1.2915	2.32873E-10	FALSE	FALSE	FALSE
FBgn0053639	CG33639	1.2914	1.28694E-06	FALSE	FALSE	**TRUE**
FBgn0017418	ari-1	1.2901	7.05496E-08	FALSE	FALSE	**TRUE**
FBgn0032897	CG9336	1.2898	6.53047E-05	FALSE	FALSE	FALSE

geneID	geneName	log2FoldChange	padj	RNA-binding protein	TF/DNA binding	Imp target
FBgn0030520	Pdcd4	1.2880	3.74088E-07	FALSE	FALSE	**TRUE**
FBgn0003514	sqh	1.2868	1.41233E-10	FALSE	FALSE	FALSE
FBgn0034091	mrj	1.2867	1.96597E-08	FALSE	FALSE	**TRUE**
FBgn0259916	CG42445	1.2858	1.71249E-04	FALSE	FALSE	FALSE
FBgn0052264	CG32264	1.2808	7.25685E-07	FALSE	**TRUE**	**TRUE**
FBgn0004436	Ubc6	1.2793	9.12422E-09	FALSE	FALSE	FALSE
FBgn0011704	RnrS	1.2791	6.56632E-04	FALSE	FALSE	**TRUE**
FBgn0086446	DCTN6-p27	1.2791	3.55016E-06	FALSE	FALSE	FALSE
FBgn0028734	Fmr1	1.2774	8.31476E-09	**TRUE**	FALSE	FALSE
FBgn0030863	CG8188	1.2759	1.61879E-08	FALSE	FALSE	**TRUE**
FBgn0021800	Reph	1.2750	4.87020E-07	FALSE	FALSE	**TRUE**
FBgn0266777	CR45242	1.2749	2.24565E-06	FALSE	FALSE	**TRUE**
FBgn0051363	Jupiter	1.2744	2.66800E-12	FALSE	FALSE	**TRUE**
FBgn0010226	GstS1	1.2738	6.26662E-09	FALSE	FALSE	**TRUE**
FBgn0001323	knrl	1.2733	9.19326E-04	FALSE	**TRUE**	FALSE
FBgn0266409	CG45049	1.2685	3.83368E-09	FALSE	FALSE	**TRUE**
FBgn0267336	Glut4EF	1.2680	3.44023E-05	FALSE	**TRUE**	**TRUE**
FBgn0264006	dysc	1.2670	5.18538E-04	FALSE	FALSE	**TRUE**
FBgn0004687	Mlc-c	1.2661	2.24717E-08	FALSE	FALSE	**TRUE**
FBgn0031908	CG5177	1.2654	6.64482E-03	FALSE	FALSE	FALSE
FBgn0011666	msi	1.2626	1.89388E-05	**TRUE**	FALSE	**TRUE**
FBgn0034802	CNBP	1.2624	4.43720E-04	FALSE	FALSE	**TRUE**
FBgn0032816	Nf-YB	1.2622	5.34801E-05	FALSE	**TRUE**	**TRUE**
FBgn0051360	CG31360	1.2609	8.91854E-04	FALSE	FALSE	FALSE
FBgn0265487	mbl	1.2600	2.80480E-04	**TRUE**	FALSE	**TRUE**
FBgn0032420	CG6583	1.2590	2.01518E-07	FALSE	FALSE	**TRUE**
FBgn0031090	Rab35	1.2542	5.34825E-07	FALSE	FALSE	FALSE
FBgn0011706	rpr	1.2533	6.13455E-06	FALSE	FALSE	**TRUE**
FBgn0039532	Mtl	1.2527	8.10207E-09	FALSE	FALSE	**TRUE**
FBgn0004169	up	1.2515	2.74375E-03	FALSE	FALSE	FALSE
FBgn0000044	Act57B	1.2509	7.47299E-03	FALSE	FALSE	FALSE
FBgn0036773	CG13698	1.2508	4.66806E-06	FALSE	FALSE	FALSE
FBgn0004567	slp2	1.2505	1.53964E-09	FALSE	**TRUE**	**TRUE**
FBgn0260943	Rbp6	1.2500	2.79148E-05	**TRUE**	FALSE	**TRUE**
FBgn0024432	Dlc90F	1.2500	3.95216E-05	FALSE	FALSE	**TRUE**
FBgn0027496	epsilonCOP	1.2495	3.76716E-03	FALSE	FALSE	FALSE
FBgn0026077	Gasp	1.2490	9.00945E-04	FALSE	FALSE	**TRUE**
FBgn0000043	Act42A	1.2477	5.01500E-04	FALSE	FALSE	FALSE
FBgn0261789	SmD2	1.2471	3.13607E-08	**TRUE**	FALSE	**TRUE**
FBgn0283535	Vha26	1.2450	1.32407E-10	FALSE	FALSE	**TRUE**
FBgn0004170	sc	1.2440	2.47841E-03	FALSE	**TRUE**	FALSE
FBgn0040942	CG12643	1.2429	1.12439E-08	FALSE	FALSE	**TRUE**

geneID	geneName	log2FoldChange	padj	RNA-binding protein	TF/DNA binding	Imp target
FBgn0029979	mahe	1.2428	1.70902E-08	**TRUE**	FALSE	**TRUE**
FBgn0020378	Sp1	1.2423	1.40777E-07	FALSE	**TRUE**	**TRUE**
FBgn0020496	CtBP	1.2396	6.13619E-10	FALSE	**TRUE**	**TRUE**
FBgn0011224	heph	1.2393	3.20177E-05	**TRUE**	FALSE	**TRUE**
FBgn0052365	CG32365	1.2373	5.87951E-05	FALSE	FALSE	FALSE
FBgn0000370	crc	1.2360	9.66252E-07	FALSE	**TRUE**	**TRUE**
FBgn0011290	Taf12	1.2329	3.66071E-07	FALSE	**TRUE**	**TRUE**
FBgn0263995	cpo	1.2314	1.76416E-03	**TRUE**	FALSE	**TRUE**
FBgn0052423	shep	1.2282	1.90400E-04	**TRUE**	FALSE	**TRUE**
FBgn0266020	CR44785	1.2253	6.75300E-03	FALSE	FALSE	FALSE
FBgn0052062	Rbfox1	1.2236	2.79943E-06	**TRUE**	FALSE	**TRUE**
FBgn0283472	S6k	1.2233	3.07616E-06	FALSE	FALSE	**TRUE**
FBgn0010424	TpnC73F	1.2230	2.16940E-03	FALSE	FALSE	FALSE
FBgn0010314	Cks30A	1.2229	1.76488E-05	FALSE	FALSE	**TRUE**
FBgn0036237	viaf	1.2228	2.48316E-09	FALSE	FALSE	FALSE
FBgn0039977	CG17454	1.2225	1.22165E-06	**TRUE**	FALSE	FALSE
FBgn0051855	CG31855	1.2223	6.49705E-07	FALSE	FALSE	**TRUE**
FBgn0044323	Cka	1.2223	6.54473E-09	FALSE	FALSE	**TRUE**
FBgn0263345	CR43426	1.2213	5.11126E-04	FALSE	FALSE	**TRUE**
FBgn0038947	Sar1	1.2193	1.25234E-06	FALSE	FALSE	**TRUE**
FBgn0026409	Mpcp2	1.2180	7.40758E-11	FALSE	FALSE	**TRUE**
FBgn0016797	fz2	1.2162	2.80619E-09	FALSE	FALSE	FALSE
FBgn0002561	l(1)sc	1.2158	2.61648E-03	FALSE	**TRUE**	FALSE
FBgn0001122	Galphao	1.2158	3.67306E-09	FALSE	FALSE	**TRUE**
FBgn0010300	brat	1.2157	2.86124E-04	**TRUE**	**TRUE**	**TRUE**
FBgn0035578	CG13707	1.2147	3.03390E-05	FALSE	FALSE	FALSE
FBgn0003165	pum	1.2139	3.06219E-04	**TRUE**	FALSE	**TRUE**
FBgn0017578	Max	1.2113	7.07889E-05	FALSE	**TRUE**	FALSE
FBgn0035917	Zasp66	1.2106	4.34987E-03	FALSE	FALSE	FALSE
FBgn0026192	par-6	1.2103	2.95782E-08	FALSE	FALSE	**TRUE**
FBgn0035677	CG13293	1.2093	1.17953E-06	FALSE	FALSE	FALSE
FBgn0039209	REPTOR	1.2068	6.73018E-05	FALSE	**TRUE**	FALSE
FBgn0015024	Cklalpha	1.2056	5.20256E-05	FALSE	FALSE	**TRUE**
FBgn0040235	c12.1	1.2054	2.49658E-06	**TRUE**	FALSE	FALSE
FBgn0266666	Sem1	1.2050	2.32135E-09	FALSE	FALSE	FALSE
FBgn0026262	bip2	1.2029	1.33879E-08	FALSE	**TRUE**	**TRUE**
FBgn0030328	Amun	1.2026	2.31569E-08	FALSE	FALSE	**TRUE**
FBgn0052512	CG32512	1.2022	6.20653E-06	FALSE	FALSE	**TRUE**
FBgn0026149	BCL7-like	1.1992	8.48402E-08	FALSE	FALSE	**TRUE**
FBgn0040765	luna	1.1985	6.39849E-04	FALSE	FALSE	**TRUE**
FBgn0038662	Mpc1	1.1981	1.25673E-04	FALSE	FALSE	FALSE
FBgn0011276	HLH3B	1.1980	1.55278E-03	FALSE	**TRUE**	**TRUE**

geneID	geneName	log2FoldChange	padj	RNA-binding protein	TF/DNA binding	Imp target
FBgn0033529	CG17765	1.1980	7.29885E-06	FALSE	FALSE	FALSE
FBgn0046763	CG17278	1.1971	3.59541E-05	FALSE	FALSE	**TRUE**
FBgn0004870	bab1	1.1966	8.94364E-04	FALSE	**TRUE**	**TRUE**
FBgn0028550	Atf3	1.1950	2.08550E-03	FALSE	**TRUE**	**TRUE**
FBgn0030309	CG1572	1.1932	2.27067E-05	FALSE	FALSE	FALSE
FBgn0002732	E(spl)malpha-BFM	1.1926	3.99375E-05	FALSE	FALSE	FALSE
FBgn0035370	Non2	1.1922	2.33463E-07	FALSE	FALSE	FALSE
FBgn0031914	CG5973	1.1921	2.08720E-03	FALSE	FALSE	FALSE
FBgn0010316	dap	1.1912	5.32055E-05	FALSE	FALSE	**TRUE**
FBgn0040907	mRpL33	1.1908	5.69219E-03	FALSE	FALSE	FALSE
FBgn0265192	Snp	1.1896	6.52263E-08	**TRUE**	FALSE	FALSE
FBgn0029676	HIP-R	1.1893	2.32135E-09	FALSE	FALSE	**TRUE**
FBgn0063670	CG40228	1.1888	1.22165E-06	FALSE	FALSE	FALSE
FBgn0002609	E(spl)m3-HLH	1.1887	2.70368E-05	FALSE	**TRUE**	FALSE
FBgn0036534	DCP2	1.1876	9.21814E-07	**TRUE**	FALSE	**TRUE**
FBgn0000286	Cf2	1.1851	4.83248E-05	FALSE	**TRUE**	**TRUE**
FBgn0004854	B-H2	1.1834	3.83760E-06	FALSE	**TRUE**	**TRUE**
FBgn0000147	aurA	1.1830	6.86595E-04	FALSE	FALSE	FALSE
FBgn0002521	pho	1.1822	3.73573E-05	FALSE	FALSE	**TRUE**
FBgn0024734	PRL-1	1.1821	6.43073E-03	FALSE	FALSE	**TRUE**
FBgn0265177	CG44242	1.1820	7.63779E-06	FALSE	FALSE	FALSE
FBgn0283651	CG46301	1.1817	6.89000E-07	FALSE	FALSE	**TRUE**
FBgn0030090	fend	1.1803	4.28039E-04	FALSE	FALSE	**TRUE**
FBgn0013718	nuf	1.1790	1.16524E-06	FALSE	FALSE	FALSE
FBgn0035193	CG9192	1.1784	3.44845E-04	FALSE	FALSE	FALSE
FBgn0010453	Wnt4	1.1758	2.90036E-08	FALSE	FALSE	**TRUE**
FBgn0261933	SmD1	1.1752	4.57394E-05	**TRUE**	FALSE	FALSE
FBgn0016041	Tom40	1.1735	1.15287E-10	FALSE	FALSE	**TRUE**
FBgn0037534	CG2781	1.1731	2.60693E-03	FALSE	FALSE	**TRUE**
FBgn0000711	flw	1.1719	1.34897E-06	FALSE	FALSE	**TRUE**
FBgn0011705	rost	1.1703	5.10991E-08	FALSE	FALSE	FALSE
FBgn0052442	Arv1	1.1623	4.57529E-05	FALSE	FALSE	FALSE
FBgn0265512	mlt	1.1610	3.13053E-07	FALSE	FALSE	**TRUE**
FBgn0023167	SmD3	1.1588	5.22346E-09	**TRUE**	FALSE	FALSE
FBgn0002723	Met	1.1573	3.14506E-05	FALSE	FALSE	FALSE
FBgn0024321	NK7.1	1.1570	4.05543E-05	FALSE	**TRUE**	FALSE
FBgn0265447	CR44347	1.1557	7.65939E-03	FALSE	FALSE	FALSE
FBgn0002789	Mp20	1.1545	1.88634E-03	FALSE	FALSE	FALSE
FBgn0023212	EloB	1.1523	2.83360E-08	FALSE	FALSE	**TRUE**
FBgn0051176	CG31176	1.1521	2.42831E-04	FALSE	FALSE	**TRUE**
FBgn0264270	Sxl	1.1508	2.52216E-05	**TRUE**	FALSE	**TRUE**
FBgn0037481	MAGE	1.1506	9.60759E-03	FALSE	FALSE	**TRUE**

geneID	geneName	log2FoldChange	padj	RNA-binding protein	TF/DNA binding	Imp target
FBgn0036556	CG5830	1.1485	2.35943E-08	FALSE	FALSE	FALSE
FBgn0023534	CG17778	1.1468	7.81254E-06	FALSE	FALSE	FALSE
FBgn0038922	Idh3b	1.1449	5.26420E-06	FALSE	FALSE	**TRUE**
FBgn0053181	CG33181	1.1425	1.11835E-03	FALSE	FALSE	**TRUE**
FBgn0263617	CR43626	1.1425	8.03158E-03	FALSE	FALSE	**TRUE**
FBgn0278608	Dsp1	1.1410	1.82060E-09	FALSE	**TRUE**	FALSE
FBgn0003371	sgg	1.1389	8.02793E-07	FALSE	FALSE	**TRUE**
FBgn0262733	Src64B	1.1389	1.90567E-07	FALSE	FALSE	**TRUE**
FBgn0038608	WRNexo	1.1381	1.30461E-04	FALSE	FALSE	FALSE
FBgn0026076	UBL3	1.1379	1.77907E-06	FALSE	FALSE	FALSE
FBgn0000179	bi	1.1375	8.15071E-04	FALSE	**TRUE**	**TRUE**
FBgn0038672	CG6005	1.1370	8.73144E-05	FALSE	FALSE	FALSE
FBgn0032642	CG5110	1.1370	1.08720E-05	FALSE	FALSE	FALSE
FBgn0086677	jeb	1.1368	6.82411E-04	FALSE	FALSE	**TRUE**
FBgn0005626	ple	1.1359	8.76614E-04	FALSE	FALSE	FALSE
FBgn0001325	Kr	1.1345	1.21196E-03	FALSE	**TRUE**	FALSE
FBgn0037342	CG2931	1.1325	5.70811E-08	**TRUE**	FALSE	FALSE
FBgn0037556	CG9636	1.1302	2.98682E-04	FALSE	FALSE	**TRUE**
FBgn0250823	gish	1.1293	1.34897E-06	FALSE	FALSE	FALSE
FBgn0266721	gammaSnap2	1.1280	2.10068E-03	FALSE	FALSE	FALSE
FBgn0014020	Rho1	1.1279	7.92248E-08	FALSE	FALSE	FALSE
FBgn0030788	Sap30	1.1259	1.88381E-06	FALSE	**TRUE**	FALSE
FBgn0261793	Trf2	1.1252	5.49146E-06	FALSE	**TRUE**	**TRUE**
FBgn0004102	oc	1.1252	1.52065E-04	FALSE	**TRUE**	FALSE
FBgn0267795	Frl	1.1245	1.27537E-05	FALSE	FALSE	FALSE
FBgn0015222	Fer1HCH	1.1219	4.75987E-04	FALSE	FALSE	**TRUE**
FBgn0031126	Cyp6v1	1.1204	3.02324E-06	FALSE	FALSE	FALSE
FBgn0024227	aurB	1.1199	8.63599E-04	FALSE	FALSE	FALSE
FBgn0015399	kek1	1.1155	4.88818E-05	FALSE	FALSE	**TRUE**
FBgn0001186	Hex-A	1.1154	1.06845E-04	FALSE	FALSE	FALSE
FBgn0264821	CR44029	1.1154	3.09573E-03	FALSE	FALSE	**TRUE**
FBgn0030653	CG7860	1.1152	2.27067E-05	FALSE	FALSE	FALSE
FBgn0026088	CG14818	1.1150	1.16162E-05	FALSE	FALSE	FALSE
FBgn0267365	l(2)SH0834	1.1145	3.07138E-04	FALSE	FALSE	FALSE
FBgn0264493	rdx	1.1144	2.21314E-06	FALSE	FALSE	**TRUE**
FBgn0051481	pb	1.1131	6.76561E-05	FALSE	FALSE	FALSE
FBgn0013799	Deaf1	1.1130	6.29137E-07	FALSE	**TRUE**	**TRUE**
FBgn0038286	CG6966	1.1119	6.35718E-06	FALSE	FALSE	FALSE
FBgn0039831	CG12054	1.1117	6.87067E-05	FALSE	**TRUE**	**TRUE**
FBgn0036820	Grx1	1.1116	1.80229E-03	FALSE	FALSE	FALSE
FBgn0034282	Mapmodulin	1.1092	2.78451E-06	FALSE	FALSE	**TRUE**
FBgn0038388	CG4287	1.1079	1.73494E-06	FALSE	FALSE	FALSE

geneID	geneName	log2FoldChange	padj	RNA-binding protein	TF/DNA binding	Imp target
FBgn0032048	Dh31	1.1025	6.82411E-04	FALSE	FALSE	FALSE
FBgn0031037	CG14207	1.1020	1.11144E-05	FALSE	FALSE	FALSE
FBgn0050094	CG30094	1.1006	1.29376E-05	FALSE	FALSE	FALSE
FBgn0262739	AGO1	1.1002	5.24647E-05	**TRUE**	FALSE	**TRUE**
FBgn0261822	Bsg	1.0995	3.87109E-05	FALSE	FALSE	**TRUE**
FBgn0013469	klu	1.0981	4.36835E-04	FALSE	FALSE	FALSE
FBgn0033556	CG12343	1.0955	3.12491E-03	FALSE	FALSE	FALSE
FBgn0000659	fkh	1.0953	2.03760E-05	FALSE	**TRUE**	**TRUE**
FBgn0001138	grn	1.0939	3.36159E-04	FALSE	**TRUE**	**TRUE**
FBgn0002734	E(spl)mdelta-HLH	1.0931	8.87371E-03	FALSE	**TRUE**	FALSE
FBgn0262858	CG43222	1.0913	8.42460E-05	FALSE	FALSE	FALSE
FBgn0053977	CG33977	1.0888	5.07084E-03	FALSE	FALSE	FALSE
FBgn0032946	nrv3	1.0865	4.05028E-07	FALSE	FALSE	**TRUE**
FBgn0035612	frm	1.0833	2.55014E-03	FALSE	FALSE	**TRUE**
FBgn0053100	eIF4EHP	1.0833	1.85074E-03	**TRUE**	FALSE	**TRUE**
FBgn0261068	LSm7	1.0826	4.76746E-06	**TRUE**	FALSE	FALSE
FBgn0033725	Cpr49Ac	1.0813	9.39299E-06	FALSE	FALSE	FALSE
FBgn0042630	Sox21b	1.0811	8.88348E-06	FALSE	**TRUE**	**TRUE**
FBgn0050096	CG30096	1.0786	9.50305E-03	FALSE	FALSE	FALSE
FBgn0033872	CG6329	1.0777	4.66216E-07	FALSE	FALSE	**TRUE**
FBgn0040985	CG6115	1.0747	2.86487E-07	FALSE	FALSE	FALSE
FBgn0014135	bnl	1.0744	2.08459E-03	FALSE	FALSE	**TRUE**
FBgn0035109	CG13876	1.0728	7.47206E-03	FALSE	FALSE	FALSE
FBgn0033378	tsu	1.0706	3.16779E-05	**TRUE**	FALSE	FALSE
FBgn0030912	CG6023	1.0691	8.13758E-03	FALSE	FALSE	**TRUE**
FBgn0030482	CG1673	1.0683	1.53257E-03	FALSE	FALSE	FALSE
FBgn0032189	Ripalpha	1.0671	7.91933E-05	FALSE	FALSE	FALSE
FBgn0266000	CG44774	1.0665	1.16543E-03	FALSE	FALSE	**TRUE**
FBgn0003520	stau	1.0660	4.89198E-04	**TRUE**	FALSE	**TRUE**
FBgn0031403	CG15387	1.0641	3.79507E-03	FALSE	FALSE	FALSE
FBgn0259176	bun	1.0631	1.69129E-04	FALSE	**TRUE**	**TRUE**
FBgn0001185	her	1.0621	5.58173E-07	FALSE	FALSE	FALSE
FBgn0264848	vih	1.0617	9.64031E-05	FALSE	FALSE	**TRUE**
FBgn0259711	CG42365	1.0614	1.70029E-03	FALSE	FALSE	FALSE
FBgn0030501	BthD	1.0599	3.44529E-06	FALSE	FALSE	FALSE
FBgn0013762	Cdk5	1.0594	2.28286E-05	FALSE	FALSE	FALSE
FBgn0003607	Su(var)205	1.0587	3.45817E-03	**TRUE**	**TRUE**	FALSE
FBgn0001139	gro	1.0577	1.75341E-07	FALSE	**TRUE**	FALSE
FBgn0029959	Rab39	1.0568	1.29319E-03	FALSE	FALSE	**TRUE**
FBgn0267487	Ptp61F	1.0562	2.03339E-05	FALSE	FALSE	FALSE
FBgn0003042	Pc	1.0555	5.48853E-05	FALSE	**TRUE**	**TRUE**
FBgn0030791	CG9132	1.0533	1.49620E-06	FALSE	FALSE	**TRUE**

geneID	geneName	log2FoldChange	padj	RNA-binding protein	TF/DNA binding	Imp target
FBgn0029962	CG1402	1.0525	7.31839E-08	FALSE	FALSE	**TRUE**
FBgn0005649	Rox8	1.0513	4.75719E-09	**TRUE**	FALSE	FALSE
FBgn0265595	CG44422	1.0509	3.19198E-03	FALSE	FALSE	**TRUE**
FBgn0013467	igl	1.0506	8.95239E-04	FALSE	FALSE	FALSE
FBgn0001248	Idh	1.0500	1.21467E-05	FALSE	FALSE	FALSE
FBgn0004889	tws	1.0499	2.35425E-05	FALSE	FALSE	**TRUE**
FBgn0034709	Swim	1.0490	4.90893E-04	FALSE	FALSE	FALSE
FBgn0033550	CG12341	1.0475	1.94122E-05	FALSE	FALSE	FALSE
FBgn0035423	eIF1	1.0464	6.09475E-04	**TRUE**	FALSE	**TRUE**
FBgn0250869	CG42240	1.0457	1.82604E-05	FALSE	FALSE	**TRUE**
FBgn0085387	shakB	1.0450	5.55326E-03	FALSE	FALSE	**TRUE**
FBgn0052369	CG32369	1.0443	1.05454E-04	FALSE	FALSE	**TRUE**
FBgn0263093	CR43361	1.0442	1.80229E-03	FALSE	FALSE	FALSE
FBgn0032400	CG6770	1.0428	8.17930E-05	FALSE	FALSE	FALSE
FBgn0086686	l(3)L1231	1.0428	3.16455E-04	FALSE	FALSE	**TRUE**
FBgn0001169	H	1.0424	1.39477E-04	FALSE	**TRUE**	FALSE
FBgn0034264	Dlish	1.0384	8.89287E-03	FALSE	FALSE	FALSE
FBgn0035023	ITP	1.0378	4.39921E-05	FALSE	FALSE	**TRUE**
FBgn0025638	Roc1a	1.0369	2.98091E-09	FALSE	FALSE	FALSE
FBgn0261955	kdn	1.0357	1.84792E-09	FALSE	FALSE	**TRUE**
FBgn0028369	kirre	1.0353	6.70796E-04	FALSE	FALSE	**TRUE**
FBgn0003721	Tm1	1.0309	8.37510E-07	FALSE	FALSE	**TRUE**
FBgn0283451	br	1.0307	6.91839E-03	FALSE	FALSE	**TRUE**
FBgn0035505	Teh2	1.0272	1.29571E-03	FALSE	FALSE	**TRUE**
FBgn0261647	Axud1	1.0251	2.61049E-04	FALSE	FALSE	FALSE
FBgn0027291	l(1)G0156	1.0240	2.54033E-06	FALSE	FALSE	**TRUE**
FBgn0034408	sano	1.0236	6.87739E-05	FALSE	FALSE	**TRUE**
FBgn0053200	VepD	1.0229	1.11299E-03	FALSE	FALSE	**TRUE**
FBgn0029693	CG6379	1.0228	1.27149E-03	FALSE	FALSE	FALSE
FBgn0005771	noc	1.0227	1.00563E-08	FALSE	FALSE	FALSE
FBgn0037930	CG14715	1.0210	3.45507E-03	FALSE	FALSE	FALSE
FBgn0030605	ND-B18	1.0185	2.76908E-05	FALSE	FALSE	FALSE
FBgn0037623	CG9801	1.0174	9.94643E-07	FALSE	FALSE	FALSE
FBgn0004237	Hrb87F	1.0170	6.42419E-08	**TRUE**	FALSE	FALSE
FBgn0030876	CG6762	1.0162	7.37134E-04	FALSE	FALSE	FALSE
FBgn0011725	twin	1.0161	1.14650E-06	FALSE	**TRUE**	**TRUE**
FBgn0001215	Hrb98DE	1.0160	1.05066E-07	**TRUE**	FALSE	**TRUE**
FBgn0040230	dbo	1.0155	6.49705E-07	FALSE	FALSE	FALSE
FBgn0052296	Mrtf	1.0148	5.17855E-04	FALSE	**TRUE**	**TRUE**
FBgn0028663	VhaM9.7-b	1.0142	4.50481E-07	FALSE	FALSE	FALSE
FBgn0010287	Trf	1.0137	1.74459E-03	FALSE	**TRUE**	FALSE
FBgn0025549	unc-119	1.0123	4.91194E-09	FALSE	FALSE	**TRUE**

geneID	geneName	log2FoldChange	padj	RNA-binding protein	TF/DNA binding	Imp target
FBgn0020255	Ran	1.0118	8.27164E-06	FALSE	FALSE	**TRUE**
FBgn0036844	Mkp3	1.0110	1.74349E-04	FALSE	FALSE	FALSE
FBgn0035692	Sf3b6	1.0102	7.77294E-07	**TRUE**	FALSE	FALSE
FBgn0030617	CG9095	1.0084	4.93558E-03	FALSE	FALSE	**TRUE**
FBgn0259239	CG42337	1.0082	4.04993E-04	FALSE	FALSE	FALSE
FBgn0003134	Pp1alpha-96A	1.0076	4.33830E-07	FALSE	FALSE	**TRUE**
FBgn0029930	CG12541	1.0056	1.36445E-05	FALSE	FALSE	FALSE
FBgn0010333	Rac1	1.0044	1.01909E-04	FALSE	FALSE	FALSE
FBgn0000575	emc	1.0035	3.13053E-07	FALSE	**TRUE**	**TRUE**
FBgn0024920	Ts	1.0030	4.18554E-03	FALSE	FALSE	FALSE
FBgn0261975	CG42806	1.0025	1.14847E-06	FALSE	FALSE	FALSE
FBgn0023528	CG2924	1.0018	4.24983E-06	FALSE	FALSE	FALSE

Table D.2 Imp RIPseq targets

geneID	geneName	log2FoldChange	padj	RNA-binding protein	TF/DNA binding	Syp target
FBgn0021895	ytr	4.4747	0.0000E+00	**TRUE**	FALSE	**TRUE**
FBgn0285926	Imp	4.3717	0.0000E+00	**TRUE**	FALSE	**TRUE**
FBgn0027339	jim	4.2917	0.0000E+00	FALSE	**TRUE**	**TRUE**
FBgn0264490	Eip93F	4.2346	0.0000E+00	FALSE	**TRUE**	**TRUE**
FBgn0262972	CR43283	4.2128	0.0000E+00	FALSE	FALSE	**TRUE**
FBgn0030897	Frq1	4.1510	4.5864E-256	FALSE	FALSE	**TRUE**
FBgn0261552	ps	4.0034	0.0000E+00	**TRUE**	FALSE	**TRUE**
FBgn0262979	CR43287	3.8851	3.0209E-17	FALSE	FALSE	FALSE
FBgn0037636	CG9821	3.7870	0.0000E+00	FALSE	FALSE	**TRUE**
FBgn0004595	pros	3.7465	0.0000E+00	FALSE	**TRUE**	**TRUE**
FBgn0000259	CkIIbeta	3.6652	0.0000E+00	FALSE	FALSE	**TRUE**
FBgn0262656	Myc	3.6486	5.8624E-290	FALSE	**TRUE**	**TRUE**
FBgn0031097	obst-A	3.6369	3.2139E-148	FALSE	FALSE	**TRUE**
FBgn0031751	CG9016	3.6303	1.1936E-122	FALSE	FALSE	**TRUE**
FBgn0263396	sqd	3.6271	0.0000E+00	**TRUE**	**TRUE**	**TRUE**
FBgn0026197	noe	3.6256	8.2219E-229	FALSE	FALSE	**TRUE**
FBgn0028397	Tob	3.6139	1.0896E-145	FALSE	FALSE	**TRUE**
FBgn0266936	CR45387	3.5848	6.0199E-133	FALSE	FALSE	**TRUE**
FBgn0063127	pncr002:3R	3.5818	0.0000E+00	FALSE	FALSE	**TRUE**
FBgn0051451	CR31451	3.5681	0.0000E+00	FALSE	FALSE	**TRUE**
FBgn0266409	CG45049	3.5594	0.0000E+00	FALSE	FALSE	**TRUE**
FBgn0003380	Sh	3.4953	1.0933E-196	FALSE	FALSE	FALSE
FBgn0267033	mamo	3.4729	2.8939E-123	FALSE	**TRUE**	**TRUE**
FBgn0000253	Cam	3.4418	9.9795E-279	FALSE	FALSE	**TRUE**
FBgn0010415	Sdc	3.4150	3.9229E-249	FALSE	FALSE	**TRUE**
FBgn0001235	hth	3.4125	0.0000E+00	FALSE	**TRUE**	**TRUE**
FBgn0034443	cer	3.4101	1.9004E-95	FALSE	FALSE	**TRUE**
FBgn0052512	CG32512	3.4034	1.0622E-141	FALSE	FALSE	**TRUE**
FBgn0037127	CG14566	3.3892	8.2149E-102	FALSE	FALSE	FALSE
FBgn0030763	CG9782	3.3822	6.0293E-91	FALSE	FALSE	**TRUE**
FBgn0266549	CR45102	3.3605	9.9686E-125	FALSE	FALSE	**TRUE**
FBgn0264738	CG43996	3.3508	9.6347E-18	FALSE	FALSE	FALSE
FBgn0023215	Mnt	3.3269	3.0747E-232	FALSE	**TRUE**	**TRUE**
FBgn0000308	chic	3.3232	2.9588E-275	FALSE	FALSE	**TRUE**
FBgn0266937	CR45388	3.3025	1.0240E-111	FALSE	FALSE	**TRUE**
FBgn0004244	Rdl	3.2925	4.4972E-236	FALSE	FALSE	FALSE
FBgn0053181	CG33181	3.2693	2.6456E-300	FALSE	FALSE	**TRUE**
FBgn0285944	para	3.2651	0.0000E+00	FALSE	FALSE	FALSE
FBgn0015946	grim	3.2507	6.3558E-111	FALSE	FALSE	**TRUE**
FBgn0013334	Sap47	3.2227	0.0000E+00	FALSE	FALSE	**TRUE**
FBgn0030940	CG15040	3.2195	2.6075E-20	FALSE	FALSE	FALSE

geneID	geneName	log2FoldChange	padj	RNA-binding protein	TF/DNA binding	Syp target
FBgn0004636	Rap1	3.1728	5.5351E-229	FALSE	FALSE	**TRUE**
FBgn0035397	CG11486	3.1713	0.0000E+00	FALSE	FALSE	**TRUE**
FBgn0032151	nAChRalpha6	3.1613	4.2419E-226	FALSE	FALSE	FALSE
FBgn0264006	dysc	3.1608	6.2299E-263	FALSE	FALSE	**TRUE**
FBgn0030328	Amun	3.1427	5.4944E-304	FALSE	FALSE	**TRUE**
FBgn0003371	sgg	3.1412	0.0000E+00	FALSE	FALSE	**TRUE**
FBgn0267912	CanA-14F	3.1374	1.6408E-257	FALSE	FALSE	**TRUE**
FBgn0035571	CG12493	3.1312	7.8740E-16	**TRUE**	FALSE	FALSE
FBgn0034802	CNBP	3.1186	8.6629E-288	FALSE	FALSE	**TRUE**
FBgn0000448	Hr3	3.1088	1.3833E-47	FALSE	**TRUE**	FALSE
FBgn0086758	chinmo	3.0987	3.3411E-237	FALSE	**TRUE**	**TRUE**
FBgn0004103	Pp1-87B	3.0945	0.0000E+00	FALSE	FALSE	FALSE
FBgn0028999	nerfin-1	3.0937	1.5224E-189	FALSE	**TRUE**	FALSE
FBgn0085387	shakB	3.0820	3.8638E-144	FALSE	FALSE	**TRUE**
FBgn0259994	CG42492	3.0660	3.8329E-248	FALSE	FALSE	FALSE
FBgn0029814	CG15765	3.0638	4.5982E-254	FALSE	FALSE	FALSE
FBgn0023214	edl	3.0563	1.1328E-150	FALSE	**TRUE**	**TRUE**
FBgn0016694	Pdp1	3.0524	2.5317E-165	FALSE	**TRUE**	**TRUE**
FBgn0053100	eIF4EHP	3.0501	4.7382E-237	**TRUE**	FALSE	**TRUE**
FBgn0028704	Nckx30C	3.0485	0.0000E+00	FALSE	FALSE	FALSE
FBgn0033403	CG13739	3.0480	1.5438E-144	FALSE	FALSE	FALSE
FBgn0052204	CG32204	3.0406	3.9651E-183	FALSE	FALSE	FALSE
FBgn0031453	Bacc	3.0375	0.0000E+00	FALSE	FALSE	**TRUE**
FBgn0035282	CNMa	2.9876	1.7289E-14	FALSE	FALSE	FALSE
FBgn0263397	Ih	2.9664	6.5612E-267	FALSE	FALSE	FALSE
FBgn0039431	plum	2.9486	6.6022E-188	FALSE	FALSE	FALSE
FBgn0262734	eIF4H1	2.9479	9.7549E-161	**TRUE**	FALSE	**TRUE**
FBgn0016041	Tom40	2.9470	0.0000E+00	FALSE	FALSE	**TRUE**
FBgn0032895	twit	2.9422	1.1524E-83	FALSE	FALSE	FALSE
FBgn0035526	CG1316	2.9062	1.4052E-242	**TRUE**	FALSE	FALSE
FBgn0004921	Ggamma1	2.9059	2.3259E-253	FALSE	FALSE	**TRUE**
FBgn0261822	Bsg	2.9053	3.7006E-150	FALSE	FALSE	**TRUE**
FBgn0263769	CR43686	2.8981	2.1845E-05	FALSE	FALSE	FALSE
FBgn0029666	CG10803	2.8892	5.2153E-94	**TRUE**	FALSE	**TRUE**
FBgn0263080	CG43348	2.8820	5.6725E-04	FALSE	FALSE	FALSE
FBgn0267690	CG46026	2.8806	1.2774E-03	FALSE	FALSE	FALSE
FBgn0029708	CG3556	2.8749	4.2844E-214	FALSE	FALSE	FALSE
FBgn0262370	mir-7	2.8693	3.8918E-07	FALSE	FALSE	FALSE
FBgn0086677	jeb	2.8634	3.0848E-213	FALSE	FALSE	**TRUE**
FBgn0010113	hdc	2.8466	5.3786E-218	FALSE	FALSE	**TRUE**
FBgn0029894	CG14440	2.8465	3.6301E-293	FALSE	FALSE	**TRUE**
FBgn0041094	scyl	2.8451	2.4944E-210	FALSE	FALSE	**TRUE**

geneID	geneName	log2FoldChange	padj	RNA-binding protein	TF/DNA binding	Syp target
FBgn0051140	CG31140	2.8328	1.9939E-190	**TRUE**	FALSE	FALSE
FBgn0263352	Unr	2.8166	4.4274E-211	**TRUE**	**TRUE**	**TRUE**
FBgn0002921	Atpalpha	2.8163	0.0000E+00	FALSE	FALSE	FALSE
FBgn0010453	Wnt4	2.8008	7.4583E-146	FALSE	FALSE	**TRUE**
FBgn0262636	dati	2.7991	0.0000E+00	FALSE	**TRUE**	FALSE
FBgn0085385	bma	2.7811	1.9556E-160	FALSE	FALSE	FALSE
FBgn0085478	CG34449	2.7803	3.3294E-216	FALSE	FALSE	FALSE
FBgn0016660	H15	2.7692	4.5766E-69	FALSE	**TRUE**	**TRUE**
FBgn0026206	mei-P26	2.7643	1.7656E-189	FALSE	**TRUE**	FALSE
FBgn0032946	nrv3	2.7552	4.8909E-174	FALSE	FALSE	**TRUE**
FBgn0086675	fne	2.7535	3.7519E-142	**TRUE**	FALSE	**TRUE**
FBgn0013343	Syx1A	2.7470	2.3776E-158	FALSE	FALSE	**TRUE**
FBgn0259143	CG42258	2.7312	1.1173E-256	FALSE	FALSE	**TRUE**
FBgn0026077	Gasp	2.7311	2.4816E-85	FALSE	FALSE	**TRUE**
FBgn0040726	dpr1	2.7310	7.0116E-176	FALSE	FALSE	FALSE
FBgn0261955	kdn	2.7287	5.4944E-304	FALSE	FALSE	**TRUE**
FBgn0019661	roX1	2.7256	1.5170E-118	FALSE	FALSE	**TRUE**
FBgn0264001	bru3	2.7234	2.8826E-162	**TRUE**	FALSE	**TRUE**
FBgn0038826	Syp	2.7145	1.3276E-124	**TRUE**	FALSE	**TRUE**
FBgn0041191	Rheb	2.7067	1.7574E-252	FALSE	FALSE	**TRUE**
FBgn0265297	pAbp	2.7038	7.7161E-208	**TRUE**	FALSE	**TRUE**
FBgn0266679	CR45169	2.6961	5.8906E-05	FALSE	FALSE	FALSE
FBgn0036677	CG13023	2.6950	2.4239E-106	FALSE	FALSE	FALSE
FBgn0027932	Akap200	2.6937	3.0243E-154	FALSE	FALSE	FALSE
FBgn0028550	Atf3	2.6930	1.1017E-129	FALSE	**TRUE**	**TRUE**
FBgn0000412	D1	2.6848	9.4383E-157	FALSE	**TRUE**	**TRUE**
FBgn0014184	Oda	2.6847	2.8949E-218	FALSE	FALSE	**TRUE**
FBgn0034657	LBR	2.6834	1.3251E-184	FALSE	FALSE	FALSE
FBgn0020496	CtBP	2.6792	1.4630E-250	FALSE	**TRUE**	**TRUE**
FBgn0266410	CG45050	2.6764	1.5216E-89	FALSE	**TRUE**	**TRUE**
FBgn0029761	SK	2.6733	5.0941E-145	FALSE	FALSE	FALSE
FBgn0085249	CG34220	2.6689	2.1050E-09	FALSE	FALSE	FALSE
FBgn0052532	CG32532	2.6650	8.2417E-154	FALSE	**TRUE**	FALSE
FBgn0036030	CG6767	2.6571	1.3736E-208	FALSE	FALSE	**TRUE**
FBgn0283499	InR	2.6554	7.5900E-97	FALSE	FALSE	FALSE
FBgn0264270	Sxl	2.6482	1.7106E-125	**TRUE**	FALSE	**TRUE**
FBgn0004828	His3.3B	2.6447	2.1909E-171	FALSE	FALSE	FALSE
FBgn0261549	rdgA	2.6368	6.4383E-90	FALSE	FALSE	**TRUE**
FBgn0000028	acj6	2.6312	3.7500E-133	FALSE	**TRUE**	**TRUE**
FBgn0030183	CG15309	2.6160	4.1550E-73	FALSE	FALSE	**TRUE**
FBgn0030912	CG6023	2.6145	2.8805E-33	FALSE	FALSE	**TRUE**
FBgn0028369	kirre	2.6128	1.9591E-119	FALSE	FALSE	**TRUE**

geneID	geneName	log2FoldChange	padj	RNA-binding protein	TF/DNA binding	Syp target
FBgn0267309	CR45745	2.6122	9.2192E-05	FALSE	FALSE	FALSE
FBgn0029155	Men-b	2.6017	7.1470E-218	FALSE	FALSE	FALSE
FBgn0025809	Paf-AHalpha	2.6009	9.6396E-163	FALSE	FALSE	**TRUE**
FBgn0003463	sog	2.5905	1.7235E-75	FALSE	FALSE	**TRUE**
FBgn0022986	qkr58E-1	2.5795	3.8041E-67	**TRUE**	FALSE	FALSE
FBgn0267253	CG32700	2.5723	8.0823E-121	FALSE	**TRUE**	**TRUE**
FBgn0262682	CR43152	2.5670	1.3817E-06	FALSE	FALSE	FALSE
FBgn0029887	CG3198	2.5641	1.3477E-193	FALSE	FALSE	FALSE
FBgn0014135	bnl	2.5641	3.8427E-53	FALSE	FALSE	**TRUE**
FBgn0030479	Rbp1-like	2.5597	1.9222E-15	**TRUE**	FALSE	FALSE
FBgn0032229	CG5045	2.5579	2.7056E-207	FALSE	FALSE	FALSE
FBgn0028862	dao	2.5579	3.7175E-131	FALSE	FALSE	FALSE
FBgn0026250	eIF1A	2.5561	2.0545E-108	**TRUE**	FALSE	**TRUE**
FBgn0265487	mbl	2.5359	8.1384E-162	**TRUE**	FALSE	**TRUE**
FBgn0260499	qvr	2.5339	2.9372E-97	FALSE	FALSE	FALSE
FBgn0262101	CG42854	2.5246	3.0375E-04	FALSE	FALSE	FALSE
FBgn0053267	CG33267	2.5236	1.8542E-11	FALSE	FALSE	FALSE
FBgn0024244	drm	2.5189	1.2498E-40	FALSE	**TRUE**	**TRUE**
FBgn0028743	Dhit	2.5148	2.2786E-146	FALSE	FALSE	**TRUE**
FBgn0028875	nAChRalpha5	2.5085	1.6717E-91	FALSE	FALSE	FALSE
FBgn0000479	dnc	2.5069	2.3655E-154	FALSE	FALSE	**TRUE**
FBgn0030439	CG12716	2.5060	3.7543E-11	FALSE	FALSE	FALSE
FBgn0017418	ari-1	2.5027	8.5390E-176	FALSE	FALSE	**TRUE**
FBgn0000108	Appl	2.4992	3.5190E-224	FALSE	FALSE	FALSE
FBgn0035813	CG8492	2.4935	2.6114E-04	FALSE	FALSE	FALSE
FBgn0261801	CG42747	2.4918	7.3171E-80	FALSE	FALSE	FALSE
FBgn0267252	Ggamma30A	2.4757	5.6710E-274	FALSE	FALSE	FALSE
FBgn0013981	His4r	2.4620	0.0000E+00	FALSE	FALSE	**TRUE**
FBgn0264511	CR43910	2.4572	2.4863E-06	FALSE	FALSE	FALSE
FBgn0085446	CG34417	2.4537	3.8965E-145	FALSE	FALSE	FALSE
FBgn0262877	CG43232	2.4519	2.8128E-14	FALSE	FALSE	FALSE
FBgn0263773	fok	2.4479	1.5650E-89	FALSE	FALSE	**TRUE**
FBgn0020238	14-3-3epsilon	2.4444	1.7812E-162	FALSE	FALSE	**TRUE**
FBgn0020556	bxd	2.4425	3.5698E-06	FALSE	FALSE	FALSE
FBgn0082598	akirin	2.4365	5.5619E-177	FALSE	FALSE	**TRUE**
FBgn0000179	bi	2.4353	1.1038E-183	FALSE	**TRUE**	**TRUE**
FBgn0023526	CG2865	2.4317	5.7472E-90	FALSE	FALSE	**TRUE**
FBgn0062978	CG31808	2.4302	1.1170E-22	FALSE	FALSE	FALSE
FBgn0035505	Teh2	2.4271	1.0571E-110	FALSE	FALSE	**TRUE**
FBgn0001122	Galphao	2.4271	1.3736E-162	FALSE	FALSE	**TRUE**
FBgn0050389	CG30389	2.4261	1.1389E-238	FALSE	FALSE	FALSE
FBgn0035469	CG14977	2.4247	1.1440E-105	FALSE	FALSE	**TRUE**

geneID	geneName	log2FoldChange	padj	RNA-binding protein	TF/DNA binding	Syp target
FBgn0011661	Moe	2.4198	5.1908E-167	FALSE	FALSE	FALSE
FBgn0028434	Ercc1	2.4176	1.7513E-55	FALSE	FALSE	FALSE
FBgn0029715	CG11444	2.4172	8.6403E-158	FALSE	FALSE	**TRUE**
FBgn0039831	CG12054	2.4054	1.5205E-127	FALSE	**TRUE**	**TRUE**
FBgn0004838	Hrb27C	2.4047	4.7889E-88	**TRUE**	FALSE	**TRUE**
FBgn0003093	Pkc98E	2.4016	7.6537E-176	FALSE	FALSE	FALSE
FBgn0028408	Drep2	2.3871	2.1206E-117	FALSE	FALSE	**TRUE**
FBgn0003435	sm	2.3849	2.8459E-131	**TRUE**	FALSE	**TRUE**
FBgn0036008	CG3408	2.3776	2.0696E-132	FALSE	FALSE	FALSE
FBgn0259224	CG42324	2.3753	8.3715E-87	FALSE	FALSE	FALSE
FBgn0035719	tow	2.3729	7.3403E-135	FALSE	FALSE	**TRUE**
FBgn0267336	Glut4EF	2.3695	3.7117E-103	FALSE	**TRUE**	**TRUE**
FBgn0030468	CG1622	2.3619	3.3141E-160	FALSE	FALSE	FALSE
FBgn0031049	Sec61gamma	2.3565	1.6551E-148	FALSE	FALSE	**TRUE**
FBgn0010226	GstS1	2.3516	2.8312E-187	FALSE	FALSE	**TRUE**
FBgn0052672	Atg8a	2.3469	4.0347E-233	FALSE	FALSE	**TRUE**
FBgn0000036	nAChRalpha1	2.3456	8.6031E-125	FALSE	FALSE	FALSE
FBgn0085391	trv	2.3417	2.9568E-114	**TRUE**	FALSE	**TRUE**
FBgn0011760	ctp	2.3266	7.0442E-76	FALSE	FALSE	**TRUE**
FBgn0000557	eEF1alpha2	2.3214	2.8179E-257	**TRUE**	FALSE	FALSE
FBgn0285925	Fas1	2.3213	8.3349E-110	FALSE	FALSE	FALSE
FBgn0038100	Paip2	2.3174	6.8201E-82	FALSE	FALSE	**TRUE**
FBgn0260943	Rbp6	2.3130	2.6121E-100	**TRUE**	FALSE	**TRUE**
FBgn0036735	Edc3	2.3116	1.7868E-94	FALSE	FALSE	FALSE
FBgn0010228	HmgZ	2.3115	1.2432E-175	FALSE	**TRUE**	**TRUE**
FBgn0025390	Mur2B	2.3078	1.8835E-77	FALSE	FALSE	FALSE
FBgn0031632	CG15628	2.3075	3.2323E-129	FALSE	FALSE	**TRUE**
FBgn0263117	CG34377	2.3026	5.2855E-78	FALSE	FALSE	FALSE
FBgn0010313	corto	2.3013	2.4572E-100	FALSE	**TRUE**	FALSE
FBgn0020279	lig	2.2973	5.3607E-174	FALSE	FALSE	FALSE
FBgn0024963	GluClalpha	2.2876	5.2843E-127	FALSE	FALSE	FALSE
FBgn0000636	Fas3	2.2854	1.5982E-97	FALSE	FALSE	FALSE
FBgn0260722	CR42549	2.2830	3.3560E-64	FALSE	FALSE	FALSE
FBgn0022959	yps	2.2806	2.6162E-164	**TRUE**	**TRUE**	**TRUE**
FBgn0052107	CG32107	2.2762	1.5812E-03	FALSE	FALSE	FALSE
FBgn0022893	Df31	2.2738	2.5912E-224	FALSE	**TRUE**	**TRUE**
FBgn0040153	l(1)G0469	2.2687	3.1319E-76	FALSE	FALSE	**TRUE**
FBgn0034135	Syn2	2.2679	1.7658E-80	FALSE	FALSE	FALSE
FBgn0038694	CG5217	2.2638	8.8204E-03	FALSE	FALSE	FALSE
FBgn0259483	Mob4	2.2607	8.5128E-242	FALSE	FALSE	FALSE
FBgn0086674	Tango13	2.2593	9.5218E-60	FALSE	FALSE	FALSE
FBgn0053140	CG33140	2.2582	2.2778E-03	FALSE	FALSE	FALSE

geneID	geneName	log2FoldChange	padj	RNA-binding protein	TF/DNA binding	Syp target
FBgn0029687	Vap33	2.2572	8.2006E-158	FALSE	FALSE	**TRUE**
FBgn0038947	Sar1	2.2535	5.6955E-240	FALSE	FALSE	**TRUE**
FBgn0022238	lolal	2.2523	2.1605E-140	FALSE	**TRUE**	**TRUE**
FBgn0051176	CG31176	2.2510	3.5662E-17	FALSE	FALSE	**TRUE**
FBgn0259745	wech	2.2452	6.7368E-96	FALSE	FALSE	FALSE
FBgn0004880	scrt	2.2370	1.1942E-137	FALSE	**TRUE**	**TRUE**
FBgn0260429	CG42524	2.2306	1.9626E-13	FALSE	FALSE	FALSE
FBgn0003447	sn	2.2301	1.3952E-138	FALSE	FALSE	**TRUE**
FBgn0029768	SPR	2.2276	1.7144E-58	FALSE	FALSE	FALSE
FBgn0000273	Pka-C1	2.2267	1.4585E-107	FALSE	FALSE	**TRUE**
FBgn0266875	CR45336	2.2262	4.9036E-03	FALSE	FALSE	FALSE
FBgn0264493	rdx	2.2215	3.4300E-110	FALSE	FALSE	**TRUE**
FBgn0010768	sqz	2.2208	1.4879E-51	FALSE	**TRUE**	FALSE
FBgn0262483	Rbp	2.2169	5.1393E-178	FALSE	FALSE	FALSE
FBgn0013342	nSyb	2.2168	6.2545E-214	FALSE	FALSE	FALSE
FBgn0051221	CG31221	2.2145	5.0343E-144	FALSE	FALSE	**TRUE**
FBgn0040324	Ephrin	2.2135	1.6081E-87	FALSE	FALSE	FALSE
FBgn0264788	CR44018	2.2118	1.6673E-41	FALSE	FALSE	FALSE
FBgn0260642	Antp	2.2109	2.4172E-112	FALSE	**TRUE**	**TRUE**
FBgn0266886	CR45347	2.2076	5.2219E-04	FALSE	FALSE	FALSE
FBgn0086686	l(3)L1231	2.2007	1.4034E-113	FALSE	FALSE	**TRUE**
FBgn0261789	SmD2	2.1957	3.5276E-169	**TRUE**	FALSE	**TRUE**
FBgn0259176	bun	2.1929	3.6124E-128	FALSE	**TRUE**	**TRUE**
FBgn0004396	CrebA	2.1805	1.1564E-44	FALSE	**TRUE**	**TRUE**
FBgn0052428	CG32428	2.1770	1.7830E-126	FALSE	FALSE	**TRUE**
FBgn0015229	glec	2.1750	6.0547E-132	FALSE	FALSE	**TRUE**
FBgn0027495	Smyd4-4	2.1744	3.9758E-135	FALSE	FALSE	FALSE
FBgn0086361	alph	2.1712	2.7061E-135	FALSE	FALSE	FALSE
FBgn0265533	CR44383	2.1662	1.7777E-18	FALSE	FALSE	FALSE
FBgn0037796	CG12814	2.1637	1.9562E-25	FALSE	FALSE	FALSE
FBgn0040569	CR14310	2.1593	6.4699E-03	FALSE	FALSE	FALSE
FBgn0043825	CG18284	2.1578	9.6498E-03	FALSE	FALSE	FALSE
FBgn0013799	Deaf1	2.1552	2.7730E-121	FALSE	**TRUE**	**TRUE**
FBgn0031294	IA-2	2.1539	7.0581E-137	FALSE	FALSE	FALSE
FBgn0029801	CG15771	2.1509	1.1975E-104	FALSE	FALSE	FALSE
FBgn0026439	Eaat1	2.1469	4.4927E-91	FALSE	FALSE	FALSE
FBgn0029799	CG15772	2.1424	8.6877E-25	FALSE	FALSE	FALSE
FBgn0042630	Sox21b	2.1385	1.7091E-58	FALSE	**TRUE**	**TRUE**
FBgn0283472	S6k	2.1381	6.3460E-121	FALSE	FALSE	**TRUE**
FBgn0030973	CG7332	2.1367	2.1140E-106	FALSE	FALSE	**TRUE**
FBgn0001105	Gbeta13F	2.1339	4.1873E-132	FALSE	FALSE	**TRUE**
FBgn0030886	CG12672	2.1289	7.1316E-07	FALSE	FALSE	FALSE

geneID	geneName	log2FoldChange	padj	RNA-binding protein	TF/DNA binding	Syp target
FBgn0034731	CG10384	2.1277	1.1675E-101	**TRUE**	FALSE	FALSE
FBgn0260026	CG42494	2.1262	2.9820E-09	FALSE	FALSE	FALSE
FBgn0040600	CG13631	2.1228	4.0067E-20	FALSE	FALSE	**TRUE**
FBgn0003118	pnt	2.1215	1.6113E-95	FALSE	**TRUE**	FALSE
FBgn0045761	CHKov1	2.1212	1.4534E-67	**TRUE**	FALSE	FALSE
FBgn0024330	MED6	2.1201	8.4574E-90	FALSE	**TRUE**	**TRUE**
FBgn0038294	Mf	2.1171	6.6317E-25	FALSE	FALSE	**TRUE**
FBgn0036134	FoxK	2.1133	3.6068E-117	FALSE	**TRUE**	FALSE
FBgn0033715	CG8490	2.1116	5.4259E-109	FALSE	FALSE	FALSE
FBgn0030893	RhoGAP16F	2.1115	7.6511E-88	FALSE	FALSE	FALSE
FBgn0262405	mir-998	2.1101	4.4769E-03	FALSE	FALSE	FALSE
FBgn0262728	Pal2	2.1087	5.0974E-135	FALSE	FALSE	FALSE
FBgn0004242	Syt1	2.1052	2.9070E-172	FALSE	FALSE	FALSE
FBgn0043070	MESK2	2.1012	1.4150E-181	FALSE	FALSE	FALSE
FBgn0000459	disco	2.0967	2.4785E-85	FALSE	**TRUE**	**TRUE**
FBgn0039647	CG14509	2.0949	1.2056E-134	FALSE	FALSE	FALSE
FBgn0015774	NetB	2.0940	8.5145E-181	FALSE	FALSE	FALSE
FBgn0035246	CG13928	2.0929	3.6453E-126	FALSE	FALSE	FALSE
FBgn0011206	bol	2.0910	6.9906E-79	**TRUE**	FALSE	FALSE
FBgn0264908	pHCl-1	2.0908	5.5607E-53	FALSE	FALSE	FALSE
FBgn0036717	CG13731	2.0892	8.7762E-07	FALSE	FALSE	FALSE
FBgn0263257	Cngl	2.0892	2.3040E-94	FALSE	FALSE	FALSE
FBgn0011766	E2f1	2.0889	4.9956E-134	FALSE	**TRUE**	**TRUE**
FBgn0041605	cpx	2.0880	8.2248E-103	FALSE	FALSE	FALSE
FBgn0011706	rpr	2.0838	3.2857E-33	FALSE	FALSE	**TRUE**
FBgn0031043	Naa20A	2.0781	5.7039E-146	FALSE	FALSE	FALSE
FBgn0031736	CG11030	2.0774	1.2015E-60	FALSE	FALSE	**TRUE**
FBgn0029979	mahe	2.0749	6.3994E-113	**TRUE**	FALSE	**TRUE**
FBgn0010488	NAT1	2.0739	3.5670E-90	**TRUE**	FALSE	FALSE
FBgn0001404	egh	2.0726	4.2654E-153	FALSE	FALSE	FALSE
FBgn0039858	CycG	2.0721	4.5723E-124	FALSE	FALSE	**TRUE**
FBgn0027527	Osi6	2.0712	4.1374E-03	FALSE	FALSE	FALSE
FBgn0051626	CG31626	2.0704	2.6549E-03	FALSE	FALSE	FALSE
FBgn0036576	CG5151	2.0698	8.6214E-69	FALSE	FALSE	**TRUE**
FBgn0051191	CG31191	2.0684	6.4586E-82	FALSE	FALSE	FALSE
FBgn0041188	Atx2	2.0681	2.1875E-76	FALSE	FALSE	**TRUE**
FBgn0035544	CG15021	2.0674	1.5158E-15	FALSE	FALSE	FALSE
FBgn0036165	chrb	2.0616	6.2658E-64	FALSE	FALSE	**TRUE**
FBgn0039584	beat-VI	2.0616	3.5459E-71	FALSE	FALSE	FALSE
FBgn0263987	spoon	2.0545	4.2653E-94	**TRUE**	FALSE	FALSE
FBgn0267758	CR46089	2.0521	6.2708E-03	FALSE	FALSE	FALSE
FBgn0263220	Hk	2.0513	6.9387E-117	FALSE	FALSE	FALSE

geneID	geneName	log2FoldChange	padj	RNA-binding protein	TF/DNA binding	Syp target
FBgn0026160	tna	2.0490	4.5948E-98	FALSE	**TRUE**	**TRUE**
FBgn0266220	CR44915	2.0483	2.0427E-03	FALSE	FALSE	FALSE
FBgn0266000	CG44774	2.0478	8.7796E-175	FALSE	FALSE	**TRUE**
FBgn0033777	CG17574	2.0449	1.5677E-90	FALSE	FALSE	FALSE
FBgn0002772	Mlc1	2.0408	1.2996E-09	FALSE	FALSE	**TRUE**
FBgn0266579	tau	2.0329	1.3217E-111	FALSE	FALSE	FALSE
FBgn0010341	Cdc42	2.0299	9.1881E-170	FALSE	FALSE	**TRUE**
FBgn0031091	Phf7	2.0263	3.5196E-53	FALSE	FALSE	FALSE
FBgn0263993	CG43736	2.0237	9.2922E-101	FALSE	FALSE	FALSE
FBgn0053200	VepD	2.0232	5.9978E-30	FALSE	FALSE	**TRUE**
FBgn0267199	CR45639	2.0205	5.0332E-05	FALSE	FALSE	FALSE
FBgn0035538	DopEcR	2.0145	9.1687E-67	FALSE	FALSE	FALSE
FBgn0265611	CR44429	2.0113	2.9972E-05	FALSE	FALSE	FALSE
FBgn0030672	CG9281	2.0101	6.8436E-158	FALSE	FALSE	FALSE
FBgn0265634	CR44441	2.0078	1.9148E-03	FALSE	FALSE	FALSE
FBgn0250869	CG42240	2.0072	3.9489E-44	FALSE	FALSE	**TRUE**
FBgn0033926	Arc1	2.0072	1.8427E-83	FALSE	FALSE	FALSE
FBgn0003429	slo	2.0064	1.9211E-81	FALSE	FALSE	FALSE
FBgn0017581	Lk6	2.0061	7.8515E-158	FALSE	FALSE	FALSE
FBgn0033166	Eaf	2.0054	5.3523E-111	FALSE	FALSE	FALSE
FBgn0033872	CG6329	2.0052	4.3551E-138	FALSE	FALSE	**TRUE**
FBgn0036516	CG7656	2.0039	1.1387E-95	FALSE	FALSE	FALSE
FBgn0035986	CG4022	2.0028	2.4118E-70	FALSE	FALSE	FALSE
FBgn0036575	CG5157	2.0022	1.8043E-16	FALSE	FALSE	FALSE
FBgn0243512	puc	2.0009	2.1777E-106	FALSE	FALSE	FALSE
FBgn0005655	PCNA	1.9998	8.2756E-128	FALSE	FALSE	**TRUE**
FBgn0038839	Ktl	1.9996	2.1356E-87	FALSE	FALSE	FALSE
FBgn0263970	CR43724	1.9967	1.3101E-04	FALSE	FALSE	FALSE
FBgn0004509	Fur1	1.9932	3.1046E-59	FALSE	FALSE	FALSE
FBgn0030617	CG9095	1.9889	3.1156E-13	FALSE	FALSE	**TRUE**
FBgn0265276	l(3)neo38	1.9823	1.5103E-92	FALSE	**TRUE**	**TRUE**
FBgn0003310	S	1.9811	3.1980E-76	FALSE	FALSE	FALSE
FBgn0011217	eff	1.9800	1.0032E-110	FALSE	FALSE	FALSE
FBgn0039675	ppk21	1.9782	1.0228E-03	FALSE	FALSE	FALSE
FBgn0010501	Dcp-1	1.9779	6.8990E-131	FALSE	FALSE	FALSE
FBgn0051687	CG31687	1.9749	4.1767E-17	FALSE	FALSE	FALSE
FBgn0265595	CG44422	1.9737	6.2780E-57	FALSE	FALSE	**TRUE**
FBgn0015024	Cklalpha	1.9726	1.6337E-158	FALSE	FALSE	**TRUE**
FBgn0031089	CG9572	1.9713	7.7948E-08	FALSE	FALSE	FALSE
FBgn0037635	CG9837	1.9681	5.0732E-08	FALSE	FALSE	FALSE
FBgn0032297	CG17124	1.9671	3.8520E-11	FALSE	FALSE	**TRUE**
FBgn0032420	CG6583	1.9652	1.5264E-35	FALSE	FALSE	**TRUE**

geneID	geneName	log2FoldChange	padj	RNA-binding protein	TF/DNA binding	Syp target
FBgn0000535	eag	1.9629	5.7091E-68	FALSE	FALSE	FALSE
FBgn0264562	Hr4	1.9627	3.4110E-06	FALSE	**TRUE**	FALSE
FBgn0052039	CG32039	1.9620	1.0110E-44	FALSE	FALSE	**TRUE**
FBgn0000382	csw	1.9607	1.5216E-89	FALSE	FALSE	FALSE
FBgn0030114	CG17754	1.9583	1.1509E-67	FALSE	FALSE	**TRUE**
FBgn0261258	rgn	1.9582	1.8684E-149	FALSE	FALSE	FALSE
FBgn0001994	crp	1.9562	3.2101E-111	FALSE	**TRUE**	**TRUE**
FBgn0010300	brat	1.9560	3.6059E-69	**TRUE**	**TRUE**	**TRUE**
FBgn0033252	CG12769	1.9483	1.4188E-07	FALSE	**TRUE**	FALSE
FBgn0243513	cnir	1.9481	2.1907E-49	FALSE	FALSE	FALSE
FBgn0033649	pyr	1.9459	5.8672E-60	FALSE	FALSE	FALSE
FBgn0036661	CG9705	1.9354	2.4409E-93	**TRUE**	**TRUE**	**TRUE**
FBgn0030351	CG1840	1.9330	7.7229E-35	FALSE	FALSE	FALSE
FBgn0052521	CG32521	1.9318	1.1896E-91	FALSE	FALSE	FALSE
FBgn0030406	CG1463	1.9300	2.0148E-67	FALSE	FALSE	FALSE
FBgn0031770	CG13995	1.9299	3.5477E-113	FALSE	FALSE	FALSE
FBgn0002525	Lam	1.9296	8.3240E-186	FALSE	FALSE	FALSE
FBgn0036198	crim	1.9272	1.4342E-57	FALSE	FALSE	FALSE
FBgn0264501	CR43900	1.9268	1.5267E-03	FALSE	FALSE	FALSE
FBgn0267590	CR45928	1.9252	7.2621E-05	FALSE	FALSE	FALSE
FBgn0027843	CAH2	1.9242	1.0064E-38	FALSE	FALSE	FALSE
FBgn0003507	srp	1.9213	1.7945E-04	FALSE	**TRUE**	FALSE
FBgn0004854	B-H2	1.9211	4.1810E-18	FALSE	**TRUE**	**TRUE**
FBgn0264821	CR44029	1.9203	4.5254E-10	FALSE	FALSE	**TRUE**
FBgn0053547	Rim	1.9197	2.7275E-86	FALSE	FALSE	FALSE
FBgn0037697	GstZ2	1.9190	9.0228E-83	FALSE	FALSE	**TRUE**
FBgn0000173	ben	1.9184	1.6214E-91	FALSE	FALSE	**TRUE**
FBgn0003165	pum	1.9169	1.1977E-96	**TRUE**	FALSE	**TRUE**
FBgn0021800	Reph	1.9150	5.4868E-63	FALSE	FALSE	**TRUE**
FBgn0033551	CG7222	1.9148	2.0224E-104	FALSE	FALSE	**TRUE**
FBgn0031629	Clect27	1.9139	8.5265E-04	FALSE	FALSE	FALSE
FBgn0030559	CG13404	1.9127	1.5026E-29	FALSE	FALSE	**TRUE**
FBgn0029903	pod1	1.9124	1.0669E-91	FALSE	FALSE	FALSE
FBgn0013759	CASK	1.9117	9.5534E-118	FALSE	FALSE	FALSE
FBgn0000489	Pka-C3	1.9081	1.9303E-13	FALSE	FALSE	**TRUE**
FBgn0014343	mirr	1.9077	4.3709E-105	FALSE	**TRUE**	FALSE
FBgn0035481	CG12605	1.9070	8.8604E-64	FALSE	**TRUE**	**TRUE**
FBgn0040285	Scamp	1.9051	1.5273E-86	FALSE	FALSE	FALSE
FBgn0036090	CG8009	1.9047	1.4919E-32	FALSE	FALSE	**TRUE**
FBgn0015519	nAChRalpha3	1.9046	1.8562E-93	FALSE	FALSE	FALSE
FBgn0005648	Pabp2	1.9027	1.7479E-92	**TRUE**	FALSE	**TRUE**
FBgn0001257	ImpL2	1.9027	5.5013E-132	FALSE	FALSE	FALSE

geneID	geneName	log2FoldChange	padj	RNA-binding protein	TF/DNA binding	Syp target
FBgn0036534	DCP2	1.9024	2.6285E-106	**TRUE**	FALSE	**TRUE**
FBgn0053639	CG33639	1.8995	2.2308E-78	FALSE	FALSE	**TRUE**
FBgn0033639	CG9003	1.8975	1.0482E-13	FALSE	FALSE	FALSE
FBgn0035023	ITP	1.8955	1.1425E-95	FALSE	FALSE	**TRUE**
FBgn0011837	Tis11	1.8950	1.9623E-71	**TRUE**	FALSE	**TRUE**
FBgn0003710	tipE	1.8904	1.4843E-66	FALSE	FALSE	FALSE
FBgn0037534	CG2781	1.8903	3.6207E-12	FALSE	FALSE	**TRUE**
FBgn0000463	Dl	1.8898	1.3466E-60	FALSE	FALSE	FALSE
FBgn0011224	heph	1.8884	1.8901E-81	**TRUE**	FALSE	**TRUE**
FBgn0053988	Mid1	1.8862	3.8553E-76	FALSE	FALSE	FALSE
FBgn0082582	tmod	1.8829	1.0698E-126	FALSE	FALSE	FALSE
FBgn0262035	CG42846	1.8826	4.2655E-03	FALSE	FALSE	FALSE
FBgn0036451	CG9425	1.8817	2.1993E-107	**TRUE**	FALSE	FALSE
FBgn0014388	sty	1.8813	5.1092E-58	FALSE	FALSE	**TRUE**
FBgn0032293	Dpy-30L1	1.8809	1.3143E-69	FALSE	FALSE	FALSE
FBgn0259222	CG42322	1.8798	8.3670E-105	FALSE	FALSE	FALSE
FBgn0001253	ImpE1	1.8792	5.7803E-07	FALSE	FALSE	FALSE
FBgn0264922	smt3	1.8777	4.4742E-88	FALSE	FALSE	**TRUE**
FBgn0035553	CG13722	1.8771	1.5485E-03	FALSE	FALSE	FALSE
FBgn0029962	CG1402	1.8716	2.6781E-67	FALSE	FALSE	**TRUE**
FBgn0004635	rho	1.8671	3.3537E-78	FALSE	FALSE	FALSE
FBgn0051324	CG31324	1.8656	7.1803E-08	FALSE	FALSE	**TRUE**
FBgn0001197	His2Av	1.8636	3.2416E-148	FALSE	FALSE	**TRUE**
FBgn0040942	CG12643	1.8617	9.5914E-46	FALSE	FALSE	**TRUE**
FBgn0027795	CG14785	1.8600	2.7952E-26	FALSE	FALSE	FALSE
FBgn0266848	wap	1.8582	3.5164E-83	FALSE	FALSE	FALSE
FBgn0035020	CG13585	1.8539	2.4103E-84	FALSE	FALSE	**TRUE**
FBgn0040571	CG17193	1.8535	1.3266E-33	FALSE	FALSE	FALSE
FBgn0029896	CG3168	1.8530	1.4621E-68	FALSE	FALSE	FALSE
FBgn0285913	red	1.8496	6.2875E-92	FALSE	FALSE	FALSE
FBgn0015222	Fer1HCH	1.8493	7.9514E-160	FALSE	FALSE	**TRUE**
FBgn0028863	CG4587	1.8453	1.3328E-44	FALSE	FALSE	FALSE
FBgn0263132	Cht6	1.8416	1.9913E-45	FALSE	FALSE	FALSE
FBgn0030377	CG1924	1.8415	8.0758E-05	FALSE	FALSE	FALSE
FBgn0263442	CR43465	1.8399	1.8295E-05	FALSE	FALSE	FALSE
FBgn0053516	dpr3	1.8358	7.2831E-72	FALSE	FALSE	FALSE
FBgn0025394	inc	1.8343	1.0486E-111	FALSE	FALSE	FALSE
FBgn0265512	mlt	1.8319	8.5627E-70	FALSE	FALSE	**TRUE**
FBgn0052296	Mrtf	1.8313	4.7696E-67	FALSE	**TRUE**	**TRUE**
FBgn0032816	Nf-YB	1.8257	1.1325E-61	FALSE	**TRUE**	**TRUE**
FBgn0038704	CG5316	1.8240	1.0124E-78	**TRUE**	FALSE	FALSE
FBgn0063498	GstE2	1.8187	1.1786E-19	FALSE	FALSE	**TRUE**

geneID	geneName	log2FoldChange	padj	RNA-binding protein	TF/DNA binding	Syp target
FBgn0036032	CG16711	1.8172	2.1388E-90	FALSE	FALSE	FALSE
FBgn0030869	Socs16D	1.8145	6.4829E-75	FALSE	FALSE	FALSE
FBgn0000015	Abd-B	1.8131	1.3589E-51	FALSE	**TRUE**	**TRUE**
FBgn0038980	Octbeta1R	1.8094	1.8592E-84	FALSE	FALSE	FALSE
FBgn0011817	nmo	1.8088	5.4541E-71	FALSE	FALSE	**TRUE**
FBgn0011704	RnrS	1.8076	6.9893E-87	FALSE	FALSE	**TRUE**
FBgn0265809	CR44598	1.8074	5.5110E-03	FALSE	FALSE	FALSE
FBgn0036428	Gbs-70E	1.8073	1.4535E-25	FALSE	FALSE	**TRUE**
FBgn0038653	CG18208	1.8069	5.3197E-64	FALSE	FALSE	FALSE
FBgn0263111	cac	1.8054	1.1607E-85	FALSE	FALSE	FALSE
FBgn0024989	CG3777	1.8033	3.5556E-27	FALSE	FALSE	FALSE
FBgn0020378	Sp1	1.8030	1.0528E-46	FALSE	**TRUE**	**TRUE**
FBgn0040918	schlank	1.8024	2.5587E-80	FALSE	**TRUE**	FALSE
FBgn0038063	Octbeta2R	1.8004	1.9051E-49	FALSE	**TRUE**	FALSE
FBgn0004362	HmgD	1.8002	1.1507E-110	FALSE	**TRUE**	FALSE
FBgn0039132	AP-1sigma	1.7990	2.0472E-69	FALSE	FALSE	FALSE
FBgn0259110	mmd	1.7974	1.5950E-143	FALSE	FALSE	FALSE
FBgn0026061	Mipp1	1.7953	3.7303E-05	FALSE	FALSE	FALSE
FBgn0265808	CR44597	1.7949	1.1609E-04	FALSE	FALSE	FALSE
FBgn0000659	fkh	1.7898	4.2228E-66	FALSE	**TRUE**	**TRUE**
FBgn0035477	CG14982	1.7862	4.3377E-78	FALSE	FALSE	FALSE
FBgn0015799	Rbf	1.7855	1.1318E-129	FALSE	**TRUE**	FALSE
FBgn0261791	SNRPG	1.7835	6.4147E-47	**TRUE**	FALSE	FALSE
FBgn0003520	stau	1.7815	2.9509E-101	**TRUE**	FALSE	**TRUE**
FBgn0025833	CG8910	1.7807	2.2832E-51	FALSE	FALSE	FALSE
FBgn0030658	CG7872	1.7755	1.4621E-65	FALSE	FALSE	FALSE
FBgn0083228	Frq2	1.7719	1.3908E-58	FALSE	FALSE	FALSE
FBgn0036734	CG7564	1.7718	3.2117E-79	FALSE	FALSE	FALSE
FBgn0014037	Su(Tpl)	1.7710	7.2977E-76	FALSE	**TRUE**	FALSE
FBgn0264491	how	1.7648	1.7252E-41	**TRUE**	FALSE	**TRUE**
FBgn0083991	CG34155	1.7636	6.7482E-47	FALSE	FALSE	**TRUE**
FBgn0030976	CG7378	1.7627	1.1227E-59	FALSE	FALSE	FALSE
FBgn0037416	Osi9	1.7622	2.5912E-04	FALSE	FALSE	FALSE
FBgn0027492	wdb	1.7603	6.7885E-88	FALSE	FALSE	FALSE
FBgn0044047	Ilp6	1.7513	3.3840E-26	FALSE	FALSE	**TRUE**
FBgn0264087	Slob	1.7491	2.0132E-51	FALSE	FALSE	FALSE
FBgn0035914	CG6282	1.7459	2.3267E-58	FALSE	FALSE	FALSE
FBgn0030890	CG7536	1.7444	1.0437E-56	FALSE	FALSE	FALSE
FBgn0283651	CG46301	1.7424	1.3874E-56	FALSE	FALSE	**TRUE**
FBgn0038492	Mur89F	1.7416	3.6909E-04	FALSE	FALSE	FALSE
FBgn0033526	Caf1-105	1.7415	1.9258E-53	FALSE	FALSE	FALSE
FBgn0264078	Flo2	1.7414	1.2672E-52	FALSE	FALSE	**TRUE**

geneID	geneName	log2FoldChange	padj	RNA-binding protein	TF/DNA binding	Syp target
FBgn0034282	Mapmodulin	1.7396	1.8215E-112	FALSE	FALSE	**TRUE**
FBgn0003134	Pp1alpha-96A	1.7377	8.6772E-132	FALSE	FALSE	**TRUE**
FBgn0013954	FK506-bp2	1.7353	2.2753E-118	FALSE	FALSE	FALSE
FBgn0030090	fend	1.7348	4.4970E-102	FALSE	FALSE	**TRUE**
FBgn0267821	da	1.7306	7.6184E-113	FALSE	**TRUE**	FALSE
FBgn0027108	Inx2	1.7289	3.0463E-82	FALSE	FALSE	FALSE
FBgn0035593	CG4603	1.7288	5.9869E-66	FALSE	FALSE	**TRUE**
FBgn0263511	Vsx1	1.7286	3.2064E-51	FALSE	**TRUE**	**TRUE**
FBgn0030809	Ubr1	1.7272	8.8609E-124	FALSE	FALSE	FALSE
FBgn0086778	nAChRalpha7	1.7201	9.8980E-26	FALSE	FALSE	FALSE
FBgn0035772	Sh3beta	1.7199	1.4456E-67	FALSE	FALSE	**TRUE**
FBgn0283451	br	1.7199	7.5544E-88	FALSE	**TRUE**	**TRUE**
FBgn0000299	Col4a1	1.7196	4.6308E-32	FALSE	FALSE	FALSE
FBgn0026144	CBP	1.7159	6.7717E-96	FALSE	FALSE	**TRUE**
FBgn0030812	wcy	1.7155	9.8860E-67	FALSE	FALSE	FALSE
FBgn0036589	CG13067	1.7119	5.7224E-05	FALSE	FALSE	FALSE
FBgn0037831	Cap-H2	1.7107	8.7568E-58	FALSE	FALSE	FALSE
FBgn0014163	fax	1.7053	4.3801E-48	FALSE	FALSE	**TRUE**
FBgn0032230	lft	1.7032	6.3348E-26	FALSE	FALSE	**TRUE**
FBgn0004907	14-3-3zeta	1.7029	4.6683E-95	FALSE	**TRUE**	**TRUE**
FBgn0030933	CG6470	1.7020	3.6614E-10	FALSE	**TRUE**	FALSE
FBgn0036746	Crtc	1.7006	4.0038E-43	FALSE	FALSE	**TRUE**
FBgn0001145	Gs2	1.7001	7.8831E-51	FALSE	FALSE	**TRUE**
FBgn0030913	CG6123	1.6980	3.3885E-38	FALSE	FALSE	FALSE
FBgn0003302	rux	1.6979	7.5897E-55	FALSE	FALSE	FALSE
FBgn0085430	CG34401	1.6971	2.3736E-58	FALSE	FALSE	FALSE
FBgn0024734	PRL-1	1.6953	5.2063E-13	FALSE	FALSE	**TRUE**
FBgn0030997	CG7990	1.6943	1.5235E-56	FALSE	FALSE	FALSE
FBgn0000490	dpp	1.6933	3.2362E-24	FALSE	FALSE	FALSE
FBgn0024985	CG11448	1.6926	8.7050E-103	FALSE	FALSE	FALSE
FBgn0029778	RhoGAP5A	1.6911	2.4603E-67	FALSE	FALSE	**TRUE**
FBgn0263503	CR43492	1.6875	9.5244E-03	FALSE	FALSE	FALSE
FBgn0000606	eve	1.6864	1.1699E-10	FALSE	**TRUE**	FALSE
FBgn0034009	CG8155	1.6854	3.3099E-70	FALSE	FALSE	FALSE
FBgn0030863	CG8188	1.6808	2.3629E-82	FALSE	FALSE	**TRUE**
FBgn0031150	bves	1.6783	2.7884E-56	FALSE	FALSE	FALSE
FBgn0037798	CG12817	1.6765	6.1562E-39	FALSE	FALSE	FALSE
FBgn0032414	CG17211	1.6735	4.5915E-70	FALSE	FALSE	FALSE
FBgn0027608	CG2082	1.6733	4.5659E-34	FALSE	FALSE	FALSE
FBgn0050009	CR30009	1.6695	1.5073E-30	FALSE	FALSE	**TRUE**
FBgn0015609	CadN	1.6641	1.1887E-70	FALSE	FALSE	FALSE
FBgn0034789	PIP5K59B	1.6637	1.9399E-75	FALSE	FALSE	FALSE

geneID	geneName	log2FoldChange	padj	RNA-binding protein	TF/DNA binding	Syp target
FBgn0035612	frm	1.6636	1.4072E-17	FALSE	FALSE	**TRUE**
FBgn0010379	Akt1	1.6622	5.3709E-53	FALSE	FALSE	FALSE
FBgn0025360	Optix	1.6620	1.6320E-93	FALSE	**TRUE**	FALSE
FBgn0029996	UbcE2H	1.6614	1.0534E-45	FALSE	FALSE	**TRUE**
FBgn0035816	CG13685	1.6610	8.6149E-33	FALSE	FALSE	**TRUE**
FBgn0028360	Cdc7	1.6599	4.2330E-66	FALSE	FALSE	FALSE
FBgn0042696	Nfl	1.6588	7.7505E-35	FALSE	**TRUE**	FALSE
FBgn0026084	cib	1.6584	9.9526E-84	FALSE	FALSE	**TRUE**
FBgn0267796	Tmc	1.6579	7.4488E-07	FALSE	FALSE	FALSE
FBgn0053542	upd3	1.6573	8.8207E-03	FALSE	FALSE	FALSE
FBgn0015622	Cnx99A	1.6569	3.7357E-101	FALSE	FALSE	FALSE
FBgn0011666	msi	1.6555	7.9078E-79	**TRUE**	FALSE	**TRUE**
FBgn0264307	orb2	1.6523	1.9721E-29	**TRUE**	FALSE	FALSE
FBgn0034534	maf-S	1.6484	1.5927E-34	FALSE	**TRUE**	FALSE
FBgn0037717	CG8301	1.6481	1.1336E-33	FALSE	**TRUE**	FALSE
FBgn0015778	rin	1.6463	1.2049E-60	**TRUE**	FALSE	**TRUE**
FBgn0001297	kay	1.6456	2.9585E-98	FALSE	**TRUE**	FALSE
FBgn0026582	Hmg-2	1.6456	5.3669E-41	FALSE	**TRUE**	FALSE
FBgn0266768	CR45233	1.6451	2.4544E-05	FALSE	FALSE	FALSE
FBgn0263617	CR43626	1.6438	8.1427E-08	FALSE	FALSE	**TRUE**
FBgn0034391	CG15080	1.6435	2.9149E-08	FALSE	FALSE	FALSE
FBgn0010348	Arf79F	1.6431	1.7151E-49	FALSE	FALSE	FALSE
FBgn0033802	CG17724	1.6397	3.7631E-44	FALSE	**TRUE**	FALSE
FBgn0002933	ng1	1.6367	5.7652E-04	FALSE	FALSE	FALSE
FBgn0036537	CG18081	1.6348	2.0420E-47	FALSE	FALSE	**TRUE**
FBgn0020443	eRF3	1.6348	1.3262E-53	**TRUE**	FALSE	FALSE
FBgn0263353	CG11000	1.6348	5.8913E-46	FALSE	FALSE	FALSE
FBgn0038282	dpr9	1.6323	1.7797E-48	FALSE	FALSE	FALSE
FBgn0261674	CG42709	1.6323	7.9391E-57	FALSE	FALSE	FALSE
FBgn0262733	Src64B	1.6279	2.2228E-39	FALSE	FALSE	**TRUE**
FBgn0051660	smog	1.6247	2.2685E-79	FALSE	FALSE	FALSE
FBgn0061515	endos	1.6211	4.3472E-125	FALSE	FALSE	**TRUE**
FBgn0034145	CG5065	1.6191	2.2911E-82	FALSE	FALSE	FALSE
FBgn0004652	fru	1.6184	6.4011E-63	FALSE	**TRUE**	FALSE
FBgn0015286	Rala	1.6183	1.8633E-34	FALSE	FALSE	FALSE
FBgn0004870	bab1	1.6168	4.7959E-37	FALSE	**TRUE**	**TRUE**
FBgn0261505	CR42653	1.6158	2.2825E-03	FALSE	FALSE	FALSE
FBgn0015524	otp	1.6155	8.2548E-52	FALSE	**TRUE**	FALSE
FBgn0264507	CR43906	1.6152	2.4443E-16	FALSE	FALSE	FALSE
FBgn0046776	CR14033	1.6128	4.8137E-05	FALSE	FALSE	FALSE
FBgn0035936	Tsp66E	1.6125	7.6121E-66	FALSE	FALSE	FALSE
FBgn0031955	CG14535	1.6113	7.0479E-52	FALSE	FALSE	FALSE

geneID	geneName	log2FoldChange	padj	RNA-binding protein	TF/DNA binding	Syp target
FBgn0023212	EloB	1.6086	1.8029E-74	FALSE	**TRUE**	**TRUE**
FBgn0035016	CG4612	1.6077	6.4483E-57	**TRUE**	FALSE	**TRUE**
FBgn0030391	Rab40	1.6076	7.5278E-50	FALSE	FALSE	FALSE
FBgn0259146	fid	1.6058	5.8983E-42	FALSE	FALSE	FALSE
FBgn0026760	Tehao	1.6009	1.1198E-03	FALSE	FALSE	FALSE
FBgn0085447	sif	1.5991	1.0366E-39	FALSE	FALSE	FALSE
FBgn0003042	Pc	1.5972	1.2099E-39	FALSE	**TRUE**	**TRUE**
FBgn0040239	bc10	1.5969	6.6561E-45	FALSE	FALSE	FALSE
FBgn0052062	Rbfox1	1.5926	2.0797E-62	**TRUE**	FALSE	**TRUE**
FBgn0029504	CHES-1-like	1.5924	3.3196E-60	FALSE	**TRUE**	FALSE
FBgn0011746	ana	1.5870	2.7618E-27	FALSE	FALSE	FALSE
FBgn0034091	mrj	1.5861	6.3993E-28	FALSE	FALSE	**TRUE**
FBgn0037481	MAGE	1.5850	4.1997E-28	FALSE	FALSE	**TRUE**
FBgn0037229	CG9766	1.5772	1.3054E-06	FALSE	FALSE	FALSE
FBgn0004573	5-HT7	1.5761	2.2225E-35	FALSE	FALSE	FALSE
FBgn0037614	TMEM216	1.5721	6.7650E-38	FALSE	FALSE	**TRUE**
FBgn0040609	CG3348	1.5717	3.4798E-03	FALSE	FALSE	FALSE
FBgn0005586	Rab3	1.5705	1.3501E-86	FALSE	FALSE	FALSE
FBgn0030766	mthl1	1.5693	2.0189E-73	FALSE	FALSE	FALSE
FBgn0003888	betaTub60D	1.5690	2.8453E-45	FALSE	FALSE	FALSE
FBgn0004177	mts	1.5674	1.9973E-79	FALSE	FALSE	**TRUE**
FBgn0040020	MED21	1.5660	2.3593E-40	FALSE	FALSE	**TRUE**
FBgn0003525	stg	1.5651	2.6479E-73	FALSE	FALSE	**TRUE**
FBgn0267319	CR45755	1.5650	2.1079E-03	FALSE	FALSE	FALSE
FBgn0003334	Scm	1.5646	8.0746E-52	FALSE	**TRUE**	FALSE
FBgn0028331	l(1)G0289	1.5640	5.2537E-72	FALSE	FALSE	FALSE
FBgn0029911	CG14435	1.5637	1.5250E-42	FALSE	FALSE	**TRUE**
FBgn0035993	Nf-YA	1.5633	1.1714E-64	FALSE	**TRUE**	**TRUE**
FBgn0003997	hid	1.5628	5.2810E-19	FALSE	FALSE	**TRUE**
FBgn0038922	Idh3b	1.5610	5.2458E-94	FALSE	FALSE	**TRUE**
FBgn0263995	cpo	1.5605	8.1743E-62	**TRUE**	FALSE	**TRUE**
FBgn0024941	RSG7	1.5584	2.3235E-46	FALSE	FALSE	**TRUE**
FBgn0033463	CG1513	1.5550	1.5030E-58	FALSE	FALSE	FALSE
FBgn0010280	Taf4	1.5548	2.5242E-77	FALSE	**TRUE**	FALSE
FBgn0004657	mys	1.5538	3.9957E-76	FALSE	FALSE	FALSE
FBgn0039479	CG14257	1.5532	7.8739E-03	FALSE	FALSE	FALSE
FBgn0033274	CG14757	1.5530	2.0833E-05	FALSE	FALSE	**TRUE**
FBgn0035423	eIF1	1.5530	2.3683E-35	**TRUE**	FALSE	**TRUE**
FBgn0002629	E(spl)m4-BFM	1.5528	3.0395E-40	FALSE	FALSE	FALSE
FBgn0039937	fd102C	1.5513	6.8588E-22	FALSE	**TRUE**	FALSE
FBgn0266124	ghi	1.5494	6.2798E-42	FALSE	FALSE	FALSE
FBgn0031896	CG4502	1.5492	9.3014E-60	FALSE	FALSE	FALSE

geneID	geneName	log2FoldChange	padj	RNA-binding protein	TF/DNA binding	Syp target
FBgn0036411	Sox21a	1.5479	1.4605E-19	FALSE	**TRUE**	FALSE
FBgn0014010	Rab5	1.5479	3.5715E-98	FALSE	FALSE	**TRUE**
FBgn0036285	toe	1.5441	1.8367E-04	FALSE	**TRUE**	FALSE
FBgn0037525	CG17816	1.5421	3.8805E-46	FALSE	FALSE	FALSE
FBgn0000575	emc	1.5416	3.3260E-46	FALSE	**TRUE**	**TRUE**
FBgn0263345	CR43426	1.5406	2.7026E-14	FALSE	FALSE	**TRUE**
FBgn0010316	dap	1.5397	7.5117E-58	FALSE	FALSE	**TRUE**
FBgn0036373	Tgi	1.5357	4.4738E-40	FALSE	FALSE	FALSE
FBgn0035148	CG3402	1.5332	1.2684E-51	FALSE	FALSE	FALSE
FBgn0022987	qkr54B	1.5325	1.0468E-37	**TRUE**	FALSE	FALSE
FBgn0037849	CG4596	1.5321	6.0486E-55	FALSE	FALSE	FALSE
FBgn0040066	wds	1.5310	4.2308E-66	FALSE	FALSE	**TRUE**
FBgn0037153	olf413	1.5299	4.0291E-72	FALSE	FALSE	FALSE
FBgn0017572	Mo25	1.5248	3.9524E-48	FALSE	FALSE	**TRUE**
FBgn0033631	Sod3	1.5248	7.3960E-29	FALSE	FALSE	FALSE
FBgn0004687	Mlc-c	1.5233	1.2786E-50	FALSE	FALSE	**TRUE**
FBgn0036111	Aps	1.5222	9.1874E-53	FALSE	FALSE	**TRUE**
FBgn0264975	Nrg	1.5222	1.7341E-73	FALSE	FALSE	FALSE
FBgn0005619	Hdc	1.5192	1.1912E-09	FALSE	FALSE	FALSE
FBgn0002773	Mlc2	1.5184	1.6207E-06	FALSE	FALSE	FALSE
FBgn0262954	Rpb12	1.5157	1.5567E-49	FALSE	FALSE	**TRUE**
FBgn0085220	Ufm1	1.5153	1.9952E-42	FALSE	FALSE	FALSE
FBgn0001319	kn	1.5151	3.1367E-35	FALSE	**TRUE**	FALSE
FBgn0030791	CG9132	1.5131	8.0693E-59	FALSE	FALSE	**TRUE**
FBgn0267571	CR45911	1.5129	2.9914E-04	FALSE	FALSE	FALSE
FBgn0085383	CG34354	1.5128	6.3196E-45	**TRUE**	FALSE	FALSE
FBgn0005775	Con	1.5123	6.4448E-50	FALSE	FALSE	FALSE
FBgn0011476	l(3)neo43	1.5122	2.9082E-15	FALSE	FALSE	FALSE
FBgn0261804	CG42750	1.5117	4.2024E-43	FALSE	FALSE	FALSE
FBgn0000547	ed	1.5051	1.2412E-69	FALSE	FALSE	FALSE
FBgn0015372	RabX1	1.5048	1.2352E-44	FALSE	FALSE	FALSE
FBgn0003984	vn	1.5029	2.9022E-19	FALSE	FALSE	FALSE
FBgn0038181	CG9297	1.5019	2.7168E-03	FALSE	FALSE	FALSE
FBgn0001090	bnb	1.5003	5.7938E-33	FALSE	FALSE	FALSE
FBgn0026149	BCL7-like	1.4998	2.7294E-76	FALSE	FALSE	**TRUE**
FBgn0263118	tx	1.4993	1.8981E-06	FALSE	**TRUE**	**TRUE**
FBgn0025549	unc-119	1.4984	3.3710E-48	FALSE	FALSE	**TRUE**
FBgn0030029	CG15343	1.4983	5.0843E-08	FALSE	FALSE	FALSE
FBgn0002565	Lsp2	1.4947	9.0089E-06	FALSE	FALSE	FALSE
FBgn0267376	SelR	1.4944	3.2106E-53	FALSE	FALSE	FALSE
FBgn0033925	CG8617	1.4928	1.4632E-55	FALSE	FALSE	FALSE
FBgn0034903	sona	1.4919	1.3120E-04	FALSE	FALSE	FALSE

geneID	geneName	log2FoldChange	padj	RNA-binding protein	TF/DNA binding	Syp target
FBgn0034435	fest	1.4889	2.4456E-03	FALSE	FALSE	**TRUE**
FBgn0000276	CecA1	1.4882	8.4582E-04	FALSE	FALSE	FALSE
FBgn0011290	Taf12	1.4878	3.9729E-73	FALSE	**TRUE**	**TRUE**
FBgn0262730	dtn	1.4875	1.7038E-54	FALSE	FALSE	FALSE
FBgn0003741	tra	1.4866	7.7063E-39	FALSE	FALSE	FALSE
FBgn0015777	nrv2	1.4853	7.0296E-62	FALSE	FALSE	FALSE
FBgn0037728	CG16817	1.4841	1.8171E-45	FALSE	FALSE	FALSE
FBgn0259734	Nost	1.4815	1.7704E-13	FALSE	FALSE	FALSE
FBgn0035699	CG13300	1.4814	3.0166E-39	FALSE	FALSE	FALSE
FBgn0028341	Ptpmeg2	1.4813	3.5307E-77	FALSE	FALSE	FALSE
FBgn0000181	bic	1.4810	8.3820E-123	FALSE	**TRUE**	FALSE
FBgn0032223	GATAd	1.4809	4.3908E-41	FALSE	**TRUE**	FALSE
FBgn0011259	Sema1a	1.4797	2.5133E-41	FALSE	FALSE	FALSE
FBgn0005694	Aef1	1.4771	1.6422E-43	FALSE	**TRUE**	FALSE
FBgn0004889	tws	1.4729	1.8093E-78	FALSE	FALSE	**TRUE**
FBgn0259171	Pde9	1.4725	2.2228E-39	FALSE	FALSE	FALSE
FBgn0031064	CG12531	1.4683	4.7615E-46	FALSE	FALSE	FALSE
FBgn0052650	CG32650	1.4681	1.6772E-04	FALSE	FALSE	FALSE
FBgn0035495	CG14989	1.4668	2.1876E-86	FALSE	FALSE	**TRUE**
FBgn0032723	ssp3	1.4649	2.4314E-48	FALSE	FALSE	FALSE
FBgn0260400	elav	1.4591	1.8083E-47	**TRUE**	FALSE	**TRUE**
FBgn0011288	Snap25	1.4581	9.9346E-37	FALSE	FALSE	FALSE
FBgn0046763	CG17278	1.4580	1.7692E-27	FALSE	FALSE	**TRUE**
FBgn0039358	CG5028	1.4563	2.5799E-70	FALSE	FALSE	FALSE
FBgn0035283	CG12024	1.4534	8.9481E-62	FALSE	FALSE	FALSE
FBgn0262511	Vha44	1.4533	1.3446E-78	FALSE	FALSE	FALSE
FBgn0052206	CG32206	1.4522	2.7711E-57	FALSE	FALSE	FALSE
FBgn0001215	Hrb98DE	1.4521	2.4508E-38	**TRUE**	FALSE	**TRUE**
FBgn0039808	CG12071	1.4510	2.2916E-74	FALSE	**TRUE**	FALSE
FBgn0028400	Syt4	1.4508	1.6829E-51	FALSE	FALSE	FALSE
FBgn0051908	CG31908	1.4502	1.5650E-59	FALSE	FALSE	FALSE
FBgn0029974	dpr14	1.4493	1.2099E-39	FALSE	FALSE	FALSE
FBgn0004567	slp2	1.4472	8.5464E-27	FALSE	**TRUE**	**TRUE**
FBgn0039465	Tsp97E	1.4465	6.3594E-82	FALSE	FALSE	FALSE
FBgn0002283	l(3)73Ah	1.4465	4.1863E-59	FALSE	**TRUE**	FALSE
FBgn0024987	ssx	1.4454	1.0646E-55	**TRUE**	FALSE	FALSE
FBgn0031652	jet	1.4440	1.2482E-22	FALSE	FALSE	FALSE
FBgn0283477	SF2	1.4432	1.9481E-37	**TRUE**	FALSE	FALSE
FBgn0261854	aPKC	1.4428	6.5638E-44	FALSE	FALSE	FALSE
FBgn0037141	DNApol-eta	1.4422	1.0945E-31	FALSE	FALSE	FALSE
FBgn0028894	GMF	1.4412	2.7504E-45	FALSE	FALSE	FALSE
FBgn0000286	Cf2	1.4404	8.8144E-34	FALSE	**TRUE**	**TRUE**

geneID	geneName	log2FoldChange	padj	RNA-binding protein	TF/DNA binding	Syp target
FBgn0034763	RYBP	1.4400	1.2042E-41	FALSE	FALSE	FALSE
FBgn0036583	CG13055	1.4380	1.4089E-14	FALSE	FALSE	FALSE
FBgn0028734	Fmr1	1.4359	4.0409E-43	**TRUE**	FALSE	**TRUE**
FBgn0015399	kek1	1.4344	1.1582E-59	FALSE	FALSE	**TRUE**
FBgn0003360	sesB	1.4334	4.2903E-66	FALSE	FALSE	FALSE
FBgn0027498	CG2061	1.4331	2.0585E-89	FALSE	FALSE	FALSE
FBgn0266687	CR45177	1.4322	4.8896E-03	FALSE	FALSE	FALSE
FBgn0259245	DIP-beta	1.4295	5.8426E-28	FALSE	FALSE	FALSE
FBgn0037556	CG9636	1.4290	3.8925E-71	FALSE	FALSE	**TRUE**
FBgn0038984	AdipoR	1.4287	1.1946E-66	FALSE	FALSE	FALSE
FBgn0037696	GstZ1	1.4285	7.6598E-05	FALSE	FALSE	FALSE
FBgn0030499	CG11178	1.4264	1.6864E-35	FALSE	FALSE	FALSE
FBgn0266051	CR44816	1.4209	2.5475E-04	FALSE	FALSE	FALSE
FBgn0266388	CR45028	1.4207	7.3497E-03	FALSE	FALSE	FALSE
FBgn0010014	CanB	1.4179	7.8382E-42	FALSE	FALSE	FALSE
FBgn0262515	VhaAC45	1.4165	2.4013E-57	FALSE	FALSE	FALSE
FBgn0001218	Hsc70-3	1.4157	4.2378E-38	FALSE	FALSE	FALSE
FBgn0027556	CG4928	1.4129	1.2633E-15	FALSE	FALSE	**TRUE**
FBgn0002735	E(spl)mgamma-HLH	1.4128	2.7426E-32	FALSE	**TRUE**	FALSE
FBgn0030049	Trf4-1	1.4116	6.5529E-64	FALSE	FALSE	FALSE
FBgn0037705	mura	1.4115	1.8493E-52	FALSE	FALSE	FALSE
FBgn0038603	PKD	1.4108	5.5189E-46	FALSE	FALSE	FALSE
FBgn0037551	Gie	1.4094	8.6893E-41	FALSE	FALSE	FALSE
FBgn0053111	CG33111	1.4093	1.1006E-23	FALSE	FALSE	FALSE
FBgn0261444	CG3638	1.4083	3.0611E-42	FALSE	FALSE	FALSE
FBgn0013750	Arf51F	1.4059	8.8846E-26	FALSE	FALSE	FALSE
FBgn0002631	E(spl)m5-HLH	1.4039	4.0751E-24	FALSE	**TRUE**	FALSE
FBgn0262739	AGO1	1.4037	3.8795E-46	**TRUE**	FALSE	**TRUE**
FBgn0039232	sosie	1.4006	1.5623E-04	FALSE	FALSE	FALSE
FBgn0030854	CG8289	1.3993	6.6013E-76	FALSE	FALSE	FALSE
FBgn0033791	Drl-2	1.3991	3.9750E-56	FALSE	FALSE	FALSE
FBgn0261793	Trf2	1.3987	7.3475E-41	FALSE	**TRUE**	**TRUE**
FBgn0004435	Galphaq	1.3969	6.2135E-39	FALSE	FALSE	FALSE
FBgn0030816	CG16700	1.3960	3.3797E-09	FALSE	FALSE	FALSE
FBgn0024944	Oamb	1.3953	2.4633E-32	FALSE	FALSE	FALSE
FBgn0262736	Vha16-1	1.3937	2.2779E-70	FALSE	FALSE	FALSE
FBgn0029881	pigs	1.3920	4.9316E-37	FALSE	FALSE	FALSE
FBgn0051522	CG31522	1.3904	1.1777E-49	FALSE	FALSE	FALSE
FBgn0015614	CanB2	1.3896	4.4344E-38	FALSE	FALSE	FALSE
FBgn0015737	Hmu	1.3876	9.5354E-76	**TRUE**	FALSE	FALSE
FBgn0031011	CG8034	1.3870	2.9918E-19	FALSE	FALSE	**TRUE**
FBgn0264000	GluRIB	1.3863	1.7268E-28	FALSE	FALSE	FALSE

geneID	geneName	log2FoldChange	padj	RNA-binding protein	TF/DNA binding	Syp target
FBgn0261085	Syt12	1.3813	1.0619E-10	FALSE	FALSE	FALSE
FBgn0031568	CG10019	1.3804	5.4013E-24	FALSE	FALSE	FALSE
FBgn0020255	Ran	1.3794	2.6324E-72	FALSE	FALSE	**TRUE**
FBgn0039816	CG11317	1.3793	2.4339E-41	FALSE	**TRUE**	FALSE
FBgn0015320	Ubc2	1.3771	8.3022E-35	FALSE	FALSE	**TRUE**
FBgn0052625	CG32625	1.3752	1.7893E-03	FALSE	FALSE	FALSE
FBgn0264823	CR44031	1.3729	6.1116E-03	FALSE	FALSE	FALSE
FBgn0003495	spz	1.3727	2.1503E-20	FALSE	FALSE	FALSE
FBgn0020767	Spred	1.3704	1.1243E-39	FALSE	FALSE	FALSE
FBgn0040718	CG15353	1.3696	1.5635E-17	FALSE	FALSE	**TRUE**
FBgn0003721	Tm1	1.3693	4.2145E-53	FALSE	FALSE	**TRUE**
FBgn0003410	sina	1.3685	7.7808E-44	FALSE	FALSE	**TRUE**
FBgn0033132	Tsp42Ej	1.3680	9.5059E-21	FALSE	FALSE	FALSE
FBgn0039209	REPTOR	1.3634	3.1252E-37	FALSE	**TRUE**	**TRUE**
FBgn0038311	CG14864	1.3624	8.5719E-06	FALSE	FALSE	FALSE
FBgn0003513	ss	1.3612	1.8495E-03	FALSE	**TRUE**	FALSE
FBgn0021738	Crg-1	1.3595	1.2088E-05	FALSE	FALSE	FALSE
FBgn0003866	tsh	1.3553	8.0042E-54	FALSE	**TRUE**	FALSE
FBgn0004606	zfh1	1.3517	2.5359E-39	FALSE	**TRUE**	FALSE
FBgn0036851	CG14082	1.3512	1.7962E-09	FALSE	FALSE	FALSE
FBgn0037807	CG6293	1.3496	1.5624E-11	FALSE	FALSE	FALSE
FBgn0030757	CG9902	1.3491	1.3062E-18	FALSE	FALSE	FALSE
FBgn0027538	beta4GalNAcTA	1.3488	9.0148E-23	FALSE	FALSE	FALSE
FBgn0026375	RhoGAPp190	1.3485	2.0378E-80	FALSE	FALSE	FALSE
FBgn0011586	e(r)	1.3470	6.8061E-45	FALSE	**TRUE**	FALSE
FBgn0053199	CG33199	1.3431	1.1678E-03	FALSE	FALSE	FALSE
FBgn0000567	Eip74EF	1.3408	5.1708E-30	FALSE	**TRUE**	FALSE
FBgn0051125	CG31125	1.3408	4.4763E-40	FALSE	FALSE	FALSE
FBgn0003300	run	1.3395	1.9439E-31	FALSE	**TRUE**	FALSE
FBgn0031816	Rchy1	1.3375	1.8053E-38	FALSE	FALSE	FALSE
FBgn0036967	SCCRO4	1.3341	8.6313E-51	FALSE	FALSE	FALSE
FBgn0265191	Glycogenin	1.3325	1.4838E-38	FALSE	FALSE	FALSE
FBgn0030719	eIF5	1.3315	5.4428E-07	**TRUE**	FALSE	FALSE
FBgn0035504	Teh4	1.3301	9.5214E-40	FALSE	FALSE	FALSE
FBgn0283535	Vha26	1.3289	4.1501E-75	FALSE	FALSE	**TRUE**
FBgn0051855	CG31855	1.3287	1.8540E-34	FALSE	FALSE	**TRUE**
FBgn0010894	sinu	1.3279	3.0010E-22	FALSE	FALSE	FALSE
FBgn0263776	CG43693	1.3261	2.3149E-32	FALSE	FALSE	FALSE
FBgn0052264	CG32264	1.3232	3.2671E-76	FALSE	**TRUE**	**TRUE**
FBgn0261648	salm	1.3222	2.5446E-40	FALSE	**TRUE**	FALSE
FBgn0263456	nwk	1.3217	1.3061E-45	FALSE	FALSE	FALSE
FBgn0266227	CR44922	1.3216	5.1538E-17	FALSE	FALSE	FALSE

geneID	geneName	log2FoldChange	padj	RNA-binding protein	TF/DNA binding	Syp target
FBgn0031059	CG14229	1.3186	2.6354E-28	FALSE	FALSE	FALSE
FBgn0052369	CG32369	1.3181	1.6745E-33	FALSE	FALSE	**TRUE**
FBgn0015380	drl	1.3162	1.0721E-41	FALSE	FALSE	FALSE
FBgn0267668	CR46006	1.3161	1.1620E-04	FALSE	FALSE	FALSE
FBgn0039178	CG6356	1.3143	3.2687E-24	FALSE	FALSE	FALSE
FBgn0030895	CG7135	1.3105	8.3484E-13	FALSE	FALSE	FALSE
FBgn0267025	CR45469	1.3094	6.9581E-04	FALSE	FALSE	FALSE
FBgn0086768	Pcmt	1.3082	6.1334E-42	FALSE	FALSE	FALSE
FBgn0266117	CR44843	1.3081	6.0860E-03	FALSE	FALSE	FALSE
FBgn0085409	smal	1.3073	1.8412E-31	FALSE	FALSE	FALSE
FBgn0000810	fs(1)K10	1.3067	9.5991E-25	FALSE	FALSE	FALSE
FBgn0032021	CG7781	1.3053	9.6470E-36	FALSE	FALSE	FALSE
FBgn0030276	Dlic	1.3053	9.1368E-57	FALSE	FALSE	FALSE
FBgn0031053	CG14223	1.3037	7.2619E-14	FALSE	FALSE	FALSE
FBgn0011481	Ssdp	1.3034	1.6108E-49	FALSE	**TRUE**	**TRUE**
FBgn0266446	CG45076	1.3019	1.5966E-03	FALSE	FALSE	**TRUE**
FBgn0003448	sna	1.2995	6.2383E-35	FALSE	**TRUE**	FALSE
FBgn0263929	jvl	1.2991	3.2085E-47	FALSE	FALSE	FALSE
FBgn0026059	Mhcl	1.2978	2.8186E-58	FALSE	FALSE	FALSE
FBgn0037468	CG1943	1.2977	4.6024E-24	FALSE	FALSE	**TRUE**
FBgn0001624	dlg1	1.2946	4.3696E-37	FALSE	FALSE	FALSE
FBgn0052647	CG32647	1.2946	3.7413E-18	FALSE	FALSE	FALSE
FBgn0039098	GILT3	1.2938	1.4428E-03	FALSE	FALSE	FALSE
FBgn0052843	Dh31-R	1.2919	1.0995E-18	FALSE	FALSE	FALSE
FBgn0028644	beat-Ic	1.2910	6.8962E-26	FALSE	FALSE	FALSE
FBgn0031952	cdc14	1.2885	4.7100E-35	FALSE	FALSE	FALSE
FBgn0010238	Lac	1.2877	1.9964E-38	FALSE	FALSE	FALSE
FBgn0085442	NKAIN	1.2877	6.0901E-55	FALSE	FALSE	FALSE
FBgn0011725	twin	1.2845	2.2690E-61	FALSE	**TRUE**	**TRUE**
FBgn0031903	Wnt10	1.2841	2.1572E-16	FALSE	FALSE	FALSE
FBgn0030581	CG14408	1.2820	1.1862E-41	FALSE	FALSE	FALSE
FBgn0024250	brk	1.2814	1.1673E-43	FALSE	**TRUE**	FALSE
FBgn0030418	CG4004	1.2813	7.1228E-34	FALSE	FALSE	FALSE
FBgn0264895	RapGAP1	1.2793	8.0326E-43	FALSE	FALSE	FALSE
FBgn0039994	conu	1.2784	7.5097E-18	FALSE	FALSE	FALSE
FBgn0267698	Pak	1.2781	2.1712E-43	FALSE	FALSE	FALSE
FBgn0000719	fog	1.2770	5.0083E-24	FALSE	FALSE	FALSE
FBgn0003975	vg	1.2769	2.3052E-16	FALSE	**TRUE**	**TRUE**
FBgn0030400	CG11138	1.2768	2.7609E-50	FALSE	FALSE	**TRUE**
FBgn0031698	Ncoa6	1.2761	4.4367E-59	FALSE	FALSE	FALSE
FBgn0086680	vvl	1.2756	5.1980E-35	FALSE	**TRUE**	**TRUE**
FBgn0283657	Tlk	1.2748	8.6478E-43	FALSE	FALSE	FALSE

geneID	geneName	log2FoldChange	padj	RNA-binding protein	TF/DNA binding	Syp target
FBgn0026409	Mpcp2	1.2738	1.5873E-34	FALSE	FALSE	**TRUE**
FBgn0030028	Corp	1.2709	1.2890E-12	FALSE	FALSE	FALSE
FBgn0030742	CG9919	1.2709	1.4455E-62	FALSE	FALSE	FALSE
FBgn0011300	babo	1.2683	3.8448E-33	FALSE	FALSE	FALSE
FBgn0264816	koko	1.2675	1.8635E-31	FALSE	FALSE	FALSE
FBgn0039532	Mtl	1.2641	2.8322E-32	FALSE	FALSE	**TRUE**
FBgn0003091	Pkc53E	1.2628	3.2126E-20	FALSE	FALSE	FALSE
FBgn0047135	CG32276	1.2606	1.7247E-43	FALSE	FALSE	FALSE
FBgn0036062	CG6685	1.2603	8.2264E-14	FALSE	FALSE	FALSE
FBgn0000370	crc	1.2586	1.7870E-30	FALSE	**TRUE**	**TRUE**
FBgn0031473	CG3104	1.2580	4.9827E-26	FALSE	FALSE	FALSE
FBgn0266721	gammaSnap2	1.2552	1.2372E-05	FALSE	FALSE	**TRUE**
FBgn0001168	h	1.2532	1.5681E-21	FALSE	**TRUE**	**TRUE**
FBgn0037770	Art4	1.2525	3.0001E-55	FALSE	FALSE	FALSE
FBgn0030174	CG15312	1.2506	7.0299E-13	FALSE	FALSE	FALSE
FBgn0013720	pck	1.2499	1.6296E-35	FALSE	FALSE	FALSE
FBgn0038419	CG14879	1.2490	7.7404E-12	FALSE	FALSE	FALSE
FBgn0028993	scro	1.2484	2.3291E-28	FALSE	**TRUE**	FALSE
FBgn0004924	Top1	1.2457	1.9660E-38	FALSE	FALSE	FALSE
FBgn0030421	CG3812	1.2450	1.4616E-32	FALSE	FALSE	FALSE
FBgn0034218	CG18467	1.2427	5.7883E-14	FALSE	FALSE	FALSE
FBgn0051363	Jupiter	1.2423	4.9123E-47	FALSE	FALSE	**TRUE**
FBgn0040697	Teh3	1.2418	1.3518E-07	FALSE	FALSE	FALSE
FBgn0019660	roX2	1.2402	6.9328E-10	FALSE	FALSE	**TRUE**
FBgn0015221	Fer2LCH	1.2397	1.2658E-72	FALSE	FALSE	FALSE
FBgn0037207	Mes2	1.2387	1.0276E-38	FALSE	FALSE	FALSE
FBgn0026076	UBL3	1.2384	2.7697E-37	FALSE	FALSE	**TRUE**
FBgn0004656	fs(1)h	1.2379	9.7100E-50	FALSE	**TRUE**	FALSE
FBgn0039303	CG11857	1.2373	4.4451E-42	FALSE	FALSE	FALSE
FBgn0259168	mnb	1.2365	1.7252E-24	FALSE	FALSE	**TRUE**
FBgn0002521	pho	1.2364	7.4557E-35	FALSE	**TRUE**	**TRUE**
FBgn0015625	CycB3	1.2359	1.0879E-52	FALSE	FALSE	FALSE
FBgn0032587	CG5953	1.2358	8.2420E-21	FALSE	**TRUE**	FALSE
FBgn0035610	Lkr	1.2357	2.2411E-12	FALSE	FALSE	FALSE
FBgn0004859	ci	1.2345	8.0397E-26	FALSE	**TRUE**	FALSE
FBgn0036725	CG18265	1.2335	1.1954E-24	FALSE	**TRUE**	FALSE
FBgn0039380	CG5890	1.2333	2.7601E-17	FALSE	FALSE	**TRUE**
FBgn0039427	CG5447	1.2289	1.1468E-27	FALSE	FALSE	FALSE
FBgn0263594	lost	1.2284	3.4766E-78	**TRUE**	FALSE	FALSE
FBgn0035989	CG3967	1.2281	5.8628E-61	FALSE	FALSE	FALSE
FBgn0038147	CCHa2	1.2276	5.4755E-08	FALSE	FALSE	FALSE
FBgn0036538	CG15715	1.2270	7.4736E-28	FALSE	**TRUE**	**TRUE**

geneID	geneName	log2FoldChange	padj	RNA-binding protein	TF/DNA binding	Syp target
FBgn0031458	aph-1	1.2260	9.5992E-30	FALSE	FALSE	FALSE
FBgn0033529	CG17765	1.2258	1.2315E-41	FALSE	FALSE	**TRUE**
FBgn0010223	Galphaf	1.2233	2.7293E-03	FALSE	FALSE	FALSE
FBgn0004395	unk	1.2227	2.8655E-30	**TRUE**	FALSE	FALSE
FBgn0267330	KdelR	1.2222	1.0148E-27	FALSE	FALSE	FALSE
FBgn0030996	CG14194	1.2212	2.8260E-47	FALSE	FALSE	FALSE
FBgn0039459	IntS12	1.2196	3.2267E-15	FALSE	FALSE	FALSE
FBgn0029959	Rab39	1.2196	1.9020E-34	FALSE	FALSE	**TRUE**
FBgn0002609	E(spl)m3-HLH	1.2179	4.7333E-26	FALSE	**TRUE**	**TRUE**
FBgn0028664	VhaM9.7-c	1.2172	1.5395E-04	FALSE	FALSE	FALSE
FBgn0024326	Mkk4	1.2163	4.8910E-41	FALSE	FALSE	FALSE
FBgn0036360	CG10713	1.2159	3.4601E-20	FALSE	FALSE	FALSE
FBgn0066292	CheB42c	1.2154	2.7543E-05	FALSE	FALSE	FALSE
FBgn0262740	Evi5	1.2153	2.2097E-52	FALSE	FALSE	FALSE
FBgn0032048	Dh31	1.2148	7.0242E-17	FALSE	FALSE	**TRUE**
FBgn0267534	CR45874	1.2139	1.9792E-04	FALSE	FALSE	FALSE
FBgn0035181	CG9205	1.2135	6.4584E-45	FALSE	FALSE	FALSE
FBgn0010638	Sec61beta	1.2129	9.5472E-63	FALSE	FALSE	**TRUE**
FBgn0004198	ct	1.2127	4.3474E-25	FALSE	**TRUE**	FALSE
FBgn0086673	CG13272	1.2111	2.8151E-03	FALSE	FALSE	FALSE
FBgn0039900	Syt7	1.2102	2.3269E-19	FALSE	FALSE	FALSE
FBgn0011276	HLH3B	1.2101	3.8061E-15	FALSE	**TRUE**	**TRUE**
FBgn0001138	grn	1.2099	2.2930E-25	FALSE	**TRUE**	**TRUE**
FBgn0037262	MED31	1.2098	1.1422E-32	FALSE	**TRUE**	FALSE
FBgn0034072	Dg	1.2081	2.5344E-46	FALSE	FALSE	FALSE
FBgn0000046	Act87E	1.2065	7.0605E-08	FALSE	FALSE	**TRUE**
FBgn0004646	ogre	1.2063	1.5815E-71	FALSE	FALSE	**TRUE**
FBgn0265180	CG44245	1.2063	2.5098E-15	FALSE	FALSE	FALSE
FBgn0051627	CG31627	1.2061	4.0328E-03	FALSE	FALSE	FALSE
FBgn0034313	CG5726	1.2060	3.2812E-24	FALSE	FALSE	FALSE
FBgn0004369	Ptp99A	1.2058	8.0763E-38	FALSE	FALSE	FALSE
FBgn0045823	vsg	1.2045	3.8826E-40	FALSE	FALSE	FALSE
FBgn0085732	CR40190	1.2039	3.0960E-04	FALSE	FALSE	FALSE
FBgn0265296	Dscam2	1.2035	7.6576E-25	FALSE	FALSE	FALSE
FBgn0004108	Nrt	1.2023	1.9346E-39	FALSE	FALSE	FALSE
FBgn0045852	ham	1.2018	7.5888E-47	FALSE	**TRUE**	FALSE
FBgn0043010	Fsn	1.2011	1.9882E-36	FALSE	FALSE	FALSE
FBgn0004436	Ubc6	1.2003	6.0659E-42	FALSE	FALSE	**TRUE**
FBgn0263219	Dscam4	1.2001	8.8473E-32	FALSE	FALSE	FALSE
FBgn0035049	Mmp1	1.1963	6.8059E-04	FALSE	FALSE	FALSE
FBgn0001087	g	1.1959	4.1067E-39	FALSE	FALSE	FALSE
FBgn0262975	cnc	1.1945	5.4894E-36	FALSE	**TRUE**	FALSE

geneID	geneName	log2FoldChange	padj	RNA-binding protein	TF/DNA binding	Syp target
FBgn0283471	wupA	1.1942	2.4048E-05	FALSE	FALSE	**TRUE**
FBgn0270928	VAChT	1.1914	8.6841E-39	FALSE	FALSE	FALSE
FBgn0000014	abd-A	1.1900	1.3827E-34	FALSE	**TRUE**	FALSE
FBgn0031397	CG15385	1.1898	9.1573E-25	FALSE	FALSE	FALSE
FBgn0003944	Ubx	1.1885	4.1736E-24	FALSE	**TRUE**	**TRUE**
FBgn0039054	Cow	1.1877	4.3890E-44	FALSE	FALSE	FALSE
FBgn0013732	sced	1.1875	1.4261E-36	FALSE	FALSE	FALSE
FBgn0002522	lab	1.1840	4.9531E-03	FALSE	**TRUE**	FALSE
FBgn0037890	CG17734	1.1834	2.5794E-28	FALSE	FALSE	FALSE
FBgn0004648	svr	1.1831	3.8744E-54	FALSE	FALSE	FALSE
FBgn0260653	serp	1.1826	4.9976E-20	FALSE	FALSE	FALSE
FBgn0030883	CG7772	1.1826	2.4507E-10	FALSE	FALSE	FALSE
FBgn0035424	CG11505	1.1811	1.6576E-47	**TRUE**	FALSE	FALSE
FBgn0015019	CCT3	1.1769	7.9716E-40	FALSE	FALSE	FALSE
FBgn0037443	Dmtn	1.1736	5.1139E-23	FALSE	FALSE	FALSE
FBgn0266020	CR44785	1.1733	1.6653E-03	FALSE	FALSE	**TRUE**
FBgn0260658	CG42541	1.1731	4.6329E-28	FALSE	FALSE	FALSE
FBgn0032614	CG13284	1.1721	1.2027E-05	FALSE	FALSE	FALSE
FBgn0262738	norpA	1.1719	1.6924E-32	FALSE	FALSE	FALSE
FBgn0035625	Blimp-1	1.1715	4.8681E-03	FALSE	**TRUE**	FALSE
FBgn0264502	CG43901	1.1706	1.3148E-24	FALSE	FALSE	FALSE
FBgn0035589	CHMP2B	1.1691	7.9958E-18	FALSE	FALSE	FALSE
FBgn0030847	CG12991	1.1685	2.3459E-29	FALSE	FALSE	FALSE
FBgn0262717	Skeletor	1.1683	9.1896E-13	FALSE	FALSE	FALSE
FBgn0022382	Pka-R2	1.1671	7.3870E-34	FALSE	FALSE	FALSE
FBgn0004858	elB	1.1670	3.4121E-30	FALSE	**TRUE**	**TRUE**
FBgn0030724	Nipsnap	1.1667	7.7171E-32	FALSE	FALSE	FALSE
FBgn0032218	CG5381	1.1649	8.4510E-03	FALSE	FALSE	FALSE
FBgn0053147	Hs3st-A	1.1637	6.3402E-22	FALSE	FALSE	FALSE
FBgn0044323	Cka	1.1630	6.1422E-45	FALSE	FALSE	**TRUE**
FBgn0250823	gish	1.1617	2.9586E-55	FALSE	FALSE	**TRUE**
FBgn0261477	slim	1.1612	1.3881E-39	FALSE	FALSE	FALSE
FBgn0037150	CG7133	1.1608	2.6414E-22	FALSE	FALSE	FALSE
FBgn0037445	CG9727	1.1606	4.0741E-25	FALSE	**TRUE**	FALSE
FBgn0029941	CG1677	1.1603	2.8008E-60	**TRUE**	FALSE	FALSE
FBgn0024184	unc-4	1.1600	5.0213E-16	FALSE	**TRUE**	FALSE
FBgn0029895	CG14441	1.1578	1.2325E-28	FALSE	**TRUE**	FALSE
FBgn0261611	CG42700	1.1566	8.6898E-12	FALSE	FALSE	FALSE
FBgn0030520	Pdcd4	1.1561	3.6009E-65	FALSE	FALSE	**TRUE**
FBgn0030634	CG9164	1.1559	8.9700E-12	FALSE	FALSE	FALSE
FBgn0266101	CG44838	1.1556	7.5616E-36	FALSE	FALSE	FALSE
FBgn0259236	comm3	1.1519	3.8261E-03	FALSE	FALSE	FALSE

geneID	geneName	log2FoldChange	padj	RNA-binding protein	TF/DNA binding	Syp target
FBgn0004956	upd1	1.1492	5.9681E-09	FALSE	FALSE	FALSE
FBgn0033453	CG1667	1.1485	2.0632E-09	FALSE	FALSE	FALSE
FBgn0026411	Lim1	1.1465	1.7900E-42	FALSE	**TRUE**	**TRUE**
FBgn0038087	beat-Va	1.1458	6.7681E-15	FALSE	FALSE	FALSE
FBgn0264489	CG43897	1.1456	1.1379E-05	FALSE	**TRUE**	**TRUE**
FBgn0024248	chico	1.1454	1.0217E-28	FALSE	FALSE	FALSE
FBgn0039381	SppL	1.1447	2.9759E-32	FALSE	FALSE	FALSE
FBgn0267378	sau	1.1447	6.6470E-35	FALSE	FALSE	FALSE
FBgn0025391	Scgdelta	1.1442	3.8306E-28	FALSE	FALSE	FALSE
FBgn0036486	Msh6	1.1440	6.9389E-29	FALSE	FALSE	FALSE
FBgn0013347	TfIIA-S	1.1425	6.5661E-44	FALSE	**TRUE**	FALSE
FBgn0053182	Kdm4B	1.1414	5.3273E-05	FALSE	**TRUE**	FALSE
FBgn0010434	cora	1.1402	1.2495E-32	FALSE	FALSE	FALSE
FBgn0033996	CG11807	1.1385	1.4740E-25	FALSE	FALSE	FALSE
FBgn0004552	Akh	1.1381	8.8028E-07	FALSE	FALSE	FALSE
FBgn0000037	mAChR-A	1.1378	2.1906E-37	FALSE	FALSE	FALSE
FBgn0027111	miple1	1.1371	4.4521E-25	FALSE	FALSE	FALSE
FBgn0015790	Rab11	1.1366	5.9136E-44	FALSE	FALSE	FALSE
FBgn0033876	Syngr	1.1360	2.9617E-39	FALSE	FALSE	FALSE
FBgn0031939	CG13796	1.1353	7.8673E-05	FALSE	**TRUE**	FALSE
FBgn0035756	unc-13-4A	1.1348	3.3150E-20	FALSE	FALSE	FALSE
FBgn0038545	pasi1	1.1334	1.0904E-14	FALSE	FALSE	FALSE
FBgn0002535	Lcp4	1.1322	6.4784E-08	FALSE	FALSE	FALSE
FBgn0051774	fred	1.1312	9.8556E-23	FALSE	FALSE	FALSE
FBgn0027291	l(1)G0156	1.1303	1.6222E-53	FALSE	FALSE	**TRUE**
FBgn0025800	Smox	1.1295	3.9569E-30	FALSE	**TRUE**	**TRUE**
FBgn0032805	CG10337	1.1290	3.2653E-03	FALSE	FALSE	FALSE
FBgn0266429	AstA-R1	1.1289	6.7089E-08	FALSE	FALSE	FALSE
FBgn0034408	sano	1.1276	3.0233E-29	FALSE	FALSE	**TRUE**
FBgn0042135	CG18812	1.1275	1.3036E-43	FALSE	FALSE	FALSE
FBgn0033405	CG13954	1.1271	1.0914E-13	FALSE	FALSE	FALSE
FBgn0265597	rad	1.1270	1.9097E-45	FALSE	FALSE	FALSE
FBgn0265974	ttv	1.1264	7.0848E-25	FALSE	FALSE	FALSE
FBgn0265605	Ric	1.1252	1.1390E-21	FALSE	FALSE	FALSE
FBgn0035542	DOR	1.1241	5.8044E-36	FALSE	FALSE	**TRUE**
FBgn0032153	CG4537	1.1232	4.8159E-07	FALSE	FALSE	FALSE
FBgn0024432	Dlc90F	1.1230	6.2274E-40	FALSE	FALSE	**TRUE**
FBgn0264794	CR44024	1.1226	4.0134E-09	FALSE	FALSE	FALSE
FBgn0011260	Sema2a	1.1205	6.1990E-30	FALSE	FALSE	FALSE
FBgn0052423	shep	1.1202	1.4399E-26	**TRUE**	FALSE	**TRUE**
FBgn0030991	CG7453	1.1168	1.4143E-26	FALSE	FALSE	FALSE

geneID	geneName	log2FoldChange	padj	RNA-binding protein	TF/DNA binding	Syp target
FBgn0265784	CrebB	1.1167	4.8006E-28	FALSE	**TRUE**	FALSE
FBgn0040396	CG3939	1.1166	3.7666E-30	FALSE	FALSE	FALSE
FBgn0051092	LpR2	1.1165	2.4020E-21	FALSE	FALSE	FALSE
FBgn0032336	AstC	1.1164	3.1259E-10	FALSE	FALSE	FALSE
FBgn0034253	CG10936	1.1162	2.6336E-04	FALSE	FALSE	FALSE
FBgn0029992	Upf2	1.1160	1.5144E-35	**TRUE**	FALSE	FALSE
FBgn0264324	spg	1.1151	1.0994E-30	FALSE	FALSE	FALSE
FBgn0011604	Iswi	1.1146	7.9156E-50	FALSE	**TRUE**	FALSE
FBgn0028899	CG31817	1.1144	5.1458E-03	FALSE	FALSE	FALSE
FBgn0036059	nudE	1.1137	2.3625E-28	FALSE	FALSE	FALSE
FBgn0266777	CR45242	1.1136	5.6724E-10	FALSE	FALSE	**TRUE**
FBgn0010314	Cks30A	1.1135	1.2558E-21	FALSE	FALSE	**TRUE**
FBgn0264822	CR44030	1.1128	2.9307E-05	FALSE	FALSE	FALSE
FBgn0036494	Toll-6	1.1120	2.0687E-32	FALSE	FALSE	FALSE
FBgn0040765	luna	1.1116	2.2671E-25	FALSE	**TRUE**	**TRUE**
FBgn0051781	CR31781	1.1108	1.1027E-15	FALSE	FALSE	**TRUE**
FBgn0004882	orb	1.1095	5.5014E-15	**TRUE**	FALSE	FALSE
FBgn0037754	CG8500	1.1087	3.0826E-32	FALSE	FALSE	FALSE
FBgn0263039	CR43334	1.1084	3.0332E-05	FALSE	FALSE	FALSE
FBgn0037016	CG13252	1.1083	1.9017E-17	FALSE	FALSE	**TRUE**
FBgn0051759	CG31759	1.1082	2.6397E-08	FALSE	**TRUE**	FALSE
FBgn0039266	CG11791	1.1079	4.1202E-23	FALSE	FALSE	FALSE
FBgn0037106	CG11307	1.1075	1.1930E-21	FALSE	FALSE	FALSE
FBgn0036893	PIG-F	1.1058	1.0854E-11	FALSE	FALSE	FALSE
FBgn0036155	CG6163	1.1058	3.6519E-17	FALSE	FALSE	FALSE
FBgn0000504	dsx	1.1049	1.2169E-05	**TRUE**	**TRUE**	FALSE
FBgn0031883	Caper	1.1025	2.9309E-36	**TRUE**	FALSE	FALSE
FBgn0050460	CG30460	1.1024	4.1596E-20	FALSE	FALSE	FALSE
FBgn0034808	CG9896	1.1019	9.0892E-08	FALSE	FALSE	FALSE
FBgn0003345	sd	1.1016	5.0540E-32	FALSE	**TRUE**	FALSE
FBgn0031992	CG8498	1.1006	5.1516E-36	FALSE	FALSE	**TRUE**
FBgn0036126	Irbp18	1.1001	5.8312E-07	FALSE	**TRUE**	**TRUE**
FBgn0051122	CG31122	1.1000	3.4383E-45	FALSE	FALSE	FALSE
FBgn0052544	CG32544	1.0995	1.3636E-15	FALSE	FALSE	**TRUE**
FBgn0036958	CG17233	1.0976	7.4592E-55	FALSE	FALSE	FALSE
FBgn0027885	Aac11	1.0971	9.6020E-14	FALSE	FALSE	FALSE
FBgn0061198	HSPC300	1.0966	2.0373E-07	FALSE	FALSE	FALSE
FBgn0039136	CG5902	1.0955	2.0983E-32	FALSE	FALSE	FALSE
FBgn0047114	CG31142	1.0955	6.2623E-05	FALSE	FALSE	**TRUE**
FBgn0267181	CR45621	1.0953	6.8258E-06	FALSE	FALSE	FALSE
FBgn0030955	CG6891	1.0952	1.6345E-18	FALSE	FALSE	**TRUE**
FBgn0032814	CG10366	1.0945	1.2794E-20	FALSE	**TRUE**	FALSE

geneID	geneName	log2FoldChange	padj	RNA-binding protein	TF/DNA binding	Syp target
FBgn0051481	pb	1.0934	1.6181E-08	FALSE	**TRUE**	**TRUE**
FBgn0031682	CG5828	1.0934	5.2419E-18	FALSE	FALSE	FALSE
FBgn0036454	CG17839	1.0895	2.4652E-38	FALSE	FALSE	FALSE
FBgn0261341	verm	1.0894	4.1702E-13	FALSE	FALSE	FALSE
FBgn0010303	hep	1.0888	3.2255E-43	FALSE	FALSE	FALSE
FBgn0036144	GlcAT-P	1.0887	3.9970E-27	FALSE	FALSE	FALSE
FBgn0031753	CG13999	1.0873	2.4268E-06	FALSE	FALSE	FALSE
FBgn0002633	E(spl)m7-HLH	1.0863	7.1257E-22	FALSE	**TRUE**	FALSE
FBgn0262737	mub	1.0861	1.3863E-30	**TRUE**	FALSE	FALSE
FBgn0050089	CG30089	1.0854	7.8810E-33	FALSE	FALSE	FALSE
FBgn0261238	Alh	1.0848	2.6894E-44	FALSE	**TRUE**	FALSE
FBgn0260970	Ubr3	1.0828	5.3973E-36	FALSE	FALSE	FALSE
FBgn0038197	foxo	1.0819	4.1667E-12	FALSE	**TRUE**	FALSE
FBgn0034068	casp	1.0812	6.3612E-33	FALSE	FALSE	FALSE
FBgn0030417	CG15725	1.0804	2.9482E-08	FALSE	FALSE	FALSE
FBgn0025776	ind	1.0786	2.7204E-03	FALSE	**TRUE**	FALSE
FBgn0020493	Dad	1.0780	2.8898E-23	FALSE	**TRUE**	FALSE
FBgn0262970	CR43281	1.0777	1.1314E-03	FALSE	FALSE	FALSE
FBgn0033934	CG17385	1.0744	2.3446E-35	FALSE	**TRUE**	FALSE
FBgn0038453	Arl6IP1	1.0725	1.7010E-35	FALSE	FALSE	FALSE
FBgn0010317	CycJ	1.0722	9.9024E-05	FALSE	**TRUE**	FALSE
FBgn0036742	CG7497	1.0715	2.5581E-06	FALSE	FALSE	FALSE
FBgn0039876	CG2126	1.0713	5.3265E-14	FALSE	FALSE	FALSE
FBgn0038126	CG8483	1.0699	5.2695E-03	FALSE	FALSE	**TRUE**
FBgn0050343	CG30343	1.0689	3.7640E-03	FALSE	FALSE	FALSE
FBgn0265052	St3	1.0684	1.7420E-07	FALSE	FALSE	FALSE
FBgn0031697	CG14024	1.0650	2.7072E-20	FALSE	FALSE	FALSE
FBgn0052163	CG32163	1.0650	3.8882E-07	FALSE	FALSE	FALSE
FBgn0262476	CG43066	1.0637	3.7103E-28	FALSE	FALSE	FALSE
FBgn0051712	CG31712	1.0636	7.9414E-03	FALSE	FALSE	FALSE
FBgn0013725	phyl	1.0633	6.4033E-23	FALSE	FALSE	FALSE
FBgn0026199	myo	1.0629	1.7259E-14	FALSE	FALSE	FALSE
FBgn0035157	CG13894	1.0623	1.3301E-27	FALSE	**TRUE**	FALSE
FBgn0030796	CG4829	1.0620	4.2279E-18	FALSE	FALSE	FALSE
FBgn0031047	Rcd-1	1.0598	6.6108E-34	FALSE	FALSE	FALSE
FBgn0259923	Sep4	1.0595	3.1741E-21	FALSE	FALSE	FALSE
FBgn0026737	CG6171	1.0584	1.3768E-17	FALSE	FALSE	FALSE
FBgn0026192	par-6	1.0579	1.5049E-25	FALSE	FALSE	**TRUE**
FBgn0262579	Ect4	1.0573	6.2260E-21	FALSE	FALSE	FALSE
FBgn0031398	CG10880	1.0518	1.0324E-15	FALSE	FALSE	FALSE
FBgn0015776	nrv1	1.0503	1.5560E-10	FALSE	FALSE	FALSE
FBgn0004865	Eip78C	1.0500	7.4371E-03	FALSE	**TRUE**	**TRUE**

geneID	geneName	log2FoldChange	padj	RNA-binding protein	TF/DNA binding	Syp target
FBgn0053914	CG33914	1.0477	6.1341E-05	FALSE	FALSE	FALSE
FBgn0052576	CG32576	1.0466	3.0258E-07	FALSE	FALSE	FALSE
FBgn0031145	Ntf-2	1.0464	1.9882E-36	FALSE	FALSE	FALSE
FBgn0004102	oc	1.0461	1.9723E-23	FALSE	**TRUE**	**TRUE**
FBgn0024183	vig	1.0457	6.6379E-25	**TRUE**	FALSE	**TRUE**
FBgn0028407	Drep3	1.0448	3.6328E-15	FALSE	FALSE	FALSE
FBgn0038975	Nrx-1	1.0443	2.0044E-33	FALSE	FALSE	FALSE
FBgn0029676	HIP-R	1.0434	1.5766E-23	FALSE	FALSE	**TRUE**
FBgn0038641	CG7708	1.0430	9.5235E-14	FALSE	FALSE	FALSE
FBgn0026262	bip2	1.0410	2.0140E-46	FALSE	**TRUE**	**TRUE**
FBgn0031378	CG15362	1.0394	1.0557E-03	FALSE	FALSE	FALSE
FBgn0086370	sra	1.0376	2.7452E-29	FALSE	FALSE	FALSE
FBgn0033683	CG18343	1.0364	2.0479E-07	FALSE	FALSE	**TRUE**
FBgn0085438	CG34409	1.0354	2.2911E-03	FALSE	FALSE	FALSE
FBgn0259112	CR42254	1.0342	1.6373E-04	FALSE	FALSE	FALSE
FBgn0264857	iab-8	1.0340	1.5855E-03	FALSE	FALSE	FALSE
FBgn0040071	tara	1.0336	8.2676E-54	FALSE	**TRUE**	FALSE
FBgn0000568	Eip75B	1.0321	3.2320E-14	FALSE	**TRUE**	FALSE
FBgn0000216	Brd	1.0320	5.3066E-07	FALSE	FALSE	FALSE
FBgn0003321	sbr	1.0314	6.0746E-23	**TRUE**	FALSE	FALSE
FBgn0023549	Mct1	1.0313	5.8722E-06	FALSE	FALSE	FALSE
FBgn0031187	Usp2	1.0312	2.3513E-38	FALSE	FALSE	FALSE
FBgn0037007	CG5059	1.0311	1.9939E-20	FALSE	FALSE	FALSE
FBgn0002632	E(spl)m6-BFM	1.0299	1.8981E-14	FALSE	FALSE	FALSE
FBgn0036476	sstn	1.0297	9.4888E-15	FALSE	FALSE	FALSE
FBgn0039186	CG5746	1.0283	3.9111E-42	FALSE	FALSE	FALSE
FBgn0004179	Csp	1.0279	5.4354E-37	FALSE	FALSE	FALSE
FBgn0262127	kibra	1.0277	2.2026E-14	FALSE	FALSE	FALSE
FBgn0085384	CG34355	1.0277	6.8898E-15	FALSE	FALSE	FALSE
FBgn0031769	CG9135	1.0259	7.6393E-37	FALSE	FALSE	FALSE
FBgn0085450	Snoo	1.0256	5.4031E-20	FALSE	**TRUE**	FALSE
FBgn0063670	CG40228	1.0255	1.4439E-14	FALSE	FALSE	**TRUE**
FBgn0039528	dsd	1.0251	1.3533E-23	FALSE	FALSE	FALSE
FBgn0035189	CG9119	1.0245	3.0289E-09	FALSE	FALSE	FALSE
FBgn0051864	Qtzl	1.0240	9.9130E-06	FALSE	FALSE	FALSE
FBgn0266654	CR45161	1.0236	9.0726E-04	FALSE	FALSE	FALSE
FBgn0039560	BOD1	1.0219	7.7825E-37	FALSE	FALSE	FALSE
FBgn0264848	vih	1.0206	1.7817E-25	FALSE	FALSE	**TRUE**
FBgn0033250	CG14762	1.0206	8.3107E-43	FALSE	FALSE	FALSE
FBgn0029663	CG10804	1.0205	3.4611E-17	FALSE	FALSE	FALSE
FBgn0003964	usp	1.0204	1.0029E-27	FALSE	**TRUE**	FALSE
FBgn0263240	Coop	1.0187	1.2827E-11	FALSE	**TRUE**	FALSE

geneID	geneName	log2FoldChange	padj	RNA-binding protein	TF/DNA binding	Syp target
FBgn0040778	CG17977	1.0183	2.6945E-09	FALSE	FALSE	FALSE
FBgn0024321	NK7.1	1.0181	1.1286E-24	FALSE	**TRUE**	**TRUE**
FBgn0002023	Lim3	1.0176	1.2306E-24	FALSE	**TRUE**	FALSE
FBgn0000524	dx	1.0175	2.4413E-25	FALSE	FALSE	FALSE
FBgn0004903	Rb97D	1.0163	6.1251E-23	**TRUE**	FALSE	FALSE
FBgn0051005	qless	1.0152	2.5732E-10	FALSE	FALSE	FALSE
FBgn0038324	CG5038	1.0151	2.2087E-10	FALSE	FALSE	FALSE
FBgn0025865	Cortactin	1.0143	1.9333E-17	FALSE	FALSE	FALSE
FBgn0037835	CG14687	1.0139	2.5280E-09	FALSE	FALSE	FALSE
FBgn0022343	CG3760	1.0125	6.2279E-33	FALSE	FALSE	FALSE
FBgn0036202	CG6024	1.0117	2.3724E-21	FALSE	FALSE	FALSE
FBgn0284408	trol	1.0116	1.9263E-31	FALSE	FALSE	FALSE
FBgn0262617	CG43143	1.0072	1.4288E-36	FALSE	FALSE	FALSE
FBgn0261262	CG42613	1.0058	1.4375E-15	FALSE	FALSE	FALSE
FBgn0032901	sky	1.0031	5.4095E-06	FALSE	FALSE	FALSE
FBgn0083963	Nlg3	1.0016	3.6084E-18	FALSE	FALSE	FALSE
FBgn0004432	Cyp1	1.0013	1.2138E-43	FALSE	**TRUE**	FALSE
FBgn0024807	DIP1	1.0008	1.7481E-25	**TRUE**	**TRUE**	FALSE
FBgn0000711	flw	1.0007	5.9949E-23	FALSE	FALSE	**TRUE**

E. *syp* mutant RNAseq comparison

Table E.1 Upregulated in *syp* mutant

geneID	geneName	log2FoldChange	padj
FBgn0033395	Cyp4p2	6.4601	6.2337E-52
FBgn0003996	w	5.7720	2.9699E-109
FBgn0015037	Cyp4p1	5.2201	1.7259E-28
FBgn0267242	CR45682	3.8978	1.2979E-54
FBgn0036288	CG10660	3.3709	1.5284E-60
FBgn0259140	CG42255	3.2329	9.2206E-25
FBgn0260874	Ir76a	3.0132	7.0521E-36
FBgn0038741	CG17186	2.8124	9.8083E-42
FBgn0035695	CG10226	2.6563	3.1054E-19
FBgn0003082	phr	2.4689	2.6507E-19
FBgn0016920	nompC	2.4065	5.2448E-17
FBgn0052581	CG32581	2.3635	1.2573E-08
FBgn0035512	Cpr64Ac	2.3055	2.3615E-07
FBgn0035770	pst	2.2857	1.5029E-31
FBgn0026176	SkpB	2.1890	4.1500E-07
FBgn0263471	scaRNA:MeU2-48	2.1381	1.4387E-10
FBgn0085788	CR41504	2.1320	5.6407E-07
FBgn0027259	Kmn1	2.0274	2.0878E-15
FBgn0040532	CG8369	2.0201	6.6905E-11
FBgn0266935	CR45386	1.9717	1.6911E-05
FBgn0021738	Crg-1	1.9589	8.5000E-07
FBgn0264835	CR44043	1.9075	7.4475E-07
FBgn0038799	MFS9	1.7649	3.0691E-08
FBgn0038354	CG5404	1.7015	7.2874E-06
FBgn0083987	snRNA:U11	1.6285	3.4333E-09
FBgn0033397	Cyp4p3	1.6283	4.0588E-05
FBgn0037387	CG1213	1.6210	2.2554E-06
FBgn0030593	CG9512	1.5905	2.3276E-04
FBgn0037205	BoYb	1.5568	4.1513E-04
FBgn0038277	RpS5b	1.5542	2.6308E-10
FBgn0263496	CR43485	1.5265	2.1656E-03
FBgn0033339	Sec31	1.5163	1.0659E-16
FBgn0283442	vas	1.4961	3.2809E-04
FBgn0261560	Thor	1.4925	5.7357E-06
FBgn0034761	CG4250	1.4593	4.6225E-04
FBgn0053509	CG33509	1.4473	9.4235E-04
FBgn0029950	CG9657	1.4397	5.6091E-06
FBgn0034010	CG8157	1.4035	1.4310E-03
FBgn0036732	Oatp74D	1.3913	1.2107E-09

geneID	geneName	log2FoldChange	padj
FBgn0031703	CG12512	1.3877	4.4349E-04
FBgn0035455	CG10862	1.3790	4.1036E-03
FBgn0036208	CG10361	1.3785	1.6937E-04
FBgn0037227	TwdlV	1.3680	4.5814E-03
FBgn0003227	rec	1.3625	2.0299E-09
FBgn0053508	ppk13	1.3522	1.7363E-03
FBgn0038020	GstD9	1.3464	1.6310E-03
FBgn0001145	Gs2	1.3325	8.6565E-08
FBgn0038095	Cyp304a1	1.3230	3.9518E-03
FBgn0053914	CG33914	1.3179	6.9648E-08
FBgn0033953	CG12861	1.3169	3.5195E-03
FBgn0013279	Hsp70Bc	1.3126	2.5016E-03
FBgn0260474	CG30002	1.3003	8.0681E-03
FBgn0265533	CR44383	1.2901	4.5860E-03
FBgn0030933	CG6470	1.2762	3.8449E-03
FBgn0261505	CR42653	1.2753	6.0995E-03
FBgn0052650	CG32650	1.2636	2.9997E-03
FBgn0028573	prc	1.2618	6.3399E-03
FBgn0033458	CG18446	1.2601	5.6657E-03
FBgn0036910	Cyp305a1	1.2561	4.4918E-03
FBgn0037788	CG3940	1.2542	1.7491E-06
FBgn0003886	alphaTub85E	1.2399	4.5729E-03
FBgn0036690	Ilp8	1.2384	1.1016E-02
FBgn0038733	CG11407	1.2261	7.3986E-03
FBgn0035942	ValRS-m	1.2258	1.5377E-08
FBgn0285926	Imp	1.2212	2.0779E-04
FBgn0030349	CG10353	1.2154	5.2840E-08
FBgn0051386	CR31386	1.2146	1.2425E-04
FBgn0052237	CG32237	1.2140	8.3776E-03
FBgn0037672	sage	1.2129	1.5407E-05
FBgn0029824	CG3726	1.2093	2.2219E-11
FBgn0050101	CG30101	1.2073	9.4884E-03
FBgn0002926	ndl	1.1982	1.0436E-02
FBgn0275434	CR46266	1.1825	8.2769E-03
FBgn0034390	CG15093	1.1815	6.9740E-05
FBgn0083004	snoRNA:Psi28S-1175b	1.1752	2.8606E-03
FBgn0011653	mas	1.1727	2.8147E-04
FBgn0031170	CG1718	1.1697	2.3893E-04
FBgn0039758	CG9737	1.1688	1.3236E-02
FBgn0010383	Cyp18a1	1.1544	1.3697E-02
FBgn0040600	CG13631	1.1452	1.9578E-03
FBgn0038732	CG11391	1.1411	1.6445E-02
FBgn0036479	CG13458	1.1314	9.0627E-03

geneID	geneName	log2FoldChange	padj
FBgn0266654	CR45161	1.1284	8.8291E-04
FBgn0035504	Teh4	1.1265	1.7929E-10
FBgn0052185	edin	1.1183	1.1852E-02
FBgn0035813	CG8492	1.1180	1.6923E-02
FBgn0038709	CG15025	1.1157	1.9109E-02
FBgn0267337	rn	1.1110	9.1877E-05
FBgn0083006	snoRNA:Psi28S-1153	1.1026	2.0045E-02
FBgn0262577	CG43117	1.0993	1.6445E-02
FBgn0029733	CG6927	1.0922	2.1545E-02
FBgn0028940	Cyp28a5	1.0889	2.2119E-02
FBgn0033952	Adgf-E	1.0873	1.7969E-02
FBgn0028699	Rh50	1.0796	3.8239E-03
FBgn0000158	bam	1.0744	2.4868E-02
FBgn0265814	CR44603	1.0702	2.7176E-02
FBgn0039749	CG11498	1.0639	1.1783E-02
FBgn0032285	CG17108	1.0638	2.9996E-02
FBgn0040837	CG8620	1.0595	1.6093E-02
FBgn0013949	Elal	1.0544	1.1497E-02
FBgn0011603	ine	1.0538	2.6467E-06
FBgn0259789	zld	1.0530	5.9907E-03
FBgn0031999	CG8419	1.0522	3.2155E-02
FBgn0031367	c-cup	1.0472	2.8606E-03
FBgn0266690	CR45180	1.0467	3.6807E-02
FBgn0001258	ImpL3	1.0451	8.4878E-03
FBgn0035921	CG13305	1.0425	5.5347E-03
FBgn0086068	snoRNA:Or-CD12	1.0403	3.2155E-02
FBgn0004852	Ac76E	1.0377	1.6795E-05
FBgn0267776	CR46107	1.0363	4.4966E-03
FBgn0039094	CG10184	1.0337	3.6878E-03
FBgn0038529	CG14323	1.0304	1.9536E-02
FBgn0038784	CG4362	1.0228	4.3273E-02
FBgn0025390	Mur2B	1.0204	6.0414E-03
FBgn0033340	CG13751	1.0191	9.7065E-03
FBgn0266243	CR44938	1.0154	2.6892E-02
FBgn0039359	RpL27	1.0132	6.0995E-03
FBgn0261429	CR42646	1.0119	4.3273E-02
FBgn0052512	CG32512	1.0095	1.0549E-04
FBgn0030005	CG2120	1.0064	3.9178E-02
FBgn0040832	CG8012	1.0010	4.7362E-02
FBgn0033558	CG12344	0.9999	1.9727E-02
FBgn0039756	CG9743	0.9997	7.2552E-03
FBgn0003149	Prm	0.9971	2.0045E-02
FBgn0053548	SmydA-8	0.9942	4.5779E-02

geneID	geneName	log2FoldChange	padj
FBgn0283440	solo	0.9848	4.3856E-02
FBgn0015801	Reg-5	0.9828	9.7959E-04
FBgn0037915	CG6790	0.9813	4.4611E-02
FBgn0051706	CG31706	0.9768	5.1885E-03
FBgn0031258	CG4297	0.9753	3.7904E-03
FBgn0029791	CG4096	0.9729	1.0658E-04
FBgn0031688	Cyp28d2	0.9681	1.3692E-02
FBgn0033367	PPO2	0.9677	3.4197E-03
FBgn0036116	CG7888	0.9675	1.1783E-02
FBgn0030272	CG15201	0.9624	3.1259E-02
FBgn0264907	CG44098	0.9566	2.1525E-06
FBgn0038938	CG7084	0.9501	3.0978E-02
FBgn0037717	CG8301	0.9473	4.4189E-04
FBgn0033926	Arc1	0.9406	1.6445E-02
FBgn0039915	Gat	0.9352	1.3740E-02
FBgn0263118	tx	0.9331	4.3273E-02
FBgn0040813	Nplp2	0.9271	2.0858E-02
FBgn0029766	CG15784	0.9156	3.7995E-03
FBgn0082925	snoRNA:Or-aca1	0.9121	1.1783E-02
FBgn0034909	CG4797	0.9107	2.8823E-03
FBgn0035207	Sherpa	0.9104	5.1780E-06
FBgn0031251	CG4213	0.9092	4.4258E-02
FBgn0010482	l(2)01289	0.8982	6.0414E-03
FBgn0035168	cep290	0.8935	3.5194E-03
FBgn0043854	slam	0.8892	3.6098E-02
FBgn0085396	CG34367	0.8890	5.0745E-03
FBgn0032706	Irk3	0.8887	2.4220E-02
FBgn0039209	REPTOR	0.8876	1.6310E-03
FBgn0010197	Gyc32E	0.8846	1.6423E-02
FBgn0027513	ana2	0.8835	1.9999E-03
FBgn0040850	CG15210	0.8811	7.0038E-03
FBgn0039428	CG14237	0.8768	3.5189E-02
FBgn0028561	sut3	0.8744	3.1447E-02
FBgn0051973	Cda5	0.8729	4.1301E-03
FBgn0032433	Oatp33Ea	0.8676	1.1277E-02
FBgn0030884	CG6847	0.8671	3.3534E-03
FBgn0053196	dpy	0.8668	1.1803E-02
FBgn0010424	TpnC73F	0.8635	3.2010E-02
FBgn0086659	snoRNA:Psi18S-176	0.8588	9.5596E-03
FBgn0038407	CG6126	0.8542	9.3316E-03
FBgn0083981	RunxA	0.8541	5.9355E-03
FBgn0030437	hec	0.8535	2.2119E-02
FBgn0084049	CR41440	0.8496	2.8057E-02

geneID	geneName	log2FoldChange	padj
FBgn0036583	CG13055	0.8468	2.4613E-03
FBgn0031971	Sirup	0.8457	1.6093E-02
FBgn0051051	CG31051	0.8445	1.8613E-03
FBgn0086665	snoRNA:Psi18S-1377a	0.8408	8.4878E-03
FBgn0266129	lov	0.8397	3.1236E-03
FBgn0037758	CG9467	0.8340	1.8803E-04
FBgn0262904	CR43259	0.8262	3.2481E-02
FBgn0265967	CR44754	0.8231	3.5740E-02
FBgn0022355	Tsf1	0.8158	4.4611E-02
FBgn0003292	rt	0.8122	4.4611E-02
FBgn0034911	CG5549	0.8055	4.0968E-02
FBgn0036194	CG11652	0.7937	2.3399E-04
FBgn0029839	CG4660	0.7861	4.5477E-02
FBgn0028473	Non1	0.7855	3.9946E-03
FBgn0250757	CG42235	0.7835	7.0506E-05
FBgn0030482	CG1673	0.7819	1.5657E-02
FBgn0036391	CG17364	0.7798	4.3403E-03
FBgn0016075	vkg	0.7798	2.5977E-02
FBgn0036260	Rh7	0.7780	2.2639E-02
FBgn0267408	AOX1	0.7775	1.9815E-03
FBgn0035267	CG13921	0.7774	5.0745E-03
FBgn0266750	CR45223	0.7742	4.7940E-02
FBgn0267524	2SrRNA:CR45864	0.7739	3.5239E-04
FBgn0263738	Ada2a	0.7704	8.8707E-04
FBgn0260655	l(3)76BDm	0.7671	9.1525E-04
FBgn0051191	CG31191	0.7657	1.8828E-02
FBgn0030304	Cyp4g15	0.7580	1.4910E-03
FBgn0083963	Nlg3	0.7557	2.2639E-02
FBgn0025833	CG8910	0.7538	4.4675E-03
FBgn0033889	CG6701	0.7516	1.2716E-02
FBgn0028888	CG4168	0.7513	6.2336E-04
FBgn0000723	FER	0.7476	4.4315E-05
FBgn0051634	Oatp26F	0.7468	9.4139E-03
FBgn0261999	CG42817	0.7420	3.1783E-04
FBgn0035205	Ctr9	0.7382	2.6470E-03
FBgn0001257	ImpL2	0.7331	4.1355E-04
FBgn0036144	GlcAT-P	0.7297	1.4310E-03
FBgn0036862	Gbs-76A	0.7263	6.1003E-04
FBgn0000299	Col4a1	0.7139	2.4868E-02
FBgn0002962	nos	0.7134	2.6684E-02
FBgn0031563	CG10031	0.7082	2.2817E-02
FBgn0027793	CG14787	0.7079	4.3273E-02
FBgn0011746	ana	0.7072	1.5003E-02

geneID	geneName	log2FoldChange	padj
FBgn0033117	CG3358	0.7042	1.1137E-02
FBgn0002629	E(spl)m4-BFM	0.7018	2.3561E-02
FBgn0014141	cher	0.7012	5.9657E-05
FBgn0035260	CG7991	0.6957	4.3403E-03
FBgn0030747	CG4301	0.6950	2.3184E-02
FBgn0003189	r	0.6909	1.9215E-03
FBgn0260486	Ziz	0.6899	3.5770E-03
FBgn0261618	larp	0.6855	1.1783E-02
FBgn0259241	CG42339	0.6823	1.3503E-03
FBgn0261625	GLS	0.6810	2.1476E-04
FBgn0030603	CG5541	0.6798	1.9697E-02
FBgn0002526	LanA	0.6795	1.8622E-02
FBgn0003396	shn	0.6793	3.7217E-02
FBgn0283427	FASN1	0.6783	1.5240E-04
FBgn0003295	ru	0.6752	3.9812E-02
FBgn0046696	RNaseP:RNA	0.6733	8.0647E-03
FBgn0000064	Ald	0.6601	3.6079E-02
FBgn0264087	Slob	0.6584	1.5060E-02
FBgn0263772	CG43689	0.6570	1.5822E-02
FBgn0039431	plum	0.6531	1.9550E-02
FBgn0037773	CG5359	0.6528	1.8828E-02
FBgn0031005	Hs3st-B	0.6468	3.0314E-03
FBgn0037238	CG1090	0.6467	2.0044E-03
FBgn0030745	CG4239	0.6399	2.5811E-02
FBgn0085395	Shawl	0.6390	2.0258E-02
FBgn0085413	CG34384	0.6315	2.9517E-02
FBgn0011204	cue	0.6269	1.5060E-02
FBgn0037521	CG2993	0.6192	2.7898E-02
FBgn0033584	CG7737	0.6185	3.7120E-02
FBgn0031065	CG14234	0.6142	1.5265E-02
FBgn0052085	CG32085	0.6124	1.9536E-02
FBgn0034731	CG10384	0.6107	2.1185E-02
FBgn0085421	Epac	0.6105	2.7176E-02
FBgn0003366	sev	0.6050	3.0750E-02
FBgn0010265	RpS13	0.6045	4.1960E-02
FBgn0033500	CG12913	0.6028	4.1960E-02
FBgn0029895	CG14441	0.6026	4.7764E-02
FBgn0033652	ths	0.5971	1.6445E-02
FBgn0033246	ACC	0.5928	1.8242E-02
FBgn0034046	tun	0.5914	7.1684E-03
FBgn0031866	Nlg2	0.5894	2.4532E-02
FBgn0038693	unc79	0.5893	3.1116E-02
FBgn0038532	CG14322	0.5891	8.3184E-03

geneID	geneName	log2FoldChange	padj
FBgn0033538	CG11883	0.5862	4.2370E-03
FBgn0041150	hoe1	0.5857	3.8705E-02
FBgn0261649	tinc	0.5854	1.6445E-02
FBgn0263776	CG43693	0.5822	6.0995E-03
FBgn0051989	Cap-D3	0.5810	1.2351E-02
FBgn0016797	fz2	0.5768	5.2165E-04
FBgn0051140	CG31140	0.5744	4.3273E-02
FBgn0010114	hig	0.5691	1.8828E-02
FBgn0002941	slou	0.5649	3.8426E-02
FBgn0263102	psq	0.5648	2.1010E-02
FBgn0003071	Pfk	0.5645	2.9996E-02
FBgn0032249	TBC1D16	0.5496	3.6480E-02
FBgn0028979	tio	0.5483	3.3043E-02
FBgn0015577	alpha-Est9	0.5477	1.0139E-02
FBgn0051721	Trim9	0.5361	1.5801E-02
FBgn0001319	kn	0.5199	2.8598E-02
FBgn0004370	Ptp10D	0.5163	4.7395E-02
FBgn0030294	Pa1	0.5134	4.8755E-02
FBgn0001098	Gdh	0.5115	1.5549E-02
FBgn0035246	CG13928	0.5106	6.0414E-03
FBgn0034718	wdp	0.4952	3.2700E-02
FBgn0034237	eIF3b	0.4834	2.0757E-02
FBgn0039508	CG3368	0.4651	2.6056E-02
FBgn0036454	CG17839	0.4632	2.7429E-02
FBgn0026438	Eaat2	0.4524	2.9808E-02
FBgn0284245	eEF1alpha1	0.4387	4.9284E-02
FBgn0024179	wit	0.4324	4.8085E-02
FBgn0034145	CG5065	0.4311	4.1915E-02
FBgn0041097	robo3	0.4287	2.0258E-02

Table E.2 Downregulated in *syp* mutant

geneID	geneName	log2FoldChange	padj
FBgn0034253	CG10936	-3.5438	8.8085E-38
FBgn0011293	a10	-2.8241	5.2021E-17
FBgn0001217	Hsc70-2	-2.7711	6.0659E-16
FBgn0038290	CG6912	-2.7101	1.3783E-22
FBgn0004191	snRNA:U2:34ABa	-2.5993	3.2495E-13
FBgn0010241	Mdr50	-2.4249	6.9675E-10
FBgn0267160	CR45600	-2.2662	4.3230E-14
FBgn0038301	CG6654	-2.2049	5.2359E-27
FBgn0033725	Cpr49Ac	-2.1942	6.0440E-18

geneID	geneName	log2FoldChange	padj
FBgn0051004	mesh	-2.1317	4.5098E-16
FBgn0040299	Myo28B1	-2.1294	1.4387E-10
FBgn0262636	dati	-2.0966	5.2482E-14
FBgn0004870	bab1	-2.0660	2.2219E-11
FBgn0033980	Cyp6a20	-2.0456	5.1396E-07
FBgn0003046	Pcp	-1.9966	5.2840E-08
FBgn0037487	thw	-1.9322	3.4790E-09
FBgn0032235	CG5096	-1.9101	1.1035E-06
FBgn0037807	CG6293	-1.8087	1.2034E-10
FBgn0034275	CG5002	-1.7747	4.8848E-13
FBgn0038826	Syp	-1.7714	7.1301E-13
FBgn0265254	CR44268	-1.7708	4.5403E-04
FBgn0032405	firl	-1.7162	2.7689E-06
FBgn0037548	CG7900	-1.7139	7.3363E-05
FBgn0264267	CR43767	-1.6997	4.9936E-06
FBgn0036816	Indy	-1.6537	5.8065E-09
FBgn0266084	Fhos	-1.6154	4.2274E-13
FBgn0263656	CG43647	-1.6073	1.2119E-04
FBgn0250839	CG2016	-1.5968	5.6544E-07
FBgn0053922	CG33922	-1.5699	1.5530E-03
FBgn0051157	CG31157	-1.5616	2.1530E-04
FBgn0038716	CG7342	-1.5580	4.4802E-05
FBgn0029807	CG3108	-1.5513	7.4579E-05
FBgn0262531	CG43085	-1.5503	1.0658E-04
FBgn0000477	DNaseII	-1.5476	1.0658E-04
FBgn0052801	CG32801	-1.5367	1.7943E-06
FBgn0035193	CG9192	-1.4630	1.0037E-04
FBgn0039955	CG41099	-1.4431	5.8604E-10
FBgn0004865	Eip78C	-1.4408	1.2470E-10
FBgn0031974	CG12560	-1.4163	1.0894E-03
FBgn0266777	CR45242	-1.4130	4.6938E-07
FBgn0262972	CR43283	-1.4096	1.2325E-05
FBgn0035484	CG11594	-1.4074	8.5373E-04
FBgn0037613	Cks85A	-1.4009	2.9239E-06
FBgn0033668	exp	-1.3927	1.7557E-05
FBgn0038720	CG6231	-1.3846	2.1638E-09
FBgn0034468	Obp56a	-1.3843	1.9815E-03
FBgn0263746	CR43671	-1.3747	3.6878E-03
FBgn0038422	CG14880	-1.3422	2.6145E-03
FBgn0032252	loh	-1.3395	4.6938E-07
FBgn0265067	CR44178	-1.3303	3.0216E-03
FBgn0063127	pncr002:3R	-1.3301	4.6900E-14
FBgn0262532	CR43086	-1.3295	5.0672E-04

geneID	geneName	log2FoldChange	padj
FBgn0263655	CG43646	-1.3227	2.3412E-03
FBgn0037811	CG12592	-1.3186	4.5403E-04
FBgn0040817	CG14132	-1.3129	6.4984E-04
FBgn0259682	Jabba	-1.3098	2.0779E-04
FBgn0039642	CG11882	-1.3044	9.0377E-06
FBgn0001089	Gal	-1.2849	2.4917E-03
FBgn0037973	CG18547	-1.2805	7.6233E-04
FBgn0038925	Cchl	-1.2780	2.5238E-07
FBgn0000153	b	-1.2739	4.5729E-03
FBgn0086662	snoRNA:Psi28S-3186	-1.2666	6.2245E-03
FBgn0030665	CG15646	-1.2625	1.2654E-03
FBgn0263047	CG43342	-1.2586	6.1036E-07
FBgn0031451	CG9961	-1.2537	2.6476E-03
FBgn0035625	Blimp-1	-1.2537	2.9681E-04
FBgn0265699	CR44506	-1.2300	2.5813E-04
FBgn0086408	stl	-1.2294	3.2302E-03
FBgn0039490	CG5882	-1.2287	5.5665E-03
FBgn0035434	Drsl5	-1.2280	9.2482E-03
FBgn0031730	CG7236	-1.2028	6.1073E-03
FBgn0003375	Sgs5	-1.1978	2.8823E-03
FBgn0052571	TwdlX	-1.1748	1.4635E-02
FBgn0035852	CG7387	-1.1693	8.0647E-03
FBgn0038071	Dtg	-1.1622	1.0964E-03
FBgn0030586	CG12539	-1.1620	1.5003E-02
FBgn0040321	GNBP3	-1.1620	2.7535E-03
FBgn0034438	CG9416	-1.1572	5.5665E-03
FBgn0053126	NLaz	-1.1568	1.0037E-04
FBgn0004910	Eip63F-1	-1.1565	8.9236E-04
FBgn0267243	CR45683	-1.1509	9.1783E-03
FBgn0030051	spirit	-1.1469	1.3997E-02
FBgn0027109	NPF	-1.1462	1.0150E-02
FBgn0052364	tut	-1.1441	1.6239E-02
FBgn0266227	CR44922	-1.1404	3.1084E-05
FBgn0033724	CG8501	-1.1302	1.5886E-02
FBgn0085325	CG34296	-1.1302	1.3193E-02
FBgn0027611	LManII	-1.1224	2.8151E-03
FBgn0037265	spartin	-1.1221	1.3703E-04
FBgn0035483	Mul1	-1.1216	1.0803E-06
FBgn0264703	CR43972	-1.1182	1.8828E-02
FBgn0263048	CG43343	-1.1117	2.5451E-05
FBgn0046689	Takl1	-1.1090	1.9697E-02
FBgn0035859	CG13678	-1.1088	2.4794E-02
FBgn0024294	Spn43Aa	-1.1062	1.3308E-02

geneID	geneName	log2FoldChange	padj
FBgn0038337	CG6125	-1.1058	6.0995E-03
FBgn0004592	Eig71Ee	-1.1020	1.9045E-02
FBgn0265052	St3	-1.0969	9.7959E-04
FBgn0029863	CG3823	-1.0939	1.4796E-02
FBgn0264562	Hr4	-1.0936	4.8405E-03
FBgn0052182	CG32182	-1.0661	1.6489E-03
FBgn0266681	CR45171	-1.0656	1.8622E-02
FBgn0034988	cN-IIIB	-1.0587	2.0836E-04
FBgn0037323	CG2663	-1.0559	3.0874E-02
FBgn0263345	CR43426	-1.0495	1.0139E-02
FBgn0034540	Lrt	-1.0494	2.9641E-05
FBgn0263507	CR43496	-1.0480	1.6458E-02
FBgn0035670	CG10472	-1.0455	1.8981E-02
FBgn0052418	vito	-1.0395	9.7780E-03
FBgn0038769	CG10889	-1.0374	1.7178E-04
FBgn0039201	CG13617	-1.0346	2.1094E-02
FBgn0264862	CR44053	-1.0339	1.4286E-02
FBgn0031182	Cyp6t1	-1.0323	3.1688E-02
FBgn0040251	Ugt86Di	-1.0284	3.5303E-02
FBgn0037515	Sp7	-1.0275	5.3306E-03
FBgn0034139	CG4927	-1.0260	3.2010E-02
FBgn0014427	CG11899	-1.0107	2.2639E-02
FBgn0039081	Irk2	-1.0058	4.3611E-03
FBgn0025525	bab2	-1.0004	1.2573E-08
FBgn0051324	CG31324	-0.9949	4.5056E-04
FBgn0003943	Ubi-p63E	-0.9897	1.3408E-02
FBgn0035300	CG1139	-0.9833	4.1242E-02
FBgn0023541	Cyp4d14	-0.9830	9.0622E-03
FBgn0031549	Spindly	-0.9827	2.4799E-03
FBgn0264325	Atg6	-0.9762	5.0478E-06
FBgn0027930	MP1	-0.9758	6.0995E-03
FBgn0035610	Lkr	-0.9741	2.7251E-03
FBgn0036565	CG5235	-0.9741	1.6724E-02
FBgn0030357	Sclp	-0.9732	4.7362E-02
FBgn0038180	Cht5	-0.9700	3.0683E-02
FBgn0034218	CG18467	-0.9549	2.4915E-02
FBgn0051032	CR31032	-0.9495	1.3697E-02
FBgn0004595	pros	-0.9479	1.8828E-02
FBgn0034126	jtb	-0.9403	3.6551E-02
FBgn0038045	NANS	-0.9361	4.1023E-02
FBgn0050359	Mal-A5	-0.9215	4.2722E-02
FBgn0039301	Nup37	-0.9056	1.4089E-02
FBgn0034443	cer	-0.9020	2.2639E-02

geneID	geneName	log2FoldChange	padj
FBgn0020445	E23	-0.8990	3.2809E-04
FBgn0029804	CG3097	-0.8935	6.0995E-03
FBgn0038880	SIFaR	-0.8899	6.0289E-04
FBgn0085354	CG34325	-0.8874	4.5919E-02
FBgn0028468	rtet	-0.8827	1.0785E-02
FBgn0015591	AstA	-0.8805	2.0470E-02
FBgn0035767	Cln7	-0.8756	2.5152E-03
FBgn0004956	upd1	-0.8750	3.3233E-02
FBgn0011297	l(2)not	-0.8745	5.1675E-05
FBgn0002174	l(2)tid	-0.8716	1.7988E-04
FBgn0001253	ImpE1	-0.8709	1.0874E-04
FBgn0026085	dgt4	-0.8705	4.3486E-02
FBgn0035290	dsb	-0.8655	5.5665E-03
FBgn0267181	CR45621	-0.8645	3.7995E-03
FBgn0032230	lft	-0.8616	4.3273E-02
FBgn0039678	Obp99a	-0.8597	4.9181E-02
FBgn0030955	CG6891	-0.8593	4.5140E-03
FBgn0005612	Sox14	-0.8583	1.0533E-03
FBgn0034879	Rrp4	-0.8563	1.8095E-02
FBgn0263493	CR43482	-0.8523	3.7543E-02
FBgn0044047	Ilp6	-0.8509	5.1603E-05
FBgn0265575	yin	-0.8456	3.1207E-02
FBgn0025712	CG13920	-0.8410	1.3745E-04
FBgn0030666	CG12708	-0.8406	3.6807E-02
FBgn0053200	VepD	-0.8354	2.3098E-02
FBgn0051323	CG31323	-0.8335	8.2015E-04
FBgn0035976	PGRP-LC	-0.8314	3.9534E-02
FBgn0025693	ZnT41F	-0.8298	2.3717E-02
FBgn0013433	beat-Ia	-0.8264	1.7557E-05
FBgn0035027	CG3511	-0.8244	2.7301E-04
FBgn0011327	Uch-L5	-0.8143	8.0493E-03
FBgn0030406	CG1463	-0.8115	4.0106E-03
FBgn0039153	GatB	-0.7918	2.9515E-02
FBgn0003255	rk	-0.7877	2.8606E-03
FBgn0004057	Zw	-0.7813	3.9923E-02
FBgn0037999	CG4860	-0.7794	2.7473E-02
FBgn0032297	CG17124	-0.7730	1.1137E-02
FBgn0001226	Hsp27	-0.7726	3.3357E-02
FBgn0259676	DNApol-alpha60	-0.7716	1.0839E-02
FBgn0034725	CG6044	-0.7705	9.2837E-03
FBgn0043455	CG5986	-0.7669	3.4755E-02
FBgn0030653	CG7860	-0.7661	2.1094E-02
FBgn0020660	eIF4B	-0.7647	1.1814E-02

geneID	geneName	log2FoldChange	padj
FBgn0004360	Wnt2	-0.7612	2.1094E-02
FBgn0004394	pdm2	-0.7590	4.0623E-02
FBgn0030241	feo	-0.7588	1.2896E-03
FBgn0260407	mRpS23	-0.7570	2.5733E-02
FBgn0037835	CG14687	-0.7556	3.7596E-02
FBgn0052441	CG32441	-0.7544	2.1185E-02
FBgn0039993	CG17691	-0.7525	3.1259E-02
FBgn0019809	gcm2	-0.7521	1.3620E-02
FBgn0002466	sti	-0.7505	4.6118E-04
FBgn0010109	dpn	-0.7503	6.8193E-03
FBgn0016076	vri	-0.7502	1.0404E-02
FBgn0032698	CG10336	-0.7470	1.9697E-02
FBgn0028546	ics	-0.7467	2.3027E-02
FBgn0052137	CG32137	-0.7447	2.1847E-03
FBgn0036641	Smn	-0.7422	2.9267E-02
FBgn0263697	Uba3	-0.7419	8.4878E-03
FBgn0052207	hpRNA:CR32207	-0.7404	2.4238E-02
FBgn0260985	RfC4	-0.7335	9.4398E-03
FBgn0000261	Cat	-0.7242	1.4452E-03
FBgn0264942	CR44111	-0.7241	3.0978E-02
FBgn0032646	mEFTs	-0.7227	3.7193E-03
FBgn0015298	Srp19	-0.7204	3.9708E-02
FBgn0003430	slp1	-0.7203	3.0314E-03
FBgn0034564	CG9344	-0.7166	4.9816E-02
FBgn0052843	Dh31-R	-0.7073	1.0879E-02
FBgn0028407	Drep3	-0.7014	6.1073E-03
FBgn0036790	AstC-R1	-0.7001	3.5291E-02
FBgn0032414	CG17211	-0.6997	3.2966E-02
FBgn0267727	Pen	-0.6981	8.3776E-03
FBgn0029676	HIP-R	-0.6969	1.5577E-03
FBgn0004364	18w	-0.6931	9.2969E-03
FBgn0038140	PK2-R1	-0.6916	1.1497E-02
FBgn0261090	Sytbeta	-0.6916	5.1885E-03
FBgn0000567	Eip74EF	-0.6916	7.3986E-03
FBgn0011606	Klp3A	-0.6906	1.8044E-03
FBgn0034430	mip40	-0.6799	3.2155E-02
FBgn0001296	kar	-0.6795	5.2183E-04
FBgn0250869	CG42240	-0.6793	6.0995E-03
FBgn0025687	LKRSDH	-0.6763	2.4465E-03
FBgn0003660	Syb	-0.6751	3.0111E-02
FBgn0050106	CCHa1-R	-0.6743	2.4238E-02
FBgn0040528	CG15864	-0.6716	1.0075E-02
FBgn0036843	Sfxn2	-0.6700	4.2955E-02

geneID	geneName	log2FoldChange	padj
FBgn0038330	CG14868	-0.6687	1.1443E-03
FBgn0052447	CG32447	-0.6596	4.8287E-02
FBgn0024732	Drep1	-0.6591	2.2150E-03
FBgn0261975	CG42806	-0.6530	2.9808E-02
FBgn0037979	GCC185	-0.6498	3.8468E-03
FBgn0035120	wac	-0.6424	4.8085E-02
FBgn0038639	CG7705	-0.6407	2.7176E-02
FBgn0010382	CycE	-0.6406	2.0089E-03
FBgn0037342	CG2931	-0.6370	2.1168E-02
FBgn0031191	Cp110	-0.6327	4.3003E-02
FBgn0005355	Su(fu)	-0.6190	1.0404E-02
FBgn0000015	Abd-B	-0.6165	4.8337E-02
FBgn0265274	Inx3	-0.6163	6.1986E-03
FBgn0038772	mdlc	-0.6121	4.9181E-02
FBgn0036199	Bmcp	-0.6058	4.8287E-02
FBgn0037978	KLHL18	-0.6011	1.7649E-02
FBgn0003720	tll	-0.5989	1.0404E-02
FBgn0011692	pav	-0.5989	3.8705E-02
FBgn0045064	bwa	-0.5978	4.7764E-02
FBgn0033000	CG14464	-0.5948	8.2974E-03
FBgn0038043	CG17202	-0.5763	2.9739E-02
FBgn0039381	SppL	-0.5692	6.8193E-03
FBgn0052176	CG32176	-0.5688	4.3825E-02
FBgn0264494	CG17646	-0.5644	4.1023E-02
FBgn0052251	Claspin	-0.5512	1.9179E-02
FBgn0026319	Traf4	-0.5502	3.6079E-02
FBgn0029113	Uba2	-0.5438	9.2160E-03
FBgn0266441	CG45071	-0.5422	8.1155E-03
FBgn0038341	AdamTS-A	-0.5394	3.5768E-02
FBgn0036279	Ncc69	-0.5366	3.6522E-02
FBgn0036480	Cep135	-0.5348	3.2964E-02
FBgn0259993	CR42491	-0.5308	3.0030E-02
FBgn0053543	CG33543	-0.5242	4.1432E-02
FBgn0030260	CG1537	-0.5203	4.8337E-02
FBgn0033639	CG9003	-0.5178	1.1497E-02
FBgn0037470	Tailor	-0.5144	3.1995E-02
FBgn0036317	CG10948	-0.4810	4.9905E-02
FBgn0010225	Gel	-0.4752	1.3419E-02
FBgn0028582	lqf	-0.4346	3.3301E-02
FBgn0028692	Rpn2	-0.4293	4.9040E-02